Role of Nano and Microsize Clay Minerals in Non-Aqueous Bitumen Extraction from Alberta Oil Sands

by

Mirjavad Geramian

A thesis submitted in partial fulfillment of the requirements for the degree of

Doctor of Philosophy

In

MATERIALS ENGINEERING

Department of Chemical and Materials Engineering

University of Alberta

Abstract

The Alberta oil sands are the third largest oil reserve in the world with 174 billion barrels of recoverable oil consisting of bituminous hydrocarbons, inorganic materials and water. The current commercial aqueous extraction processes produce large amounts of tailings and is the major obstacle to recovery of bitumen from the oil sands. Solvent-based bitumen extraction is an alternative process and has been investigated since 1950, due to its high bitumen recovery and dry solids/tailings (gangue). During non-aqueous extraction, it is expected that some minerals, particularly nano and microsize minerals (NMM), change the processability of the oil sands ore due to their interaction with other ingredients such as water, bitumen and solvent. The gap of knowledge on the influence of mineralogical and chemical composition of the NMM during non-aqueous extraction directed us to the present study.

The aim of this study was first to identify the mineralogy, chemistry and surface properties of four petrologic end member samples from Syncrude's North Mine collected in 2009 (NM09) and 2012 (NM12), i.e., marine claystone (MC), marine sand (MS), estuarine claystone (EC) and estuarine sand (ES). The as-received (ASRE) petrological end members and their different size fractions were examined in this study by various analytical techniques and the results were compared with samples taken from the Aurora Mine in 2010 (AM10) of Syncrude Canada Ltd. (Fort McMurray, Alberta).

Quantitative x-ray diffraction (XRD) analysis revealed that bulk samples of the clay end members were composed of significantly higher amounts of clay minerals and lower amounts of quartz

compared with the bulk samples of the sand end members. XRD analysis of oriented preparations (air dried-54 % RH and ethylene glycolated) of the < 0.2 μm fractions of the four end members showed that interstratified illite-smectite of high (~30 %) and low (~10 %) expandability were observed only in clay-rich end members, i.e., NM12-EC and MC, respectively. Kaolinite-smectite was only found in the < 0.2 μm fraction of the NM12-MC with an expandability between 5 and 10 %. Interstratification of illite-smectite was observed in the < 0.2 μm fraction of NM09-MC and EC samples, but the expandability was only 10 % for both fractions. ES and EC had the highest and lowest bitumen contents, respectively, for the NM12, NM09 and AM10 samples.

The second underpinning aim of this research was to determine the mechanism of preferential clay segregation during the solvent-based bitumen extraction process. Different adsorption amounts of hydrocarbon components by clay minerals, which is due to their different properties, may affect the processability of oil sands ore during the extraction process. However, due to the highly heterogeneous nature of the clay minerals in the oil sands, it is difficult to determine the effect of individual clay minerals on bitumen recovery when testing the whole ore sample. For this purpose, an experimental set up was designed and investigated to examine the effect of individual clay minerals (swelling and non-swelling clays) on the non-aqueous bitumen extraction process. Artificial mixtures of bitumen with standard clays (from the Clay Minerals Society) were prepared and the influence of individual clays on the extraction process was investigated.

Elemental analysis (CHNS) revealed that the highest residual organic carbon content was observed for swelling clay-bitumen mixtures at 95% relative humidity (RH). Swelling clays are significantly affected by increasing RH; however, RH has minimal effect on non-swelling clays. After bitumen treatment, the residual organic carbon content increased and the cation exchange capacity (CEC)

and SSA decreased for all samples. Scanning electron microscopy (SEM) observations showed that swelling clays formed larger aggregates than non-swelling clays, which was consistent with the decrease in SSA for the swelling clays. Bitumen was not observed in the interlayer space of swelling clay-bitumen mixtures at 95% RH; bitumen was only observed at the surface of clay particles.

The third aim of the study was to identify the most important species affecting the non-aqueous bitumen extraction process and bitumen quality. This investigation was carried out on four petrologic end member samples taken from Syncrude's North Mine in 2012 (NM12). Each end member was separately mixed with cyclohexane at a ratio of 40:60 (cyclohexane:end member), and the bitumen-cyclohexane solutions were collected at different settling times (1 min to 30 min). These solutions were analyzed to characterize the suspended fine solids (SFS) and water content, as well as the bitumen content, using various analytical techniques.

Quantitative x-ray diffraction (XRD) analysis showed that the SFS were composed of mainly illite and kaolinite after cyclohexane extraction from MC, MS, EC and ES. Although mixed layer expandable clay minerals (i.e., illite-smectite and kaolinite-smectite) were identified in the original clay end members (EC and MC), illite-smectite and kaolinite-smectite were not observed in the SFS of the bitumen-cyclohexane solutions obtained from the four petrologic end members. The SFS content and bitumen quality of the bitumen product were affected by the end member composition and settling time, respectively. Illite and kaolinite were identified as the main minerals in the SFS of the bitumen products after relatively long settling times. Transmission electron microscopy (TEM) investigations showed the presence of kaolinite and rutile in the supernatant of EC at 1 min and 7.5 min of settling time. Kerogen and/or asphaltene were also present in the SFS

of end members based on the N/C ratio (>0.018). XRD and SEM analysis showed that the amount of large grains decreased with increasing settling time. The solids were mostly fine clay particles (kaolinite and illite) and were typically several microns in size. Some heavy minerals, such as Fe–Ti oxide minerals and pyrite (both single particle and framboidal pyrite), were found in the suspended solids from MC after 1 min and 7.5 min settling.

Preface

This research thesis is focused on the characterization of the four petrologic end members and their various fractions, particularly nano and microsize clay minerals (NMCM) as well as determination of the influence of NMCM during non-aqueous bitumen extraction process. The materials presented in this research thesis are under the supervision of Dr. Thomas H. Etsell, Dr. Qi Liu and Dr. Douglas G. Ivey and was financially supported by the Institute for Oil Sands Innovation (IOSI) at the University of Alberta and NSERC.

Chapter 4 of this thesis has been partially published as M. Osacky, M. Geramian, Q. Liu, D.G. Ivey and T.H. Etsell, Energy Fuels, 28 (2014), 934–944, DOI: 10.1021/ef402150z. Some parts of this Chapter were presented as M. Geramian, T. H. Etsell, D. G. Ivey and Q. Liu, April 28 -29, 2014, at the Oil Sands 2014 Conference, University of Alberta, Edmonton, AB, Canada. Some other parts of this Chapter were published as M. Geramian, O. H. Ardakani, H. Sanei, T. H. Etsell, D. G. Ivey and Q. Liu, April 28-29, 2015, in the proceedings of the COSIA/PTAC Oil Sands Clay Workshop and Conference, University of Alberta, Edmonton, AB, Canada.

This Chapter summarizes the research conducted in collaboration work with Dr. Marek Osacky (a former postdoctoral fellow in our group). He performed and contributed to some parts of the sample preparations, characterization techniques and interpretation of those results. The collection of various size fractions and different characterization techniques (i.e., SA, CEC, LCD and XRD), as well as interpretation of the corresponding results, were mostly performed by myself.

Chapter 5 has been published as M. Geramian, D. G. Ivey, Q. Liu and T. H. Etsell, Canadian Journal of Chemical Engineering, 9999: (2017), 1–13, DOI: 10.1002/cjce.23034. I was responsible for whole parts of this paper including the experimental design, sample preparations, data collection and interpretation of results, as well as the manuscript composition.

Chapter 6 has been published in two well-respected journals: M. Osacky, M. Geramian, D. G. Ivey, Q. Liu and T. H. Etsell, Energy Fuels, 29 (2015), 4150-4159, DOI: 10.1021/acs.energyfuels.5b00269 and M. Geramian, M. Osacky, D. G. Ivey, Q. Liu and T. H. Etsell, Energy Fuels, 30 (10), (2016), 8083–8090, DOI: 10.1021/acs.energyfuels.6b01026. Also, some parts of this Chapter were published as M. Geramian, M. Osacky, L. Zheng, D.G. Ivey, Qi Liu and T.H. Etsell, in the proceedings of the 3rd Oil Sands Clay Conference and Workshop, CONRAD, University of Alberta, February 20-21, 2013, Edmonton, AB, Canada.

This Chapter summarizes the research accomplished in collaboration with Dr. Marek Osacky. He performed and contributed to some of the sample preparations, characterization techniques and interpretation of those results. He also performed BWA analysis and calculated TMEAN and CTD for five standard clay minerals. The collection of <2 μm size fractions and different characterization techniques (i.e., SA, CEC, LCD and XRD), as well as interpretation of the corresponding results, were mostly performed by myself.

Chapter 7 has also been submitted for publication as M. Geramian, Q. Liu, D.G. Ivey and T.H. Etsell, Canadian Journal of Chemical Engineering, 2017, Manuscript ID: CJCE-17-1124. I was responsible for the entire paper including the experimental design, sample preparations and data collection, as well as the interpretation of results and the manuscript composition. The collected supernatants (CS) at different settling times were performed primarily by Farhad Azam (MSc student in our group) and Komal Dhankhar (Research Assistant in our group).

In all mentioned publications, Dr. Thomas H. Etsell, Dr. Qi Liu and Dr. Douglas G. Ivey contributed to the manuscript composition and edits.

It should be expressed that the format of this thesis is paper-based and there is likely some repetition, particularly in the “Materials and Methods” sections in a few Chapters.

Dedication

This thesis is dedicated

To Maryam-my beloved wife

To Sam-my delightful son

To my respectful parents

Acknowledgments

Herewith, I would like to thank the people who helped me in the journey of my dissertation:

First of all, I would like to express my gratitude and appreciation to Dr. Thomas H. Etsell, Dr. Douglas G. Ivey and Dr. Qi Liu for their guidance and supervision during my research. Their great suggestions, guidance and enlightening advice have helped me in performing laboratory experiments, analyzing and interpreting scientific data and editing scientific publications.

Thanks to Dr. Arek Derkowski for his great help and guidance, especially in the beginning of my research. Special thanks to Dr. Marek Osacky for his guidance and collaboration in running many experiments during the first two years of my research.

I would also like to thank my office mates and my friends Dr. Ali Hooshiar, Dr. Marek Osacky, Limin Zhang, Dr. Igor Stricek, Dr. Cheng Wang, Dr. Amir Hanifi, Farhad Azam, Dr. Mehdi Mohammadalipour and Taghi Amiri for always being very helpful and nice. They helped me a lot in this research and I really enjoyed the pleasant work experience.

I would like to thank the amazing technicians who trained me to use various instruments in the IOSI laboratories: Dr. Xiaoli Tan, Dr. Kavithaa Logan, Keith Draganiuk, Lisa Brandt, Jeremiah Bryksa and Brittany Mackinnon.

I would also like to thank the wonderful people who trained me to use several instruments in the CME, Nano-FAB and OSCIEF laboratories: Andree Koenig (for the centrifuge), Dr. Nancy Zhang (for BET, Freeze dryer, XRD-Rigaku), Shiau-Yin Wu (for TGA) and Ni Yang (for UV-Vis spectrometer, Dynamic and Static Light Scattering-ALV).

I want to thank the amazing people who provided me with various data: Shiraz Merali for XRD, Dr. Peng Li and Dr. Anqiang He for TEM imaging, Martin Kupsta, Doug Vick and Kai Cui for the FIB-SEM sample preparation for TEM and Dr. Nathan Gerein for SEM.

I am very grateful to Jonathan Calotes, Farhad Azam, Joshua Seens, Komal Dhankhar and Taghi Amiri for all their assistance during preparation of samples and running experiments. I also want to thank to my great friend Dr. Mehdi Mohammadalipour for his help in editing the current thesis.

I would like to thank the Institute for Oil Sands Innovation (IOSI) for funding my PhD project and Syncrude Energy Ltd. for the samples from different deposit sites.

I also would like to thank to Dr. Qi Liu for letting me to use his laboratory fume hood, to Dr. Douglas G. Ivey for his guidance and performing transmission electron microscopy (TEM) and nano-diffraction and to Dr. Thomas H. Etsell for his guidance, insights and knowledge at any time during my research, which helped me to reach my goals.

Last, but not least, I would like to special thank my wife Maryam, whose love and support mean the world to me. I can never thank her enough for her great help and patience during my research.

TABLE OF CONTENTS

LIST OF FIGURES

LIST OF TABLES

LIST OF ABBREVIATIONS

AM10: Aurora Mine samples collected in 2010

ASRE: As-received

BET: Brunauer-Emmett-Teller

BF: Bright field

BWA: Bertaut, Warren and Averbach

CDB: Cyclohexane-diluted bitumen

Cc: Calcite

CCa-2: Chlorite from California

CEC: Cation exchange capacity

Ch: Chlorite

CIOC: Cyclohexane insoluble organic carbon

CL: Chord length

CLD: Chord length distribution

Cor: Corundum

CS: Collected supernatants

CTB: Clay−toluene−bitumen

CTD: Crystallite thickness distribution

Cu_{TRIEN}: Copper-(II)-triethylenetetramine

Do: Dolomite

DS: Dean-Stark extraction

EC: Estuarine claystone

EDX: Energy dispersive X-ray

EG: Ethylene glycol

ES: Estuarine sand

FBRM: Focused beam reflectance measurement

FEP: Fluorinated ethylene propylene

FIB: Focused ion beam

FIB-SEM: Focused ion beam-scanning electron microscopy

FEG: Field emission gun

FTIR: Fourier transform infrared spectroscopy

G: Gypsum

HRTEM: High-resolution transmission electron microscopy

I: Illite

ICP-MS: Inductively coupled plasma-mass spectroscopy

IMt-1: Illite from Montana

IOSI: Institute for Oil Sands Innovation

ISCz-1: Illite-smectite from Slovakia

I-S: Illite-smectite

K: Kaolinite

KGa-2: Kaolinite from Georgia

K-feldspar: Potassium feldspar

KF titration: Karl Fischer titration

K-S: Kaolinite-smectite

LCD: Layer charge density

LOD: Loss-on-drying

LOI: Loss-on-ignition

MC: Marine claystone

MB: Methylene blue

MS: Marine sand

NAE: Non-aqueous extraction

NM09: North Mine samples collected in 2009

NM12: North Mine samples collected in 2012

NMCM: Nano and microsize clay minerals

NMM: Nano and microsize minerals

C_{org}: Organic carbon

PTFE: Polytetrafluoroethylene

PSD: Particle size distribution

Q: Quartz

QXRD: Quantitative X-ray diffraction

R6G: Rhodamine 6G

RCF: Relative centrifugal force

RH: Relative humidity

ROI: Region of interest

SA: Surface area

SAD: Selected area diffraction

SAGD: Steam assisted gravity drainage

Sd: Siderite

SDS: Second-derivative spectra

SE: Secondary electron

SEM: Scanning electron microscopy

SFS: Suspended fine solids

SG: Specific gravity

SSA: Specific surface area

SWy-2: Smectite from Wyoming

TC: Total carbon

TCD: Thermal conductivity detector

TEM: Transmission electron microscopy

TGA: Thermogravimetric analysis

TH: Total hydrogen

TIC: Total inorganic carbon

TIOC: Toluene insoluble organic carbon

T_{MEAN}: Mean crystallite thickness

TN: Total nitrogen

TOC: Total organic carbon

TPD: Temperature programmed desorption

TS: Total sulfur

TSSA: Total specific surface area

XRD: X-ray diffraction

CHAPTER 1

1 INTRODUCTION AND LITERATURE REVIEW

INTRODUCTION

The Alberta oil sands, with 174 billion barrels of recoverable oil, represent the third largest oil reserve in the world [1,2]. Peace River, Athabasca, and Cold Lake are three main oil sands deposits in Alberta [3]. Oil sands composition is primarily a mixture of bitumen (4-18 wt%), inorganic materials (non-clays and clays minerals (55-80 wt%)) and salty water (2-15 wt%) [2]. Considering the oil sands composition, the bitumen extraction processes are substantially more difficult than that of conventional crude reserves [4]. The extracted bitumen from oil sands has high molecular weight organic compounds, very high viscosity and high density, with relatively high concentrations of heavy metals and a low hydrogen to carbon ratio in comparison with conventional oil [5].

The Alberta oil sands can be classified in two categories depending on the depth of deposits: shallow (depth less than 75 m beneath the ground) and deep deposits. The extraction of bitumen from shallow and deep sections is performed by the conventional extraction method (hot water process) and steam assisted gravity drainage (SAGD) technologies, respectively [5]. According to Alberta Energy Resource's report in 2013, total raw bitumen recovery from Alberta resources was 2.1 million barrels per day. 53% of this amount was produced from in-situ and 47% by surface mining [6]. In conventional extraction, the efficiency of extraction depends on three main factors: water chemistry, mineralogy of the ore, and bitumen chemistry [2,7,8]. Currently, oil sands tailings ponds cover 180 square kilometers of land area in northern Alberta [6,9]. Bitumen production will reach 4.1 million barrels per day by 2023, which means a larger area of tailings ponds. It was reported that oil sands tailings are produced at a rate of two hundred million liters per day, and the volume of tailings is expected to increase by 30% by 2020 [6]. The water-based bitumen extraction

process is consuming high amounts of fresh water and energy as well as requiring a large area of land for tailings ponds, which are the most significant disadvantages of the conventional method. Thus, non-aqueous solvent bitumen extraction processes have been investigated as an alternative method for more than 50 years and are expected to have less environmental impact as well as their potential advantage of high bitumen recovery from different grades of ores (low, medium and high grade oil sands ores) [10]. It is believed that the most important factor affecting bitumen extraction processes (aqueous or non-aqueous) is oil sands composition. Therefore, it is crucial to understand the influence of water, bitumen and solids particularly nano and microsize species on the extraction process [10,11].

1.1 ALBERTA OIL SANDS FORMATION AND COMPOSITION

Deposits of oil sands are found in some areas of the world. In Venezuela and Canada, the oil sands deposits are mainly evident within Cretaceous rocks. The oil sands deposits in Canada are mostly located in northern Alberta in three deposits in the McMurray area. These deposits are layers of oil sand and sandstone, which formed during in the Cretaceous era [12]. The oil sands mined in northeastern Alberta are shown in Figure 1-1. Peace River, Athabasca and Cold Lake deposits are named for the rivers which meander through them and have their own distinct characteristics.

Figure 1-1 Location of oil sands in northeastern Alberta [12].

Most petroleum geologists believe that the origin of fossil fuels (conventional oil, natural gas, coal and oil sands) was formed in the same way, when the organic matter died and decomposed under layers of sediments for millions of years. The organic matter was affected by sufficient pressure and temperature to be altered into oil.

Alberta was mostly covered by a warm sea in the middle of the Devonian period (410–353 million years ago - mya), many years before the Rocky Mountains reach their top heights (Figure 1-2). When the sea water retrograded, the organic marine mud was trapped and converted into oil [12]. Since several plates lurched to slide underneath the North American Plate and re-formed, the oil migrated to the north of Alberta and was trapped by the large amounts of quartz sands. Viscous bitumen was created due to elimination of lighter hydrocarbons either through evaporation or consumption by bacteria [12].

Figure 1-2 Alberta was mostly covered by warm sea in the middle of the Devonian period (410–353 mya) [12].

The oil sands mined in the Fort McMurray area belong to the stratigraphic unit called the McMurray Formation. These oil sands display a composition of four petrologically different types of rocks called ‘petrologic end members’ i.e., estuarine sand, estuarine clay, marine sand and marine clay, which were deposited in two main sedimentary environments (marine and estuarine) [13]. The outcrops of estuarine and marine ore sections in the Syncrude mine, Fort McMurray, Alberta are shown in Figure 1-3 [14]. The oil sands mined in different areas consist of different

mixtures of these end members and have different mineralogical and chemical compositions. The difference in oil sands compositions affects the bitumen extraction processes (either aqueous or non-aqueous). The coarse particles do not usually have a negative effect on the bitumen extraction process; however, nano and microsize minerals, mainly clay minerals, are the most problematic minerals [15–18]. Wik *et al*. have shown that the small particles and their mineralogical compositions are the two most important parameters affecting bitumen recovery [19].

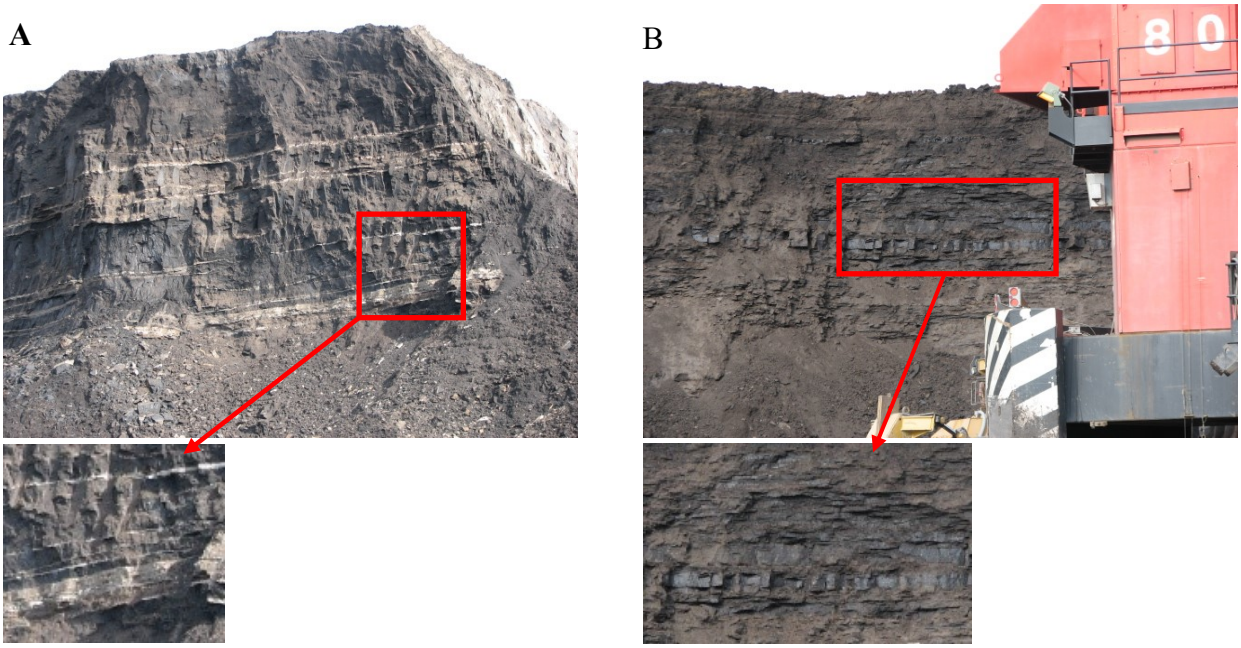

Figure 1-3 Ore sections in the Syncrude mine, Fort McMurray, Alberta, A) Estuarine ore is a black bitumen-rich sand interbedded with a light laminated claystone, B) Marine ore is a bitumen-rich sand interbedded with black or very dark claystone, Height of the outcrops are ~15-20 m [11].

Recent studies have shown that quartz and carbonates are usually the main non-clay minerals and kaolinite and illite are the major clay minerals of Alberta oil sands [4,20,21]. Low quantities of chlorite, smectite and mixed-layer clay minerals have also been reported in Alberta oil sands. Although smectite and mixed-layer clay minerals i.e., illite–smectite and kaolinite–smectite are present in low amounts, they can significantly affect the bitumen extraction process and tailings management [4,19]. Mercier *et al*. have demonstrated that clay minerals are playing the main role in the water-based bitumen extraction process [22]. Clay minerals have a negative influence on bitumen extraction, bitumen recovery and waste management due to their small particle size, high

specific surface area, swelling capacity, cation exchange capacity and layer charge properties. Different types of clay minerals may behave differently towards the processability of oil sands ore during the bitumen extraction process. It has been also reported that montmorillonite and kaolinite have negative effects on the aqueous bitumen extraction process [8]. Both extraction recovery and product quality are significantly affected by interactions between organic materials and clay minerals. These interactions produce clay-organic matter complexes, which make the bitumen extraction process more complicated [23].

1.2 OIL SANDS EXTRACTION PROCESS

As mentioned before, bitumen extraction can be classified into two main process groups; first, aqueous bitumen extraction processes, second, non-aqueous bitumen extraction processes [24]. In the following paragraphs, different extraction techniques for water-based extraction and solvent extraction processes will be explained.

1.2.1 AQUEOUS BITUMEN EXTRACTION

Two aqueous bitumen extraction techniques are currently used in Alberta oil sands, depending on the depth of deposits; shallow (depth less than 75 m beneath the ground) and deep deposits. The extraction methods of bitumen from shallow and deep sections are performed by conventional extraction methods (i.e., a hot water extraction process) and steam assisted gravity drainage (SAGD) technology, respectively [5].

1.2.1.1 OPEN PIT MINING OR SURFACE MINING

The Clark Hot Water Extraction (CHWE) technique was developed by Karl Clark at the University of Alberta in 1926. The CHWE process is still used to extract bitumen from the surface mined oil sands by Syncrude and Suncor. In this technique, the oil sands ore is dug out and crushed, then mixed with hot water at 80˚C and caustic (NaOH) at a pH ~ 8.5, and the slurry is agitated very well in order to produce a separable froth. Recently, the hot water technique has been modified to a warm-water hydro transport process, in which the ore is mixed with warm water (up to 55˚C) at a pH between 7 and 8.5 before froth separation. The produced slurry is fed into hydro transport pipelines and sent to the extraction plant, where the bitumen can be removed by froth flotation

[25,26]. The flow sheet of the hot/warm-water extraction process used in open pit mining is shown in Figure 1-4 [4].

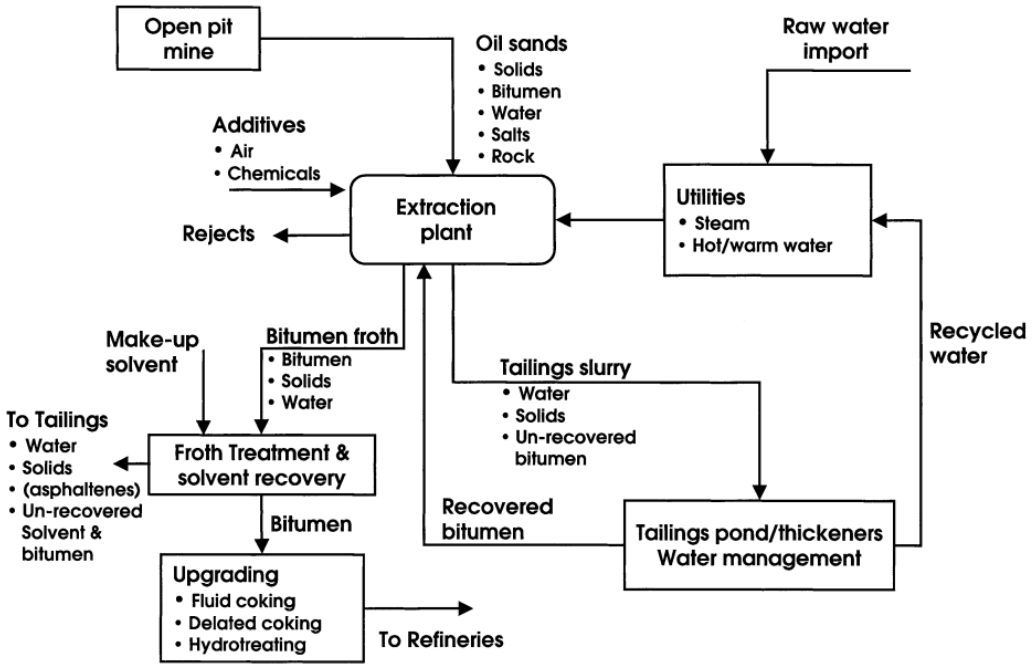

Figure 1-4 Schematic of hot/warm-water extraction process used in open pit mining [4]**.**

Unfortunately, the CHWE process is consuming large amounts of water; a mixture of 2.6 m^3 of water and two tons of ore is required for production of one barrel of oil (0.16 m^3) [27]. Although more than 75% of the water is ultimately recycled, the rest of the water remains in oil sands tailings ponds (a waste mixture of water, residual organics, sands and clays) [28]. It was reported that over 840 million cubic meters of oil sands byproduct is stored in tailings ponds and this will be increased to over a billion cubic meters by 2020 [29].

1.2.1.2 IN-SITU BITUMEN EXTRACTION

In-situ bitumen extraction is used for deeper deposits, which are accessed through various in-situ technologies such as steam-assisted gravity drainage (SAGD), cyclic steam stimulation (CSS) and the process of vapor extraction (VAPEX). The SAGD process is a thermal production method for

heavy oil, which is widely used for the in-situ extraction method. In this technique, parallel pairs of horizontal wells are drilled through the oil sands deposit. The steam injected into the upper well, which is about five meters above the lower horizontal well, increases the temperature and reduces the viscosity of bitumen. Under gravity, the low viscosity bitumen will drain to the production well (the lower horizontal well) and is transported to the surface [5]. A schematic of a SAGD process used in situ is shown in Figure 1-5 [30]. The CSS technology requires one well bore and production consists of two phases. The first phase is injection, which injects the steam for several weeks, increases the temperature and reduces the viscosity of bitumen in the oil sands deposit. The second phase is production, where bitumen flows and is transported through the same well bore to the surface. VAPEX is a non-thermal production technique similar to the SAGD method. In this method, a solvent vapor is used to reduce the viscosity of bitumen. The bitumen is expanded and diluted by contact with injected solvent vapor. The diluted bitumen will flow by gravity to the production well and is pumped to the surface [31].

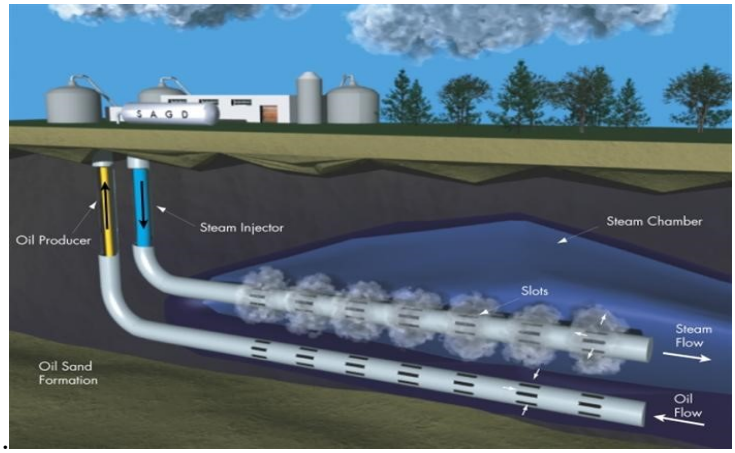

Figure 1-5 Schematic of a SAGD process used in situ [30].

1.2.2 NON-AQUEOUS BITUMEN EXTRACTION

The aqueous bitumen extraction (i.e., open pit mining and in-situ) processes has been commercially applied for many years; however, the mining and extraction process have three main environmental issues: very high water consumption, a large area/volume of tailings ponds generated as well as greenhouse gas emissions. Among these problems, a large area/volume of tailings ponds, particularly the mature fine tailings (MFT) which are generated from this process,

is a major environmental issue for the oil sands industry due to the fact that settling and reclamation of MFT may take several decades. Organic solvent-based bitumen extraction (non-aqueous extraction) from oil sands is the most promising method as it requires much lower fresh water consumption and energy input. Therefore, non-aqueous extraction overcomes the major water consumption and a large area/volume of tailings ponds. However, this process is at the laboratory stage; it requires more investigation to achieve significant progress for transferring the know-how knowledge to industrial plants.

Recently, Hooshiar, *et al*. investigated a non-aqueous bitumen extraction procedure and studied various ratios of toluene and heptane (representing aromatic and paraffinic organic solvents). They found that such an extraction method was not affected by the ore grade and composition (fines and clay contents) [32]. Nikakhtari, *et al*. studied different light hydrocarbon solvents and found that cyclohexane is a suitable solvent for a non-aqueous bitumen extraction process due to its higher bitumen extraction efficiency and faster evaporation [33]. In the following paragraphs, the different mineral compositions present in Alberta oil sands i.e., clay and non-clay minerals will be briefly explained. Studying the oil sands mineralogy will lead to a better understanding of important minerals that affect bitumen extraction processes and subsequent solvent recovery.

1.3 OIL SAND MINERALOGY

Previous researchers have observed that the oil sands deposits in Alberta contain a wide variety of minerals including four petrologically different kinds of rocks. The combination of different end members affects the properties of the oil sands. The four petrological end members consist of quartz, clay minerals (kaolinite, illite, mixed-layer clay minerals and chlorite), carbonates (calcite, dolomite and siderite), K-feldspar and TiO_2 minerals (anatase and rutile) [10]. In general, it is believed that the coarse sands do not cause any issue for the bitumen extraction process and tailings management. However, nano and microsize minerals (NMM), mostly clay minerals (NMCMs), are significantly harmful [10,15,21]. Since NMCMs have small particle size and high specific surface area, swelling capacity, cation exchange capacity and layer charge, and specific physicochemical properties, they may react with the solvent, bitumen and/or water during the extraction process. Previous studies showed that Athabasca oil sands are made up of kaolinite and

illite minerals as the main clay minerals with smaller amounts of chlorite, discrete smectite and mixed-layer clay minerals [20,22,34,35].

1.3.1 NON-CLAY MINERALS

In the oil sands industry, the solids are classified into coarse-grained and fine-grained minerals with a particle size range larger and smaller than 44 μm, respectively. Although the majority of sands in Alberta oil sands are quartz (82%) and feldspars (5%) and are concentrated in the size range larger than 44μm, they has a very small effect on a bitumen extraction process [2,36,37]. Several studies have shown the presence of nanoscale non-clay minerals i.e., SiO_2 and Ti-, Zr- and Fe-bearing minerals in the bitumen froth from Alberta oil sands [38–41]. It was speculated that the presence of these nanoscale heavy minerals in the bitumen froth is due to patches on surfaces of clay particles, and/or association with nanosize clay minerals and toluene insoluble organic matter to create an aggregate (mineral-organic) [38]. In the following sections, some of the mainly observed and identified non-clay minerals either coarse- or fine-grained (i.e., quartz, feldspars, carbonates, Fe-bearing, TiO2 minerals, zircon and calcium sulfate minerals) will be described.

1.3.1.1 QUARTZ MINERALS

Quartz is the second most predominant mineral and is present almost everywhere in the Earth's crust. It can be found in three different groups of rock i.e., igneous, metamorphic and sedimentary rocks [42]. Quartz crystal structure is hexagonal and can be melted at 1723°C. The crystal structure contains a continuous array of tetrahedra of SiO4, whereby oxygen is shared between two tetrahedra [42]. Colourless quartz crystals are observed when they are pure; however, other types are found with various colours such as yellow, red, white, milky-white and black, which were reported in the large grain sizes (> 40 mesh) due to impurities [43]. Many studies have shown that α-quartz (SiO_2) is the main mineral in Alberta oil sands [44]. Bichard reported the amount of quartz is between 70 – 90 wt% of ore samples from Beaver Creek-Mildred Lake oil sands [43]. The percentage of this mineral for the particle fractions >44 μm is significantly higher than that with particle fractions <44 μm [10]. Previous researchers have observed well-formed quartz in Alberta oil sands with the trigonal trapezohedral type of the hexagonal crystal class system. The majority

of quartz grains are conical with sharp ends. Smooth, twisted and bent quartz crystals were also observed in oil sands ores [43].

1.3.1.2 FELDSPAR MINERALS

Feldspar minerals (Na-, K- and Ca-) are the most dominant minerals (almost 60%) on the Earth's surface. It is believed that clay minerals are most likely formed by the hydrothermal alteration of the feldspar minerals [42,45]. The quantity of feldspar minerals are less than that of quartz in Alberta oil sands [46]. As mentioned in the previous section, quartz is the abundant mineral in Alberta oil sands; however, Spiers *et al*. (1989) revealed that K-, Na- and Ca-feldspars are the second, third and fourth most abundant minerals overall in Alberta oil sands, which has been reported by other scientists [4,43,46]. Microcline and plagioclase were identified as a source of potassium and a solid solution of Na-Ca feldspars, respectively, which were concentrated in the >45 μm fraction [4]. Microcline has also been detected in the <45 μm fraction due to the presence of some fine particle sizes as well as being associated with some hydrophobic particles [4,10].

1.3.1.3 CARBON MINERALS (CARBONATE)

Geologically, carbonates are classified as a sedimentary rock such as limestone, which formed from deterioration of marine organisms like coral forams, mollusks and plankton [47]. Limestone can be transformed into dolomite, if it was exposed to the right conditions i.e., pressure, time (over millions of years) and high salinity water. Most of the large conventional oil reservoirs in the Middle East around the Persian Gulf are hosted within carbonate rocks [47]. Siderite ($FeCO_3$), dolomite ($CaMg(CO_3)_2$, calcite ($CaCO_3$), and ankerite $Ca(Mg,Fe)(CO_3)_2$ are four major sources of carbon minerals (carbonate), which were identified in Alberta oil sands by Couillard *et al*. [48]. Siderite and dolomite are isomorphs of calcite and ankerite, respectively [49]. Ankerite and dolomite have similar optical properties and crystalline structure making them difficult to identify in sedimentary rocks [49]. Baker *et al*. (1985) stated that both dolomite and ankerite were formed in many areas of ocean sediments and controlled by the depositional environment such as magnesium, iron and bicarbonate (hydrogen carbonate or HCO_3^-) concentrations [50].

Hepler *et al*. (1989) identified the presence of carbonate minerals i.e., calcite, siderite, dolomite and aragonite in Alberta oil sands [51]. Trace amounts of calcite, dolomite and siderite were

reported in the clay fraction of tailings by Kasperski (1992) [52]. Kaminsky (2008) found siderite in all fractions (>45µm, 2-45 µm and < 2 µm) of ore, primary froth and tailings samples; however, it was mostly in the coarse (>45µm) fractions [4]. Sparks *et al*. (2003) observed calcite and siderite minerals in the oil sands ore. These minerals have usually hydrophilic surface properties; however, some have been identified as a biwettable with hydrophobic surface properties and/or associated with organic matter [36]. These observations were consistent with Wills textbook "Mineral Processing Technology" (2006), which claimed siderite is more hydrophobic than some other non-clay minerals such as rutile, ilmenite, hematite and magnetite, which might be due to siderite being associated with hydrophobic spices [53].

The single largest carbonate bitumen reservoir in the world is located in the Upper Devonian Grosmont in Alberta. It was estimated that more than 400 billion barrels of ultra-heavy bitumen exist in north central Alberta in the carbonate triangle areas: Peace River, Athabasca and Cold Lake, which are shown in Figure 1-6. Chopra (2000) reported that the chemical characteristics of oil from a carbonate reservoir is similar to the oil from oil sands from the above area, which might be due to same oil source [54].

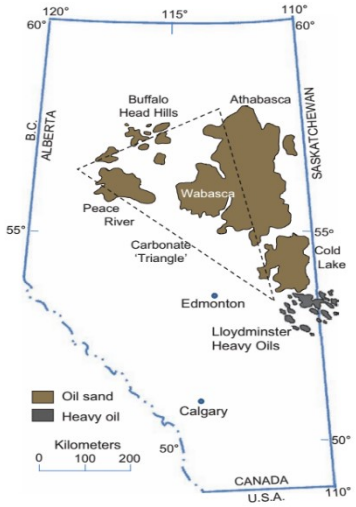

Figure 1-6 Alberta oil sand, carbonate triangle, and heavy oil areas. Modified from Proctor et al., 1984 [55].

Rassenfoss (2013) also reported that the bitumen product from this kind of formation is a bit heavier than that of common oil sands, because it is formed from light crude oil via extensive biodegradation. However, he did not report any issue about bitumen production and price [56]. Hein *et al* (2008), Wo *et al* (2011) and Machel *et al* (2012) estimated that the Upper Devonian

Grosmont platform in north central Alberta contains at least 400 billion barrels of initial oil-in-place (IOIP), which is retained in the carbonate formations at depths of 250 -400 m [56–59]. A schematic of thickness, shape and angle of a stratigraphic section of the Devonian Grosmont carbonates platform in Alberta is shown in Figure 1-7 [48,56,59].

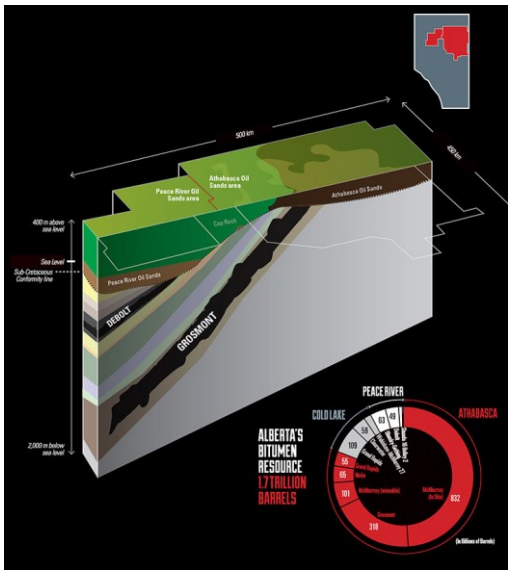

Figure 1-7 Schematic of thickness, shape and angle of stratigraphic section of the Devonian Grosmont carbonates platform in Alberta [60].

1.3.1.4 IRON-BEARING MINERALS

The McMurray Formation contains iron-bearing minerals. Siderite ($FeCO_3$) and pyrite (FeS_2), two main sources of iron-bearing minerals, were detected in Alberta oil sands [4,61]. The amounts of pyrite and siderite compared with quartz and feldspars are small in Alberta oil sands. In addition, ilmenite ($FeTiO_3$), schorl ($NaFe_2+3Al_6(BO_3)3Si_6O_{18}(OH)_4$), hematite ($Fe_2O_3$) and lepidocrocite (γ-FeO(OH)) were reported either in Alberta oil sands or in primary froth [4,61]. Kaminsky (2008) reported that the majority of these minerals except schorl were detected in the <45 μm fraction [4]. According to a report prepared by the Geology Division of the Alberta Research Council, large siderite nodules, siderite spherulites and siderite-cemented siltstones can be found in the lower, middle and upper part of the McMurray Formation, which is shown in Figure 1-8 [61]. Siderite spherulites occur in coarse-grained oil sands while siderite-cemented siltstones happen in the form of small crystals and contain a large amount of organic material [61]. It was also reported that

pyrite minerals outcrop in the form of nodules in the lower part of the McMurray Formation as shown in Figure 1-8. In addition, many iron-bearing minerals, especially nanoparticles, are expected to appear more in the primary forth and fine fractions than tailings due to association with organic matter and/or clay minerals [38,61]. Previous researchers have reported that a surface property, i.e., hydrophobicity, plays a key role in the distribution of iron-bearing minerals between the primary froth or tailings [4,53].

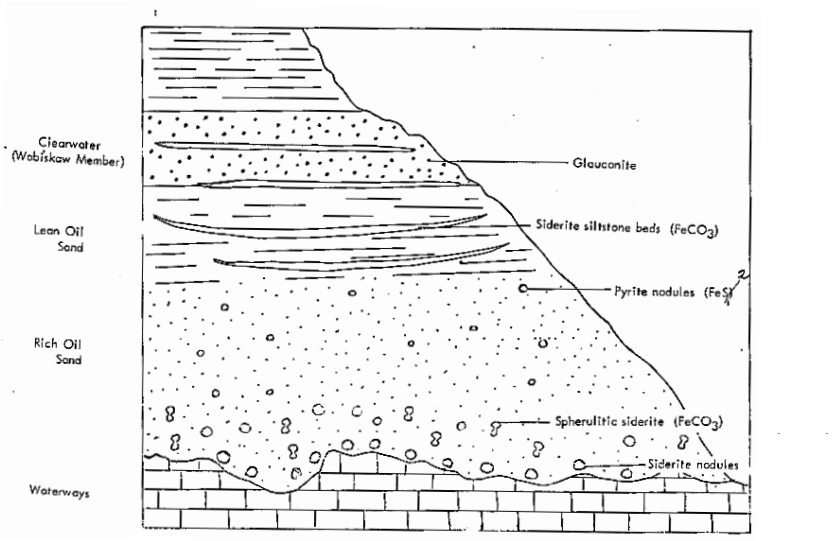

Figure 1-8 Schematic of iron-bearing minerals occurrence in the McMurray Formation [61].

The siderite mineral was identified by Sparks *et al*. in oil sands ore [36]. It can be speculated that the hydrophobicity decreases from pyrite to siderite to hematite to ilmenite minerals according to Wills textbook "Mineral Processing Technology" [53]. Therefore, less ilmenite is expected in the froth relative to other iron-bearing minerals; however, it was reported that ilmenite was highly concentrated in the froth. Siderite, on the other hand, was assumed to concentrate in the froth, while more than half of the siderite was detected in the tailings [4].

1.3.1.5 TI-OXIDE MINERALS

Rutile, anatase, brookite, pseudorutile ($Fe_2Ti_3O_9$), pseudobrookite (Fe_2TiO_5), ilmenite ($FeTiO_3$), leucoxene (the altered forms of ilmenite) and titanite ($CaTiSiO_5$) are sources of the titanium-bearing minerals, which have been identified in Alberta oil sands by researchers [39,43,62–64].

Omotoso *et al*. reported that the amounts of Ti-bearing minerals vary between 0.05 to 0.50 wt% in the McMurray Formation [63]**.** Rutile and leucoxene, the two main sources of titanium-bearing minerals, were detected in Alberta oil sands [63]**.** Like the iron-bearing minerals, the Ti-oxide minerals are concentrated in the <45 μm fraction (76%) [4]. It was also reported that titanium-bearing minerals were mostly concentrated in the primary froth; brookite had the finest particles among all the detected Ti-bearing minerals [4]. Most of the studies revealed that heavy minerals like Ti-bearing minerals are mostly concentrated in the primary froth due to their hydrophobic surfaces [63]. Although the presence of Ti-bearing minerals was less than 0.5 wt% in the oil sands feed, their concentrations increase to the range 4 to 15 wt% in the froth solids after bitumen extraction [63,65].

1.3.1.6 ZIRCONIUM SILICATE MINERALS

Zirconium silicate (zircon) is a mixed oxide of zirconium with silicon ($ZrSiO_4$). Zircon is the first heavy mineral, which was identified in the oil sands by Clark [43]. Iron, rare elements, i.e., hafnium (Hf), uranium (U), thorium (Th) and rare earths were the main impurities characterized in zircon minerals in the Athabasca oil sands by Bichard [43]. Zircon grains are usually very small (the smallest of the heavy minerals), have a high specific gravity (4.6 g/cm^3) and display partially or completely rounded particles. It is interesting to note that zircon particles sizes were mostly uniform between 44-149 μm (100-325 U.S. mesh size) fractions for many samples from Alberta oil sands [43]. Zircon particles were mostly concentrated in the primary froth; more than 90% of this mineral was detected in the primary froth by Kaminsky [4]. The perfect crystal of zircon has a tetragonal crystal structure and displays a glassy luster and is colorless using emission spectrographic analyses. However, some of the zircon particles in the oil sands appear colorful from amber to red due to adsorption of different impurities on the surface. Bichard stated that this is the most important reason for the flotation of zircon in the primary froth over others [43].

1.3.1.7 CALCIUM SULFATE MINERALS

Anhydrite and gypsum are two forms of calcium sulfate which occur in nature. Anhydrite is an anhydrous calcium sulfate with the chemical composition of $CaSO_4$. It is willingly replaced by gypsum in the presence of water. Gypsum is a calcium sulfate dihydrate with the chemical

composition of $CaSO_4 \cdot 2H_2O$ [66,67]. This mineral is not usually pure, due to the presence of other species (i.e., organic matter, iron or Fe-bearing minerals, clays, silica, calcium carbonate and magnesium carbonate) during mineral formation or deposition [67]. The color of gypsum is usually gray, ocher-yellow, honey-yellow, flesh-red or blue; however, its color may be brown, red or reddish brown and black due to impurities. The pure crystalline form is usually pearly white and glistening [67]. Anhydrite and/or gypsum may be formed from decomposition of siderite/calcite in the presence of high-sulfate waters. Gypsum is not stable over 50°C and anhydrite will be formed [51]. The common and twinned forms of gypsum crystals, and the anhydrite crystal are shown in Figure 1-9 [68].

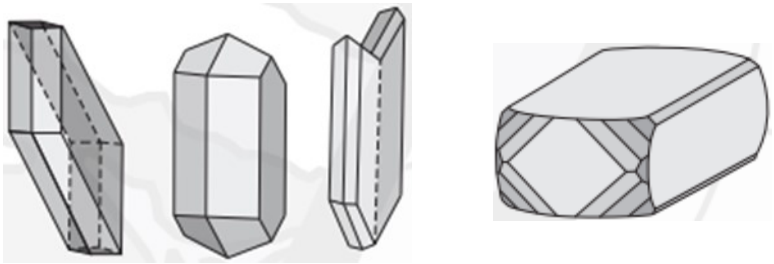

Figure 1-9 Gypsum crystals, a) and b) common forms, c) twinned form, d) anhydrite crystal [68].

In tailings technology, gypsum is used as a coagulant for control, rectification and optimization of the consolidated tailings (CT) process [69,70]. Chalaturnyk *et al*. introduced a new method for the CT process by using lime ($Ca(OH)_2$) and CO_2 instead of gypsum, which improved it [71].

Calcium sulfates were identified only in the <2 μm fraction of MS. Both sulfates (i.e., gypsum and bassanite) are most likely mineral products of pyrite oxidation [72–74]. Borrero identified anhydrite and gypsum in the heavy oil deposit hosted in the Upper Devonian Grosmont carbonates platform in Alberta [75].

1.3.2 CLAY MINERALS

Clay minerals are classified as layered silicates or phyllosilicates, which vary in chemical composition and physical properties. Most clay minerals have perfect (001) cleavage due to their layered crystal structures, and their particle size is smaller than 2 μm (equivalent spherical

diameter). Most layered silicates are made up of at least two sheets: tetrahedral and octahedral. The geometrical shapes of oxygen atoms around a central cation are composed of tetrahedra and octahedra. A tetrahedral sheet is made of a cation (T) with four oxygen atoms fitting around it; it forms an infinite two-dimensional hexagonal pattern by sharing oxygen atoms at all three corners with three adjacent tetrahedra (Figure 1-10). In each tetrahedron, the O-O and Si-O bond distances are 2.64 Å and 1.62 Å. The main cation in the tetrahedral sheet is Si^{4+}, but it can be substituted with other cations such as $Al^{3+}$and Fe^{3+} [76,77].

The octahedral sheet is made of octahedral units, and consists of two planes of close-packed oxygen and hydroxyl ions which are surrounding cations (M) that are occupying octahedral spaces between the two planes. The octahedra are connected by sharing edges of neighboring octahedra forming an infinite two-dimensional hexagonal or pseudo-hexagonal pattern (Figure 1-11). These octahedral spaces are usually occupied by Al^{3+}, Mg^{2+}, $Fe^{2+}$and Fe^{3+}, but other cations such as Li^{+}, Mn^{2+}, Co^{2+}, Ni^{2+}, Cu^{2+}, Zn^{2+}, V^{3+}, Cr^{3+} and Ti^{4+} have also been reported [78,79].

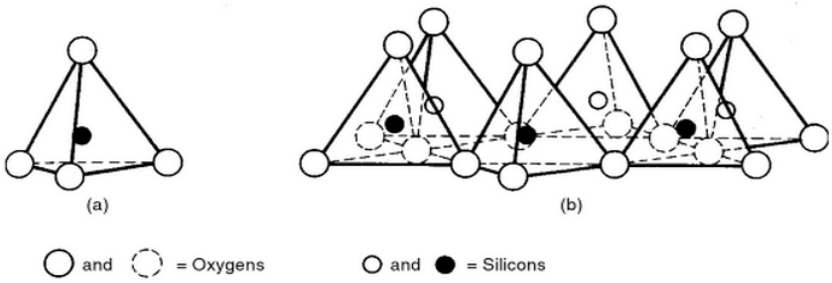

Figure 1-10 Schematics of silicon tetrahedron; a) single silica tetrahedron, b) Isomeric view of the tetrahedral sheet [77].

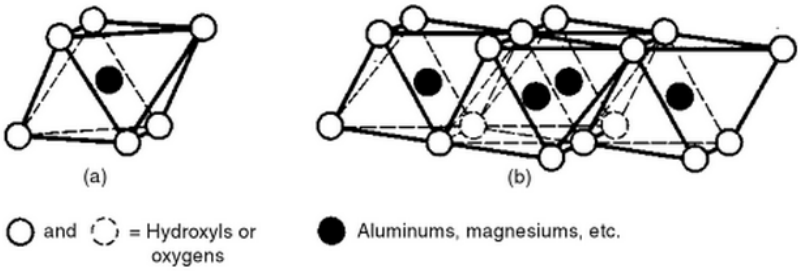

Figure 1-11 Schematics of aluminum/magnesium octahedron, a) single aluminum/magnesium octahedron, b) isomeric view of the octahedral sheet [80]

An octahedral sheet can be classified as either trioctahedral or dioctahedral due to the cation to anion ratio. When the cation:anion ratio is 1:2, the cation is divalent (e.g. Mg^{2+}) all three positions are filled, and the sheet is called a trioctahedral sheet like brucite (e.g. $Mg(OH)_2$, Figure 1-12 a). On the other hand, when the cation:anion ratio is 1:3, the cation is trivalent (e.g., Al^{3+}), therefore, only two of three positions are occupied by trivalent cations leading to a dioctahedral sheet like gibbsite (e.g. $Al(OH)_3$, Figure 1-12 b) [77, 78].

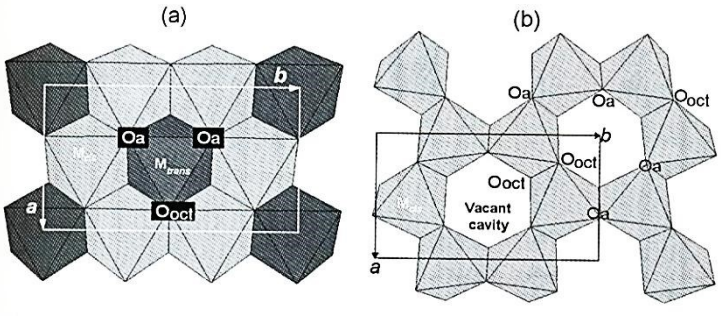

Figure 1-12 a) Trioctahedral sheet, b) dioctahedral sheet. O_a is the apical oxygen atoms shared with tetrahedral sheet, and O_{oct} is the anionic site shared between octahedral neighbors. The unit-cell parameters are a and b [79].

Clay minerals are also categorized based on their unit structure. The unit structure of clay minerals is made up of octahedral and tetrahedral sheets joined together in layers and may have a gap between layers. Two main unit structures of individual clay minerals are the 1:1 (TM) layer and the 2:1 (TMT) layering types. The TM clay minerals are usually a tetrahedral sheet and an octahedral sheet, which mostly has either a very small layer charge or no layer charge. The TMT layering type is an octahedral sheet sandwiched between two tetrahedral sheets, which may either have a neutral layer (e.g., talc- and pyrophyllic-like layer) or the layer is mostly negatively charged (e.g., mica-, smectite-, vermiculite- and chlorite-like layer) [76].

1.3.2.1 1:1 LAYER CLAY MINERALS

The layer of 1:1 clay minerals (TM) usually consists of a tetrahedral sheet and an octahedral sheet. Since the octahedral and tetrahedral sheets almost have the same dimensions (in their a and b axes) in the 1:1 layer structure, these two sheets are joined together. The thickness of each layer in the 1:1 layer clay minerals or TM phyllosilicates is about 0.7 nm (see Figure 1-13). The 1:1 layer mostly has a very small layer charge or no layer charge because the cation sites in tetrahedral

sheets are mostly all filled by Si^{4+} and the cation sites in octahedral sheets are all occupied by either Al^{3+} or Mg^{2+} such as dioctahedral kaolinite ($Al_4Si_4O_{10}(OH)_8$) and trioctahedral serpentine ($Mg_6Si_4O_{10}(OH)_8$). The total charges generated in the tetrahedral and octahedral layers are identified by the amount and type of substitution. Extra charges on one sheet neutralize substitutions in the other sheet. The surface of the tetrahedral sheet consists entirely of oxygen atoms (O_b), while the surface of the octahedral sheet is composed of O_{oct} (mostly OH groups) (see Figure 1-13) [78,79].

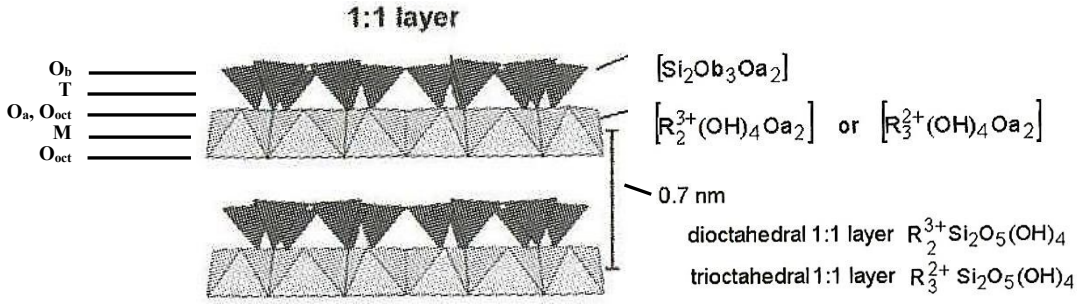

Figure 1-13 Model of 1:1layer structure (i.e. kaolinite and serpentine). O_a, O_b, and O_{oct} indicate tetrahedral apical, tetrahedral basal and octahedral anionic sites, respectively. M and T refer to octahedral and tetrahedral cation, respectively [77].

In the 1:1 layer structure, hydrogen bonds keep the unit layers firmly together, but the plane between the unit layers is a cleavage plane. Due to strong hydrogen bonding, kaolinite shows less cleavage than other clay minerals display. Grim reported that these strong hydrogen bonds do not allow small particles of kaolinite to disperse in water [79].

1.3.2.2 2:1 LAYER CLAY MINERALS

The layer of 2:1 clay minerals (TMT) usually consists of two tetrahedral sheets and one octahedral sheet (see Figure 1-14). The tetrahedral sheets of such a TMT layer are inverted and two-thirds of the hydroxyl groups from the octahedral sheet are substituted by apical oxygen atoms from thetetrahedral sheets. Both surfaces of this layer contain tetrahedral basal oxygen atoms O_b. The c-axis is between 0.91 nm to 0.95 nm for the first type of 2:1 layer (e.g., talc and pyrophyllite). Pyrophyllite and talc have a dioctahedral and trioctahedral layer, respectively, and both are electrically neutral [77,78].

In other types of 2:1 phyllosilicates, the layer is mostly negatively charged like in micas (true and brittle micas), smectite, vermiculite and chlorite groups. The interlayer spaces of talc and pyrophyllite are empty, while this space for the second type of 2:1 layer (i.e., mica-like layer) is filled by anhydrous alkali and alkaline-earth cations, and the c-axis is around 1 nm (Figure 1-15 a). The magnitude of the layer charge is approximately -1 for true mica and close to -2 for brittle mica. The third category of 2:1 clay minerals (i.e., smectite- and vermiculite-like layers) contains hydrated alkali or alkaline-earth cations (see Figure 1-15 b). The c-axis varies and can be about 1.2 nm to 1.5 nm, which depends on the occupation of interlayer position by cations and water molecules.

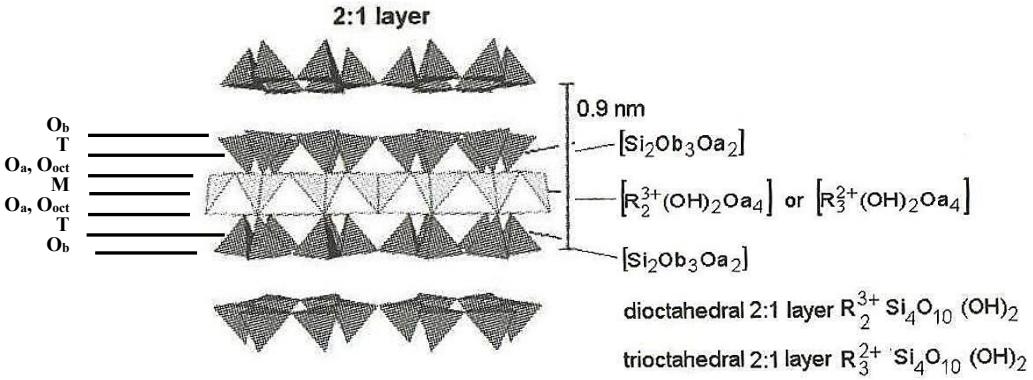

Figure 1-14 Model of 2:1 layer structure i.e. pyrophyllite (dioctahedral) and talc (trioctahedral). O_a, O_b, and O_{oct} indicate tetrahedral apical, tetrahedral basal and octahedral anionic sites, respectively. M and T refer to octahedral and tetrahedral cation, respectively [77].

The d-space can be even more than 1.5 nm when the water molecules are replaced by different polar molecules. The fourth category of 2:1 clay minerals is the chlorite group, where the interlayer is replaced by a continuous octahedral sheet (see Figure 1-15 c). Therefore, it can be shown as $TMTM_{int}$, where M_{int} is the octahedral interlayer sheet. Chlorite was named as a 2:1:1 or a 2:2 layer silicate before 1978, when the AIPEA Nomenclature Committee chaired by Bailey clearly explained that chlorite is a 2:1 layer clay with octahedrally coordinated interlayer cations. In the chlorite structure, the presence of a positively charged octahedral sheets in the interlayer space neutralizes the negative layer charge. The most abundant chlorite structure on earth is trioctahedral in both octahedral sheets. The dioctahedral chlorite and intermediate forms are rare [78,79].

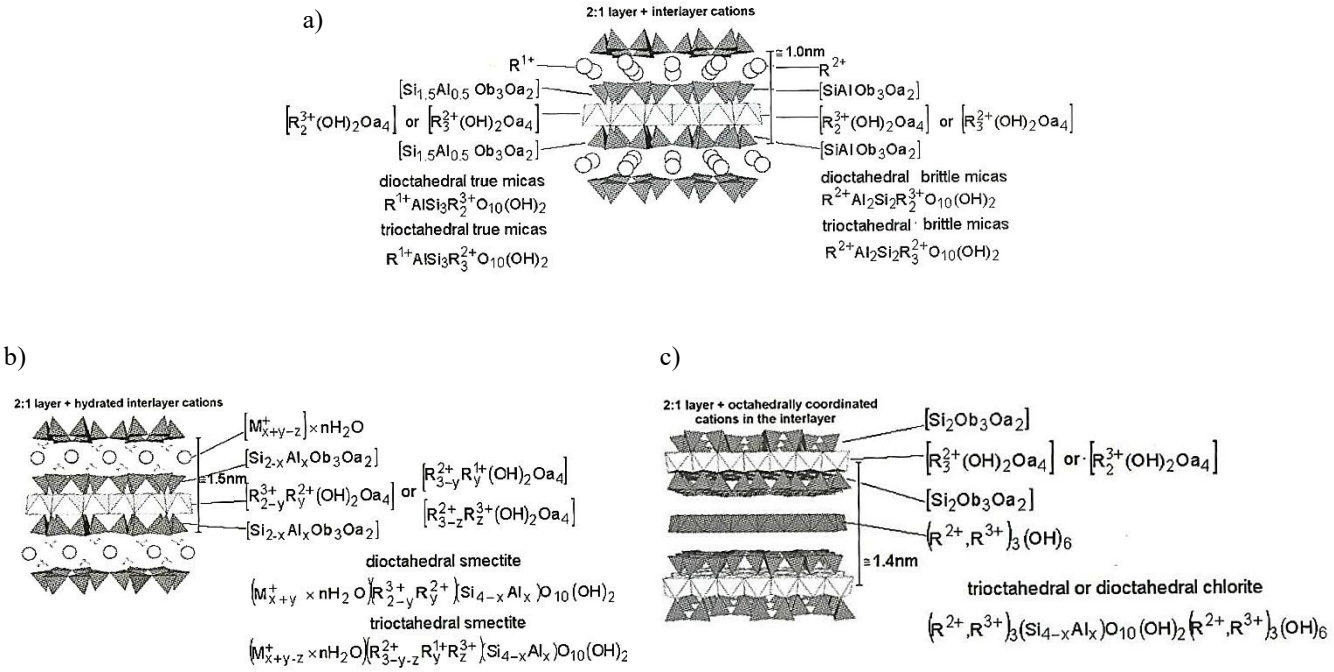

Figure 1-15 Different layer structure for 2:1 clay minerals: (a) 2:1 layer structure with anhydrous interlayer cations i.e. the mica-like layer; (b) 2:1 layer structure with hydrated interlayer cations i.e. smectite- and vermiculite-like layer; (c) 2:1 layer structure with a continuous octahedral sheet interlayer i.e. chlorite-like layer [77].

1.3.2.3 MIXED-LAYERED CLAY MINERALS

A mixed-layered clay mineral or interstratified phyllosilicates can be built up by two or more different components, which cause the stacking order of silicate layers along the c* direction. The stacking order may have either regular or irregular mixed-layer structures. The ordered or regular mixed-layer structures are produced when different layers are alternately placed along the c* direction in a periodic pattern. For example, two generic types of A and B layers can be stacked and produced …ABABAB… or …AABAABAA… or …AAAABAAAABAAAAB… and so on. These types of mixed-layer clay minerals have a characteristic unlike those of the original layers. Rectorite is an example of regular stacking order and can be considered to be made of dioctahedral mica and dioctahedral smectite layers. The disordered or irregularly mixed-layer structures are produced when the type A and B layers are randomly stacked along the c* direction (e.g., …ABBABAA… or ……AAABABBAAAAABABA…) (see Figure 1-16). The disordered or

irregular mixed-layer does not have a unique name. These types of mixed-layer clay minerals have their component names such as kaolinite-smectite, illite-smectite and chlorite-vermiculite. The typical thickness for a single layer of mixed-layered clay mineral is three or four silicate layers [76,77,79].

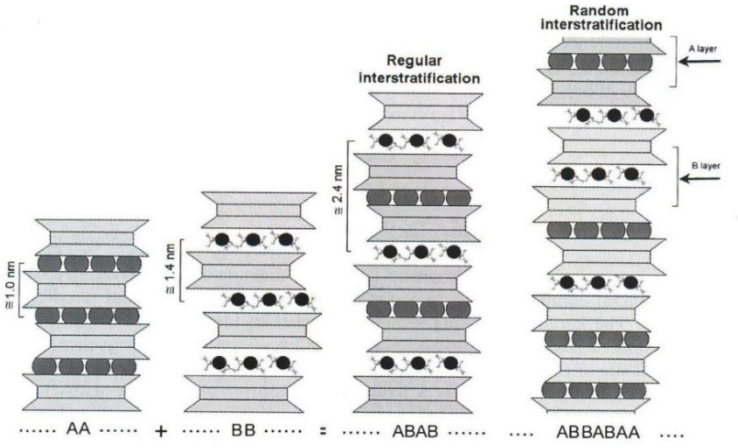

Figure 1-16 Regularly and randomly mixed-layer phyllosilicates or interstratified phyllosilicates. A and B are two different types 2:1 layers, which are located with different periodicity along the c direction [79].

1.4 ROLE OF CLAY MINERALS IN OIL SANDS BITUMEN EXTRACTION

Clay minerals present in the oil sands have a very high surface area and layer charge density. Therefore, clay species are the most reactive minerals in oil sands ore, which may react with bitumen molecules and produce clay-organic complexes during the extraction process. This reaction significantly changes the chemical and physical properties of the clay minerals and bitumen as well as the efficiency of the extraction process [80,81]. Clementz stated that the interaction of organic matter with the clay mineral surfaces may affect the layer charge density (LCD), cation exchange capacity (CEC) and expandability of clay minerals, particularly swelling clays (i.e., smectites or/and mixed-layer clay minerals such as illite-smectite and kaolinite-smectite) [80]. It has also been reported that the asphaltene molecules might be attracted to the surfaces of clay minerals due to the positive charge of nitrogen groups in the asphaltene structures and the negative charge of clay surfaces. Liu *et al*. have reported that the bitumen recovery from ore was decreased by increasing clay content in the ore [8]. Kasongo *et al*. observed that the bitumen recovery was significantly reduced by adding smectite (e.g., montmorillonite) and calcium ions during a water-based bitumen extraction process [82]. Kaminsky reported that the clay minerals directly influenced the settling behavior of tailings [4]. It has also been shown that a small quantity of swelling clays (i.e., smectite or/and other mixed-layer clay minerals) also has a

severe impact on the settling and consolidation of tailings [21]. This impact was not severe on bitumen recovery by adding kaolinite and illite [82]. Tu *et al*. have shown that bitumen recovery may be negatively influenced by the presence of ultrafine clay minerals (<0.3μm fraction) due to the gelation and sludging behavior of ores during an aqueous extraction process [83]. All these studies indicated that the clay minerals in the oil sands have mainly negative roles in bitumen recovery as well as tailings management, because they have a very small particle size, high total surface area (TSA) and high surface charge, which make water-based extraction more problematic [4].

Several studies have shown that the main clay minerals in the Alberta oil sands are kaolinite and illite. Smectite, chlorite, vermiculite and mixed-layer clay minerals are also present [4,10,21]. Omotoso *et al.* (2004) revealed that the TSA and CEC of oil sands extraction tailings are significantly higher than those values for kaolinite and illite due to existence of mixed-layer clay minerals, i.e., kaolinite-smectite and illite-smectite [20]. Although the role of clay minerals in the aqueous extraction process has been recognized, there is inadequate research on the role of various clay minerals (i.e., nano and microsize clay minerals - NMCMs) on a non-aqueous bitumen extraction process and bitumen recovery. A better understanding of clay minerals particularly swelling clays is ultimately leading to improved bitumen extraction processes with no or very small water consumption or perhaps an alternative non-aqueous bitumen extraction process.

1.5 ORGANIC MATTER

Nowadays, more than 90% of all transportation fuels and lubricants are provided by petroleum. Only ~ 4% of fossil fuels (i.e., petroleum and natural gas) are used as raw materials for different products, i.e., chemicals, pharmaceuticals, plastics, elastomers, paints and so on [44]. Scientists believed that sedimentary organic matter (i.e., petroleum, coal, natural gas, and kerogen) is derived from the debris of living organisms by photosynthesis. During the long geological history, most living organisms are decomposed and recycled to small molecules; however, the rest are preserved in organic matter forms during burial. Figure 1-17 shows the schematic evolution of sedimentary organic matter and hydrocarbons sources in geological situations [44]. Geochemical fossils and kerogen degradation represent a first and second source of hydrocarbons in the subsurface.

Three terms (i.e., diagenesis, catagenesis and metagenesis) describe the stages in the progressive transformation of organic matter to hydrocarbons, which are combinations of temperature, pressure and time. Diagenesis is a shallow burial and near-surface with temperatures up to 60°C and consists of methane, carbon dioxide, water and kerogen. Liquid hydrocarbons are produced from the kerogen in the catagenesis stage at temperatures between 60 – 175 °C. In the metagenesis stage at temperatures between 175 to 200 °C (or higher), methane and light hydrocarbons are formed from kerogen and bitumen. In the following subsections, two main organic matters present in Alberta oil sands, i.e., bitumen and kerogen, will be briefly discussed.

1.5.1 BITUMEN

Conventional crude oil flows freely at room temperature; however, bitumen looks like cold molasses, a highly viscous liquid, classified as a pitch, and does not freely flow. It flows when either heated or diluted. Bitumen is made up of hydrocarbons/organic compounds (mostly carbon and hydrogen). It contains more carbon than hydrogen compared with conventional crude oil. Bitumen consists of many impurities, i.e., nitrogen, sulfur and heavy metals. Therefore, these impurities must be removed for synthetic crude production. The early consumption of bitumen was as a binder mixed with sand and gravel for use in road construction.

According to accepted theory, bitumen migrated from western source rocks and became trapped in the McMurray Formation area. During the long dynamic geological history, different environments, i.e., terrestrial, estuarine and marine were successively formed in the upper, middle and lower intervals, respectively, in the McMurray Formation. A significant amount of kerogen (insoluble organic) as well as soluble organics (i.e., bitumen, coal, etc.) are present in Alberta oil sands ores.

The chemistry of bitumen is a very challenging and complex area for scientists. However, studies show that it consists of wide range of organic molecules from the simplest organic molecule (i.e., methane) to huge polymeric molecules with a MW exceeding 15,000. Paraffinic, olefinic, aromatic and heterocyclic structures with several functional groups have been characterized in Alberta oil sands bitumen [44].

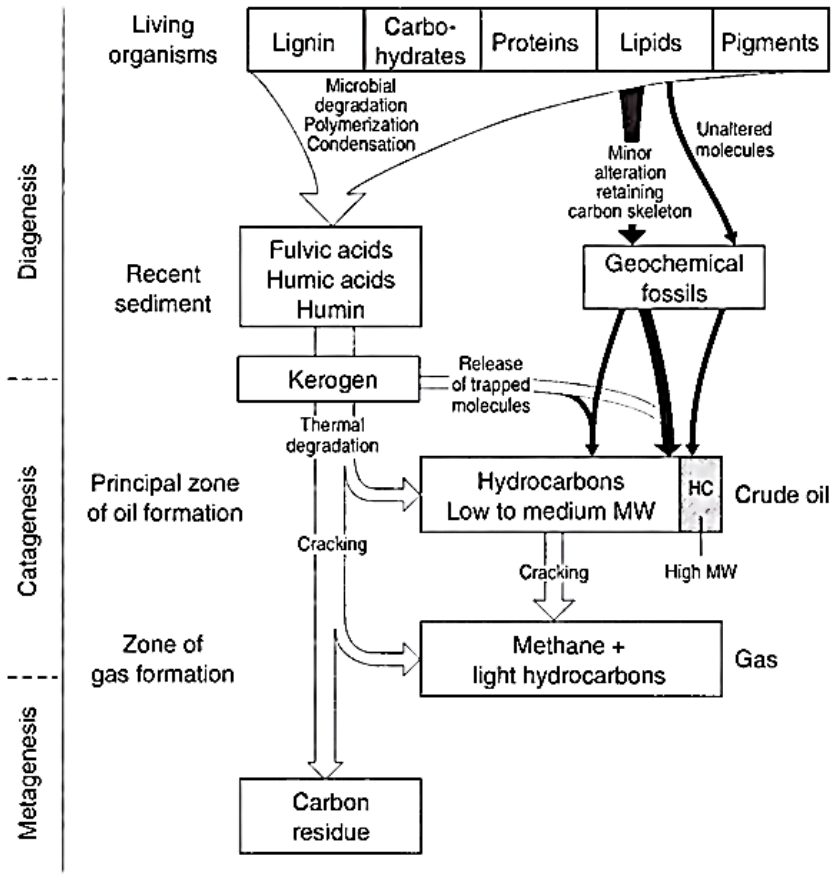

Figure 1-17 Schematic evolution of sedimentary organic matter and hydrocarbon sources in geological situations [44].

Commonly, bitumen consists of three main components, i.e., maltenes (aromatics and saturates), resins and asphaltenes. Paraffinic solvents can completely dissolve maltene; however, resins and asphaltenes are only soluble in aromatic and relatively polar solvents (i.e., benzene or toluene) [84]. Table 1-1 shows the chemical composition of bitumen extracted from Peace River, Wabasca, Athabasca and Cold Lake oil sands ores.

Table 1-1 The elemental composition of bitumen extracted from Athabasca (A), Peace River (P), Cold Lake (C), and Wabasca (W) oil sands ores [44].

Fraction	Source*	C	H	N	O	S	H/C	mw
		%						
Whole Bitumen	A	83.98	10.22	0.65	1.97	4.57	1.46	620
	P	81.68	9.98	0.14	2.08	5.60	1.46	520
	C	83.93	10.46	0.23	0.94	4.70	1.49	490
	W	82.44	10.32	0.42	0.82	5.51	1.49	600
Asphaltenes	A	81.31	7.88	1.06	2.79	7.53	1.16	5,920
	P	79.87	8.15	0.78	2.08	8.82	1.21	3,500
	C	80.54	7.39	1.15	1.78	6.51	1.10	8,140
	W	80.46	8.20	0.99	1.16	8.40	1.21	5,760
Deasphaltened Oil	A	84.38	10.63	0.07	0.87	3.91	1.51	435
	P	82.89	10.61	0.08	1.27	5.41	1.53	440
	C	84.19	11.01	0.27	0.61	3.89	1.54	430
	W	82.99	10.74	0.28	1.04	5.25	1.54	530

1.5.2 KEROGEN

Kerogen is a metastable sediment and forms at mild temperatures and pressures in young sediments (Figure 1-17). It is also known that kerogen is insoluble in organic solvents and consists of large molecules. The molecular weights of kerogen might be several thousand and even more, which is unique for each kerogen molecule, due to the random combination made from many small molecular pieces. Kerogen likely remains stable due to the lack of further sedimentation and the burial process of organic matter. However, it may also generate oil, gas and bitumen after sufficient time, temperature and pressure environments, and the successive burial stages (i.e., diagenesis, catagenesis and metagenesis) in sedimentary rock [85].

Kerogen is usually combined with small quantities of bitumen. Kerogen maturation or degradation will occur during the burial stages. These maturations vary due to different origins of kerogen. Scientists categorized four different types of kerogen based on chemical composition and the ratio of hydrogen, carbon and oxygen contents in the sample [86]. Figure 1-18 shows three types of kerogen on the modified van Krevelen diagram, which is calculated from a hydrogen index (HI; mg HC/g TOC) and oxygen index (OI; mg CO2/g TOC) using Rock-Eval pyrolysis [87].

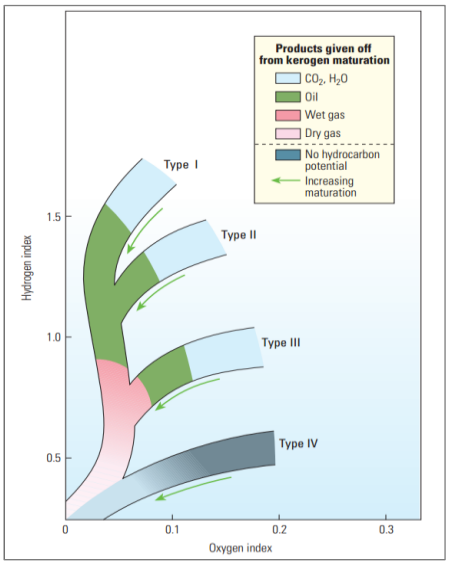

Figure 1-18 Modified van Kreveln diagram [87]

1.6 CLAY PROPERTIES

1.6.1 CHARGE DISTRIBUTION

Clay minerals have a very specific and unique surface chemistry due to their interlayer and edge surfaces. The most important parameters that define the surface chemistry of clay minerals are type of exchangeable cation, layer charge and their distributions, as well as size of the particles [88]. Since clay minerals carry charges, they are very reactive minerals. Structural (permanent) and surface (pH dependent) charges are two types of charges in clay minerals. Ion substitutions and imperfections are classified as the structural charge. The most permanent negative charges in smectitic clay minerals can be provided by ionic substitutions of Al^{+3} for Si^{+4} and/or Mg^{+2} or Fe^{+2} for Al^{+3} in the tetrahedral and octahedral sheets, respectively.

Cation exchange capacity (CEC) is one of the most important clay mineral properties. CEC of clay minerals is identified by the number of available cations for exchange, which is commonly indicated in milliequivalents (meq)/100 g of calcined clay [77]. In other words, CEC can be measured by the concentration of unfixed cations in the interlayers and surface layers. Isomorphous substitutions in the silicate layers (both tetrahedral and octahedral sheets) are the main reason for surface charges in clay minerals. The rotation of layers relative to each other and disordering of stacking layers have also been reported as other reasons for CEC in clay minerals.

Clay minerals usually adsorb ions on their surfaces to retain electrical neutrality. The distribution of ions in the interlayer surfaces is related to the layer charge distribution. The interaction of clay minerals with the adjacent area can be controlled by the layer charge. The majority of CEC in smectite is provided by isomorphous substitutions [76,79].

Some other clay minerals contain exchangeable cations at their edges due to broken bonds, which make an unbalanced charge. In addition, hydrogen can also be replaced by other cations when it is exposed to hydroxyls [89]. The CEC in kaolinite is mostly provided by broken bonds [77]. Cation adsorption via broken bonds along edges plays a major role in illite and chlorite. However, clays with an exchangeable cation interlayer (swelling clays) have much higher CEC than clays without an accessible interlayer (non-swelling clays). Therefore, total CEC of a clay mineral is the sum of exchangeable cations in both the interlayer and the edges of the crystal.

The clay properties may be influenced significantly by exchanging cations in the interlayer with other cations. Many researchers in the clay industry have reported that clays display an inclination for larger cations compared with smaller ones [77,90,91]. This tendency for exchangeable cations in swelling clay minerals (smectite) follows the order:

$$Li^+ < Na^+ < K^+ < Rb^+ < Cs^+ < Mg^{2+} < Ca^{2+} < Sr^{2+} < Ba^{2+}$$

The CEC for some common clay minerals appears in Table 1-2, which indicates the wide range of values. Kaolinite, mica and illite have significantly lower CEC than montmorillonite and vermiculite.

Table 1-2 Cation exchange capacity of some common clay minerals (meq/100 g) [77].

Clay minerals	Kaolinite	Illite	Micas (biotite, muscovite)	Chlorite	Montmorillonite	Vermiculite	Sepiolite, palygorskite
CEC (meq/100gr)	3-15	10-40	up to 5	10-40	70-120	130-210	20-30

The cation exchange is affected by many determinants, such as temperature, particle size distribution, the exchangeable cations nature, concentration of solutions, and the existence of organic matter. Therefore, the exchange capacity is defined at pH=7 (neutral condition).

1.6.2 DEGREE OF INTERSTRATIFICATION

The properties of clay minerals are directly and/or indirectly determined by their structure. The properties obtained from the interaction of clay minerals with other media (mainly water) will be explained in this section. The water chemistry (i.e., impurity ions, size of ions and charge distribution) affects the water interaction. The characteristic properties of clay minerals (i.e., plasticity, ion exchange capacity, suspension capacity, bonding, compaction and many more) are related to the quality and quantity of water adsorbed on the surfaces (interlayer surface and external surface areas) and the edges of clays. Some clay minerals may swell in the presence of water due to received water and held as three different types (i.e., a single, double and triple discrete pseudo-layer of water) in the interlayer space [76]. Smectitic clay minerals can adsorb three or less discrete pseudo-layers of water in the interlayer space [77]. This will only cause expansion of smectite along the [001] direction. Three important factors controlling the expandability of swelling clays are the nature of the water molecule (polarity), cations in the interlayer space (type and size), and the influence of charges on the neighboring silicate layers.

Smectite and kaolinite minerals are classified as the extremes of gel-forming and hydration capacity potentials; however, illites and chlorites represent the intermediate clay minerals [77]. Moore and Hower reported that the expandability of swelling clay minerals (Na-saturated smectite SWy-1) is related to water uptake in the interlayer space [92]. The number of adsorbed water molecules is an integer, i.e., 0, 1, 2 or 3 and corresponds to a discrete d (001) of 9.6, ~12.4, ~15.2 and ~18.0 Å, respectively. Figure 1-19 shows the experimental results of correlation of values of d (001) vs. relative humidity (RH) for Na-saturated smectite (SWy-1). The intermediate values of apparent d(001) is a combination of two discrete values of hydrates. For instance, the apparent d (001) for a very low RH is between 9.6 and 12.4 Å due to the presence of one sheet of water with dehydrated clay minerals.

The most common mixed-layer clay mineral in nature is illite-smectite (I/S). Kaolinite-smectite is not a regular mixed-layer clay mineral [93]. The X-ray diffraction (XRD)-oriented specimen method is the major technique for identification of mixed-layer clay minerals. The identification is based on the position of 001 reflections of an oriented specimen in four different conditions: air-dry at 54%RH, after solvation with ethylene glycol, and heated at 300 and/or 550°C. The amount of smectite (%S) in mixed-layer clay minerals can be determined by applying and comparing the

XRD patterns of two or more of these tests [77]. For identification of expandability of illite-smectite, the most common technique is comparing the position of the 001 reflections for air-dry at 54%RH and after saturation with ethylene glycol using the procedures described by Moore and Reynolds, Środoń and Dudek *et al.* [76,94,95]. The principles behind each technique will be explained and the pros and cons for each technique will be highlighted in the section 2.4.2.

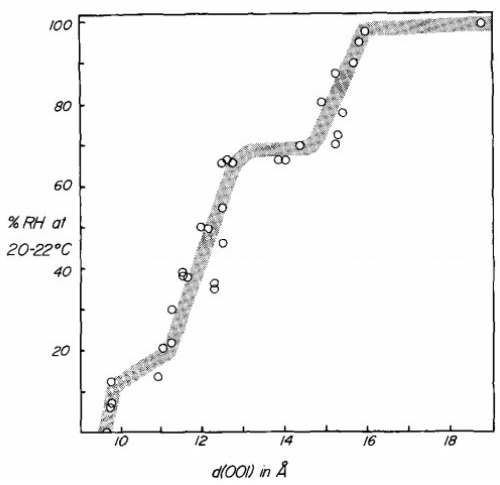

Figure 1-19 The experimental values of d(001) vs. relative humidity (RH) from 0% to 100%RH for Na-saturated smectite from Crook County Wyoming (SWy-1) [92].

1.6.3 MEAN THICKNESS AND THICKNESS DISTRIBUTION:

The physical and chemical properties of a substance, i.e., rheology, surface area, cation exchange capacity and ion solubility may significantly be affected by particle size and vice versa. Therefore, it is important to find an accurate and convenient method for measuring particle size distributions. Clay minerals are too fine to be observed by light microscopy. The laser scattering technique is able to measure only average particle sizes and cannot be performed for determination of particles in a specific crystallographic direction (for instance in the c-direction). TEM and atomic force microscopy (AFM) are accurate and direct observation techniques to determine the thickness of the particles; however, these methods are very tedious, expensive and time consuming. Moreover, the observations may not be representative of mean thickness of the particles due to lack of adequate data on distribution of sizes. Dudek *et al.* compared two independent techniques: XRD and high-resolution transmission electron microscopy (HRTEM), and found that the XRD-

determined distributions are quick, statistically reliable and very accurate compared with HRTEM measurements. He has also indicated that the HRTEM measurements underestimated the proportion of coarse particles, which caused inaccurate counting statistics for determination of the thickness of the crystals [96].

The particle size distribution can also be measured by the XRD technique. The XRD peaks are the average diffraction pattern, which is influenced by billions of individual crystals, particles and aggregates in the sample. Moreover, this technique can be used to identify the thickness of a specific mineral in a composition of several minerals, as well as the mean thickness of the particles in a particular crystallographic direction of the same mineral [96,97].

Drits *et al.* measured the mean crystallite thickness (T_{MEAN}) and the crystallite thickness distribution (CTD) for clay minerals using the BWA theory, which is based on previous research by Bertaut, Warren and Averbach, that used XRD patterns for studying metals [97]. The BWA can accurately be performed to measure the mean crystallite sizes for the periodic crystals with the size range between 2 nm and 100 nm. There is a correlation between the broadening of XRD peaks and the reduction of crystallite size.

The shape of XRD peaks from the oriented air-dried preparations was used to calculate the mean crystallite thickness (T_{MEAN}) and the crystallite thickness distribution (CTD) by BWA analysis, using the MudMaster computer program [97,98]. Eberl *et al.* measured the mean crystal thicknesses for fundamental illite particles by different techniques such as BWA analysis, integral peak width, fixed cation content and TEM, and obtained almost similar values for fundamental illite particles [99,100]. The principles of the BWA analysis will be explained and highlighted in the pros and cons section (section 2.10).

1.6.4 STACKING THE LAYERS

A polytypic series occurs when layers of identical structure and composition are stacked in different ways while the two-dimensional translations within the layers are (basically) maintained. The polytypic series can be described by rotation and/or translation (of one layer with respect to the one under it along the z-axis or (001) direction). The polytypes can be created if there are systematic displacements (rotations and/or translations), which means that the distributions of displacements follow some pattern while the disorder is generated by unsystematic displacements

[101]. For phyllosilicates, small deviations from stoichiometry (up to 0.20 atoms per formula unit) within a same polytypic series are allowed [77]. Takeda and Ross, Baronnet and Bergaya have defined the principles of polytypism when it is described by relevant features of clay mineral structures [77,102,103]. Many types of clay minerals (i.e., 1:1 or 2:1 layers) are configured along the z-axis or (001) direction depending on the type of layer ordering. In the kaolin group, kaolinite, dickite and nacrite are classified as polytypes and are all based on a 1M structure. The general composition of kaolin is $Al_2Si_2O_5(OH)_4$ and consists of dioctahedral 1:1 layer structures. In the octahedral sites of the kaolin group minerals, the main positions are occupied by Al^{3+}; however, for some isomorphous types, this cation may be substituted by Mg^{2+}, Fe^{3+}, V^{3+} and Ti^{4+}. For kaolinite, the stacking sequence contains the identical layers with an interlayer shift (translation) of 2a/3 and the location of the vacancy in the octahedral site is the same in adjacent layers (Figure 1-20). However, for dickite and nacrite, the vacancies in octahedral sites alternate between two distinct sites (Figure 1-20) [101]. Figure 1-20 shows a schematic of the layer stacking of kaolinite, dickite and nacrite viewed normal to the (001) plane. A, B and C are three octahedral sites, where only two of them (circles) are occupied and the B position is almost always unoccupied.

The polytypes of mica are examples of 2:1 clay minerals. The chemical composition of the mica group is $XY_{2-3}Z_4\ O_{10}(OH,F)_2$ with X =K, Na, Ba, Ca, Cs, (H_3O), (NH_4); Y = Al, Mg, Fe^{2+}, Li, Cr, Mn, V, Zn; and Z =Si, Al, Fe^{3+}, Be, Ti. The structural and chemical detail of more than 200 mica crystals have been studied by Brigatti and Guggenheim [104]. They identified true micas as main minerals that belong to the 1M, $2M_1$, 3T, $2M_2$ and 2O polytypes.

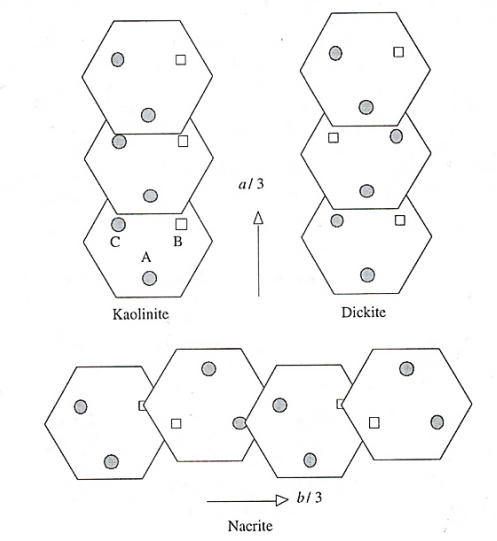

Figure 1-20 Schematic of layer stacking of kaolinite, dickite and nacrite viewed normal to the (001) plane. The shifts are exaggerated for clarity of understanding [76].

The most common stacking sequence for trioctahedral true micas is 1M. However, the dominant polytype for dioctahedral micas is $2M_1$. Anandite and phlogopite minerals were identified as a trioctahedral brittle mica with the 2O structure [77,105]. Figure 1-21 shows, schematically, A. the layer rotation, which causes a translation in the X-Y plane, B. the 1M stacking, C. the $2M_1$ polytype due to plus and minus 120° rotations, and D. the 3T polytype due to consecutive 120° rotations.

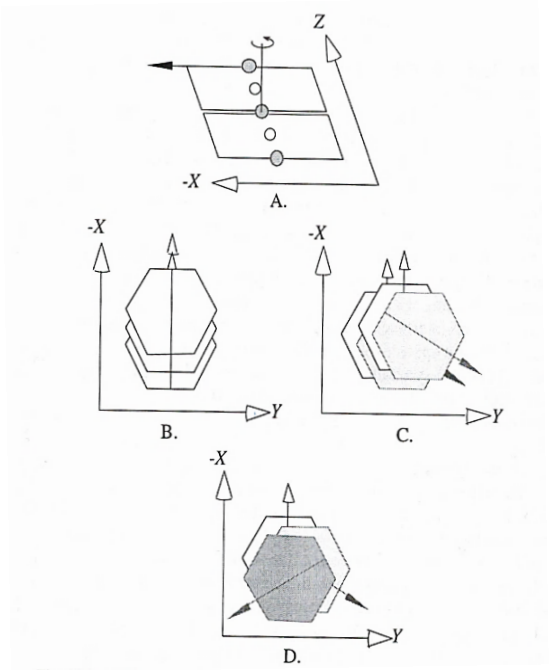

Figure 1-21 Schematics of A. a translation of cell in the X-Y plane due to a layer rotation in micas, B. the 1M stacking, C. plus and minus 120° rotations causes the $2M_1$ polytype, and D. the 3T polytype due to consecutive 120° rotations. All translation magnitudes are not to scale [76].

Unsystematic displacements (rotations and/or translations) are classified as a stacking disorder. Turbostratic disorder is the superlative type of stacking disorder. Halloysite and most smectite minerals are two different types of clay minerals (1:1 and 2:1) which contain turbostratic disorder. Halloysite is a hydrated polymorph of kaolinite with the general formula of $Si_2Al_2O_5(OH)_4.2H_2O$ and a basal spacing close to 1 nm (10 Å). Water is present in the interlayer space and can be easily and irreversibly removed by heating and the basal spacing of dehydrated halloysite (metahalloysite) decreases to about 0.72 nm [76,77,106]. Figure 1-22 shows the water present in the interlayer space of halloysite - 1nm (10 Å) and layer periodicity. Different morphologies of halloysite particles, i.e., spheres, tubes, plates have been reported by Zvyagin, and García *et al* [77,107,108]. The most widely known morphology is the tubular halloysite, which is extensively used in biological applications [77,109,110].

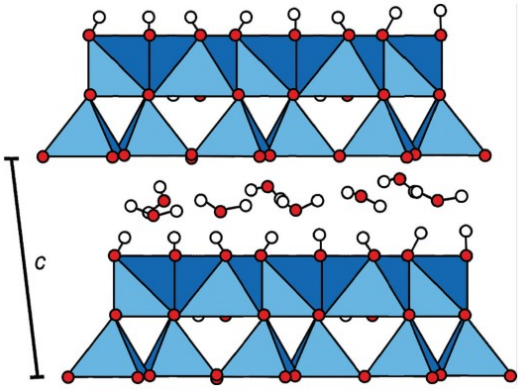

Figure 1-22 The water present in the interlayer space of halloysite-1nm (10 Å) and layer periodicity [111].

For smectite, turbostratic disorder is occurring when layer displacements are arbitrary in rotation and/or translation due to the weak attraction between exchangeable cations and the adjacent 2:1 layers. The turbostratic disorder is not observed for micas and chlorites due to the repeatable and fixed positions between the interlayer ions or hydroxide structure and adjacent layers. Figure 1-23 shows an example of arbitrary rotation, which is rotated between the lower (dash lines) and the upper (solid lines) hexagonal net by 3° to the right. K atoms (open circles) are in the center of each hexagonal site, and the K colored black (filled circle) is the center of rotation. The alignment will be poorer from the center of rotation, which means misalignment is increased by increasing the distance from the center.

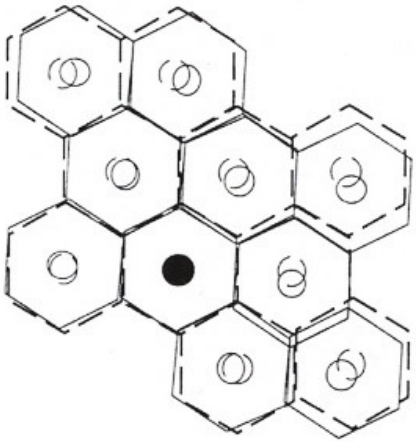

Figure 1-23 Schematic of misalignment of 2:1 interlayer by a layer rotation of 3°. K atoms are in the center of each hexagon consisting of K atom site (open circle), and the K colored black (filled circle) is the center of rotation [76].

1.6.5 SURFACE AREA

The clay mineral surface properties are under the influence of different parameters such as types of surface atoms (i.e., oxygen and hydrogen), chemical composition, type and size of defect sites,

the type of exchangeable cations and layer charge distribution [77]. The effect of surface phenomena is very important, particularly for swelling clays, which contain much higher surface area, both specific surface area (external surface area) and total specific surface area (interlayer surface and external surface areas). Brunauer-Emmett-Teller (BET) method is a technique to determine the specific surface area (SSA). The BET method uses adsorption of chemically inert gases, such as helium, nitrogen, argon or krypton, to measure the external surface area of the particles. The BET technique is able to measure the surface area contained in micropores, mesopores and macropores [112,113]. Several studies have reported that the presence of organic matter in the rocks may influence the analytical methods for measuring surface properties [114–117]. Although many studies have revealed that organic matter positively affects the results of SSA-BET from soil, high amounts of organic carbon lowers SSA-BET results due to larger aggregates forming from smaller particles by attaching to organic matter and/or blocking holes with sticky organic carbon [24,118–120]. Therefore, in the present study, the Dean-Stark extraction procedure was performed on all petrologic end-members to remove bitumen to prevent its influence on surface properties.

Bergaya *et al.* have reported that the BET technique is generally performed to measure the SSA of non-swelling clay minerals such as kaolinite, illite and chlorite [77]. For expandable clay minerals (swelling), on the other hand, the internal/interlayer surfaces are not accessible for inert gases. Moreover, the BET method is not accurate to measure total specific surface area (TSSA) values, since the amount of adsorbed gases strongly depends on the sample preparation and the nature of the exchangeable cation [121,122]. For swelling clay minerals, however, the ethylene glycol monoethyl ether (EGME), methylene blue (MB), and para-nitrophenol (PNp) methods are used to measure the TSSA [77,123–125]. Each of these methods has their own advantages and disadvantages but the different principles implemented in the measurements makes comparison between them difficult. For instance, some researchers have reported that the accuracy of TSSA from MB technique is doubtful due to the selectivity of the exchangeable dye cations and extra adsorption of cations [126–128]. This excess adsorption of MB cations may be due to molecular aggregation of MB on the surface of clay minerals, which leads to higher CEC and TSSA values than those provided by other techniques [126,128,129]. In this research, BET and MB techniques were performed for determining the SSA and TSSA, respectively. The results of these two methods are compared in chapters 3 and 4.

CHAPTER 2

2 CHARACTERIZATION TECHNIQUES

Several characterization techniques were used to examine several standard clays from the Clay Minerals Society and the four as-received (ASRE) petrologic end members from the North Mine samples taken in 2009 (NM09) and 2012 (NM12), and from Aurora Mine samples taken in 2010 (AM10) by Syncrude Canada Ltd. (Fort McMurray, Alberta). Bitumen, solids and water contents for all sets of four petrologic end members were separated and determined using the Dean-Stark (DS) extraction method [130]. After DS extraction, the bulk solids were separated into several size fractions using first wet sieving to collect >45µm and <45µm fractions and then centrifugation of the <45µm fraction at different g-force to separate 2–45 µm, 0.2–2 µm and <0.2 µm fractions. The dried fractions (overnight at 60˚C) were ground gently in an agate mortar and then subsequently prepared for further characterization.

The water content of supernatants (bitumen and solvent mixture) of the four petrologic end members was also measured by the Karl Fischer (KF) titration technique using a Mettler Toledo DL39 system. The accuracy of measurements was repeatedly verified by measuring a standard solution (0.1% water content).

XRD analysis was used to identify the expandability ($\%S_{XRD}$) of mixed-layered clay minerals (i.e., illite–smectite and kaolinite-smectite). This identification was performed on oriented preparations specimens (<2µm, 0.2-2µm and <0.2µm fractions) and suspended solids (SS) from the bitumen product (supernatant) of four petrologic end members. The $\%S_{XRD}$ of illite–smectite and kaolinite-smectite was identified by comparison between two treatments: air-dried (54% relative humidity - RH) and ethylene glycolated (vapor solvation with ethylene glycol at 60°C overnight) [76,94]. Quantitative X-ray diffraction (QXRD) was performed on random preparations specimens using the RockJock-11 program to determine the quantitative mineralogy of these fractions and bulk samples [131].

Fourier transform infrared (FTIR) spectroscopy was performed on pressed-disc samples composed of KBr and solids (from synthetic samples and various size fractions of the end members). The pressed-disc samples were heated at 120°C overnight, then FTIR spectra were measured in the middle infrared region (MIR, 4000–400 cm^{-1}) and compared with the reference IR spectra [132]. The quantity of total C (C_{total}), H, N and S was measured with a Vario MICRO cube elemental analyzer. Inductively coupled plasma-mass spectroscopy (ICP-MS) was performed to determine the chemical composition of the samples (synthetic samples and various size fractions from the end members - NM09) using a Perkin–Elmer Elan 6000 ICP-MS. An EDAX Orbis Micro energy dispersive X-ray fluorescence (XRF) spectrometer was also used to determine the chemical composition of the petrologic end members (NM09).

A TA Instruments thermogravimetric analyzer (TGA) was utilized to determine loss-on-drying (LOD) at 105°C for 90 min and loss-on-ignition (LOI) at 1000°C after 120 min for the different size fractions of the four petrologic oil sands end members. Cation exchange capacity (CEC) was determined using two techniques; copper-(II)-triethylenetetramine $[Cu\ (Trien)]^{2+}$ and methylene blue index (MBI). Total specific surface area (TSSA) and specific surface area (SSA) were determined by the methylene blue (MB) method and Brunauer−Emmett−Teller (BET) adsorption isotherm measurements, respectively [112,133].

Scanning electron microscopy (SEM) was applied to examine the fractions from petrologic end members (NM09) by using a Zeiss EVO MA 15 operated at 20 kV with a Bruker energy dispersive X-ray (EDX) analyzer. Both secondary electron (SE) and backscattered electron (BSE) detectors were used for imaging. Transmission electron microscopy (TEM) was also performed to study collected solids from the supernatant of the four petrologic end members (NM12) by using a Philips CM20 FEG TEM/STEM operated at 200 kV with an Oxford energy dispersive X-ray (EDX) analyzer and selected area electron diffraction (SAED). In the following sections, the principles behind each technique will be explained and the pros and cons for each technique will be highlighted.

2.1 CATION EXCHANGE CAPACITY (CEC)

In this study, two methods, copper(II)-triethylenetetramine $[Cu(Trien)]^{2+}$ and methylene blue (MB) were performed to determine CEC of the samples. In the copper(II)-triethylenetetramine

technique, 0.01 M solution of $[Cu(Trien)]^{2+}$ was prepared by mixing solutions of copper(II) sulfate and triethylenetetramine [134]. The dried sample (overnight at 105˚C) of ~200 mg was added and dispersed into 30 mL of distilled water using an ultrasonic for 5 min. Then 6 mL of the $[Cu(Trien)]^{2+}$ solution was added to the suspension. Afterwards, the suspension was agitated for 1 h at 120 rpm in a laboratory water bath. The supernatant was collected by using a centrifuge for 10 min at 31000 g, and then passed through a Whatman syringe filter with 0.2 μm pores to remove solid particles. Ultraviolet-visible (UV-vis) spectrophotometry (Varian Cary 50) at 578 nm was performed to determine the concentration of Cu^{2+} ions in the supernatant. The CEC value was calculated using the following equation which was reported by Pentrák *et al.* [129]:

$$CEC = \frac{2(1-\frac{A_i}{A_B}) \cdot C_{Cu^{2+}} \cdot V}{m_s} \qquad \textit{Equation 2-1}$$

where A_i represents the absorption of the supernatant after adsorption on the clay, A_B is the absorption of the stock solution $[Cu(Trien)]^{2+}$, $C_{Cu}{}^{2+}$ represents the concentration of the stock solution $[Cu(Trien)]^{2+}$, V is the volume of the dispersion, and m_s represents the mass of the sample. The average and the standard deviation of the CEC measurements were calculated from three replicates (at least) determined for three different weight loads.

In the methylene blue (MB) titration method, ~2 g (250 mg for samples with very small quantities available and 5 g for very sandy samples) [135] of dried bulk samples and different fractions (at 105°C for 24 h) was placed in a clean glass bottle (250 mL wide mouth); 50 mL of 0.015 M $NaHCO_3$ along with 2 mL of 10% w/w NaOH were added. After soaking the sample overnight, the slurry sample was completely dispersed using a hotplate/stirrer (slurry should be kept less than 60°C) and then transferred to an ultrasonic bath (each step for 20 min). The bottles were kept in a water bath (25°C) for 5 min, then 2 mL of 10% v/v H_2SO_4 was added into the dispersed mixture. The sample on the stirring plate was then titrated in 1 mL increments (0.5 mL or even less when near the endpoint) with a daily fresh solution of 0.006 N MB. In each step, a disposal pipet was used to transfer one drop of the titrated mixture onto a Whatman #42 qualitative ashless filter paper. The droplet on the filter was visually evaluated for observation of a light blue halo. When a blue halo was observed around the drop, the sample was re-examined after stirring for an additional 2 min. The end point was reached upon observation of a blue halo in the re-dropped

sample. According to the Hang and Brindley method, the recorded volume of MB added to the slurry was used to calculate the methylene blue index (MBI) [133]:

$$MBI\left(meq/100\ g\right)=\frac{\left(V_{MB}\times N_{MB}\right)}{Weight\ sample}\times 100 \qquad \textit{Equation 2-2}$$

where V_{MB} and N_{MB} are the volume and the normality of MB added, respectively. The standard deviation and the values of the methylene blue index (MBI) were based on the measurement of three replicates.

2.2 LAYER CHARGE DENSITY (LCD)

In this research, two different dyes, rhodamine 6G (R6G) and methylene blue (MB) were used to study the layer charge density for the four petrologic end members (bulk samples and different size fractions). Samples were prepared following the techniques described in Bujdák and Komadel, and Šucha *et al.* [126,136]. For each fraction, two samples were prepared and well dispersed; the first and second dispersions were prepared in distilled water and a dye solution (R6G) to reach the final suspensions with a concentration of $5\cdot10^{-2}$ g·dm^{-3} and $5\cdot10^{-6}$ mol·dm^{-3}, respectively. The UV-vis spectrophotometer Varian Cary 50 was used to measure the visible spectra after 24 h of dispersion of the fraction in the R6G solution. The prepared solid-R6G dispersions were then centrifuged and filtered using 0.2 μm filters. The specific spectra for the adsorbed dye can be calculated by subtraction of the spectra of the solid dispersions without R6G from the spectra with the solid-R6G suspension. The second-derivative spectroscopy (SDS) graph was used to analyze the spectra. A Bujdák *et al.* report was used for identification and interpretation of species (H-aggregates, H-dimers, monomers and J-aggregates) and the band positions in the SDS (Table 2-1) [137]. Figure 2-1 shows a schematic of adsorbed dye cations (Rhodamine 6G) at the surface of clay minerals. The presence of free R6G molecules was monitored by the absorption spectroscopy measurements. For instance, when the absorption spectra of supernatants did not display any traces of R6G, it indicates that solids completely adsorbed all R6G cations.

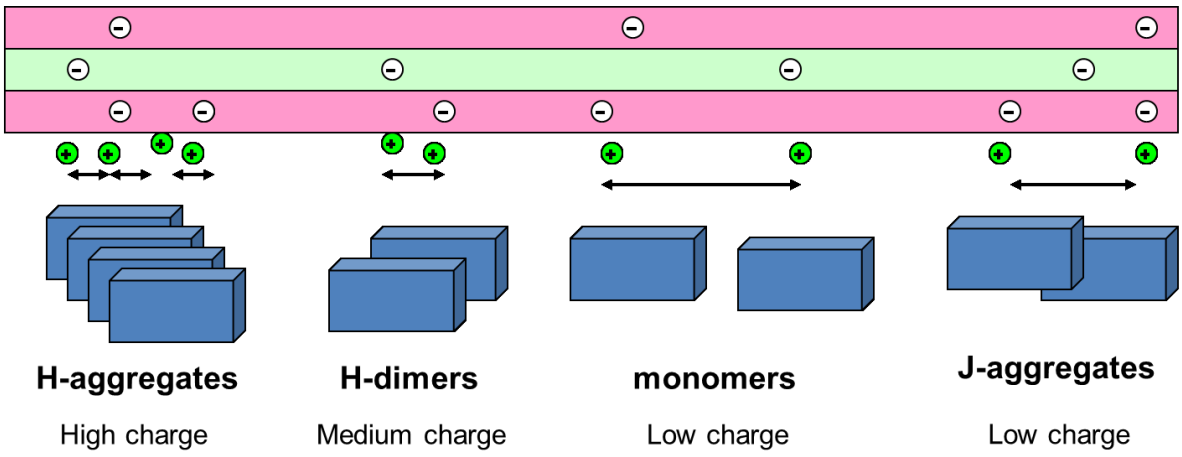

Figure 2-1 Dye cations (Rhodamine 6G) are adsorbed at the surface of clay minerals by an ion-exchange reaction at the sites of negative charge [129].

For the methylene blue (MB) dye, the same experimental procedure was performed as for rhodamine 6G (R6G). The Breen and Rock study was used for identification of assigned bands in the MB second-derivative spectra (SDS) (Table 2-1) [138].

Table 2-1 Species adsorbed on clay minerals and band positions for R6G and MB.

Species/ Dye	Rhodamine 6G (R6G)	Methylene Blue (MB)
	λ_{MAX} (nm)	λ_{MAX} (nm)
H-aggregates	466-500	570-590
H-dimers	498-525	600
monomers	535-540	650-675
J-aggregates	550	770

2.3 SURFACE AREA

The specific surface area (SSA) and total specific surface area (TSSA) of the four petrologic bulk samples and different size fractions (after bitumen removal) were determined by the BET

(Brunauer-Emmett-Teller) adsorption isotherms measurement and the methylene blue (MB) method, respectively [112,113,139]. In the BET method, the SSA measurement is based on the amount of monolayer gas (N_2) adsorption. The samples were outgassed overnight (~24 h) at 130°C under vacuum using a Quantachrome Model Autosorb-1 MP instrument. After outgassing, the amount of nitrogen adsorption was measured for every sample using seven adsorption points over the relative equilibrium adsorption pressure (P/P_0) range of 0.05 to 0.3. In such a low pressure region, adsorption takes place on the surface of micropores (D = 0-2 nm) and the external surface of particles [139]. The final value and the standard deviation of the SSA-BET were based on the measurement of two different weight loads for each sample.

In the methylene blue (MB) titration method, the sample preparation was explained in section 2.1 Cation Exchange Capacity. The methylene blue index (MBI) obtained from Equation 2-2 was then used to calculate methylene blue total specific surface area ($TSSA_{MB}$) [133]:

$$TSSA_{MB} = MBI(meq/100\ g) \times 130 \times 0.0602 \qquad \textit{Equation 2-3}$$

where the number 0.0602 represents Avogadro's constant (m^2/g) and the number 130 represents the surface area of a molecule of MB ($Å^2$). The standard deviation and the values of the $TSSA_{MB}$ were again based on the measurement of three replicates.

2.4 X-RAY DIFFRACTION (XRD)

When the X-ray beam collides with the specimen, the x-ray photons interact with electrons in the atoms from specimen and the photons from the incident beam will be scattered in all directions (with/without losing energy). These processes are called elastic scattering (Thompson Scattering) and inelastic scattering process (Compton Scattering), respectively. W.H. Bragg and his son, W.L. Bragg, discovered the geometric relationship between the atomic distances and the peaks in the X-ray diffraction pattern [140]. They proposed Bragg's law, which is the most important law for interpreting X-ray diffraction data. Figure 2-2 displays the Bragg condition [141,142]:

$$2d\sin\theta = n\lambda \qquad \textit{Equation 2-4}$$

where d is the interplanar distance of the lattice planes, λ is the wavelength of the X-rays, θ is the scattering angle and n is the order of the diffraction peak, which is an integer [143].

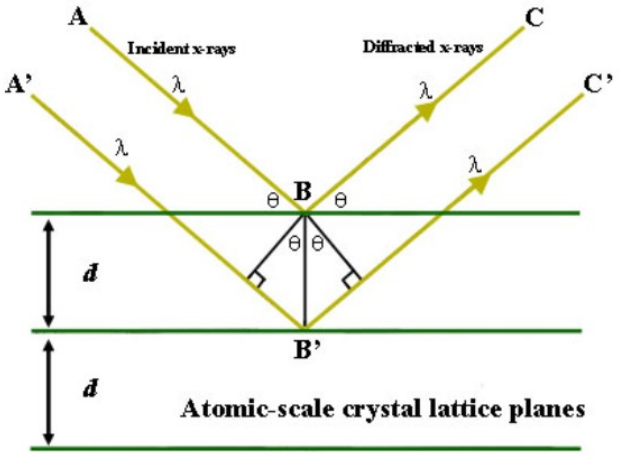

Figure 2-2 Incident and diffracted X-ray and Bragg diffraction [141].

Identification of positions, intensities, widths and symmetries of peaks are required for analyzing the X-ray diffraction (XRD) patterns. The hkl reflections from randomly ordered powder XRD is used for identification of many minerals, either clay or non-clay polytypes. Since clay minerals have a particular crystal structure (similar crystal structure in the x-y plane), it is extremely important to measure the XRD patterns from both oriented and random preparation specimens. An oriented specimen is used to improve the intensity of the (00l) reflections for identification of clay minerals by XRD. Two methods, the Millipore filter and glass slide techniques, are performed to prepare preferred orientation specimens. In addition, many other treatments, i.e., saturation with various cations, air-drying at 54% relative humidity, ethylene glycol solvation and heat treatments (350 and 550°C) are essential for characterization of the clay minerals [76,77]. The principles and/or the procedure behind oriented and random preparation specimen techniques are explained in the following sections:

2.4.1 RANDOM ORIENTATION

The mineralogical composition of bulk samples and the various size fractions for the end members were determined by quantitative X-ray diffraction (QXRD) analysis on random preparation

specimens using a Rigaku Ultima IV diffractometer, operating at 44 mA and 40 kV, with a graphite monochromator and Cu Kα radiation and the RockJock-11 program [131]. This program determines the mineralogical composition of powdered specimens by comparing the integrated X-ray diffraction (XRD) intensities of individual minerals with the intensities of a pattern from an internal standard in the complex mixtures [131]. The addition of an internal standard (e.g., corundum) allows for the calculation of each individual mineral, so the calculation will not be affected by other mineral's identification/calculation. Sample preparation was based on a modified technique by Omotoso and Eberl [144], which was also reported by Środoń [145]. A sample was sieved using a 250 μm sieve. Then exactly 1.000 g of the sieved sample and 0.250 g of an internal standard (corundum powder) were placed into a grinding cylinder with zirconia grinding balls, to which 4 mL of ethanol was added. The sealed grinding cylinder was mounted on a McCrone micronizing mill, mixed and the sample was ground for 5 min. The mixture was poured into a ceramic bowl and dried overnight at about 80°C. The dried mixture was put into a 25 mL plastic vial with three plastic balls (10 mm diameter) and shaken to mix and homogenize the contents. Then 0.5 mL of vertel (DuPont™ Vertel XF) was added to the mixture that was shaken again for 10 min using a Retsch MM 200 mill. The amount of vertel added was estimated according to the RockJock user's guide (a ratio of 0.5 mL vertrel to 1 g of pure clay) [131,145]. Next, the powder was sieved using a 250 μm sieve and loaded into an XRD side loading holder, which was against frosted glass. The specimen was run from 2θ = 4º to 2θ = 65.5º. JADE 7 software was used to extract the XRD profiles that were entered into the RockJock program to calculate the mineral composition.

2.4.2 PREFERRED ORIENTATION

X-ray diffraction (XRD) patterns were measured for oriented specimens using a Rigaku Ultima IV diffractometer, operating at 44 mA and 40 kV, with a graphite monochromator and Cu Kα radiation. The step size for both preparations was 0.02° 2θ and the exposure time was 2 s per step. Frosted glass slides were used for oriented preparation samples by fully dispersing a suspension of clay fractions (90 mg) in distilled water (approximately 1.2 mL) using a small glass bottle (8 mL). In order to disperse the clay particles in distilled water, the suspension was stirred for 5 min using a small magnetic stirring bar (Teflon^{TM} coated-PTFE, 2 mm in length and 2 mm in diameter) and sonicated in an ultrasonic bath for 5 min. The suspension was transferred by a plastic pipette

onto a frosted glass slide (2.8×2.8 cm) and left at ambient conditions to dry. According to the procedure described by Moore and Reynolds (1997), the dried glass slides were saturated first at 54% relative humidity and then with ethylene glycol (EG) prior to XRD analysis after each treatment [76]. The specimens were run from 2θ = 3º to 2θ = 60º. The expandability of kaolinite-smectite and illite–smectite were identified by comparison of XRD patterns of oriented preparations after these treatments according to the procedures described by Moore and Reynolds[76], Środoń [94] and Dudek *et al.* [95].

The Środoń procedure was performed to measure the following criteria to identify the expandability and the type of interstratification (ordering) of illite–smectite [94]:

(i) The position of the low-angle reflection for illite-smectite (between 6-8° 2θ) of the glycolated specimen;

(ii) The intensity ratios (Ir) of the 001 and 003 reflections peaks for air dried-54% relative humidity and after ethylene glycol solvation specimens [94]:

$$Ir = \frac{(001/003)\ air\ dried}{(001/003)\ glycolated} \qquad \textit{Equation 2-5}$$

Ir is the most effective tool for identification of trace expandable clay minerals. If Ir equals 1.0, the specimen is 100% discrete illite. On the other hand, the presence of expandable clay minerals is obvious when the Ir parameter exceeds 1.0.

(iii) The joint broadness (common width) of 001 illite and adjoining illite-smectite reflections where the peak tails reach the X-ray background (measured in 2θ) for the ethylene glycol solvation specimen, named BB1 (see Figure 2-3);

(iv) The joint broadness of 004 illite and adjoining illite-smectite reflections where the peaks' tails reach the X-ray background (measured in 2θ) for the ethylene glycol solvation specimen, named BB2 (see Figure 2-3) [94].

BB1, BB2 and the position of the low-angle reflection for illite-smectite (between 6-8° 2θ) of the glycolated specimen are measured to determine the types of interstratification [118]. In addition, BB1 and BB2 values can be used for controlling identification as they are not influenced by the discrete illite reflections, since both illite and adjoining illite-smectite peaks are measured. Środoń

found that samples with BB1 and BB2 values larger than 4° 2θ, with the position of the low-angle reflection illite-smectite smaller than 7.5° 2θ, are dominated by IS ordering type of illite-smectite [94].

The reflections at 6-8° and 33-35° 2θ are two sensitive regions for identification of the type of interstratification and the expandability of illite–smectite. However, the reflection at 6-8° 2θ is usually influenced by the strong adjacent 001 illite reflection with a shoulder on the 001 illite reflection generally observed, so it may not be suitable for identification purposes [94]. The reflection at 33-35° 2θ, on the other hand, seems to be more appropriate due to the lack of discrete illite reflections in this region. Figure 2-3 displays the XRD patterns for four different illitic samples after ethylene glycol solvation. Table 2-2 shows the obtained and calculated data from above procedure (i.e., the position of the low-angle reflection for illite-smectite (between 6-8° 2θ) and the amount of Ir, BB1and BB2). Figure 2-4 shows the empirical curve for calculation of the expandability (thick solid line) and the type of ordering in illite-smectite (thin solid lines) for these specimens using the reflection at 33-35° 2θ from XRD patterns after ethylene glycol solvation. The expandability results from this technique are compared with the method described by Moore and Reynolds [76].

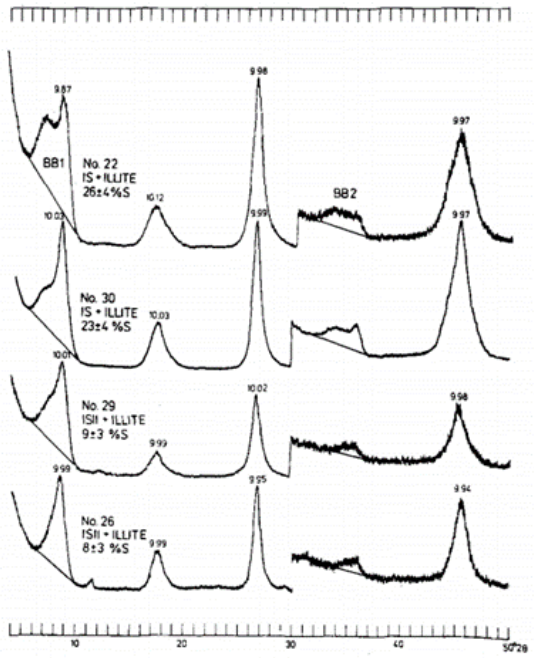

Figure 2-3 XRD patterns after ethylene glycol solvation for four different illitic samples. The units of the d(001) values are in Angstrom. The manner of measuring BB1, BB2 and Ir are shown. The type of ordering and percentage of smectite are obtained from Figure 2-4 [94].

Table 2-2 XRD data for ordered illite-smectite from four different illitic specimens. The manner of measuring BB1, BB2 and Ir is shown. The type of ordering and percentage of smectite are obtained from Figure 2-4 [94].

Sample	Reflections after glycolated (°2θ CuKα radiation)					BB1	BB2	Ir	%S	Type of Illitic materials
# 22	7.30	8.9	17.52	26.79	33.85	4.9	5.2	2.61	26	IS+I
# 26	-	8.84	17.74	26.87	35	3.6	2.8	1.83	8	I+ISII
# 29	shoulder	8.83	17.76	26.68	34.84	4.7	3.5	1.52	9	I+ISII
# 30	shoulder	8.81	17.67	26.76	34	4.5	5.0	1.5	23	I+IS

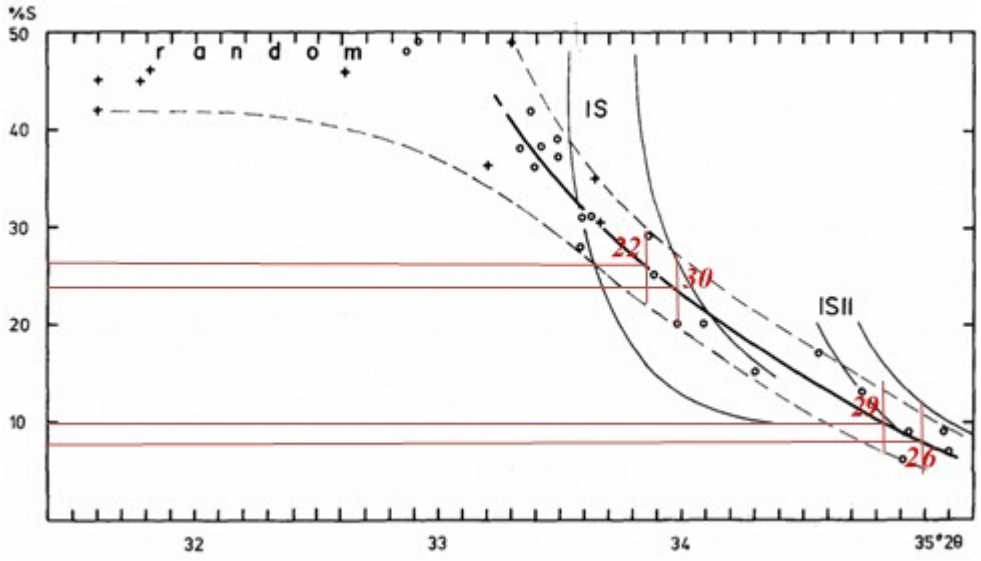

Figure 2-4 Measuring the expandability (thick solid line) and the type ordering in mixed-layer clay minerals (illite-smectites) based on the 33-35°2θ reflection. Thin solid lines represent plots of IS and ISII types of ordering. The error is shown by the dashed lines [94]

2.5 ORGANIC ELEMENTAL ANALYSIS

The total C, H, N and S contents were determined using two instruments: a Vario MICRO cube elemental analyzer and Flash 2000 organic elemental analyzer. In a vario MICRO cube elemental analyzer with "elementar vario MICRO cube" software (Version 1.5.4), the sample was burned in the presence of an oxygen stream (small amount) at 1150°C in a combustion zone; these combustion gases were then passed into a reduction zone using carrier gas He/Ar and produced CO_2, N_2, H_2O and SO_2. The formed analyte gases were trapped and separated by a temperature programmed desorption (TPD) column and quantified by a thermal conductivity detector (TCD) [146,147]. The same instrumental principles were performed by Flash 2000 organic elemental analyzer with Eager Xperience software. In order to improve the accuracy and reliability, approximately 25 mg of sample was accurately weighed and used for each run and the average of five replicates (at least) were recorded. Meanwhile, the total inorganic carbon (TIC) content was obtained by calculation of the carbon content in the carbonate minerals (calcite, dolomite and siderite). The amount of total organic carbon (TOC) for each sample was the difference between the total carbon measured by the elemental analyzer and TIC calculated by QXRD (RockJock program). The amount of TOC after Dean-Stark extraction can be considered as toluene insoluble organic carbon (TIOC).

2.6 ELECTRON MICROSCOPY

This section discusses the two main types of electron microscopes; the scanning electron microscope (SEM) and transmission electron microscope (TEM). These techniques were mostly performed to study the topography, morphology, crystal structures and chemical composition of five standard clay minerals from the Clay Repository of the Clay Minerals Society, four petrologic bulk samples and different size fractions (after bitumen removal) investigated.

2.6.1 SCANNING ELECTRON MICROSCOPY (SEM)

The surfaces of the samples were coated with a thin carbon film (electrically conductive carbon film) using a Leica EM SCD005 carbon coater. The coated specimen was then examined using a Zeiss EVO MA 15 SEM operated at 20 kV. A Bruker energy dispersive X-ray (EDX) silicon drift

detector was used for elemental microanalysis. Both secondary electron (SE) and backscattered electron (BSE) detectors were applied to record images.

2.6.2 TRANSMISSION ELECTRON MICROSCOPY (TEM)

A Philips CM20 TEM/STEM with a Schottky field-emission source was used in this study. The TEM specimen was operated at 200 kV for high resolution microstructural characterization using an ultra-thin window (UTW) X-ray detector. The size of the interaction volume through the specimen depends on the atomic number and density of the specimen as well as the energy of electron beam, which hits specimen (Figure 2-5). Unlike SEM, the interaction volume is much smaller and depends on thickness. These interaction and scattering processes determine the information from the specimen and can be collected by the TEM's detectors. In addition to the detected interactions in SEM, elastic and inelastic interactions between primary electrons from the beam and electrons of the specimen can lead to transmitted (no effect in primary beam), absorbed and/or scattered beams in the TEM, which can generate diffraction patterns and cause alteration of the transmitted electron intensities.

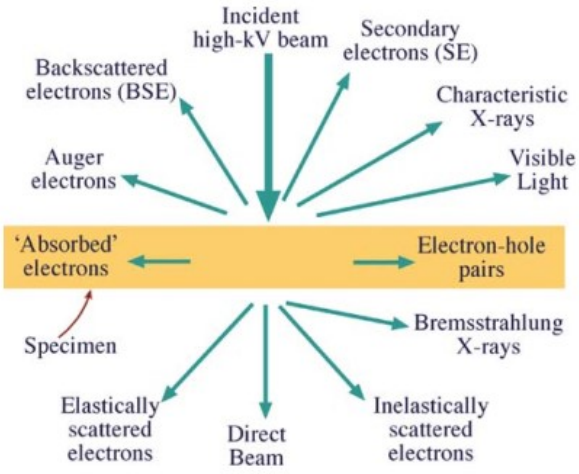

Figure 2-5 Diagram illustrating the phenomena resulting when a high-energy beam of electrons interacts with a thin specimen [148].

Some TEM instruments are capable of high-resolution imaging (~50 pm), which is related to TEM sample preparation. Two types of samples were prepared for TEM investigations. The first type

was prepared by producing a very dilute suspension of solids in solvent (cyclohexane or toluene) or distilled water and then a droplet of the prepared suspension was placed on a carbon-coated copper grid. Since the suspension was very dilute, isolated particles could be imaged. Clay mineral particles tend to orient along their basal planes due to their large planar shape. This technique was used for mineral and chemical identification of residual solids in bitumen products.

The second type of TEM sample preparation was the cutting of ultrathin sections of clay minerals using focused ion beam (FIB) methods. First an air-dried oriented specimen was placed onto a frosted glass slide (1cm ×1 cm). The sample was dried in an oven overnight at 105°C and placed in the FIB-SEM instrument. This technique consisted of an ion beam and an electron beam; the former provided the cutting/milling and latter beam was used for monitoring the milling processes. This is relatively fast technique (compared with microtoming) and an accurate technique to cut clay minerals perpendicular to the basal planes by preserving the original relations within individual grains. The procedure is described in detail in section 2.6.4. This sample preparation technique was performed to obtain useful information about clay mineralogy; i.e., smectite vs. illite and kaolinite, as well as to observe and distinguish the presence and location (a particular place) of organic matter (bitumen) on the surfaces or edges of clay minerals.

2.6.3 ELECTRON DIFFRACTION

Selected area diffraction (SAD) is a technique in TEM for obtaining diffraction patterns from small regions (<1 μm) as a result of electron beam diffraction by a thin specimen. The principles of electron diffraction are similar to X-ray diffraction, which was described in section 2.4.

In the selected area diffraction (SAD) pattern in the TEM, the specimen is struck by a near parallel beam of electrons, and diffraction spots are formed on the TEM viewing screen or CCD camera at the bottom of TEM column. Figure 2-6 show the diffraction pattern that can be seen on the screen [148].

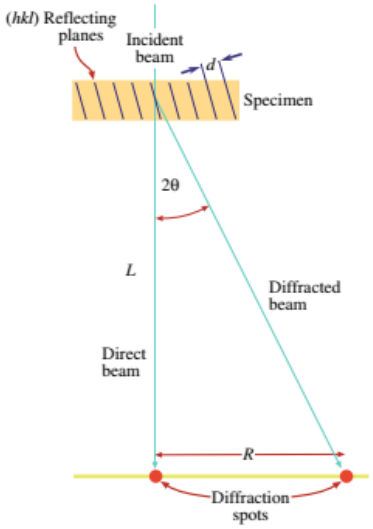

Figure 2-6 Schematic showing diffraction of electrons from a single crystal [148].

Since, the angle θ is very small (1° - 2°), then the following can be written:

$$Rd = \lambda L \qquad \textit{Equation 2-6}$$

where R is the measured distance of the diffraction spot on the screen, L is the camera length. The d spacing can be calculated, by measuring the R, L and λ values. The combined parameter λL is the camera constant and can be determined for TEM by using a standard specimen. The Miller indices (h k l) are calculated by using the d-spacing formulae for the seven different crystal systems [149].

2.6.4 FOCUSED ION BEAM-SCANNING ELECTRON MICROSCOPY (FIB-SEM)

Focused ion beam-scanning electron microscopy (FIB-SEM) is a dual-beam or crossbeam system, consisting of two column beams (i.e., focused ion and electron beams), where their focal points coincide. Commonly, the SEM column is placed in a vertical position and right above the sample, and the FIB column is held at an angle of 52° to 56°. Figure 2-7 shows different stages in preparing a TEM specimen from Si using a FEI Helios Nanolab 600 dual-beam FIB/SEM [150].

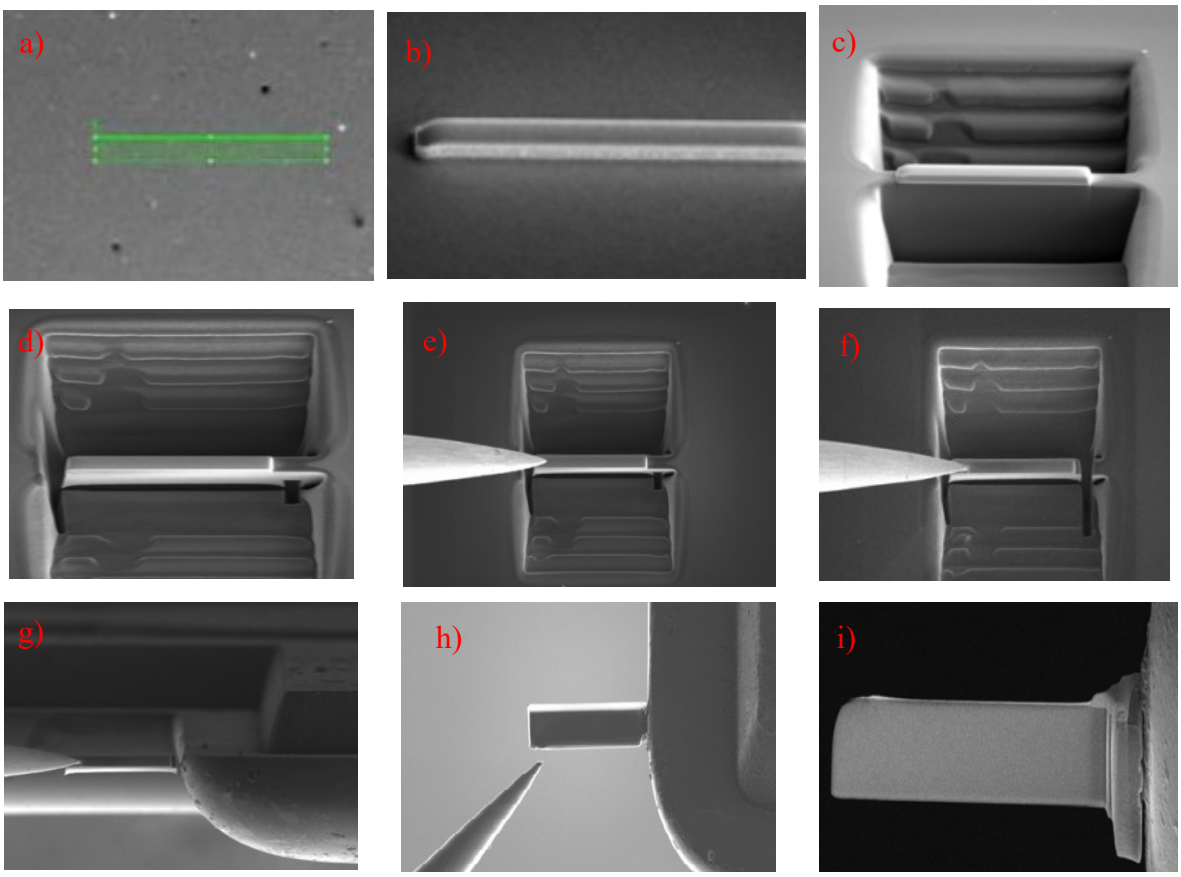

Figure 2-7 Various stages in preparing a TEM specimen from Si using a FIB-SEM instrument. a) The region of interest (ROI) is marked. b) A Pt/W strip is deposited on the ROI to protect this area from the Ga beam. c) Two stair step trenches are milled. d) The bottom and sides of the slice are milled (U-Cut). f) The slice is welded to the probe. g) The slice is lifted out and transferred to a TEM grid and attached to it. h) The probe is detached from the slice. i) The sample is milled for thinning and cleaning [150].

The region of interest (ROI) of the sample was coated with a thin Au layer by sputter deposition prior to Pt/W deposition as part of the FIB sample preparation process. Platinum and/or tungsten layers were deposited for protection by ion beam induced deposition. Bulk cutting/milling and polishing processes were carried out using a Ga^+ beam at 40 keV and 10 keV, respectively. The approximate thickness of the final thin section, prepared by FIB and placed on Cu grids, was ~100 nm. In addition to controlling the cutting process, the SEM column with a field emission source operated at 5 kV was also utilized for imaging the ROI during each step of the thin section preparation process.

2.7 FOURIER TRANSFORM INFRARED SPECTROSCOPY (FTIR)

Fourier transform infrared spectroscopy (FTIR) is an economical, rapid and common technique, which has a long and successful history as an analytical technique [151,152]. Commonly, this is a complementary technique to other methods (e.g., XRD, TGA, DSC, etc.) used to identify organic and inorganic materials. The FTIR instrument is capable of obtaining a spectrum in a few minutes. Moreover, this instrument exists in many laboratories due to its relatively cheap cost. Each material has a particular IR spectrum and can be denoted as a fingerprint for materials characterization. The principle of infrared spectroscopy is based on the vibration of atoms of a molecule. The IR spectrum is taken by passing IR radiation through a specimen and identifying the absorbance fraction from the incident radiation at a specific energy. The absorption spectrum is related to the frequency of the vibration of a part of the molecule in a sample [151].

Farmer found that IR spectroscopy of minerals can be used to collect specific information about the mineral structure, group type of minerals, the nature of isomorphic substituents, the type and presence of impurities (either crystalline or non-crystalline) and so on [153,154]. Lazarev also figured out that the IR spectrum is intensively influenced by the degree of crystalline order [155,156]. Many researchers in different industries (i.e., clay, oil and oil sands industries) have had extensive investigations on the interpretation of absorption IR spectra in the mid-IR region (MIR) (i.e., 4000 – 400 cm^{-1}) for a variety of samples such as standard clay minerals, bitumen froth and oil sands ore [153,156–159].

In this study, Fourier transform infrared (FTIR) spectra in the middle infrared region of 4000-400 cm^{-1} were measured using a Nicolet 6700 spectrometer. The KBr pellet method was used for transmission measurements of all samples. 0.5 mg of samples were fully dispersed in 200 mg of powdered KBr and completely homogenized by using an agate mortar and pestle. The KBr pellets were dried in an oven overnight at 120°C to reduce or prevent the effect of water absorption on FTIR spectra. The spectra of each sample were measured at 128 scans with a resolution of 4 cm^{-1}. OMNIC software was utilized for spectral manipulations, i.e., automatic baseline correction and normalization of FTIR spectra.

For liquid and paste samples, e.g., bitumen, FTIR spectra may be obtained by smearing the samples (dilute sample with solvent) between two KBr windows. The thickness of the bitumen film on the windows was not accurately determined. However, the applied thickness was adjusted by using a

trial and error method until an FTIR spectrum with sharp peaks for the major absorption bands was observed.

2.8 KARL FISCHER (KF) TITRATION

Karl Fischer (KF) titration is an analytical titration technique to measure the amounts of water in a sample, i.e., solids, liquids and gases. There are two types of titration equipment, which are related to the level of water in the sample: the coulometric and volumetric titration are suitable for trace amounts (1 ppm to 5% H_2O) and for a major component (100 ppm to 100% H_2O), respectively. A German chemist Karl Fischer invented this technique in the 1930's [160]. The titration method rapidly developed and became known as the Karl Fischer titration technique. The technique is performed to identify the unknown concentration of an element in solution by adding it to a standard reagent. The unknown concentration of substance (water) is determined when a reaction of definite and known proportions is completed since the same quantities of both (i.e., reagent and water) are needed for completion. The KF reaction occurs in the two following steps [160]:

$$H_20 + I_2 + S0_2 + 3Py \rightarrow 2PyH^+ I^- + PyS0_3 \qquad \text{Equation 2-7}$$

$$PyS0_3 + CH_3OH \rightarrow PyH^+ CH_3S0_3^- \qquad \text{Equation 2-8}$$

where Py is pyridine (base) and CH_3OH is alcohol (methanol).

Commonly, a mixture of iodine, sulfur dioxide, pyridine and methanol is used for the KF reagent. Except iodine, a surplus amount of all the compounds is used for the titration; the exact consumption of iodine is required for calculation of the amount of water. The solution contains I^- and a trace amounts of I_2 just before the equilibrium point. However, at the equilibrium point, the surplus amount of I_2 leads to a sudden current increase, which reveals the titration is completed.

In this research, the water content of the supernatant was determined by the coulometric Karl Fischer (KF) titration method (Mettler Toledo DL39 system), due to the trace quantities of water in the mixture. A weight of ~0.1 mL of sample was measured by transferring the mixture/supernatant using a syringe equipped with a needle. The entire sample then was quickly injected into the titration vessel. The titration usually took a few minutes. When the titration was

completed, the screen display showed the amount of water detected in every analysis. The percentage of water content was recorded for further calculation. Each supernatant was measured at least four times and the mean value and standard deviation were calculated. The accuracy of titration was repeatedly controlled (every five measurements) by using a standard sample (0.1% water content).

2.9 BERTAUT-WARREN-AVERBACH (BWA) TECHNIQUE

The crystallite thickness and the crystallite thickness distribution are important characteristics of clay minerals. Eberl *et al.*, Kile *et al.* and Środoń *et al.*, reported the identification of these factors is an effective tool for understanding the technological properties of clay minerals [161–163]. Moreover, many researchers in the oil sands industry have reported that bitumen recovery is significantly influenced by the ultrathin 2:1 clay mineral (illite and illite-smectite) particles in the oil sands ores in water-based bitumen extraction [21,39,164]. It is expected that the ultrathin clay mineral particles, particularly 2:1 clay minerals, play a negative role during a non-aqueous bitumen extraction process.

As described in section 1.6.3 the thickness of the particles is influenced by the type and valence of exchangeable cations. For instance, Na^{+}-montmorillonite is considered to consist of about 3-5 layers per particle while Ca^{2+}-montmorillonite (divalent cation) includes 10 layers. Moreover, Na^{+}-montmorillonite has a much larger interlayer spacing than that of Ca^{2+}-montmorillonite [77]. The particle thickness can be identified by two main methods: high-resolution transmission electron microscopy (HRTEM) and calculation of the peak broadening in XRD pattern of oriented specimens.

In this research, the mean crystallite thickness (T_{MEAN}) and the crystallite thickness distribution (CTD) of five standard clay minerals from the Clay Repository of the Clay Minerals Society, the Na-form of pure clay fractions and artificial mixtures of bitumen-clay were individually determined by the Bertaut-Warren-Averbach X-ray diffraction technique, using the MudMaster computer program [97,98]. The air-dried oriented specimen was prepared and scanned using a Rigaku Ultima IV diffractometer (40 kV, 44 mA) with Cu Kα radiation. To collect a high quality XRD pattern a step size of 0.02° 2θ, an exposure time >2 s per step, a graphite monochromator and a stable generator were used. The specimens were run from 2θ = 2º to 2θ = 60º. JADE 7

software was used to extract the XRD profiles, the data was then entered into the MudMaster computer program to calculate the mean crystallite thickness (T_{MEAN}) and the crystallite thickness distribution (CTD).

2.10 FOCUSED BEAM REFLECTANCE MEASUREMENT

Focused beam reflectance measurement (FBRM) is a technique for measuring/studying solid size distribution in-situ in a dark and/or opaque slurry [165,166]. This technique directly tracks changes to the number, shape and dimension of particles in the slurry [167]. The immersed FBRM probe in the slurry counts the reflected laser light from a particle, which impinges upon the probe window (Figure 2-8). Thousands of individual particles per second hit the window and create pulses of backscattered light, which generates a chord length distribution (CLD) [167]. Measuring the chord length instead of the particle diameter is due to the improbable likelihood of detecting of the centre of a particle by the laser beam [168]. In this research, FBRM model G-400 (Mettler-Toledo, Canada) was used to measure the chord length distribution, which is similar, but not identical, to particle size distribution [165,168]. The two main advantages of this technique are: a wide range of detection from 0.5 to 2000 μm and no sample preparation [167].

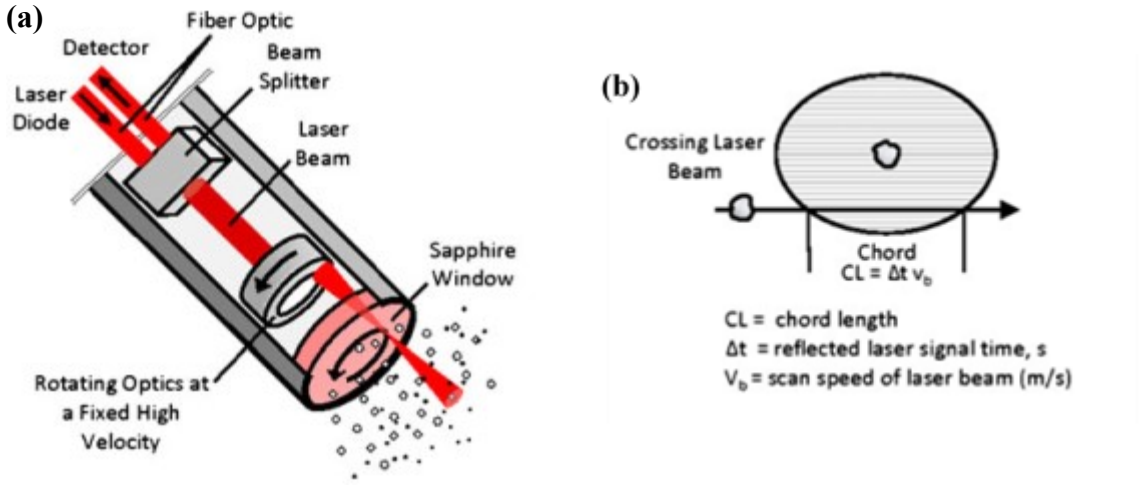

Figure 2-8 Schematic of a) the FBRM probe and b) chord length measurement [169] .

For each sample analysis, ~150 mL of pure cyclohexane was placed in a 500 mL beaker. The dual-blade impeller and the FBRM probe were immersed into the pure cyclohexane. The same position and depth of the probe were used for all measurements. The sampling interval measurement was

2s to get the best test resolution. The background medium (pure cyclohexane) was measured with the mixing speed set at 300 rpm (the optimum stirring speed for testing); the counts must be less than 300. Next ~100 mL of collected supernatant was slowly added into the beaker. Then pure cyclohexane (approximately 150 mL) was again added to the supernatant bottle to reach a total mixture of 400 mL. For each measurement, the mixture (collected supernatant and cyclohexane) was recorded after 2 min of premixing time to allow the mixture to completely disperse and stabilize. For the next 10 min (from 2 min to 12 min), the desired data (i.e., unweighted chord length distribution, mean square weighted chord lengths, percentile c (10), percentile c (50), percentile c (90) and counts of particles were monitored and recorded throughout the analysis.

The D10, D50 and D90 chord length (CL) values were calculated with the software icFBRM 4.2 from a cumulative percent distribution, which was produced from the CLD. The cumulated percent of CL size that accounts for 50% or less of the CL (which is the 50th percentile) is called D50 [169]. The same procedure was used for determination of D10 and D90.

CHAPTER 3

3 OBJECTIVES AND EXPERIMENTS

3.1 OBJECTIVES

As mentioned before, organic solvents provide an alternative method to extract bitumen from oil sands and shales, without consuming large quantities of fresh water. During non-aqueous extraction, it is, however, expected that some minerals particularly nano and microsize minerals (NMM) may change the processability of the oil sands ore. These components may interact with other ingredients such as water, bitumen and solvent due to their small particle size distribution, high surface area, high ion exchange capacity, solvent-insolubility and specific physicochemical properties.

It has been demonstrated by many scientists that the oil sands deposit in Alberta has a high geologically-driven heterogeneity, which consists of a wide variety of mineral compositions. Therefore, this heterogeneity should be considered during sampling from the oil sands ore deposit. The mineral compositions and textural variability of the mined ore can be identified in terms of a mixture of the four petrologic end members, i.e., estuarine sand, estuarine clay, marine sand and marine clay. It is also believed that the properties of different ore zones are an averaged combination of the properties of these four petrologic end members. Hence, understanding the four petrological end members will lead to a better understanding of the entire deposit. In this study, special attention is drawn to the type and quantities of NMM in the four end members as well as the behavior and influence of these NMM (particularly clay minerals) on the organic solvent.

The overall objective of this research is to characterize the mineralogical and chemical composition of the four petrologic end members comprising the oil sands deposit, specifically “nano and microsize minerals (NMM)”, i.e., clay minerals, whose particles are carried into the

solvent-bitumen solution. Identification of the NMM will help to understand their effects on non-aqueous bitumen extraction efficiency and bitumen recovery.

There are three key specific objectives: the first objective is to determine the mineralogical and chemical composition of the four petrologic end members, i.e., estuarine sand, estuarine clay, marine sand and marine clay, which were deposited in two main sedimentary environments (marine and estuarine) sampled from two different mine locations at various times. Another underpinning objective of this study is to identify the mechanism of preferential clay segregation. For this purpose, an experimental set up was designed and investigated to examine the effect of individual clay minerals (swelling and non-swelling clays) on a non-aqueous bitumen extraction process. Since it is impossible to collect individual types of clay minerals from the oil sands and because of the highly heterogeneous nature of these samples, artificial mixtures of bitumen with standard clays (from the Clay Minerals Society) were prepared and the influence of individual clays on the extraction process was investigated.

Finally, for the third objective, an experimental set up for a non-aqueous extraction procedure was designed to collect the suspended fine solids from bitumen products after cyclohexane extraction. The type and quantity of these migrated fine solids, specifically different clay species, were identified for the four petrologic end members from Alberta oil sands to better understand the most important parameters affecting non-aqueous bitumen extraction and bitumen quality.

3.2 EXPERIMENTAL SECTION

The first objective is to determine the mineralogical and chemical composition of the four petrologic end members, which will be provided in Chapters 4 and 5. The identification will pave the way for a better understanding of important factors affecting bitumen extraction processes (either aqueous or non-aqueous) and subsequent solvent recovery. Two sets of four petrologic end member samples collected at two different times from Syncrude's North Mine (i.e., NM09 and NM12) were studied for this research. Although the oil sands deposit in Alberta has a variety of mineral and chemical compositions, these variabilities can be classified in terms of a mixture of four petrologic ''end members'', i.e., estuarine sand, estuarine clay, marine sand and marine clay [170,171].

In this study, the sands and clays were manually separated from the as-received (ASRE) samples, disaggregated and passed through a sieve (aperture size of 6.3 mm, according to ASTM E.11) [172]. Then, the solids, bitumen and water contents for all four petrologic end members were separated and measured by the Dean-Stark (DS) extraction method [173]. Particle size fractions (i.e., >45 μm, 2–45 μm, <2 μm, 0.2–2 μm and <0.2 μm) were collected using wet sieving and centrifugation techniques. The samples were dried overnight at 60°C and ground gently in an agate mortar. The original bulk samples and different size fractions from the four petrologic end members after bitumen removal were characterized by XRD, FTIR, ICP-MS, elemental analysis, CEC, LCD, SSA, SEM, EDX spectroscopy and TEM. Figure 3-1 shows the schematic experimental set-up for characterization of four petrologic end member samples from Syncrude's North Mine.

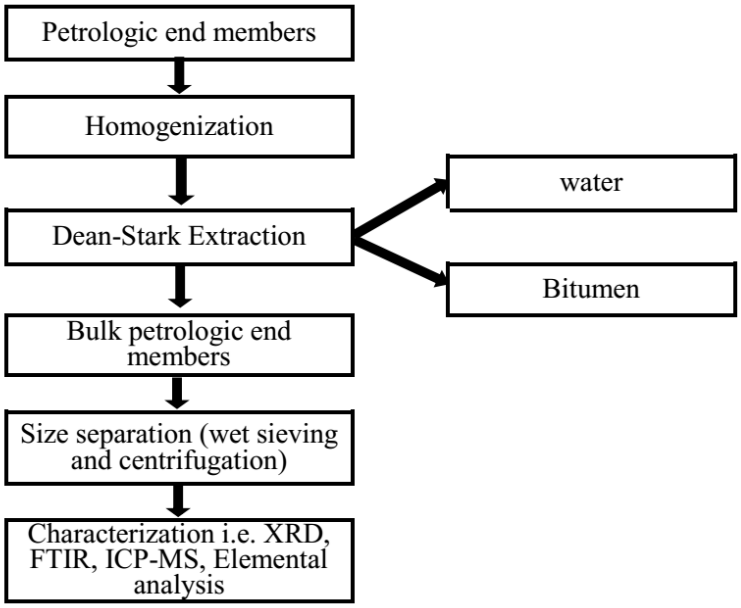

Figure 3-1 The schematic experimental set-up for mineralogical and chemical composition characterization of four petrologic end members.

The second objective is to understand the effect of individual non-swelling and swelling clay minerals on a non-aqueous bitumen extraction process, which will be explained in Chapter 6. Three non-swelling clays, KGa-2 (kaolinite, Georgia), IMt-1 (illite, Montana), and CCa-2 (chlorite, California) and two swelling clays, ISCz-1 (illite-smectite, Slovakia) and SWy-2 (smectite, Wyoming) from the Clay Mineral Repository of the Clay Minerals Society, and isolated bitumen from Alberta oil sands were used to make artificial mixtures. Mixtures of the individual clay minerals (<2 μm size fraction, Na-exchanged form and freeze dried) with toluene-diluted

bitumen were prepared and agitated with a magnetic stir bar for 24 hours. The mixtures were then stirred and left at 40°C for 7 days in open bottles inside a fume hood to allow the toluene to evaporate. The resulting clay-bitumen mixtures were washed three times with cyclohexane to extract the bitumen. The clays were separated by centrifugation and characterized by XRD, FTIR, ICP-MS, CEC, LCD, SSA, SEM, EDX spectroscopy and FIB-SEM. The experimental set-up is shown schematically in Figure 3-2.

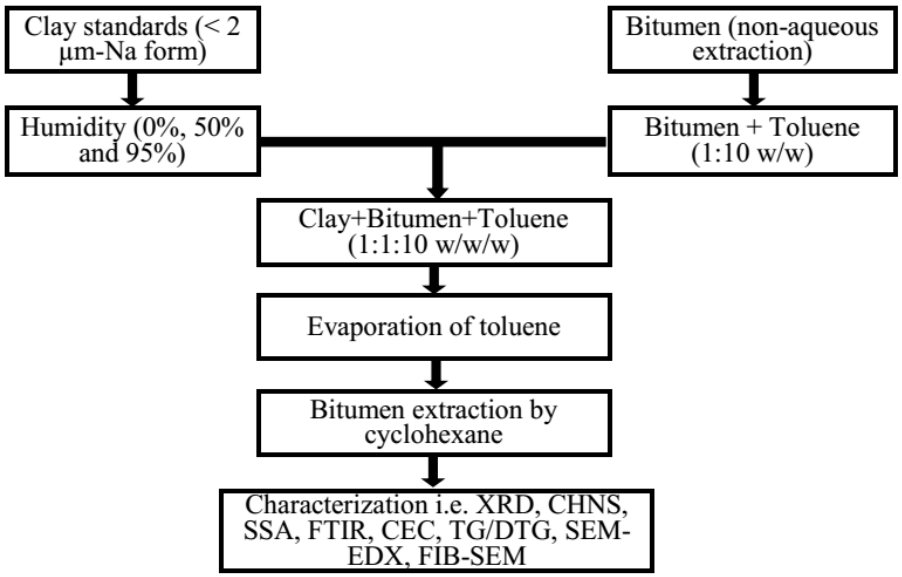

Figure 3-2 The schematic experimental procedure for preparation and characterization of artificial mixtures.

Chapters 7 contains the third objective, which was to study the migration of different clay species to the bitumen solution during non-aqueous bitumen extraction using cyclohexane as the solvent of interest. This investigation was carried out on four petrologic end member samples from Syncrude's North Mine collected in 2012 (NM12), i.e., MC, MS, EC and ES. Each end member/ore was separately mixed with cyclohexane at a ratio of 40:60 (cyclohexane:end member), and the bitumen-cyclohexane solutions were collected at different settling times (1 min to 30 min). These solutions were analyzed to determine the amount, particle size distribution and mineralogical composition of suspended fine solids (SFS), water content, as well as the bitumen content using a focused beam reflectance measurement (FBRM) particle size analyzer, Karl Fischer (KF) titration, XRD, quantitative XRD (QXRD) and elemental analysis. The experimental procedure is shown schematically in Figure 3-3.

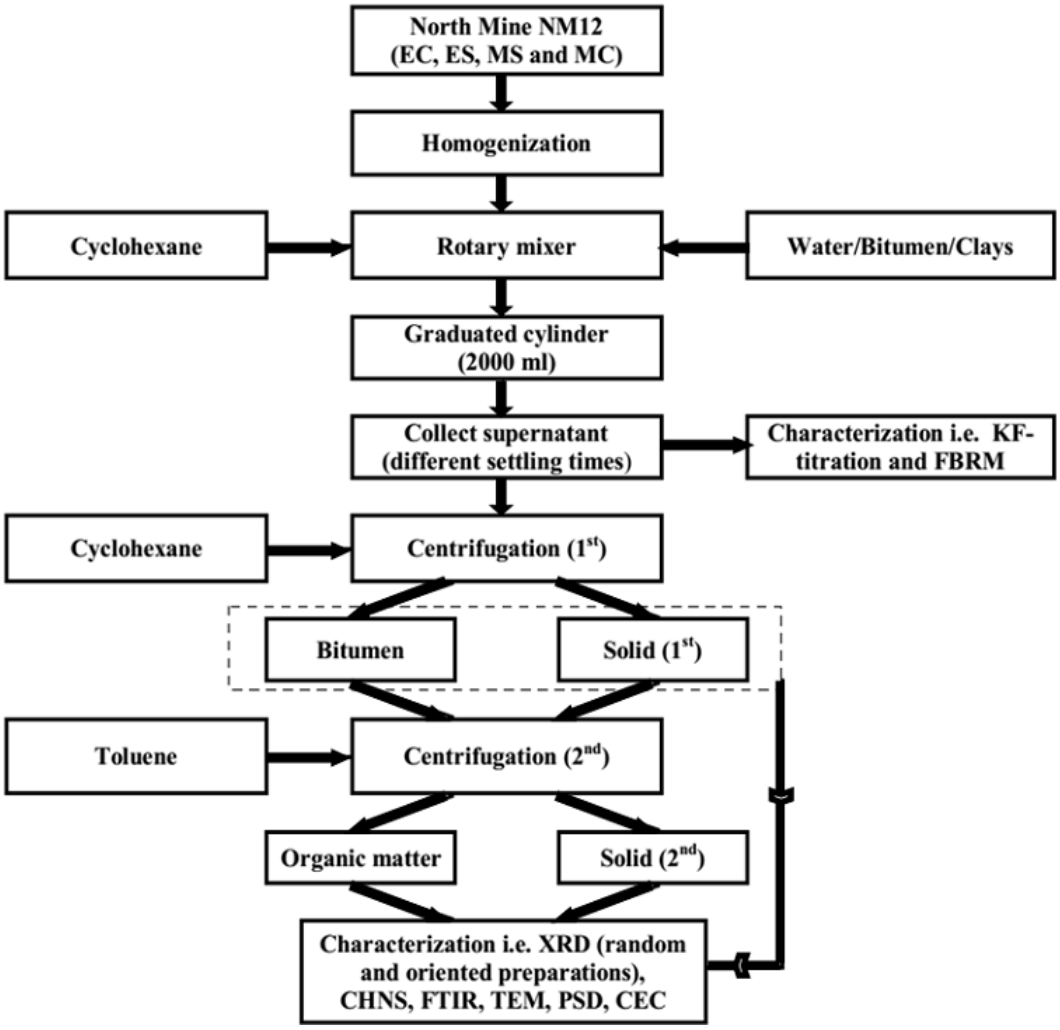

Figure 3-3 The schematic experimental procedure for understanding the migration of different clay species to bitumen solution during non-aqueous bitumen extraction process using cyclohexane.

CHAPTER 4

4 CHARACTERIZATION OF FOUR PETROLOGIC END MEMBERS FROM ALBERTA OIL SANDS AND THEIR RELATIONSHIP WITH SURFACE PROPERTIES

The contents of this chapter have been published in the following well-respected journal and presented at two peer-reviewed international conferences:

M. Osacky, **M. Geramian**, Q. Liu, D.G. Ivey and T.H. Etsell, Surface properties of petrologic end members from Alberta oil sands and their relationship with mineralogical and chemical composition, Energy Fuels, 28 (2014), 934–944.

M. Geramian, T. H. Etsell, D. G. Ivey and Q. Liu, Migration of Fine Solids to Bitumen Solution after Cyclohexane Extraction of the Four Petrological End Members of Alberta Oil Sands", was presented at the Oil Sands 2014 Conference, University of Alberta, Edmonton, April 28 -29, 2014.

M. Geramian, O. H. Ardakani, H. Sanei, T. H. Etsell, D. G. Ivey and Q. Liu, Nano and Micro-Sized Species in NonAqueous Bitumen Extraction from Alberta Oil Sands", COSIA/PTAC Oil Sands Clay Workshop and Conference April 28-29, 2015, Edmonton, Alberta.

4.1 INTRODUCTION

The oil sands deposit in Northern Alberta, Canada, consists of a significant resource of bituminous hydrocarbons, inorganic materials and water. The Alberta oil sands represent the third largest oil reserve in the world. The current commercial water-based processes are producing vast amounts of tailings, which is a major difficulty in recovering bitumen from the oil sands. The solvent-based bitumen extraction process is an alternative process and has been investigated since 1950, due to its high bitumen recovery and dry solids/tailings (gangue) [32,174–176].

The particle size distribution, mineral composition, residual organics and water chemistry influence the extraction process as well as settling and consolidation of the tailings [20,177]. The Alberta oil sands deposit can be described in terms of a mixture of four petrologic "end members", i.e., estuarine sand, estuarine clay, marine sand and marine clay. The mined ores in Alberta are a mixture of these four petrologically different types of rocks, which were deposited in marine and estuarine sedimentary environments. Thus, a profound understanding of these four petrologic end members/rocks will pave the way for a better perception of the entire deposit.

Alberta oil sands ores and their tailings ponds consist of quartz, feldspars, kaolinite, illite, chlorite, discrete smectite and mixed layer clay minerals [20,164,177–179]. Many scientists in the oil sands industry have reported that the coarse particles, i.e., quartz and feldspar, do not cause any problems during the bitumen extraction process, while nano and microsize clay minerals have negative effects on bitumen extraction, bitumen recovery and tailings treatment [16,17,20,37,164,180]. In addition to clay minerals, variable amounts of nanosized Fe-bearing minerals (oxyhydroxides/oxides), such as lepidocrocite, feroxyhyte, magnetite, hematite, wustite and amorphous Fe, and Ti and Al mineral oxides have been observed in Alberta oil sands deposits [21,34,38,181]. These species are the most likely minerals susceptible to interaction with bitumen, solvent and/or water and may contribute to unexpected behavior in bitumen extraction due to their high specific surface areas, high cation exchange capacities or redox activities, layer charges and specific physicochemical properties. Therefore, it is crucial to understand the mineralogical and physicochemical properties of nano and microsize minerals (particularly clay minerals), which can lead to improvements in both bitumen recovery and waste management.

Previous studies on the mineral composition of Alberta oil sands reported that the mineral composition varies across the deposits. The clay fraction (<2 μm) mostly contains kaolinite and

illite, with some chlorite, discrete smectite and mixed layer clay minerals [33]. However, some other researchers have not observed any discrete smectite or mixed layer clay minerals [189, 190]. Mixed layer clay minerals, i.e., illite-smectite and kaolinite-smectite, with low expandability (10 – 40% of the clay minerals) have been observed in Alberta oil sands [20,21,23,181]. The presence of smectitic clay minerals usually has an intense influence on the physical and chemical properties of soils and sediments due to their layer charge, large surface areas and swelling properties. The most important parameter of clay minerals is layer charge at their surfaces, which can be permanent or variable. The permanent charge at the surfaces usually occurs in the tetrahedral and octahedral sheets of clay minerals due to non-equivalent isomorphic substitutions. The variable charge, on the other hand, generally arises from the edges of clay particles due to the interaction of broken bonds and H^+ or OH^- at these locations.

Many researchers have extensively studied the mineral and chemical composition; however, there is limited information about the effect of these compositions on the surface properties of Alberta oil sands, i.e., cation exchange capacity, surface area and layer charge density [20,22,23,34,35,38,181,182]. The current chapter is focused on two main topics. The first topic is characterization of the minerals and the chemical composition of the four end members from the North Mine samples provided in 2009 (NM09) by Syncrude Canada Ltd. (Fort McMurray, Alberta). The second topic is to study the surface properties of the same set of samples to determine any correlation between surface properties, mineralogical composition and chemical composition of the petrologic end members of Alberta oil sands.

4.2 MATERIALS AND METHODS

4.2.1 MATERIALS

The current work was performed on the four petrologic end members collected from Syncrude Canada Ltd. in 2009 (North Mine, Fort McMurray, Alberta, Canada). These end member oil sands were deposited in marine and estuarine environments and are labelled as MC (marine clay), MS (marine sand), EC (estuarine clay) and ES (estuarine sand). The as-received (ASRE) samples were manually disaggregated, homogenized and kept frozen (–20 °C) in sealed plastic bags.

4.2.2 SAMPLE PRETREATMENT

The four petrologic end member samples were defrosted overnight at room temperature prior to use. The solids, water and bitumen from raw samples were separated by the Dean Stark (DS) extraction process [130]. Then the solids were isolated and separated into several size fractions (i.e., >45, 2 – 45, <2, 0.2 – 2 and <0.2 μm) using three techniques. The first technique was to collect the coarse fraction (>45 μm) from the solids by wet sieving in a Sepor sieve shaker, using distilled water. The second technique was to separate different size fractions (2 – 45 and <2 μm) by settling. The last technique was to isolate the <2 μm fraction into the two sub-size fractions (0.2–2 and <0.2 μm) by centrifugation of solids suspended in distilled water. The fine size fractions (<2, 0.2 – 2 and <0.2 μm) were then treated four times overnight with a 0.1 M solution of $CaCl_2$ to prepare the homoionic Ca^{2+}-exchanged form of clays [76]. In order to remove the extra soluble salt, these samples were washed by distilled water using centrifugation (at least three times) followed by dialysis. Each sample was dried at 60 °C overnight and ground gently in a diamond mortar prior to further analysis under laboratory conditions.

4.2.3 METHODS

To study the mineralogical and chemical composition, the original bulk samples and different size fractions from the four petrologic end members after bitumen removal were examined by XRD, FTIR, ICP-MS, elemental analysis (CHNS), CEC, LCD, SSA analysis, SEM and EDX spectroscopy.

In the current chapter, the layer charge of the oil sands is characterized and estimated by performing CEC and LCD measurements. The CEC is a quantification of the balance for negative charge sites of clay and consists of both permanent and variable charges [183]. The LCD is based on the molecular aggregation of organic dyes on the surface of clay minerals [126,129,136,184]. Quantitative data on the changes in the charge density are obtained from the interaction of organic dye with clay minerals, which can be identified from the absorption spectra [185].

The Vario MICRO cube elemental analyzer was performed to measure C_{tot}, H, N and S contents. For quantification of C_{org} content, sample was treated by phosphoric acid then followed by combustion at 1300 °C using a LECO carbon analyzer. The C_{inorg} was calculated from the difference between C and Corg, which both measured by a LECO carbon analyzer.

The SSA and the total specific surface area (TSSA) were identified by the Brunauer-Emmett-Teller (BET) and the methylene blue (MB) techniques, respectively. The BET technique uses an inert gas (i.e., helium, nitrogen, argon or krypton) to determine the external surface area of the particles including micropores, mesopores and macropores [112,113]. This technique is not able to identify the internal/interlayer surfaces due to inaccessibility of the inert gas. On the other hand, the TSSA can measure both external and internal/interlayer surfaces since the dye cations (i.e., MB) and polar molecules dissolved in water and water molecules are able to reach small pores and interlayer spaces [136]. The principles and/or the procedure behind the characterization techniques were explained in Chapter 2.

4.3 RESULTS

4.3.1 DEAN STARK ANALYSIS AND PARTICLE SIZE DISTRIBUTION

Table 4-1 shows the bitumen, solids and water contents of the bulk oil sands ores, which were identified by Dean Stark analysis. Except for ES, the solid contents were similar in the three other end members (MS, MC and EC). The bitumen and water contents clearly varied in all samples. The sand samples (MS and ES) had lower amounts of water and higher amounts of bitumen, while the clay samples (MC and EC) contained the relatively reverse amounts of water and bitumen (higher amounts of water and lower amounts of bitumen).

Table 4-1 Bitumen, solids and water contents of the bulk end members identified by Dean Stark analysis.

Sample	Bitumen (wt%)	Solids (wt%)	Water (wt%)
MS	8.1	90.6	1.3
MC	3.4	90.7	5.9
ES	16.6	82.1	1.3
EC	0.5	94.3	5.2

The particle size distribution (PSD) of the four petrologic end members is reported in Table 4-2 . The results clearly reveal the differences among these end members. MS and ES consist of

significantly higher amounts of the coarse fraction (>45 µm) and lower amounts of the finer fractions (2 – 45, <2 and <0.2 µm) compared with the clay end members.

Table 4-2 Particle size distribution of the four petrologic end members.

Sample	Size fraction (µm)				
	>45 (wt%)	2 – 45 (wt%)	<2 (wt%)	0.2 – 2 (wt%)	<0.2 (wt%)
EC	10.7	51.8	37.5	19.6	17.9
MC	33.4	46.9	19.7	6.9	12.8
ES	98.0	1.0	1.0	0.9	0.1
MS	80.9	11.4	7.7	6.4	1.3

4.3.2 X-RAY DIFFRACTION

Table 4-3 shows the mineral composition of the bulk samples and their size fractions identified using the RockJock procedure. The bulk samples were composed of quartz (52.3 – 94.5 wt%), 1.7 – 41 wt% of clay minerals (kaolinite, chlorite and 2:1 clays), 0.2 – 7 wt% of carbonates (calcite, dolomite and siderite), 2.7 – 3.9 wt% of K-feldspar and traces (<1 wt%) of TiO2 minerals (anatase and rutile). Figure 4-1 shows the XRD patterns of random preparations of the bulk samples with an internal standard (corundum) after Dean-Stark extraction. Sand samples (ES and MS) had higher amounts of quartz and lower amounts of clay minerals compared with the clay samples (EC and MC). The highest quartz content (88.5 – 94.7 wt%) was identified for the size fractions >45 µm for all samples. The clay mineral and quartz contents increased and decreased, respectively, with decreasing particle size fractions. The highest amounts of kaolinite (37 – 38.4 wt%) and 2:1 clay minerals (sum of discrete illite and illite-smectite) (55.1 – 64.9 wt%) were observed for the size fractions of 0.2 – 2 µm and <0.2 µm, respectively. QXRD for the fine size fractions of sand samples (MS and ES) was not performed by the RockJock procedure, due to insufficient material.

Table 4-3 Mineral composition of the bulk samples and their size fractions determined by RockJock procedure. Total 2:1 clays – the sum of illite and illite-smectite, DS – Dean Stark extraction.

Sample	Size fraction (μm)	Quartz	K-feldspar	Calcite	Dolomite	Siderite	TiO_2 minerals	Kaolinite	Total 2:1 clays	Chlorite
EC after DS	Bulk	52.3	2.7	0.0	0.3	3.0	0.7	14.4	25.3	1.3
	>45	89.3	3.3	0.0	0.1	0.5	0.2	3.3	3.3	0.0
	2–45	69.0	3.3	0.0	0.1	0.7	0.8	9.5	14.8	1.8
	<2	4.2	1.0	0.8	0.3	1.0	0.3	28.9	58.9	4.6
	0.2–2	6.9	0.6	0.0	0.2	0.1	0.3	37.0	52.6	2.3
	<0.2	1.2	0.9	1.3	0.3	1.1	0.0	21.4	64.9	8.9
MC after DS	Bulk	72.2	3.9	5.5	1.4	0.1	0.3	8.9	7.5	0.2
	>45	88.5	3.8	1.8	0.8	0.0	0.0	3.0	2.1	0.0
	2–45	55.2	4.6	9.5	2.8	0.4	0.1	14.2	10.9	2.3
	<2	8.2	0.0	13.8	1.2	0.4	0.0	30.4	40.8	5.2
	0.2–2	16.4	1.3	7.7	1.0	0.3	0.0	38.4	33.7	1.2
	<0.2	1.9	2.4	7.4	0.7	0.9	0.0	20.9	55.1	10.7
ES after DS	Bulk	94.5	3.6	0.0	0.1	0.1	0.0	0.8	0.7	0.2
	>45	94.7	4.0	0.0	0.1	0.1	0.0	1.1	0.0	0.0
	2–45	63.6	8.5	0.0	0.0	0.2	0.5	18.2	7.7	1.3
MS after DS	Bulk	87.0	3.7	1.4	0.8	0.3	0.2	4.1	2.5	0.0
	>45	93.2	2.8	0.4	0.4	0.3	0.2	1.5	1.2	0.0
	2–45	59.2	4.5	2.9	2.2	0.6	0.2	17.6	10.4	2.4
	<2	18.7	4.1	7.1	1.8	1.6	0.0	31.2	32.1	3.4

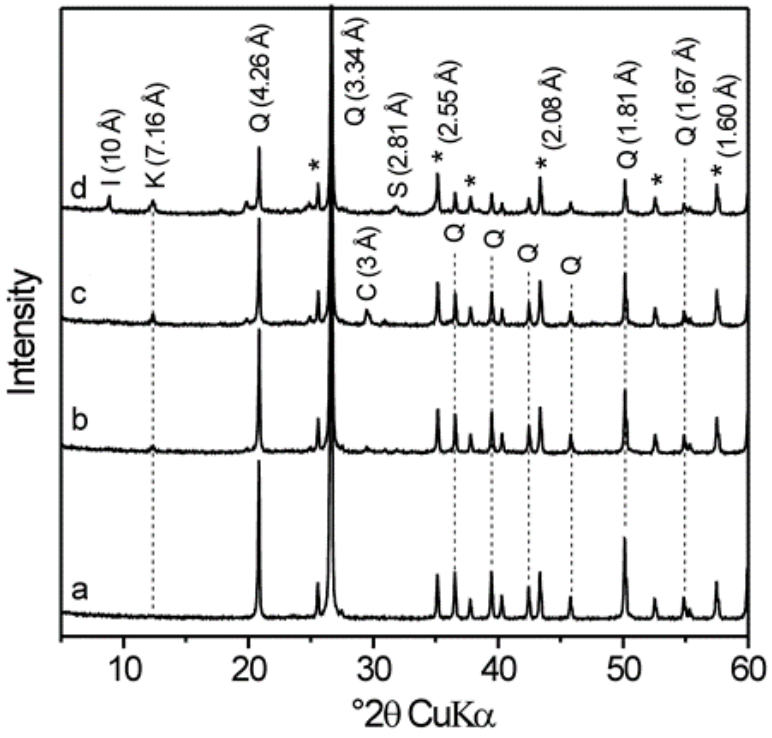

Figure 4-1 XRD patterns of random preparations of the bulk samples of (a) ES, (b) MS, (c) MC and (d) EC with an internal standard (corundum) after Dean-Stark extraction.

*I – illite; K – kaolinite; Q – quartz; C – calcite; S – siderite. * – corundum (internal standard).*

The XRD patterns of the oriented preparations for the fine size fractions (<2, 0.2 – 2 and <0.2 μm) were also obtained for detailed study of clay minerals. Figure 4-2 shows the XRD patterns of oriented preparations of EC (size fractions 0.2 – 2, <2 and <0.2 μm). The 001 and 002 reflections for illite and kaolinite were observed at d = 10 and 3.34 Å and d = 7.16 and 3.57 Å, respectively. These two clay minerals were the main minerals in the XRD patterns of the oriented preparations for the fine size fractions of all end members.

It was speculated that mixed layer clay minerals were present due to the weak shoulder near 12 Å on the left side of the discrete illite 001 reflection (d = 10 Å) (Figure 4-2). The shoulder near 12 Å of the basal reflection was increased and broadened by decreasing the size fraction from the <2 μm to the <0.2 μm fraction. Therefore, the presence of mixed layer clay minerals is more visible in the finer fractions. The presence of mixed layer illite-smectite can be distinguished and determined from the differences in the XRD patterns for the air-dried and ethylene glycol solvation oriented specimens. XRD patterns of an oriented specimen of the <0.2 μm fraction for EC after air drying-54%RH and ethylene glycol treatments are shown in Figure 4-3.

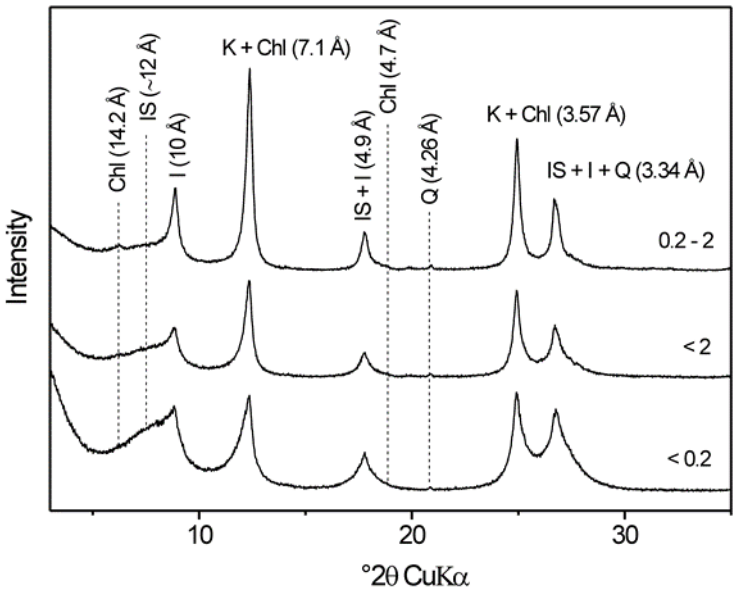

Figure 4-2 XRD patterns of oriented specimens of the fine fractions (0.2 – 2, <2 and <0.2 μm) for EC.

Chl – chlorite; IS – illite-smectite; I – illite; K – kaolinite; Q – quartz.

The procedures described by Moore and Reynolds and Środoń were applied to the <0.2 μm fractions of EC and MC [76,94]. Comparison of the XRD patterns of oriented preparations after these treatments showed that both clay samples consist of discrete illite and ordered illite-smectite with expandability of 9%. The kaolinite 001 reflection (d = 7.16 Å) without interstratification of expandable layers was identified due to lack of changes in intensity and position after ethylene glycol solvation (Figure 4-3). The weak reflection at d = 14.2 Å may be related to the presence of chlorite and/or vermiculite and was not correlated to smectite, because this reflection was not affected after ethylene glycol solvation in the oriented specimens. To verify the presence of chlorite and vermiculite, the homoionic K^+-exchanged form of the oriented specimen was prepared. Then, the sample was heated to 300 °C for 1h. Since there were no changes observed at the 14 Å basal spacing after this treatment, the presence of chlorite was confirmed. Vermiculite collapses from the 14 Å basal spacing to 10 Å after heat treatment. In addition, the reflections of some non-clay minerals such as calcite (d = 3.03 Å), dolomite (d = 2.89 Å) and siderite (d = 2.81 Å) and weak reflections of quartz (d = 4.26 and 2.12 Å) were observed in the XRD patterns of oriented preparations.

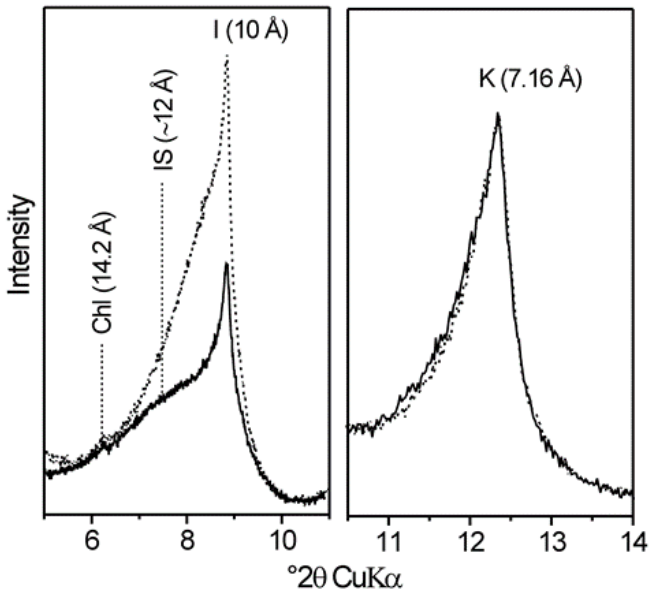

Figure 4-3 XRD patterns of oriented specimen of the <0.2 μm fraction for EC after air dried-54%RH (solid line) and ethylene glycol (dash line) treatments.

Chl – chlorite; IS – illite-smectite; I – illite; K – kaolinite.

4.3.3 FOURIER TRANSFORM INFRARED SPECTROSCOPY

Fourier transform infrared (FTIR) spectra of bulk samples and their size fractions are shown in Figure 4-4 and Figure 4-5, respectively. The four absorption bands in the 3700 – 3620 cm^{-1} range are related to AlAlOH vibrations of kaolinite [132]. The assigned absorption bands for the vibration of inner-surface OH groups are observed at 3697, 3669 and 3652 cm^{-1}. The OH-stretching band of illite near 3620 cm^{-1} overlaps with the two absorption bands (3697 and 3620 cm^{-1}) of kaolinitic vibrations. Therefore, the absorption band for illite at 3620 cm^{-1} has the same or even higher intensity as the absorption band at 3697 cm^{-1}.

Figure 4-4 shows three absorption bands in the 3000 – 2700 cm^{-1} range, which belong to the aliphatic CH groups of organic matter (i.e., bitumen) [159,186]. The two absorption bands at 2953 and 2853 cm^{-1} and one absorption band at 2925 cm^{-1} belong to the stretching vibration of CH_3 and CH_2 groups, respectively. The intense bands of the aliphatic CH groups are eliminated/significantly reduced after bitumen removal for all samples. The most intense bands of aliphatic CH groups are observed for ES before bitumen removal.

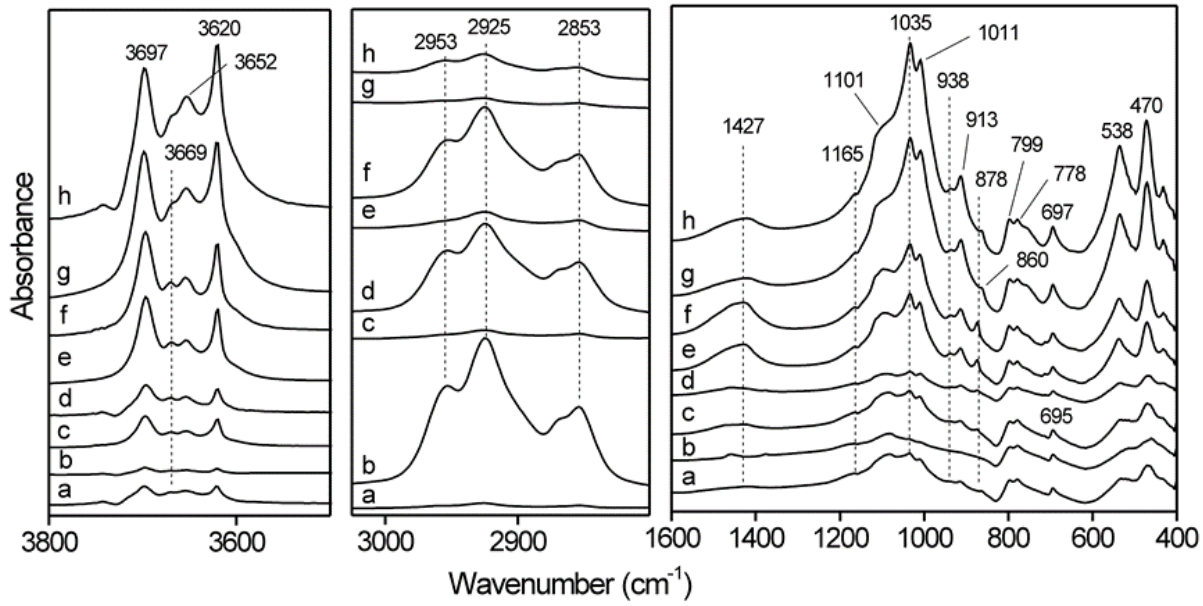

Figure 4-4 FTIR spectra for bulk samples before bitumen removal (b) ES, (d) MS, (f) MC, (h) EC and after bitumen removal (a) ES, (c) MS, (e) MC and (g) EC.

The absorption band near 830 cm^{-1} corresponds to the AlMgOH bending vibration of illite, which is only visible in the fine fractions (<2, 0.2 – 2 and <0.2 μm) of all samples (Figure 4-5) [187]. The stretching vibration of AlFeOH of the clay minerals is also visible and is displayed as a curvature near 3598 cm^{-1} in the spectra for the fine fractions (<2, 0.2 – 2 and <0.2 μm) for all end members (Figure 4-5) [188]. The bands near 1011, 1035 and 1101 cm^{-1} are assigned to Si-O stretching vibrations from the position of tetrahedral sheets for kaolinite. The absorption bands near 913 and 938 cm^{-1} correspond to the bending vibrations of the inner OH groups and the inner-surface OH groups of kaolinite, respectively. The assigned absorption bands for the bending vibration of Si-O-Al and Si-O-Si for kaolinite are displayed near 538 and 470 cm^{-1}. Furthermore, the absorption bands near 1427, 875, 860 and 713 cm^{-1} are related to carbonates [189,190]. The characteristic bands of quartz are observed near 1165 and 695 cm^{-1}. The intensity of absorption bands related to CH vibrations (3000 – 2700 cm^{-1}) is higher in the finer size fractions than those in the coarse fractions (not shown).

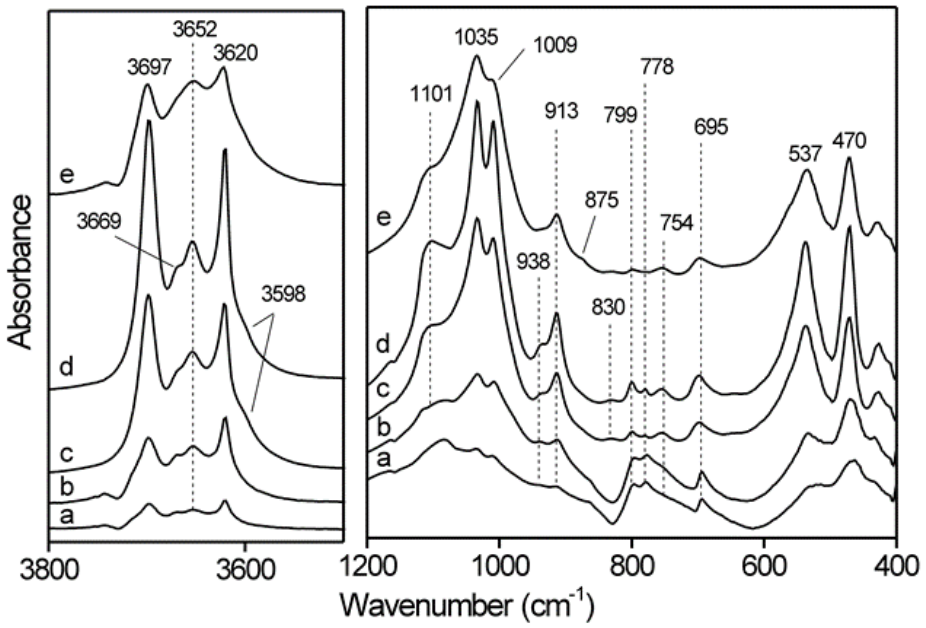

Figure 4-5 FTIR spectra for size fractions: (a) >45 µm, (b) 2 – 45 µm, (c) <2 µm, (d) 0.2 – 2 µm and (e) <0.2 µm for EC after bitumen removal.

4.3.4 INDUCTIVELY COUPLED PLASMA – MASS SPECTROSCOPY

The chemical compositions of the bulk end members and their size fractions after bitumen removal were characterized by inductively coupled plasma-mass spectroscopy (ICP-MS) and are reported in Table 4-4. Comparison of the bulk samples shows that there are clear differences between clay (MC and EC) and sand (MS and ES) samples. The amounts of Al, K, Na, Mg and Ti for the bulk clay samples (MC, EC) are higher than those for the bulk sand samples (MS, ES). The highest Ca content was detected for the marine samples (MC and MS). The highest amounts of K and Fe were detected for EC. Higher Al and K contents were observed in the fine size fractions (<2, 0.2 – 2 and <0.2 µm) compared with the coarse fractions (>45 and 2 – 45 µm). The amount of Na increased as the size fraction decreased, and the highest amount of Na was detected in the <0.2 µm for all clay samples (MC and EC).

Figure 4-6 Al content versus total clay minerals + K-feldspar content determined for bulk petrologic end members and their size fractions after bitumen removal.

Table 4-4 Chemical composition (in wt%) of the bulk petrologic end members and their size fractions characterized by ICP-MS. DS – Dean Stark extraction.

Sample	Size fraction (μm)	Al	Ca	Na	Mg	K	Fe	Ti
EC after DS	Bulk	6.49	0.22	0.27	0.40	1.44	2.61	0.38
	>45	2.13	0.08	0.10	0.10	0.86	0.89	0.15
	2–45	5.23	0.14	0.12	0.27	1.46	2.95	0.43
	<2	11.54	0.17	1.05	0.68	2.85	3.02	0.71
	0.2–2	10.23	0.26	0.15	0.54	2.70	2.86	0.85
	<0.2	9.76	0.37	1.34	0.64	2.45	3.61	0.52
MC after DS	Bulk	4.47	4.32	0.17	0.54	0.87	0.64	0.23
	>45	1.46	1.31	0.06	0.18	0.64	0.25	0.14
	2–45	4.35	5.78	0.09	0.62	1.07	0.82	0.34
	<2	7.39	7.71	0.29	0.76	1.35	1.05	0.41
	0.2–2	9.39	4.77	0.06	0.42	1.43	0.94	0.36
	<0.2	9.36	6.86	0.73	0.75	1.65	1.36	0.52
ES after DS	Bulk	0.60	<0.01	0.03	<0.01	0.47	0.05	0.03
	>45	0.77	0.01	0.04	0.01	0.67	0.06	0.04
	2–45	5.52	0.04	0.14	0.13	1.85	0.83	0.34
MS after DS	Bulk	1.46	1.16	0.08	0.20	0.55	0.55	0.09
	>45	1.35	1.30	0.05	0.22	0.70	0.85	0.09
	2–45	3.25	4.69	0.10	0.62	0.99	1.97	0.30

Similarly, Figure 4-7 displays the correlation between K content determined by ICP-MS and minerals consisting of K (i.e., total 2:1 clay minerals and K-feldspar) determined by QXRD for the bulk petrologic end members and their size fractions after bitumen removal. The results show that the amount of Al and K are raised by increasing the total clay minerals/total 2:1 clay minerals and K-feldspar content.

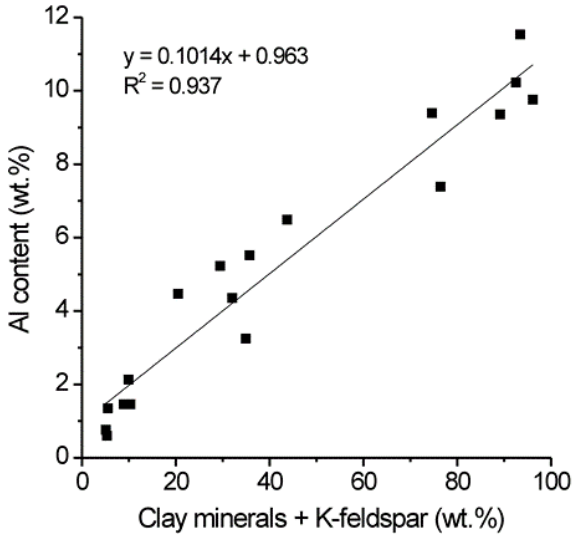

Figure 4-6 Al content versus total clay minerals + K-feldspar content determined for bulk petrologic end members and their size fractions after bitumen removal.

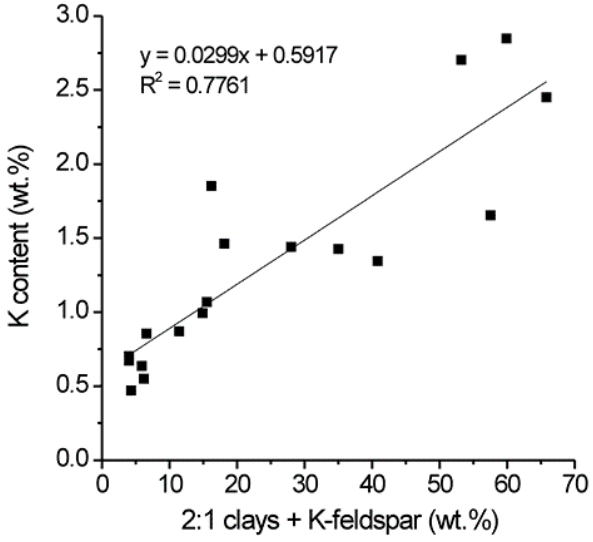

Figure 4-7 K content versus total 2:1 clays (sum of illite and illite-smectite) + K-feldspar content determined for the bulk petrologic end members and their size fractions after bitumen removal.

4.3.5 ELEMENTAL ANALYSIS

Table 4-5 shows the results of elemental analysis i.e., C (organic, inorganic and total), H, N and S contents for the four bulk end members (before and after bitumen removal) and their size fractions after bitumen removal.

Table 4-5 C (i.e., organic, inorganic and total), H, N and S contents (in wt%) of the bulk petrologic end members (before and after bitumen removal) and their size fractions after bitumen removal characterized by elemental analysis. C_{org} and C_{inorg} were measured and calculated by a LECO carbon analyzer, respectively. C_{tot}, H, N, S were measured by a Vario MICRO cube elemental analyzer. DS – Dean-Stark extraction.

Sample	Size fraction (µm)	C_{org}	C_{inorg}	C_{tot}	H	N	S
EC before DS	Bulk	-	-	2.032	0.579	0.178	0.124
EC after DS	Bulk	1.62	<0.01	1.615	0.514	0.198	0.094
	>45	0.59	<0.01	0.850	0.162	0.170	0.057
	2–45	1.24	<0.01	1.128	0.370	0.176	0.064
	<2	1.58	<0.01	1.545	1.155	0.423	0.121
	0.2–2	1.40	<0.01	1.770	1.149	0.436	0.075
	<0.2	1.77	<0.01	2.038	1.386	0.362	0.147
MC before DS	Bulk	-	-	8.753	0.935	0.425	0.641
MC after DS	Bulk	5.20	0.31	4.972	0.576	0.358	0.256
	>45	1.34	0.29	1.824	0.197	0.346	0.144
	2–45	4.61	1.47	6.642	0.670	0.382	0.349
	<2	5.78	1.60	7.625	1.092	0.465	0.445
	0.2–2	6.34	0.98	7.217	1.465	0.377	0.200
	<0.2	6.15	2.14	6.953	1.482	0.358	0.219
ES before DS	Bulk	-	-	13.465	1.696	0.408	0.813
ES after DS	Bulk	0.15	0.01	0.513	0.123	0.163	0.051
	>45	0.04	<0.01	0.080	0.042	0.148	0.027
	2–45	-	-	1.748	0.529	0.370	0.170
	<2	-	-	6.357	1.672	0.300	0.765
MS before DS	Bulk	-	-	8.415	1.025	0.395	0.616
MS after DS	Bulk	1.22	0.08	2.220	0.245	0.380	0.318
	>45	0.81	0.06	0.637	0.092	0.363	0.167
	2–45	3.54	0.84	4.305	0.562	0.360	0.786
	<2	-	-	6.735	1.487	0.480	0.756

C_{tot}, H, N and S contents were measured by a Vario MICRO cube elemental analyzer. C_{org} was measured by a LECO carbon analyzer. The total C was also measured by the LECO instrument. The C_{inorg} was calculated from the difference between the total C and C_{org}. Since two different techniques and instruments were used to measure the total carbon content, the sum of C_{org} and C_{inorg} (measured and calculated by LECO) were not equal to C_{tot} (measured by Vario MICRO cube), in some bulk samples and size fractions.

The amount of total carbon for the bulk samples before bitumen removal clearly varied between 2.0 to 13.4 wt%. The same bulk ores after bitumen removal contained 0.5 – 4.9 wt% carbon. This carbon mainly consists of toluene insoluble organic carbon due to the results of analysis of organic and inorganic carbon (Table 4-5). A high inorganic carbon content was detected in the finer fractions. The high inorganic carbon content was only observed for marine samples (MC and MS). The amount of inorganic carbon was higher in the finer fractions.

Except for the MC sample, for the three other samples the same evolution trend was detected for organic carbon and hydrogen contents. The toluene insoluble organic carbon and hydrogen levels were elevated in the finer size fractions. In the clay samples (EC and MC), the same trend for organic carbon evolution was detected after bitumen removal (Figure 4-8).

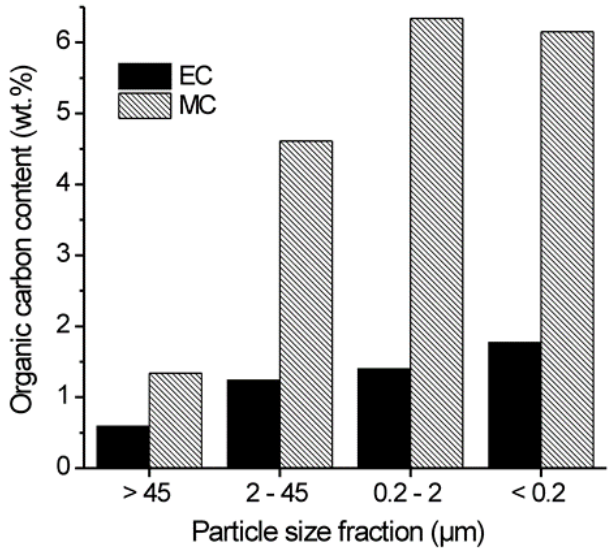

Figure 4-8 Distribution of organic carbon content in the different size fractions of clay samples (EC and MC) after bitumen removal.

Figure 4-9 shows the correlation between hydrogen and total clay mineral (sum of kaolinite, total 2:1 clays and chlorite) contents for the bulk end members and their size fractions after bitumen

removal. The lowest amounts of organic carbon, total carbon, hydrogen, nitrogen and sulfur were found for the >45 µm fraction in all samples.

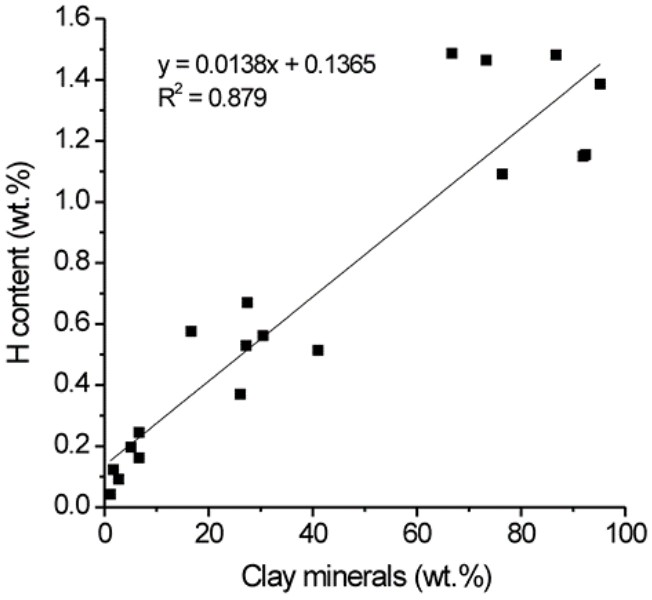

Figure 4-9 Correlation of H and total clay mineral (sum of kaolinite, total 2:1 clays and chlorite) contents determined for the bulk end members and their size fractions after bitumen removal.

4.3.6 CATION EXCHANGE CAPACITY

The CEC values determined by two techniques i.e., Cu_{TRIEN} and MB, are shown in Table 4-6. The comparison shows clear differences for the CEC values for the four bulk petrologic end members and their size fractions.

Higher CEC values were obtained using both methods for the bulk clay petrologic end members (7.1 ± 0.17 – 5.8 ± 0.20 meq/100g for Cu_{TRIEN} and 7.2 ± 0.40 – 6.5 ± 0.09 meq/100g for MB) compared with bulk sand petrologic end members (0.5 ± 0.14 – 3.1 ± 0.04 meq/100g for Cu_{TRIEN} and 0.4 ± 0.00 – 1.4 ± 0.27 meq/100g for MB). The CEC for the >45 µm fractions in all samples was the lowest value among the other fractions using both methods (i.e., 0.5 ± 0.14 – 3.5 ± 0.20 meq/100g for Cu_{TRIEN} and 0.4 ± 0.00 – 1.9 ± 0.07 meq/100g for MB). On the other hand, the highest CEC were identified in the <0.2 µm fractions for all samples (27.3 ± 0.25 – 30.7 ± 0.05 meq/100g for Cu_{TRIEN} and 33.0 ± 0.63 – 33.8 ± 0.71 meq/100g for MB).

Table 4-6 Cation exchange capacity (CEC) results determined by Cu_{TRIEN} (CEC-Cu_{TRIEN}) and MB (CEC-MB) techniques. Total surface area (TSSA) calculated using MB (TSSA-MB) technique and specific surface area (SSA) identified by the BET (SSA-BET) method for the four bulk petrologic end members and their size fractions.

Sample	Size fraction (µm)	Cation exchange capacity (CEC)		Surface area (SA)	
		CEC-Cu_{TRIEN} (meq/100g)	CEC-MB (meq/100g)	TSSA-MB (m^2/g)	SSA-BET (m^2/g)
MC	Bulk	5.8 ± 0.20	6.5 ± 0.09	51.0 ± 0.71	10.2 ± 1.04
	>45	3.5 ± 0.20	1.9 ± 0.07	14.6 ± 0.52	2.4 ± 0.09
	2–45	8.2 ± 0.42	3.5 ± 0.05	27.1 ± 0.38	5.2 ± 0.34
	<2	23.0 ± 0.25	14.2 ± 0.03	111.5 ± 0.27	15.3 ± 0.74
	0.2–2	17.3 ± 0.33	12.8 ± 0.14	99.9 ± 1.09	18.6 ± 0.06
	<0.2	27.3 ± 0.25	33.8 ± 0.71	264.6 ± 5.54	26.1 ± 6.53
EC	Bulk	7.1 ± 0.17	7.2 ± 0.40	56.7 ± 3.14	17.6 ± 0.40
	>45	1.1 ± 0.16	0.9 ± 0.01	7.0 ± 0.06	1.1 ± 0.02
	2–45	3.8 ± 0.08	3.4 ± 0.01	26.6 ± 0.04	7.5 ± 0.42
	<2	21.6 ± 0.09	19.6 ± 0.65	153.5 ± 5.07	50.7 ± 0.49
	0.2–2	13.5 ± 0.07	10.6 ± 0.05	82.7 ± 0.36	27.6 ± 0.71
	<0.2	30.7 ± 0.05	33.0 ± 0.63	258.6 ± 4.96	74.2 ± 0.15
MS	Bulk	3.1 ± 0.04	1.4 ± 0.27	10.8 ± 2.07	1.7 ± 0.80
	>45	2.8 ± 0.08	1.4 ± 0.04	10.7 ± 0.33	1.4 ± 0.09
	2–45	5.3 ± 0.21	1.7 ± 0.13	13.6 ± 1.04	2.3 ± 0.24
	<2	n.a.	11.5 ± 0.07	90.0 ± 0.52	23.3 ± 3.39
ES	Bulk	0.8 ± 0.11	0.7 ± 0.01	5.4 ± 0.05	0.4 ± 0.02
	>45	0.5 ± 0.14	0.4 ± 0.00	3.5 ± 0.04	0.2 ± 0.02
	2–45	2.1 ± 0.01	n.a.	n.a.	7.3 ± 1.41
	<2	n.a.	n.a.	n.a.	25.0 ± 1.15

The same trend was observed for the CEC values using both techniques (Cu_{TRIEN} and MB) as shown in Figure 4-10. The CEC values increased as the size fractions were reduced. For bulk and coarse fractions (>45 and 2 – 45 µm) of estuarine end members, there was good agreement between CEC values determined by Cu_{TRIEN} and MB techniques; however, small discrepancies were found for their fine fractions (<2, 0.2 – 2 and <0.2 µm). For marine samples, the discrepancies were identified for CEC values determined by Cu_{TRIEN} and MB methods in all fractions (with the exception of bulk MC).

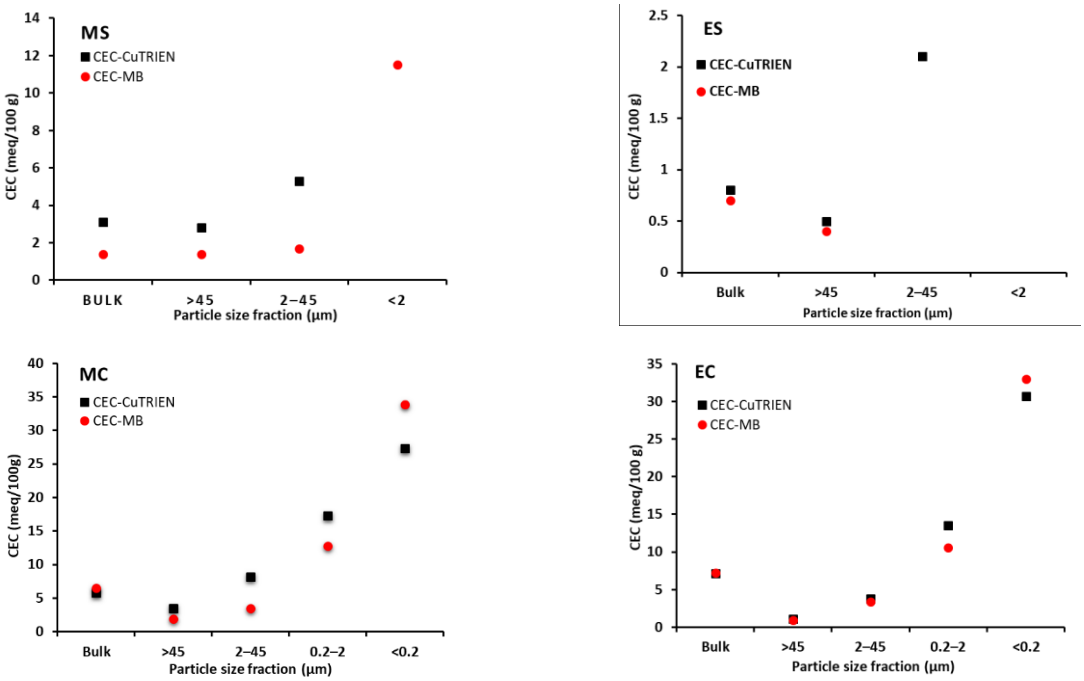

Figure 4-10 Cation exchange capacity (CEC) determined by Cu_{TRIEN} and MB techniques for bulk samples and their size fractions for the four petrologic end members.

4.3.7 SURFACE AREA

The total surface area and the specific surface area characterized by the methylene blue (TSSA-MB) and the BET method (SSA-BET), respectively, are summarized in Table 4-6. The bulk sand-rich petrologic end members (MS and ES) had lower surface area values using both the MB and BET techniques than those for the bulk clay-rich petrologic end members (MC and EC), which is likely due to the lower clay minerals content in sand bulk samples compared with clay bulk

samples. The same trend (increasing values) was found for both MB and BET techniques (Figure 4-11). The surface areas values (TSSA-MB and SSA-BET) were higher for smaller size fractions for all petrologic end members. The lowest surface area values occurred for the >45 µm fractions (3.5 ± 0.04 – 14.6 ± 0.52 m^2/g for TSSA-MB and 0.2 ± 0.02 – 2.4 ± 0.09 m^2/g for SSA-BET), whereas the highest were measured for the <0.2 µm fractions (258.6 ± 4.96 – 264.6 ± 5.54 m^2/g for TSSA-MB and 26.1 ± 6.53 – 74.2 ± 0.15 m^2/g for SSA-BET). Higher surface area values were measured by the MB technique (TSSA-MB) compared with the BET method (SSA-BET) for bulk samples and their size fractions for the four petrologic end members. In addition, the discrepancies increased with decreasing size fractions.

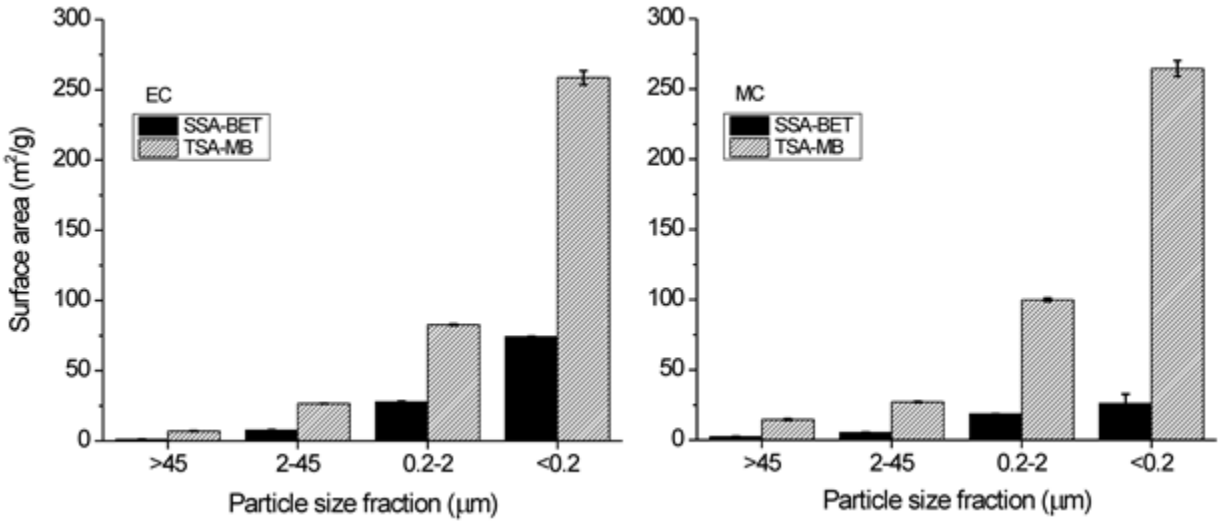

Figure 4-11 Specific surface area (SSA) characterized by BET (SSA-BET) and total surface area (TSSA) characterized by MB (TSSA-MB) for bulk samples and their size fractions of two clay-rich petrologic end members (EC and MC).

4.3.8 LAYER CHARGE DENSITY

R6G and MB dye cations were used to study the interaction between dye cations and the surface of clay minerals for bulk samples and their size fractions of the four petrologic end members using UV-Vis spectroscopy. The positions of the adsorption bands of dyes cations (R6G and MB) on the surface of clay minerals are summarized in Table 2-1.

Figure 4-12 shows the second-derivative spectra (SDS), which are calculated from the absorption spectra of R6G in dispersions of the fine size fractions (0.2 – 2 and <0.2 µm) of EC and MC. Three intensive bands at ~466, ~497 and ~535 nm are indicated for the SDS spectra of R6G in the dispersion of fine size fractions (0.2 – 2 and <0.2 µm) of EC and MC (Figure 4-12). Figure 4-13 shows the SDS calculated from the R6G absorption spectra in dispersions for the bulk and the coarse size fractions (>45 and 2 – 45 µm) of the four petrologic end members. A comparison of these figures shows obvious discrepancies between the R6G SDS for the fine (0.2 – 2 and <0.2 µm) and bulk and coarse (>45 and 2 – 45 µm) size fractions of the four petrologic end members (Figure 4-12 andFigure 4-13).

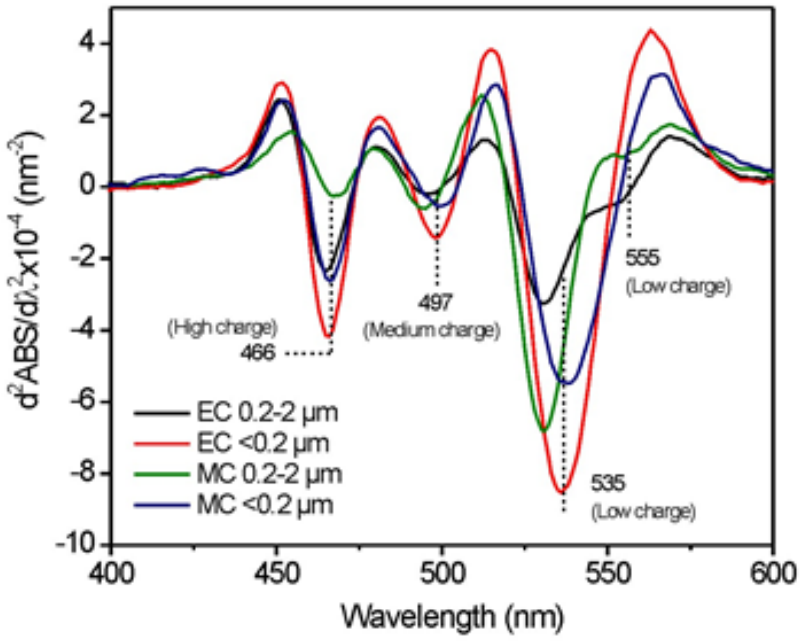

Figure 4-12 SDS calculated from the R6G absorption spectra for the 0.2 – 2 and <0.2 µm fractions of EC and MC.

The formation of H-aggregates (sandwich-type of dye cations) is displayed near the band at 466 nm; these are mostly created on the clay surfaces with high negative charges [191,192]. The band at ~535 nm is characteristic of monomers which are usually formed on the low charged layer sites. The band for H-dimers, which is preferentially created on the medium charged surfaces, was observed near 497 nm. Moreover, the formation of J-aggregates on the low charged sites is indicated as a small band shoulder near 555 nm in the R6G SDS spectra for the 0.2 – 2 µm size fractions of EC and MC [193]. A comparison between different fine fractions shows that the charged layer for the 0.2 – 2 µm size fractions of EC and MC is reduced relative to the <0.2 µm

size fractions, which shows up as a reduction in intensities for the band of H-aggregates near 466 nm along with the appearance of the J-aggregate shoulder near 555 nm in the SDS spectra of the 0.2 – 2 µm fractions of EC and MC.

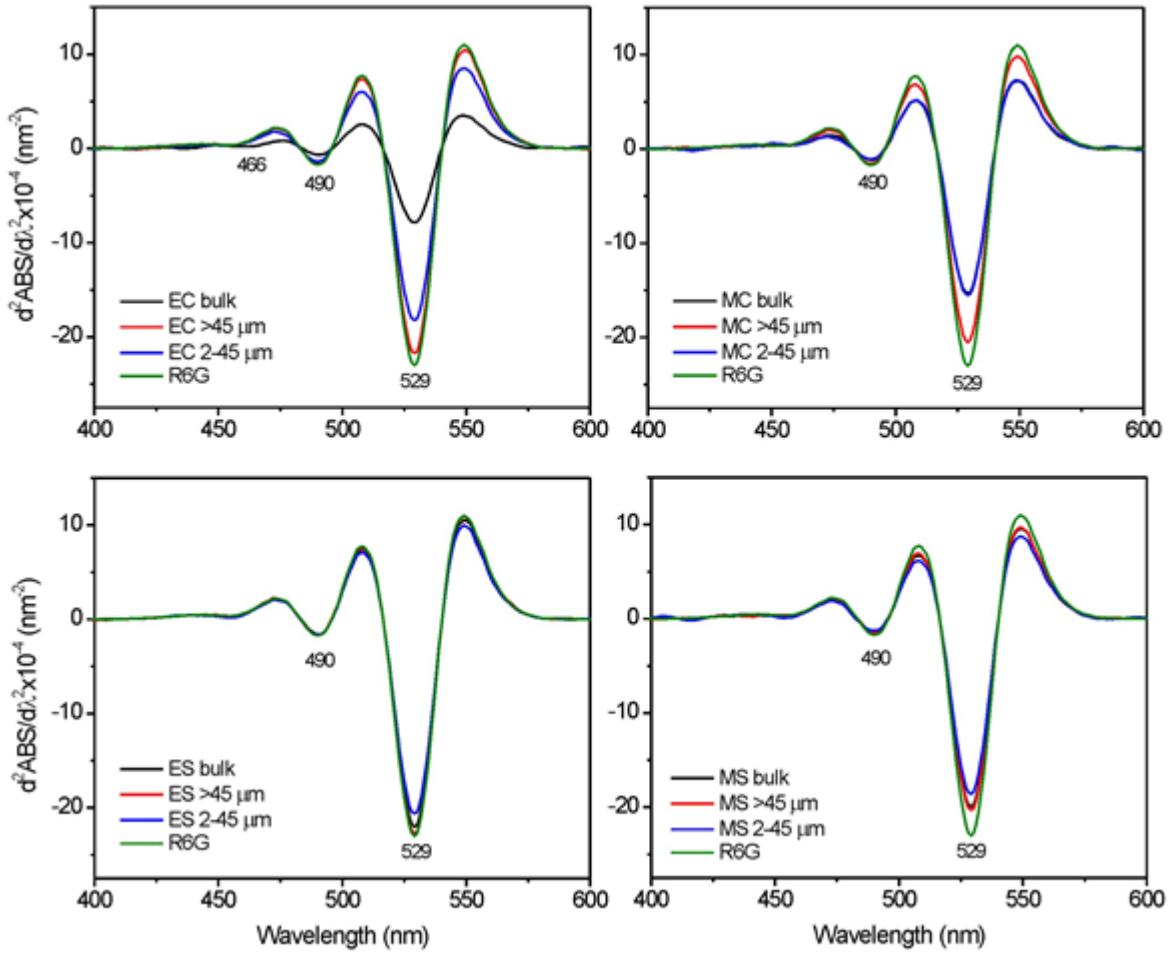

Figure 4-13 SDS calculated from the R6G absorption spectra in dispersions for the bulk and the coarse size fractions (>45 and 2 – 45 µm) of the four petrologic end members.

Except for the bulk EC sample, there was not any molecular aggregation of R6G in the dispersions of bulk samples and coarse fractions (>45 and 2 – 45 um) of the four petrologic end members. The intensity of the bands near 529 and 490 nm were only reduced in the R6G SDS spectra for bulk EC (Figure 4-13). The small inflection near 466 nm, which is related to the formation of H-aggregates, only appeared in the R6G SDS spectra for the bulk EC sample.

The SDS calculated from the MB absorption spectra in dispersions for the fine (0.2 – 2 and <0.2 µm) size fractions of the clay petrologic end members and the bulk samples, and the coarse (>45 and 2 – 45 µm) size fractions for all four petrologic end members are shown in Figure 4-14 and Figure 4-15, respectively. The comparison shows that the same correlations are observed for the R6G and MB SDS spectra in all bulk samples and their size fractions of the four petrologic end members (Figure 4-14 andFigure 4-15).

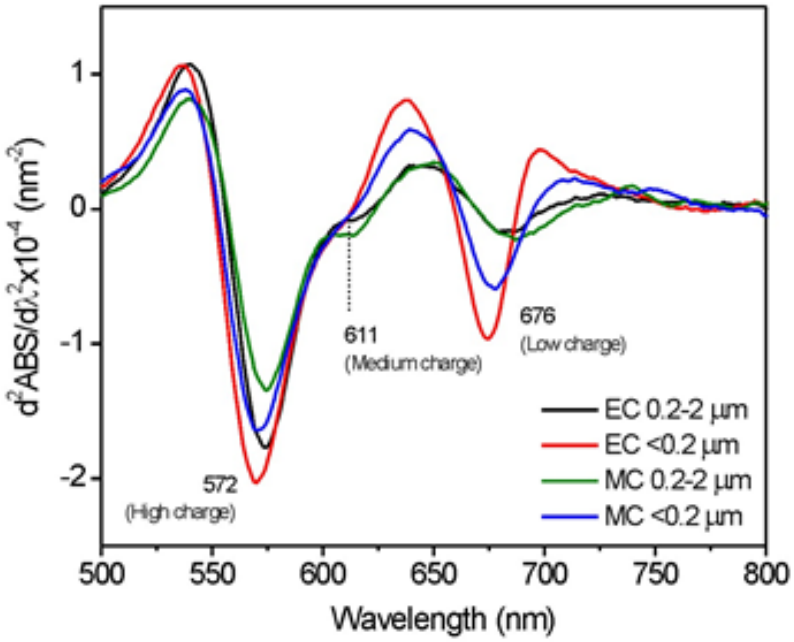

Figure 4-14 SDS calculated from the absorption spectra of MB in dispersions for the 0.2 – 2 and <0.2 µm size fractions of clay petrologic end members (EC and MC).

The two intense bands at ~572 and ~676 nm are related to the formation of H-aggregates (with highly negatively layer charged surfaces) and monomers (with low negatively layer charged surfaces), respectively, for the MB absorption spectra in dispersions of the fine (0.2 – 2 and <0.2 µm) size fractions (Figure 4-14) [194,195]. Moreover, the formation of H-dimers on the medium charged surfaces appears as a small inflection near 611 nm in the MB SDS spectra for the 0.2 – 2 µm size fractions of EC and MC. The lowest amounts of the monomers (~676 nm) and H-aggregates (~572 nm) are identified in the SDS of the 0.2 – 2 µm size fraction of MC, whereas the highest amounts of monomers and H-aggregates are found in SDS of the <0.2 µm size fraction of EC.

The molecular aggregation of MB was only observed for the bulk EC sample (Figure 4-15). The band at 577 nm, which is correlated with the formation of H-aggregates, was revealed in SDS of

MB for the bulk EC sample. A reduction in intensity of the bands near 667 and 608 nm occurs in the SDS spectra of MB for the bulk and the coarse size fractions (>45 and 2 – 45 µm) of all petrologic end members compared with the SDS spectrum of a pure MB solution (Figure 4-15).

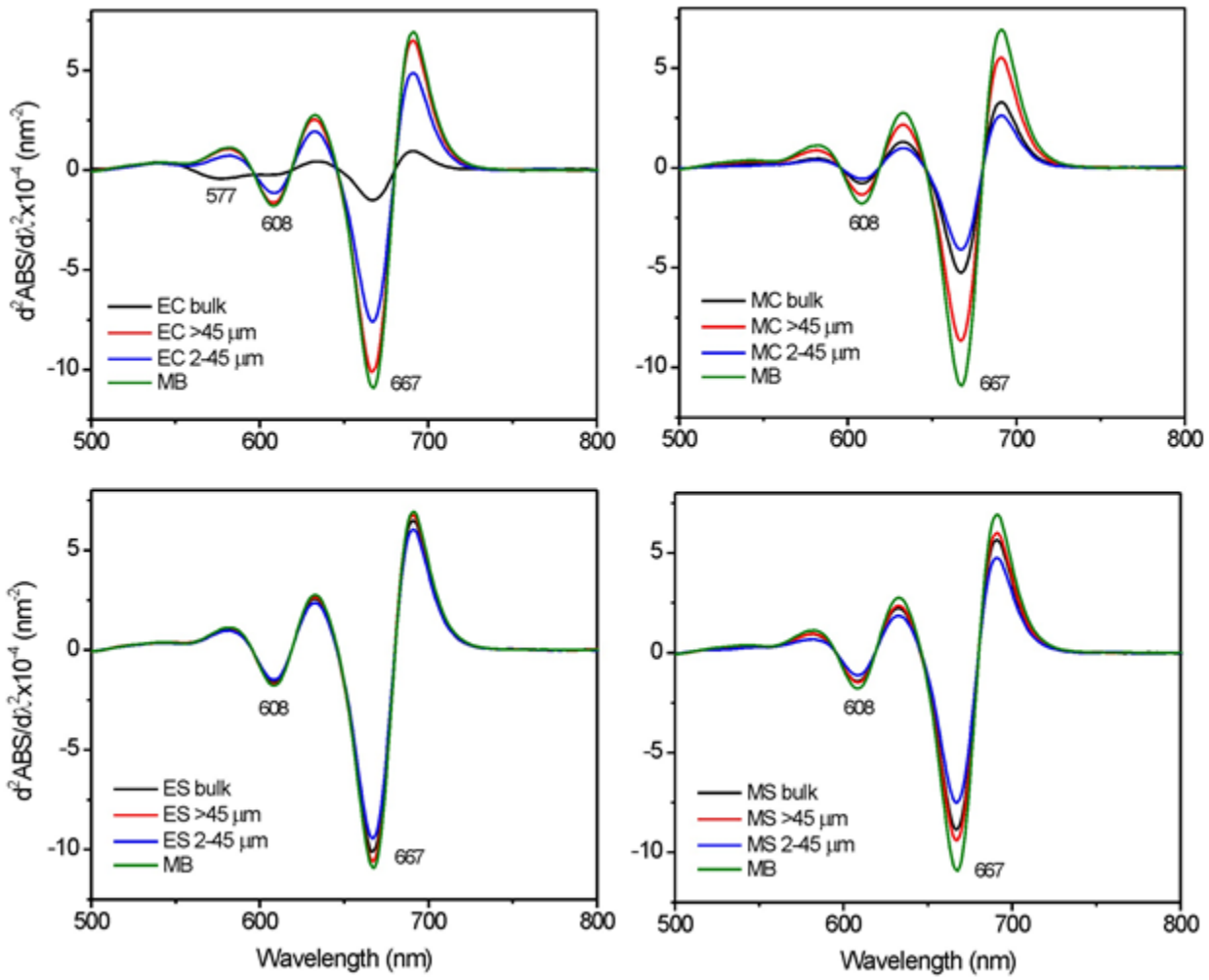

Figure 4-15 SDS calculated from the absorption spectra of MB in dispersions for the bulk and the coarse size fractions (>45 and 2 – 45 µm) of the four petrologic end members.

4.4 DISCUSSION

The bulk clay-rich end members (MC and EC) have low bitumen and high water contents, which is likely correlated to high clay fraction (<2 µm) content in these petrologic end members. This conjecture is in agreement with published data, which reported the reduction in bitumen content is

due to increased amounts of clay size fractions in the oil sands ore [196]. In addition, the high amount of water collected by the Dean-Stark extraction process can be related to the higher clay minerals content of clay-rich end members (Table 4-1). The higher water content in the clay-rich samples is correlated to removal of water from exterior surfaces as well as partial removal from interlayer surfaces in clay minerals, due to sample treatment with hot toluene during the Dean Stark extraction procedure. The high amount of bitumen (16.6 wt%) likely caused the low amount of solids in the bulk ES.

The total, organic and inorganic carbon in the bulk and their size fractions in the four petrologic end members are shown in Table 4-5. High amounts of inorganic carbon were present in the marine samples, which was correlated to carbonate minerals (i.e., calcite, dolomite and siderite). These results are in agreement with the QXRD data. Elevated toluene insoluble organic carbon was found in the finer fractions, which demonstrated the correlation between toluene insoluble organic carbon and the clay minerals (Figure 4-8). After bitumen removal, the >45 μm size fraction in all samples contained the lowest toluene insoluble organic carbon content for all fractions. The results indicate that bitumen was completely/mostly removed from the coarse size fractions (with a minimal quantity of clay minerals) by the Dean-Stark extraction process (the soxhlet extractor with hot toluene) relative to other fractions.

Figure 4-9 shows the correlation between hydrogen and clay mineral content. The presence of organic matter likely caused detection of hydrogen (~ 0.14 wt%) for samples with a lack of clay minerals. The presence of organic matter in the samples after Dean Stark extraction confirmed the increased amount of organic carbon (C_{org}) in finer size fractions (Table 4-5). The hydroxyl (OH) groups, water in the interlayer and on the exterior surfaces of clay minerals, and the residual organic matter after bitumen removal were the most relevant source assumptions for the presence of hydrogen in the oil sands samples.

According to Środoń *et al.* and Omotoso *et al.*, QXRD is unable to accurately quantify separate amounts of the 2:1 clay minerals in the mixture ores. Therefore, only the sum of 2:1 clay minerals is reported, which consists of discrete illite, smectite and mixed layer clay minerals [145,197]. The highest relative amount of mixed layer clay minerals was identified in the <0.2 μm size fractions using the XRD patterns of oriented preparations for oil sands samples (Figure 4-2).

Figure 4-6 and Figure 4-7 show a connection between the chemical (ICP-MS) and mineral composition (QXRD) of the oil sands. There were clear correlations between aluminum, potassium and mineral composition; however, the trend lines cross the potassium and aluminum axes at ~0.59 and ~0.96 wt% (instead of zero wt%), respectively, for zero amount of minerals (i.e., K-feldspars + total 2:1 clay minerals/total clay minerals). This may reveal the presence of amorphous and/or poorly crystallized Al, K-bearing phases, which cannot be identified by XRD and/or the heterogeneity of the end members. Kotlyar *et al.* found amorphous Al and Fe oxides in the clay size fractions from Alberta oil sands ores [198]. Moreover, it has been reported that Alberta oil sands deposit is highly heterogeneous in nature; thus, the deposit consists of a variety of mineral compositions. The trend lines also revealed that the aluminum and potassium contents are related to the higher K-feldspars and total 2:1 clay minerals/total clay minerals content in the samples.

The amount of sodium was elevated with increasing smectite and mixed layer clay minerals (illite-smectite) contents in the MC and EC samples. High amounts of siderite and calcite content are likely responsible for the higher iron content in EC and calcium content in the marine samples (MC and MS), respectively. The presence of TiO_2 minerals (anatase and rutile) are responsible for the titanium content in some fractions. The magnesium content is due to the presence of dolomite and chlorite minerals in the clay samples (MC and EC). The QXRD results are consistent with the ICP-MS data.

Although the sample/KBr ratio was fixed for all FT-IR pellets, the intensity of kaolinite absorption band at near 3697 cm^{-1} varied for different bulk end members, due to the variable kaolinite content (Figure 4-4). Russell and Fraser estimated the relative amount of kaolinite from the intensity of the absorption band at ~3699 cm^{-1} [158]. The highest and lowest relative amount of kaolinite were observed in the bulk samples of EC and ES, respectively, which is consistent with the QXRD data.

The absorption band near 3598 cm^{-1} correlates with the AlFeOH vibration in the IR spectra of the fine fractions, which assumes the presence of Fe^{3+} in the octahedral sheets of the clay minerals [188]. It is impossible to identify the type of clay minerals from the position of iron in the clay structure, due to the polymineral character of the oil sands ores, which consist of different types of clay minerals, i.e., illite, kaolinite, chlorite and illite-smectite. Each clay may contain structural iron.

Three absorption bands in the 3000 – 2700 cm^{-1} range in the IR spectra of oil sands after bitumen removal indicate the presence of residual toluene insoluble organics. The elevated amounts in the finer size fractions is in good agreement with the elemental analysis data.

Clear differences observed in the CEC values among the clay-rich (EC and MC) and sand-rich (ES and MS) petrologic end members, may be due to variations in mineral composition between these samples. The formation of negative charges and the ability to exchange the charge-compensating cations commonly create the CEC minerals. The clay minerals, particularly 2:1 clay minerals, have relatively high CEC values. Since these minerals have relatively large layer substitution and high negative charges in their structure, the compensating cations are mostly exchangeable. Non-clay minerals, i.e., quartz and feldspars, on the other hand, do not contribute to the total CEC values due to lack of exchangeable cations for charge-compensation. Therefore, the CEC values are mostly correlated to the swelling clay minerals content (i.e., smectite and illite-smectite) in the studied petrologic end members.

The CEC values increased with decreasing size fractions for all four petrologic end members, due to the higher clay minerals content, particularly total 2:1 clay minerals (Figure 4-16 and Table 4-3). The lowest CEC values were identified for the >45 μm size fractions, which are the quartz-rich size fractions with small quantities of 2:1 clay minerals. In contrast, the highest CEC values were observed for the <0.2 μm size fraction for clay samples (EC and MC) due to the high amount of 2:1 clay minerals. This conjecture is consistent with previous works showing that the type and amount of clay minerals are the two most important factors affecting the CEC values for the majority of sedimentary rocks [199–201].

Discrepancies were observed for the CEC values between the two techniques (i.e., Cu_{TRIEN} and MB); however, the most significant differences were identified for marine end members (MS and MC). Except for the CEC values for the <0.2 μm fractions of the clay samples (EC and MC), the CEC values determined by the MB method were generally lower than those by the Cu_{TRIEN} method. This result is in a good agreement with the observations of Hooshiar *et al.* [21], who reported lower CEC values obtained by the MB technique than those by the Cu_{TRIEN} technique for the primary froth of Alberta oil sands. The authors found a correlation between Fe content and elevated CEC values from the Cu_{TRIEN} technique. They also obtained the same CEC values from both techniques after Fe removal from the samples using the Jackson procedure (by sodium dithionite). A similar

outcome for the relative sensitivity of the Cu_{TRIEN} method in the presence of high Fe content was also determined by Grygar *et al.* [202].

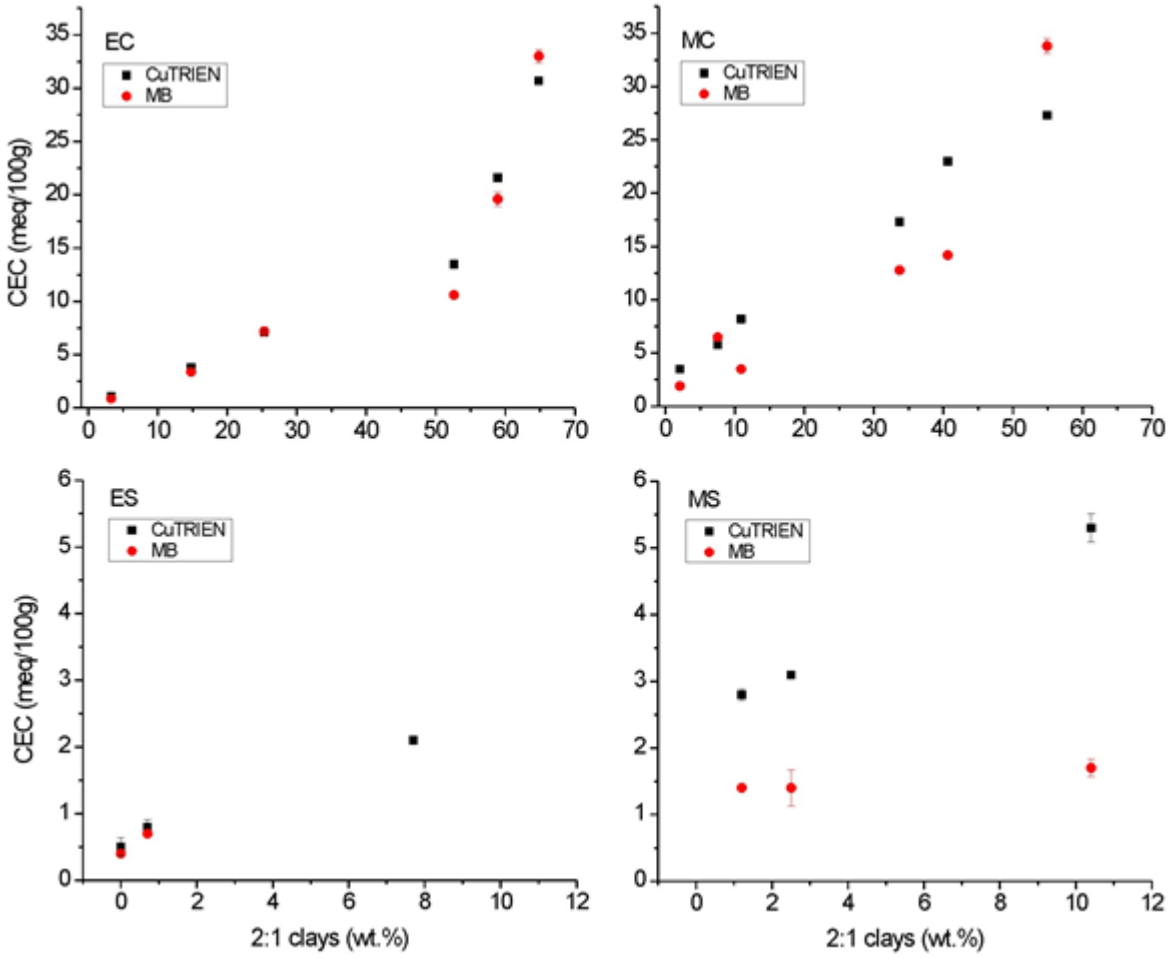

Figure 4-16 Correlation between CEC values determined by Cu_{TRIEN} and MB techniques and total 2:1 clay minerals content for different size fractions of the four petrologic end members.

The amount of total Fe identified in our previous study was significantly lower than that reported by Hooshiar *et al.* [21,203]. In addition, iron was found to be mainly bound in the structure of the clay minerals (mostly chlorite) and Fe carbonate (siderite) in the petrologic end members. The small amount of lepidocrocite (source of Fe oxyhydroxide) was identified only in the <2 µm size fractions of EC, ES and MS [203]. It was assumed that the influence of Fe on CEC values obtained by the Cu_{TRIEN} technique was negligible due to low amount of iron in the chlorite, carbonate and lepidocrocite minerals in the currently studied samples (Figure 4-17). Higher CEC values (CEC-

Cu_{TRIEN} and CEC-MB) and total Fe, total carbonates (sum of calcite, dolomite and siderite) and organic carbon (C_{org}-toluene insoluble organic carbon), along with a reduction in size fractions for clay end members (EC and MC), are observed in Figure 4-17. Significant discrepancies in the CEC values (CEC-Cu_{TRIEN} and CEC-MB) were identified for MC samples, which is related to the carbonate and toluene insoluble organic carbon (C_{org}) contents. The CEC values were more affected by C_{org} and carbonate contents than the Fe content in the studied petrologic end members (NM09).

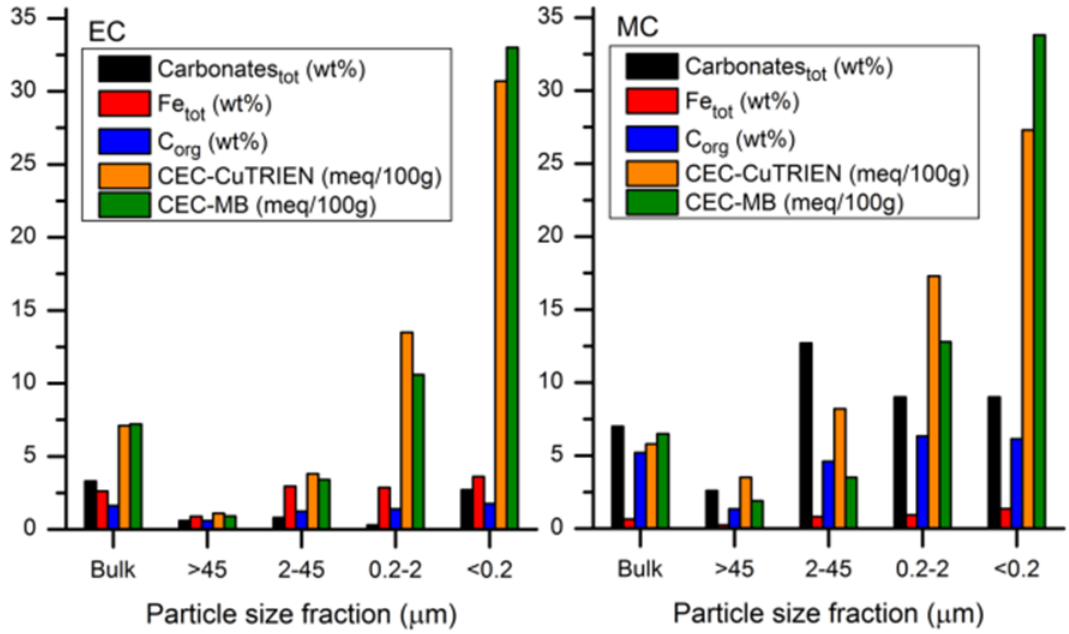

Figure 4-17 CEC values determined by CEC-Cu_{TRIEN} and CEC-MB compared with the amounts of carbonates (sum of calcite, dolomite and siderite), total Fe (Fe_{tot}) and toluene insoluble organic carbon (C_{org}) for the different size fractions of clay end members (EC and MC).

Previous studies by Dohrmann *et al.*, Derkowski *et al.*, and Kaufhold showed a similar relationship between carbonates and organic matter using CEC measurements [204,205]. The investigations revealed that other techniques for determination of CEC such as silver-thiourea, ammonium acetate, barium chloride, and Co(III)-hexamine can be also problematic due to the release of Ca^{2+} from carbonates during CEC measurements which influences the accuracy of CEC values. The elevation in Ca^{2+} content may lead to competitive cation exchange between the solution and the

clay sample, which can alter the initial exchange quantities on the negative charge of clay mineral surfaces [204,206] Therefore, significantly high CEC values will be obtained due to high Ca^{2+} concentrations, exchangeable Ca^{2+}, and the sum of exchangeable cations which lead to the excessive negative charge content [204,207,208].

Since the organic matter consists of a variety of functional groups, the surface can develop a negative charge, which is compensated by exchangeable cations. Particularly, terrigenous and marine humic compounds mostly contain CEC values equivalent to or greater than that of pure smectite due to the weak hydrogen bond on carboxyl and phenolic hydroxyl groups [209,210]. Moreover, underestimation of CEC values is possible in the presence of organic matter in samples due to the influence of absorbance for the CEC-Cu_{TRIEN} determination technique using ultraviolet-visible (UV-Vis) spectrophotometry [205].

The <0.2 μm size fractions of EC and MC show higher MB-CEC values than the CEC-Cu_{TRIEN} values, due to the presence of residual organic matter in these samples, which leads to excess adsorption of MB molecules on clay mineral surfaces. In oil sands industries, the CEC values are usually determined by the methylene blue (MB) technique; however, many scientists have stated that the accuracy of this method is not reliable, due to the selectivity for the type of exchangeable cations and extra adsorption of the dye cations [127,128]. Molecular aggregation on clay mineral surfaces causes the extra uptake of MB cations, which leads to slightly higher CEC values than those measured by other CEC methods [128,211].

There are some discrepancies in the CEC values obtained by Cu_{TRIEN} and MB, which may be due to different analytical principles, techniques and procedures. According to Kaufhold *et al.*, the mixture for the CEC-MB method is treated by H_2SO_4 solution [128]. Such a treatment causes a drop in the pH of the acidic solution, in which the negative charges of the functional groups on the edges of clay crystals are saturated by protons. Thus, MB molecules are only adsorbed on permanent charge sites and not on variable charge sites [128]. The adsorption of Cu_{TRIEN} complex molecules, on the other hand, is possible on sites with both charges (i.e., permanent and variable).

Figure 4-18 shows the correlation between surface areas determined by TSSA-MB and SSA-BET techniques and the total amount of 2:1 clay minerals for different size fractions of the four petrologic end members. A clear increase in the surface area (SSA-BET and TSSA-MB) with

increasing amount of 2:1 clay minerals and reducing size fraction for the four petrologic end members was observed (Figure 4-18).

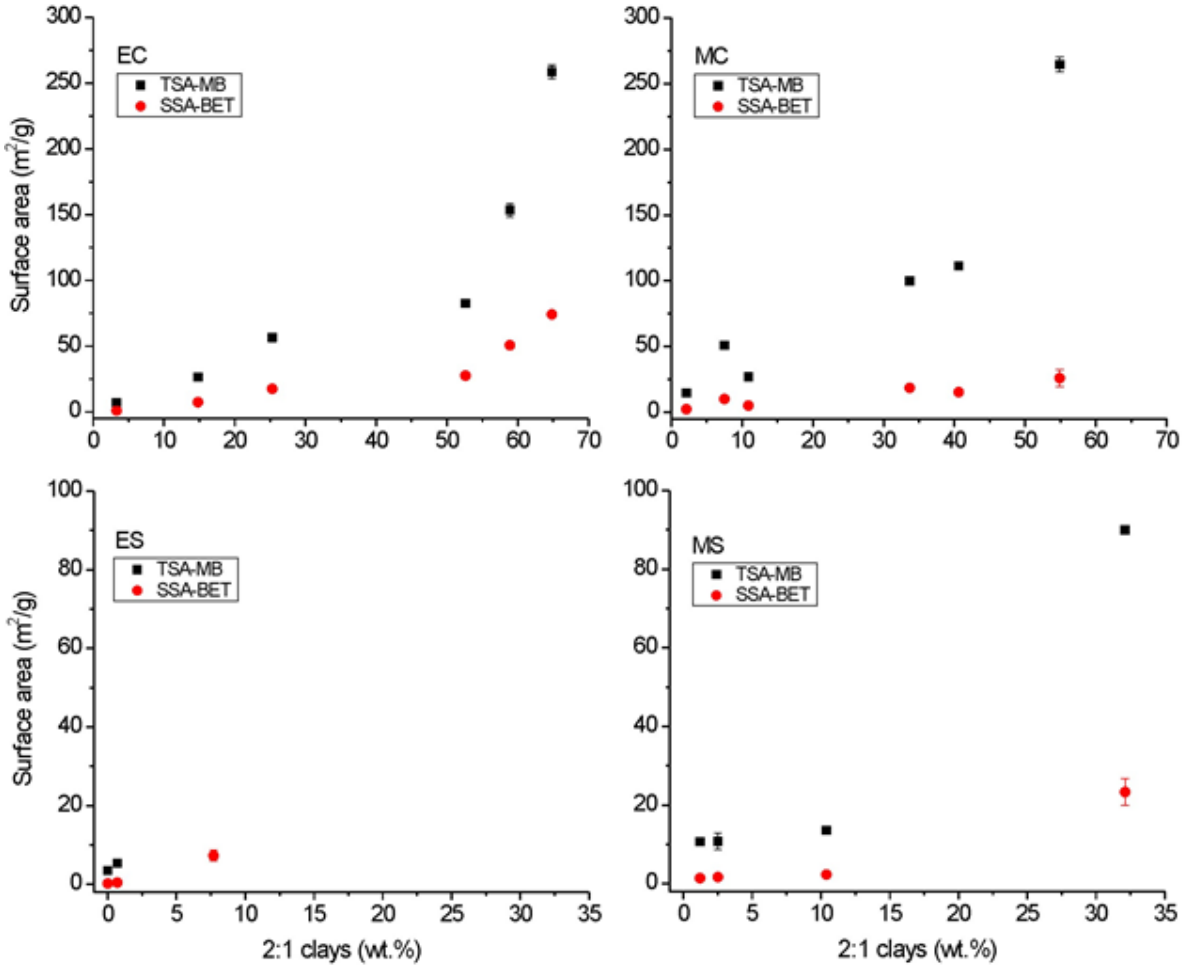

Figure 4-18 Correlation between surface areas determined by TSSA-MB and MB SSA-BET techniques and total amount of 2:1 clay minerals for different size fractions of the four petrologic end members.

There is also an interrelationship between the cation exchange capacity (CEC-MB and CEC-Cu_{TRIEN}) and the surface area (SSA-BET and TSSA-MB), in which the cation exchange capacity increases with higher surface area (Figure 4-19). This conjecture is consistent with published data, which has reported that cation exchange capacity and surface area are both interrelated and primarily controlled by the type and quantity of clay minerals present in the samples [199,200,205].

A comparison between the two techniques for measuring the surface area (TSSA-MB and SSA-BET) revealed that the total surface areas measured by the MB method (TSSA-MB) have systematically higher values than those values measured by the BET method (SSA-BET). The explanation seems to lie in different sample pretreatment and, in particular, different physical principles for determining the total surface area (TSSA) and specific surface area (SSA). The TSSA-MB technique measures the adsorption of methylene blue molecules on external surfaces of particles and on interlayer spaces of swelling clay minerals (illite-smectite and smectite). The SSA-BET method measures nitrogen adsorption in a vacuum at a temperature of 77 K on external surfaces of the particles. Nitrogen gas is not able to enter interlayer spaces of swelling clay minerals, since the swelling clay minerals are dehydrated with their interlayers collapsed in vacuum condition. Thus, nitrogen gas is mostly adsorbed by external surfaces of minerals [114,212,213].

Several scientists performed other techniques such as ethylene glycol monoethyl ether (EGME) to measure TSSA using polar organic liquid adsorption coefficients; however, the liquid reacted with the natural organic matter in the ore leading to artificially high TSSA values [114–117,205]. Although the accuracy of CEC values identified by the MB technique have been criticized by some researchers, the CEC-MB is more reliable than those determined by EGME, particularly for samples with organic-rich content [205]. Studies by Środoń, Derkowski and Bristow show that the EGME technique is not suitable for identification of TSSA when the amount of organic matter is more than 3 wt% [199,205]. Therefore, in the present study, the bitumen was removed from all petrologic end members by the Dean Stark extraction procedure to minimize the interference between analytical techniques and organic matter (i.e., bitumen) prior to measuring CEC, SA and LCD.

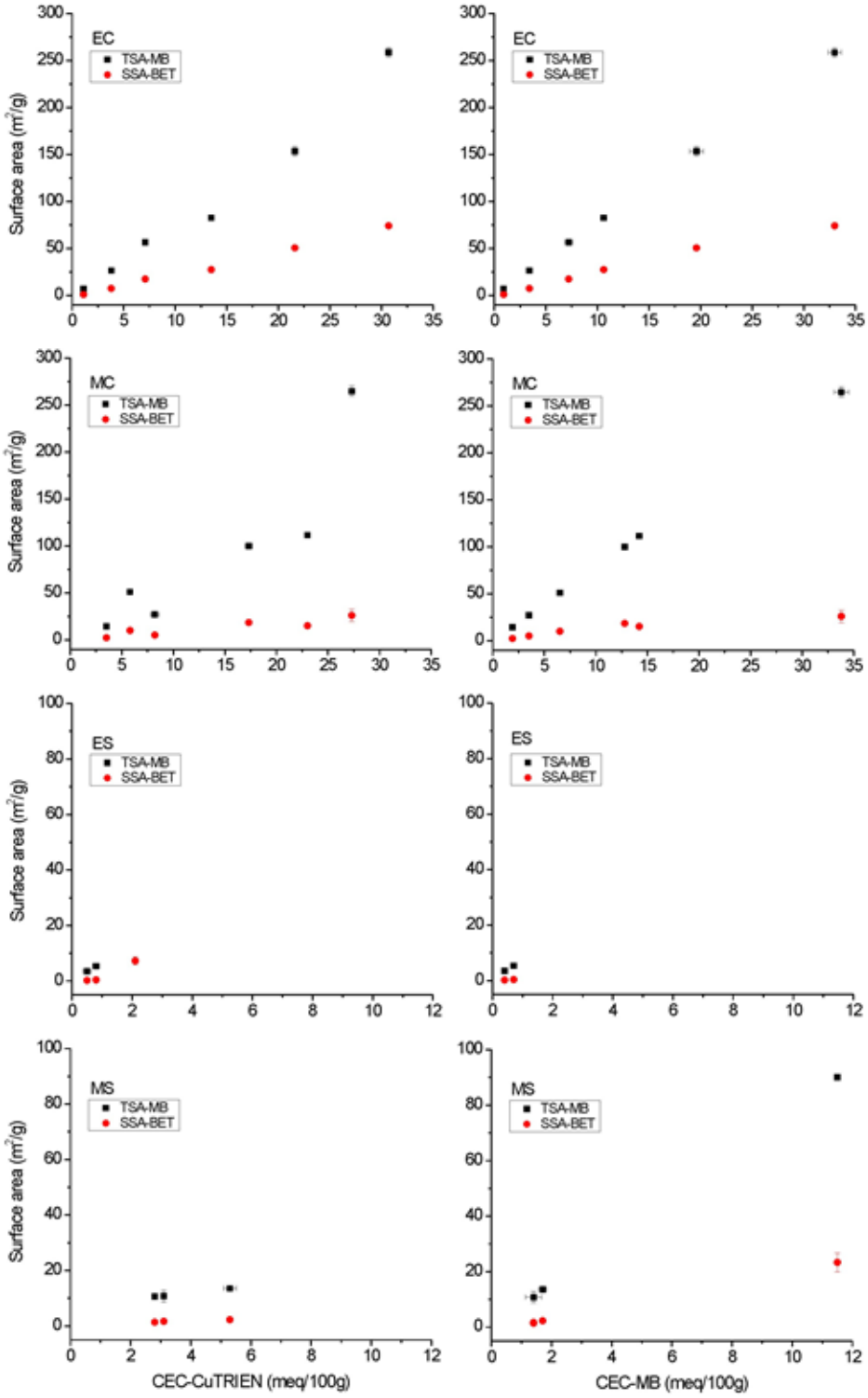

Figure 4-19 Correlation between surface areas determined by TSSA-MB and SSA-BET techniques and cation exchange capacity (CEC) measured by CEC-Cu$_{TRIEN}$ and CEC-MB procedures for different size fractions of the four petrologic end members.

Figure 4-20 shows the correlation between surface area (determined by TSSA-MB and SSA-BET methods) and toluene insoluble organic carbon (C_{org}) content for the different size fractions of clay-rich end members (EC and MC). The TSSA-MB and SSA-BET values increased with increasing amount of C_{org} for EC and MC samples. This finding is consistent with previous works, which showed that the amount of organic carbon in the ore is positively correlated to the SSA-BET values; however, the high organic matter content of the ore reduces the SSA-BET values [119,120,214]. The inaccessibility of organic matter and organic matter filled pores by nitrogen gas and/or the gluing of mineral particles to larger aggregates by organic macromolecules are the main possible reasons responsible for the lower SSA-BET values for organic matter-rich samples [117,215–217]. The lower SSA-BET values are related to the amount of organic matter adsorbed and type of mineral [214]. There was not observed any significant reduction of SSA-BET values in clay-rich petrologic end members (EC and MC), due to the low amount of C_{org} (negligible effect of C_{org} on SSA-BET values) and relatively high clay mineral content (Figure 4-20).

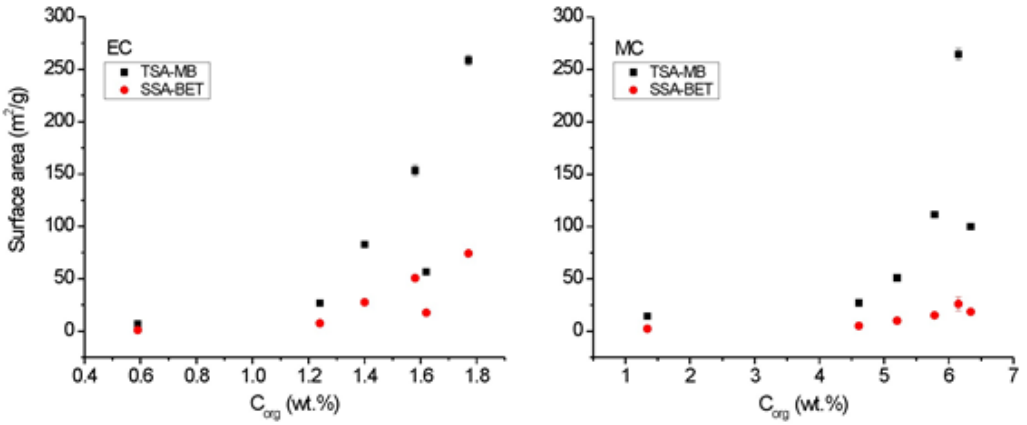

Figure 4-20 Correlation between surface area measurements (determined by TSSA-MB and SSA-BET) and toluene insoluble organic carbon (Corg) content for the different size fractions of clay-rich end members (EC and MC).

Correlations were observed among surface area (TSSA-MB and SSA-BET), particle size and mineral composition. The surface areas (TSSA-MB and SSA-BET) were elevated by decreasing and increasing the size fractions and the total 2:1 clays content, respectively (Table 4-6 and Figure

4-18). In other words, the quantity of swelling clays (mainly illite-smectite) was a more effective parameter than the C_{org} content in terms of affecting surface area in the fine size fractions of Alberta oil sands.

A lower intensity of H-aggregates in the SDS spectra for the dispersions of R6G and MB was observed for the 0.2 – 2 µm size fraction compared with the <0.2 µm size fraction of EC and MC (Figure 4-12 and Figure *4-14*). These results also indicate the highest layer charge for the finest (<0.2 µm) size fraction. Moreover, except for the bulk EC sample, the lowest negative layer charge was detected in the dispersions of the bulk and coarse fractions (>45 and 2 – 45 µm), with no observation of molecular aggregation of organic dye (R6G and MB). It is presumed that the distribution of the negative layer charge varied in the different size fractions of petrologic end members due to the amount of mixed layer clay minerals (illite-smectite). The highest illite-smectite content was found for the <0.2 µm size fractions, while the 0.2 – 2 µm size fraction mostly containing kaolinite (Table 4-3). The bulk and coarse size fractions (>45 and 2 – 45 µm) included only a small quantity of clay minerals. This result is also supported by the relation between the 2:1 clay mineral content and the variation of H-aggregates, which indicates the negative layer charge increased with increasing amount of 2:1 clay (mainly illite-smectite) content in the petrologic end members (Figure 4-21). This observation is consistent with previous studies, which indicate that the number of H-aggregates and the size of negative layer charge are directly related to the quantity of 2:1 clay minerals [126,136,211,218,219].

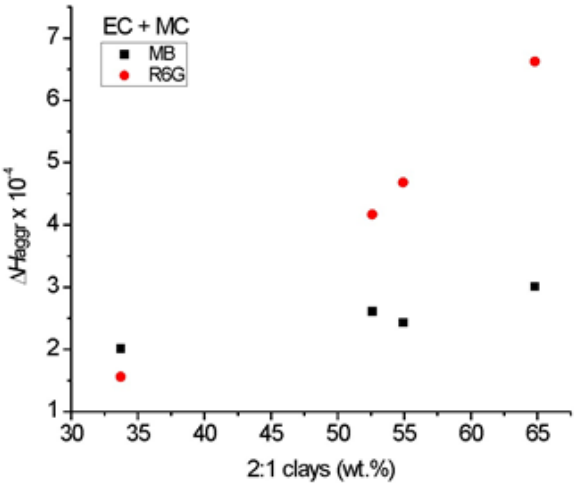

Figure 4-21 Correlation between the amplitude of SDS peaks related to H-aggregates and the quantity of 2:1 clays (sum of illite and illite-smectite) for the 0.2 – 2 and the <0.2 µm size fractions of EC and MC. ΔH_{aggr} displays the amplitude of the peaks at 466 and 572 nm of R6G and MB SDS spectra, respectively.

The SDS spectra of the bulk and coarse size fractions (>45 and 2 – 45 µm) of petrologic end members showed that the absorption of monomer sites (low layer charge density) of R6G and MB dye was found at near 529 and 667 nm, respectively. The quantity of monomers in the bulk and coarse fractions varied with the quantity of clay minerals (recall Figure 4-13 and Figure 4-15). This speculation was supported by the relationship among the 2:1 clays content and the amplitude of the peaks at 667 and 529 nm of MB and R6G SDS spectra, respectively, which indicates that the reduction in the number of monomers is related to the increasing amount of swelling 2:1 clays (illite-smectite) (Figure 4-22).

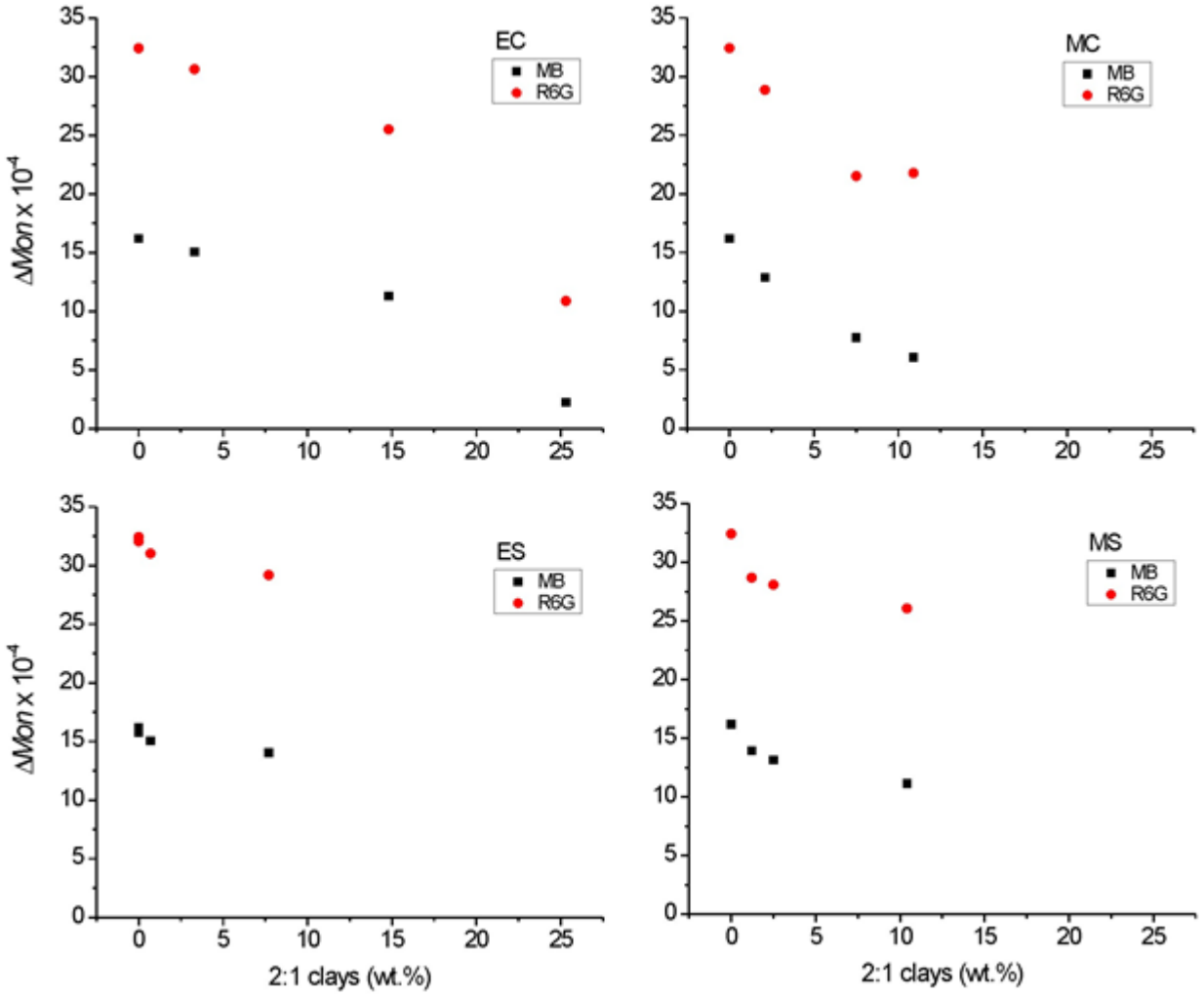

Figure 4-22 Correlation among the amplitudes of the SDS peaks related to monomers and the 2:1 clays content for the bulk and coarse fractions (>45 and 2 – 45 µm) of petrologic end members. Δ_{Mon} displays the amplitude of the peaks at 529 and 667 nm of R6G and MB SDS spectra, respectively.

Due to low amount of clay minerals, in particular swelling 2:1 clay minerals (illite-smectite), no H-aggregate sites (high layer charge position) were observed in the R6G and MB SDS spectra of the bulk and coarse size fractions (with the exception of bulk EC). The exception for bulk EC was due to the significant presence of the 2:1 clays (>25 wt%).

4.5 CONCLUSIONS

The four petrologic end members of Alberta oil sands, i.e., marine clays, estuarine clays, marine sands and estuarine sands, contain between 0.5 to 16.6 wt% of bitumen. The presence of 0.04 – 6.34 wt% of toluene insoluble organic carbon after bitumen removal was found in the four end members using elemental analysis (CHNS). The higher amount of toluene insoluble organic carbon with finer fractions was mostly due to its association with the clay minerals. Most of the bitumen was removed from the coarse size fractions during Dean-Stark extraction compared with the other size fractions due to a lower quantity of clay minerals in the coarse size fractions. The four end members of Alberta oil sands contained a different quantity of non-clay minerals, i.e., quartz, carbonates (calcite, dolomite and siderite), K-feldspar and TiO_2 minerals (anatase and rutile) and clay minerals such as kaolinite, illite, mixed layer illite-smectite and chlorite. The highest relative amount of mixed layer clay minerals was identified in the finest size fractions (<0.2 μm) using XRD analysis of oriented preparations. The expandability (S_{XRD}) of illite-smectite was about 9 %. Correlations were found among the mineral and chemical composition of the four petrologic end members.

Cation exchange capacity (CEC), layer charge density (LCD) and surface area (SA) values were characterized for the four petrologic end members of Alberta oil sands. The quantity and type of clay minerals present in the petrologic end members affected the surface properties (i.e., CEC, LCD and SA). The LCD (R6G and MB), SA (TSSA-MB and SSA-BET) and CEC (Cu_{TRIEN} and MB) values increased with increasing quantity of total 2:1 clay minerals, particularly with mixed layer clay minerals (illite-smectite). The CEC (Cu_{TRIEN} and MB) values increased with increasing the SA (SSA-BET and TSSA-MB) values.

Due to the different amounts of 2:1 clays, particularly interstratified illite-smectite, different layer charge distributions were found for the different size fractions of petrologic end members.

Correlation among the amount of 2:1 clays and the amplitudes of H-aggregates and monomers was found. A higher quantity of 2:1 clay minerals in a given fraction displayed larger numbers of H-aggregates, lower numbers of monomers and greater layer charge. Molecular aggregation in the SDS spectra of organic dye (MB and R6G) was only observed for the petrologic end members with more than 25 wt% of 2:1 clay minerals.

The highest SA (TSSA-MB and SSA-BET), CEC (Cu_{TRIEN} and MB) and LCD (R6G and MB) values were identified for the <0.2 μm size fractions of the petrologic end members, due to their highest relative amounts of illite-smectite. Higher SA, CEC and LCD values were determined for the fine size fractions of the petrologic end members, which is likely due to higher amounts of illite-smectite compared with other clay minerals in this fraction.

CHAPTER 5

5 CHARACTERIZATION OF FOUR PETROLOGIC END MEMBERS FROM ALBERTA OIL SANDS AND COMPARISON BETWEEN DIFFERENT MINES AND SAMPLING TIMES

The contents of this Chapter have been published in the Canadian Journal of Chemical Engineering.

M. Geramian, D. G. Ivey, Q. Liu and T. H. Etsell "Characterization of Four Petrologic End Members from Alberta Oil Sands and Comparison between Different Mines and Sampling Times" Canadian Journal of Chemical Engineering, (Published on 31st October 2017, DOI: 10.1002/cjce.23034).

5.1 INTRODUCTION

The oil sands in Canada are mostly located in northern Alberta in three deposits (Peace River, Athabasca, and Cold Lake), which are located in the McMurray area [220]. The Alberta oil sands, with 174 billion barrels of recoverable oil, represents the third largest oil reserve in the world [1,6]. Petroleum geologists believe that the origin of fossil fuels, i.e. conventional oil, natural gas, coal, and oil sands, occurred in the same way, when the organic matter died and was covered by layers of sediments for millions of years. The organic matter was subjected to sufficient pressures and temperatures to be altered into oil [85,220]. The oil sands mined in the Fort McMurray area belong to the stratigraphic unit called the McMurray Formation. It is divided into three different depositional paleoenvironments: fluvial, estuarine, and shallow marine, corresponding to the lower, middle, and upper intervals, respectively [221]. The estuarine and marine rocks are the two-main geological sub-units mined at the Syncrude site. The estuarine rocks are the most prominent intervals. The estuarine ore is a black bitumen-rich sand interbedded with a light laminated claystone, while the marine ore is a mixture of interbedded black sand and a very dark grey claystone [2]. The oil sands ore usually displays a combination of four petrologically different types of rocks called 'petrologic end members,' i.e. estuarine sand (ES), estuarine clay (EC), marine sand (MS), and marine clay (MC), which were deposited in two main sedimentary environments (marine and estuarine) [13]. The mined oil sands ores consist of these four end members in different proportions, which significantly affects the process-related properties of the oil sands [10]. As learned from previous studies, random sampling can be detrimental due to the heterogeneity of the oil sands [23,32]. Therefore, a better understanding of these end members will help considerably in interpreting the behavior of the entire ore deposit as well as the bitumen quality during either an aqueous or non-aqueous extraction process.

The oil sands are primarily a mixture of bitumen (4–18 wt%), inorganic materials, i.e. non-clays and clay minerals (55–80 wt%), and salty water (2–15 wt%) [2]. The oil sands deposit in Alberta displays a high variety of mineral compositions [2,10]. Many researchers in the oil sands industry have reported that the coarse particles do not have any negative effects during bitumen extraction. Recent studies have shown that quartz and carbonates are usually the main non-clay minerals and kaolinite and illite are the major clay minerals in Alberta oil sands. Low quantities of chlorite, smectite, and mixed-layer clay minerals have also been reported in Alberta oil sands

[4,10,20,21,203]. Although smectite and mixed layer clay minerals, i.e. illite-smectite and kaolinite-smectite, are present in low amounts, they can significantly affect the bitumen extraction process and tailings management [4,19]. Mercier *et al.* demonstrated that clay minerals play the main role in the water-based bitumen extraction process [22]. Clay minerals have a negative influence on the bitumen extraction process, bitumen recovery, and waste management due to their small particle size, high specific surface area, swelling capacity, cation exchange capacity, and layer charge properties. The various types of clay minerals may have different effects on the processability of oil sands ore during the bitumen extraction process. Wik *et al.* also showed that the small particles and the mineralogical compositions are the two most important parameters which affect the bitumen extraction processes as well as bitumen recovery [19]. It has also been reported that montmorillonite and kaolinite have negative effects on aqueous bitumen extraction [8]. Both extraction recovery and product quality are significantly affected by interactions between organic materials (i.e. bitumen, asphaltene, and kerogen) and clay minerals. These interactions produce clay-organic matter complexes which make the bitumen extraction process more complicated [23]. Therefore, it is crucial to understand the influence of water, bitumen, and solids, particularly nano- and microsize species, on the extraction process [11].

There is virtually no knowledge about the processability of different petrologic end members during non-aqueous bitumen extraction. Detailed analysis of the compositions of the petrologic types and the suspended fine solid content in the bitumen product after non-aqueous extraction are necessary in order to interpret the "non-aqueous processability" of the end member rocks. The goal of the present Chapter is to characterize the four end members in order to determine and better understand the most important species affecting non-aqueous bitumen extraction and bitumen quality. In this Chapter, the results from the current study are reported and compared with those published in our previous work, which characterized both the mineralogical and chemical composition of the petrologic end members of Alberta oil sands that were collected during September 2009 (NM09) [10,203]. Comparison of these papers shows the heterogeneous nature of the Alberta oil sands, due to either different mine locations or when the ore was mined. The effect of oil sands composition on bitumen quality during non-aqueous bitumen extraction is reported in Chapter 7.

5.2 MATERIALS AND METHODS

5.2.1 MATERIALS

Four oil sands ores mined in the Fort McMurray area, collected by Syncrude Canada Ltd. from the North Mine in November 2012 (NM12), were used in the current study. Each mined ore was essentially a sample of one of the four petrologic end members, namely: estuarine sand (ES), estuarine clay (EC), marine sand (MS), and marine clay (MC) [10,203]. The sands and clays were manually separated from the as-received (ASRE) samples, disaggregated, and passed through a sieve (aperture size of 6.3 mm, according to ASTM E.11). Then, each end member sample was homogenized, wrapped with two plastic zipper bags, stored in sealed containers, and kept frozen at –20 ℃ to avoid/stop any weathering degradation [222]. The solvent used for this study was toluene, which was purchased from Fisher Scientific, Canada and certified as ACS grade.

5.2.2 EXPERIMENTAL PROCEDURE

Figure 5-1 shows the methodology for collecting the different size fractions and ore characterization. The prepared samples were defrosted for 24 h at room temperature (20–25 °C) in sealed containers and then used for subsequent analysis.

The solids, bitumen, and water contents for all four as-received (ASRE) petrologic end members were separated and measured by the Dean-Stark (DS) extraction method [173]. Then each solid after bitumen removal was mixed with distilled water (1:5 ratio) and treated in an ultrasonic water bath for 20 min. The particle size fractions were collected by using different methods. First, the >45 μm and <45 μm fractions were separated by wet sieving using a 45 μm aperture sieve and a vibrating Sepor sieve shaker. Then the 2–45 μm, <2 μm, 0.2–2 μm, and <0.2 μm fractions were separated from the <45 μm fraction by centrifugation. The particle size diameter from centrifugation was calculated by Stokes' Law. The samples were dried overnight at 60 °C and ground gently in an agate mortar. The original bulk samples and all fractions of the four petrologic end members after bitumen removal (Dean-Stark) were characterized (see Figure 5-1).

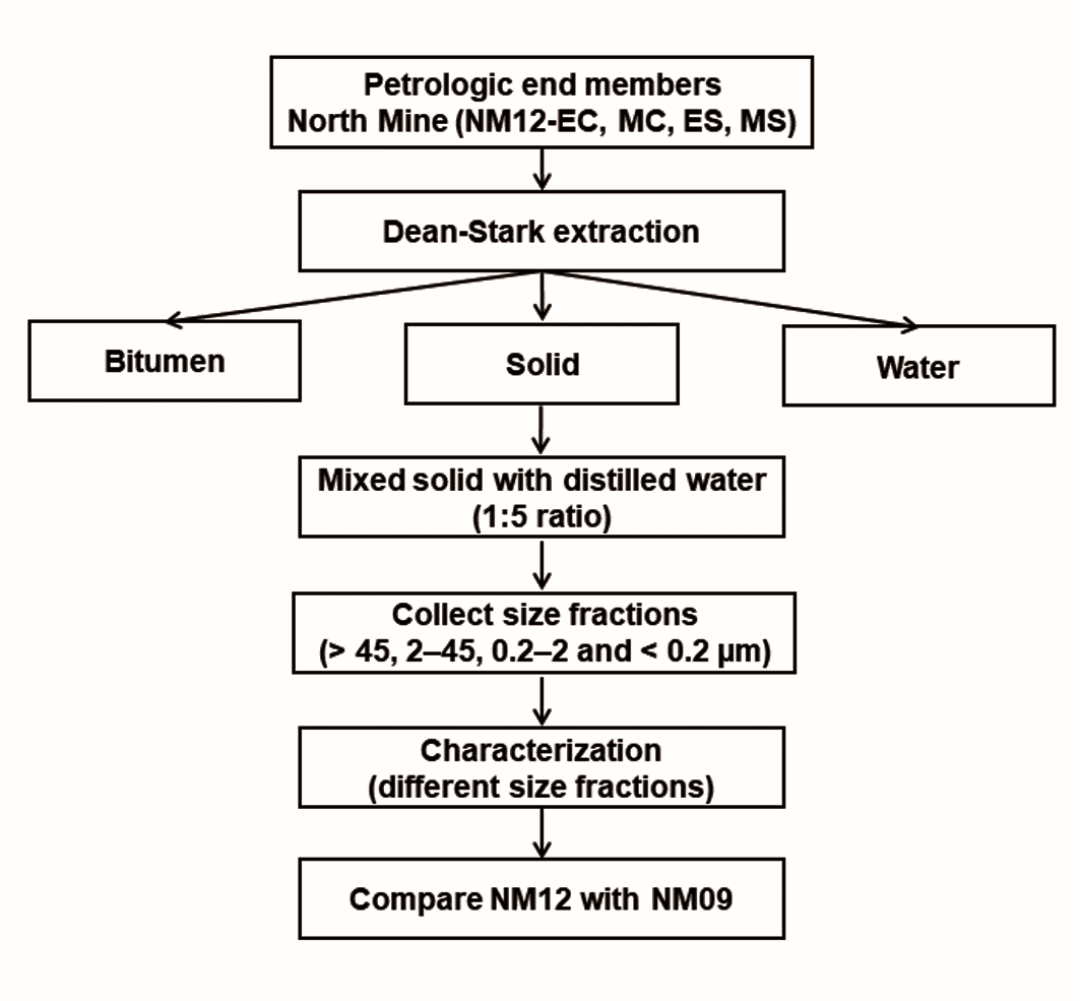

Figure 5-1 Schematic experimental setup for mineralogical and chemical composition characterization of the four petrologic end members [223].

5.2.3 ANALYTICAL METHODS

5.2.3.1 X-RAY DIFFRACTION

X-ray diffraction (XRD) patterns were measured for oriented and random preparation specimens using a Rigaku Ultima IV diffractometer, operating at 44 mA and 40 kV, with a graphite monochromator and Cu Kα radiation. The step size for both preparations was 0.02° 2θ and the exposure time was 2 s per step. Frosted glass slides were used for oriented preparation samples by fully dispersing a suspension of clay fractions (90 mg) in distilled water (approximately 1.2 mL)

using a small glass bottle (8 mL). In order to disperse the clay particles in distilled water, the suspension was stirred for 5 min using a small magnetic stirring bar (Teflon^{TM} coated-PTFE, 2 mm in length and 2 mm in diameter) and sonicated in an ultrasonic bath for 5 min. The suspension was transferred by a plastic pipette onto a frosted glass slide (2.8 × 2.8 cm) and left at ambient conditions to dry. According to the procedure described by Moore and Reynolds [76], the dried glass slides were saturated first at 54 % relative humidity and then with ethylene glycol (EG) prior to XRD analysis after each treatment [76]. The specimens were run from 2θ = 3º to 2θ = 60º. The expandability of kaolinite-smectite and illite-smectite were identified by comparison of XRD patterns of oriented preparations after these treatments according to the procedures described by Moore and Reynolds, Środoń, and Dudek *et al* [76,94,95].

The Środoń procedure was performed to measure the following criteria to identify the expandability and the type of interstratification (ordering) of illite-smectite [94]:

(i) The position of the low-angle reflection illite-smectite (between 6–8° 2θ) of the glycolated specimen.

(ii) The intensity ratios (Ir) of the 001 and 003 reflections peaks for air dried-54 % relative humidity and after ethylene glycol solvation specimens [94]:

$$Ir = \frac{(001/003)\ air\ dried}{(001/003)\ glycolated} \qquad \textit{Equation 5-1}$$

Ir is the most effective tool for identification of trace expandable clay minerals. If Ir equals 1.0, the specimen is 100 % discrete illite. On the other hand, the presence of expandable clay minerals is obvious when the Ir parameter exceeds 1.0.

(iii) The joint broadness of 001 illite and adjoining illite-smectite reflections where the peaks' tails reach the X-ray background (measured in 2θ) for the ethylene glycol solvation specimen, named BB1.

(iv) The joint broadness of 004 illite and adjoining illite-smectite reflections where the peaks' tails reach the X-ray background (measured in 2θ) for the ethylene glycol solvation specimen, named BB2 [94].

BB1, BB2, and the position of the low-angle reflection illite-smectite (between 6–8° 2θ) of the glycolated specimen were measured to determine the types of interstratification [118]. In addition, BB1 and BB2 values were used to control identification as they were not influenced by the discrete illite reflections since both illite and adjoining illite-smectite reflections peaks were measured. Środoń found that samples with BB1 and BB2 values larger than 4° 2θ, with the position of the low-angle reflection illite-smectite smaller than 7.5° 2θ, are dominated by IS ordering type of illite-smectite [94].

The mineralogical composition of bulk samples and the various size fractions for the end members were determined by quantitative X-ray diffraction (QXRD) analysis on random preparation specimens using the RockJock-11 program [131]. This program determines the mineralogical composition of powdered specimens by comparing the integrated X-ray diffraction (XRD) intensities of individual minerals with the intensities of an internal standard in the complex mixtures [131]. The addition of an internal standard (corundum) allows the calculation of each mineral individually; therefore, the calculation will not be affected by other minerals' identification/calculation. Sample preparation was followed according to a modified technique by Omotoso and Eberl, which was also reported by Środoń [144,145]. A sample was sieved using a 250 μm sieve. Then exactly 1.000 g of the sieved sample and 0.250 g of an internal standard (corundum powder) were placed into a grinding cylinder with zirconia grinding balls, to which 4 mL of ethanol was added. Then the sealed grinding cylinder was mounted on a McCrone micronizing mill and the sample was mixed and ground for 5 min. The mixture was poured into a ceramic bowl and dried overnight at about 80 °C. The dried mixture was put into a 25 mL plastic vial with three plastic balls (10 mm diameter) and shaken to mix and homogenize the contents. Then 0.5 mL of vertel (DuPont™ Vertel XF) was added to the mixture that was shaken again for 10 min using a Retsch MM 200 mill. The amount of vertel added was estimated according to the RockJock user's guide (a ratio of 0.5 mL vertrel to 1 g of pure clay) [131,145]. Next, the powder was sieved using a 250 μm sieve and loaded into an XRD side loading holder, which was against frosted glass. The specimens were run from 2θ = 4º to 2θ = 65.5º. JADE 7 software was used to extract the XRD profiles that were entered into the RockJock program to calculate the mineral composition.

5.2.3.2 ELEMENTAL ANALYSIS

The total C, H, N, and S contents were determined using a Vario MICRO cube elemental analyzer. The sample was burned in the presence of an oxygen stream at 1150 °C and the products of combustion, including CO_2, N_2, H_2O, and SO_2, were identified by a thermal conductivity detector. In order to improve the accuracy and reliability, approximately 25 mg of sample was accurately weighed and used for each run and the average of five replicates (at least) were recorded. The total inorganic carbon (TIC) content was obtained by calculation of the carbon content in the carbonate minerals (calcite, dolomite, and siderite). The amount of total organic carbon (TOC) for each sample was the difference between the total carbon measured by the elemental analyzer and TIC calculated by QXRD (RockJock program). The amount of TOC after Dean-Stark extraction can be considered as toluene insoluble organic carbon (TIOC).

5.2.3.3 SURFACE AREA

Specific surface area (SSA) and total specific surface area (TSSA) of the four bulk samples were determined by the BET (Brunauer-Emmett-Teller) adsorption isotherm measurement and the methylene blue (MB) method, respectively [112,113,139]. In the BET method, the SSA measurement is based on amount of monolayer gas (N_2) adsorption. The samples were outgassed overnight (~24 h) at 130 °C under vacuum using a Quantachrome Model Autosorb-1 MP instrument. After outgassing, the amount of nitrogen adsorption was measured for every sample using seven adsorption points over the relative equilibrium adsorption pressure (P/P_0) range of 0.05 to 0.3. In such a low pressure region, adsorption takes place on the surface of micropores (D = 0–2 nm) and the external surface of particles [139]. The final value and the standard deviation of the SSA-BET were based on the measurement of three different weight loads for each sample.

In the methylene blue (MB) titration method, ~2 g (or 5 g for MS and ES)[135] of dried bulk sample (105 °C for 24 h) were placed in a clean glass bottle (250 mL wide mouth); 50 mL of 0.015 mol/L $NaHCO_3$ along with 2 mL of 10 % w/w NaOH were added. After soaking the sample overnight, the slurry sample was completely dispersed using a hotplate/stirrer (slurry was kept below 60 °C) and then transferred to an ultrasonic bath (each step for 20 min). The bottles were kept in a water bath (25 °C) for 5 min; then 2 mL of 10 % v/v H_2SO_4 were added into the dispersed mixture. The sample on a stirring plate was then titrated in 1 mL increments (0.5 mL or even less when near the endpoint) with a daily fresh solution of 0.006 N MB. In each step, a disposal pipet

was used to transfer one drop of the titrated mixture onto a Whatman #42 qualitative ashless filter paper. The droplet on the filter was visually evaluated for observation of a light blue halo. When a blue halo was observed around the drop, the sample was re-examined after stirring for an additional 2 min. The end point was reached upon observation of a blue halo in the re-dropped sample. According to the Hang and Brindley methods, the recorded volume of MB added to the slurry was used to calculate the methylene blue index (MBI) and methylene blue total specific surface area (TSSA-MB) [133]:

$$MBI\left(meq/100\ g\right)=\frac{\left(V_{MB}\times N_{MB}\right)}{Weight\ sample}\times 100 \qquad \text{Equation 5-2}$$

$$TSSA\text{-}MB=MBI\left(meq/100\ g\right)\times 130\times 0.0602 \qquad \textit{Equation 5-3}$$

where V_{MB} and N_{MB} are the volume and the normality of MB added, respectively; the number 0.0602 represents Avogadro's constant (m^2/g) and the number 130 represents the surface area of a molecule of MB ($Å^2$). The standard deviation and the values of the TSSA-MB method were based on the measurement of three replicates.

5.3 RESULTS

5.3.1 DEAN-STARK ANALYSIS

Bitumen, solid, and water contents, determined by Dean-Stark analysis of the four petrologic end members from the North Mine (NM12), are reported in Table 5-1. The Dean-Stark extraction for NM12 samples was performed in the Institute for Oil Sands Innovation (IOSI) labs at the University of Alberta. The final value and the standard deviation for NM12 were based on the measurement of five replicates. The solid, bitumen, and water contents were significantly different for all three sets of samples, i.e., NM09, NM12, and Aurora Mine samples taken in 2010 (AM10). Both sand samples (ES and MS) contained higher amounts of bitumen and lower amounts of water compared with the clay samples (EC and MC) for all three sets of samples. The highest and lowest bitumen contents were observed for ES and EC, respectively. MC contained the highest water content for all three sets of samples (NM09, NM12, and AM10).

Table 5-1 Amounts of bitumen, solids and water as determined by Dean-Stark analysis of the four petrologic end members from NM12, NM09 [10] *and AM10* [224].

Mine Site	Samples	Bitumen (wt%)	Solids (wt%)	Water (wt%)
North Mine (NM09)	Estuarine Clay (EC)	0.4±0.3	95.1±0.9	4.5±1.0
	Marine Clay (MC)	4.0 ±0.8	91.0±0.1	5.3±0.8
	Estuarine Sand (ES)	16.4±0.4	83.3±1.1	0.7±0.8
	Marine Sand (MS)	8.2±0.1	89.7±0.6	2.0±1.0
North Mine (NM12)	Estuarine Clay (EC)	0.03±0.01	92.9±0.3	7.1±0.3
	Marine Clay (MC)	1.3±0.4	88.5±0.5	10.2±0.3
	Estuarine Sand (ES)	15.3±0.2	84.1±0.1	0.6±0.3
	Marine Sand (MS)	10.4±0.5	87.4±0.7	2.2±0.4
Aurora Mine (AM10)	Estuarine Clay (EC)	0.1±0.0	97.4±2.1	2.5±2.1
	Marine Clay (MC)	1.3±0.1	94.5±3.1	4.2±3.2
	Estuarine Sand (ES)	9.3±0.1	87.7±0.1	3.0±0.0
	Marine Sand (MS)	8.8±0.1	87.3±0.4	3.9±0.5

5.3.2 PARTICLE SIZE DISTRIBUTION

The particle size distributions for the four petrologic end members for NM12 appear in Table 5-2. There are clearly differences among the studied samples. The amounts of fine and ultrafine fractions (< 2 and < 0.2 μm) are noticeably higher in the clay samples. The sand samples, on the other hand, contained significantly higher amounts of the coarse fractions (> 45 and 2–45 μm). The results of the current research (NM12) were compared with those published in our previous study (NM09). Similar results, with some small discrepancies, are observed for the NM09 samples [10]. Three end members from NM12 (with the exception of ES) contained lower amounts of the ultrafine (< 0.2 μm) fraction than those from NM09 samples.

Table 5-2 Particle size distribution for the four petrologic end members from NM12 and NM09 [10].

Mine Site	Samples	Size fraction (wt%)				
		> 45µm	2 – 45µm	0.2-2µm	<0.2µm	Total
NM12	Marine Clay (MC)	24.98	59.05	13.61	2.36	100
	Estuarine Clay (EC)	20.04	62.21	14.27	3.48	100
	Marine Sand (MS)	90.71	6.05	2.70	0.54	100
	Estuarine Sand (ES)	94.01	4.13	1.34	0.52	100
NM09	Marine Clay (MC)	44.84	41.85	4.66	8.65	100
	Estuarine Clay (EC)	16.72	57.85	13.28	12.15	100
	Marine Sand (MS)	80.97	11.35	6.43	1.25	100
	Estuarine Sand (ES)	97.94	1.02	0.91	0.13	100

5.3.3 X-RAY DIFFRACTION

The mineral composition of the bulk samples and their size fractions for the four petrologic end members for NM12 were determined using the RockJock program and are listed in Table 5-3. The bulk samples included two main groups: non-clay and clay minerals. The non-clay minerals mostly contained quartz (51.7–99 wt%), carbonates (calcite, dolomite, and siderite - 0–14.1 wt%), and feldspars (K, Na, and Ca feldspars - 0.1–3.8 wt%), with small amounts of pyrite (< 0.2 wt%), TiO_2 minerals (anatase and rutile - < 0.4 wt%), and calcium sulphate (gypsum - < 0.5 wt%). High amounts of quartz were observed in ES (99 wt%) and MS (93 wt%) in the bulk samples (Figure 5-2). On the other hand, high amounts of clay minerals were identified in EC (32.4 wt%) and MC (29.5 wt%) in the bulk samples [225]. The highest amount of carbonate minerals was observed in the clay samples, especially in the MC fractions. Figure 5-2 shows the clear peak positions of the internal standard among other mineral peaks and no evidence of

overlap with other minerals.

The quartz and clay mineral contents gradually decreased and increased, respectively, with decreasing size fraction. The highest amount of quartz accumulated in the > 45 µm size fractions for all samples (> 90.3 wt%). The < 2 µm size fractions mainly consisted of kaolinite (28.7–46 wt%) and 2:1 clay minerals (21.8–55.9 wt%). The < 0.2 µm fractions of clay samples mostly

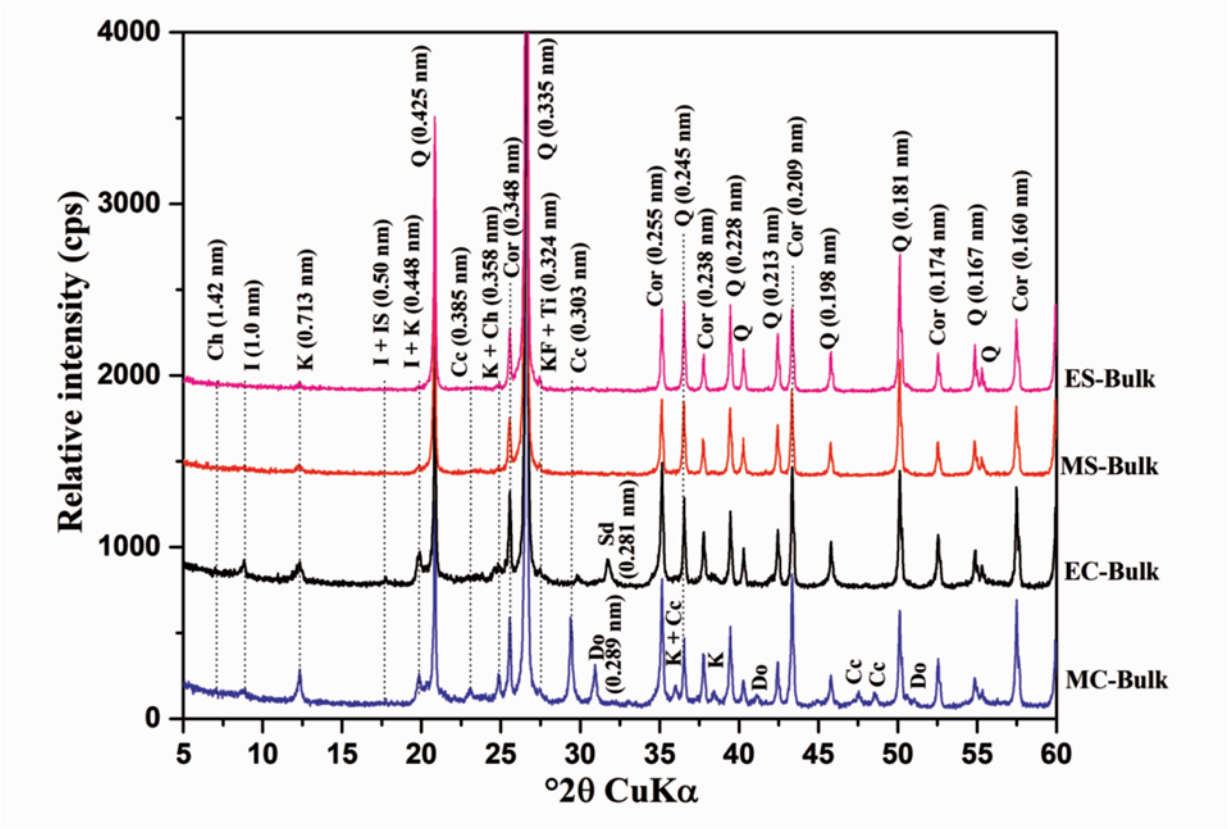

Figure 5-2 XRD patterns for random preparations of bulk samples of EC, MC, ES, and MS from NM12 with an internal standard. Ch, chlorite; I, illite; K, kaolinite; G, gypsum; Q, quartz; Cc, calcite; Do, dolomite; Sd, siderite; KF, potassium feldspar; Ti, TiO_2 minerals (rutile and anatase); Cor, corundum (internal standard).

contained 2:1 clay minerals (sum of discrete illite and illite-smectite) (~82.7 wt%). Kaolinite content was significantly enriched in the < 2 µm size fractions of the sand samples, and the highest kaolinite content was observed in NM12-ES. The collected amounts of the 0.2–2 and < 0.2 µm fractions for MS and ES were insufficient for mineral characterization by QXRD.

Table 5-3 Mineral composition (in wt%) of the bulk samples and their size fractions from the four petrologic end members for NM12 using the RockJock program. Total 2:1 clays – sum of illite and illite–smectite; DS – Dean-Stark extraction; Calcium sulfate – i.e., gypsum. Sum fractions - the mineral composition of the bulk samples was calculated from the mass weighted quantification of the sub-samples (all fractions, i.e., > 45, 2–45, 0.2–2, and < 0.2 μm).

Sample	Size fraction (μm)	Quartz	Feldspar (K, Na, Ca)	Calcite	Dolomite	Siderite	Calcium sulfate	TiO_2 minerals	Pyrite	Kaolinite	Total 2:1 clays	Chlorite
EC after DS	Bulk	62.9	2	0	0.1	2.2	0	0.4	0	12.2	20.2	0
	>45	94.3	2.9	0	0	0.2	0	0.2	0	1.5	0.9	0
	2-45	58.1	1.8	0	0.2	2.4	0	0.3	0	14.9	21.4	0.9
	<2	12.4	1.1	0	0	0	0	1.2	0	28.7	55.9	0
	0.2-2	15.7	1	0	0	0	0	1	0	33.5	48.8	0
	<0.2	0	1.7	0	0	0	0	0.7	0	14.9	82.7	0
	Sum fractions	57.3	1.9	0	0.1	1.5	0	0.4	0	14.9	23.3	0.6
MC after DS	Bulk	51.7	3.8	9	4.9	0.2	0.5	0.2	0.2	11.7	17.8	0
	>45	90.3	3.9	2.5	1.1	0	0	0	0	1.2	1	0
	2-45	48.3	4.2	12.1	7.3	0.3	0.8	0.2	0.3	14.7	11.8	0
	<2	6.6	0.9	2.9	0	0	0	0.5	0	36.7	52.4	0
	0.2-2	10.8	0.8	3	0	0	0	0.5	0	40.8	44.1	0
	<0.2	0	2.4	2.5	0	0	0.5	0.7	0	11.3	82.6	0
	Sum fractions	52.5	3.6	8.2	4.6	0.2	0.5	0.2	0.2	14.8	15.2	0.0
ES after DS	Bulk	99	0.1	0	0	0	0	0	0	0.9	0	0
	>45	100	0	0	0	0	0	0	0	0	0	0
	2–45	46	11.1	0	0.1	0.5	0.5	0	0	27.1	12.9	1.8
	<2	10.1	13.8	0.1	1	0.5	2.9	1.3	0.4	46	21.8	2.1
	Sum fractions	96.1	0.7	0.0	0.0	0.0	0.1	0.0	0.0	2.0	0.9	0.1
MS after DS	Bulk	93	0.7	0	0	0	0	0	0	3.5	2.8	0
	>45	99	0.1	0	0	0	0	0	0	0.9	0	0
	2–45	39.6	4	0	0.1	0.3	0.5	0.3	0.6	25.4	27.4	1.8
	<2	8	4.6	0	0.3	0.6	2.3	0	0	39.1	43.7	1.4
	Sum fractions	92.5	0.5	0.0	0.0	0.0	0.1	0.0	0.0	3.6	3.1	0.2

The mineral composition of bulk samples was also calculated from the mass weighted quantification of the sub-samples (all fractions, i.e. > 45, 2–45, 0.2–2, and < 0.2 μm), named sum fractions in Table 5-3, and compared with direct mineral calculations for each bulk end member. The comparison revealed relatively good agreement between these two calculations (internal check), which confirmed that the mineral composition of bulk samples from direct measurement matched fairly well with the sub-samples (sum of mineral fractions for each end member).

XRD patterns were obtained from oriented preparations of ultrafine size fractions (< 0.2 μm) for detailed study of the clay minerals (Figure 5-3c). Illite and kaolinite minerals were identified in the < 0.2 μm size fractions for all end members. Discrete illite reflections were observed at d = 1.0 nm and 0.334 nm for MS and ES, d = 1.05 nm and 0.332 nm for MC, and d = 1.0 nm and 0.332 nm for EC. Discrete kaolinite reflections were observed at d = 0.713 nm for MS and ES and 0.719 nm for MC and EC. The presence of mixed-layer minerals (illite-smectite and/or kaolinite-smectite) was revealed in the < 0.2 μm size fractions of MC and EC due to changes in the positions, shapes, and relative intensities of 00l reflections after ethylene glycol treatment (Figure 5-3c). The method described by Środoń was used to calculate the expandability and ordering types of illite-smectite based on the XRD patterns from oriented preparations of the < 0.2 μm fractions for EC and MC [10,94]. The calculated Ir (Equation 5-1) for MC and EC was 1.67 and 1.43, respectively, indicating the presence of expandable clay minerals for both clay samples. The measured BB1 and BB2, and the position of the low-angle reflection illite-smectite for MC were 5.21°, 4.10°, and 7.30° 2θ (1.21 nm), respectively, indicating that the ordering type of illite-smectite was dominated by IS. Since the BB2 value for EC was 3.05° (smaller than 4.0°) 2θ, the ordering type of illite-smectite at this stage cannot be determined.

The reflections at 6–8° and 33–35° 2θ are two sensitive regions for identification of the type of interstratification and the expandability of illite-smectite. However, the reflection at 6–8° 2θ is usually influenced by the strong adjacent 001 illite reflection with a shoulder on the 001 illite reflection generally observed, so it may not be suitable for identification purposes [94]. The reflection at 33–35° 2θ, on the other hand, seems to be more appropriate due to the lack of discrete illite reflections in this region. The reflection for MC was observed at 33.65° 2θ, indicating this specimen consisted of discrete illite and illite-smectite with 30 ± 4 % expandability. The ordering type of illite-smectite was dominated by IS (R1). An EC peak was observed at 34.85° 2θ, signifying discrete illite and illite-smectite with 10 ± 3 % expandability. The ordering type of illite-

smectite was mainly ISII (R3) and partially IS (R1). The expandability results are also in agreement with the method described by Moore and Reynolds [76].

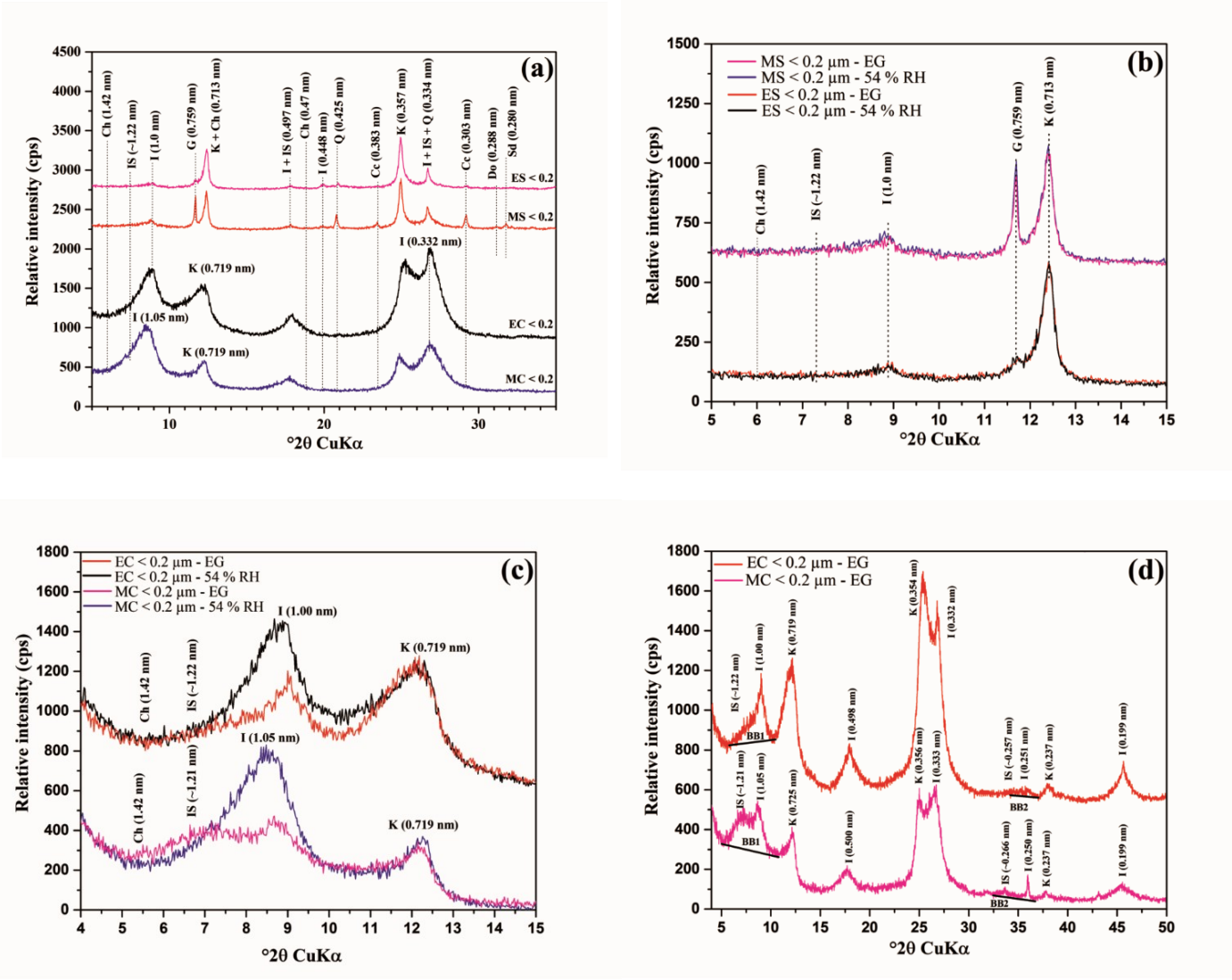

Figure 5-3 XRD patterns for oriented preparation specimens of the < 0.2 µm size fraction for (a) EC, MC, ES, and MS of air dried-54 % RH, (b) MS and ES of air dried-54 % RH (black and blue lines) and glycolated (red and pink lines), (c) MC and EC of air dried-54 % RH (black and blue lines) and glycolated (red and pink lines), (d) MC and EC of glycolated. Ch, chlorite; G, gypsum; I, illite; IS, illite-smectite; K, kaolinite; Q, quartz; Cc, calcite; Do, dolomite; Sd, siderite.

The intensity of the kaolinite peak for the 001 reflection was slightly changed after the ethylene glycol saturation treatment, which indicates the possible presence of interstratification of 2:1 clay

minerals. Kaolinite-smectite (K-S) was also observed by Dudek *et al.* and Srivastava *et al.* in their studies [95,226]. Visible reflection changes were observed between d = 0.719 nm (air dried) and d = 0.725 nm (after ethylene glycol solvation) for the < 0.2 μm fraction of the MC sample (Figure 5-3c). It has been recommended to use Δ2θ as well as the peak positions for determining the composition of randomly interstratified K-S [94]. The shift of the kaolinite peak at d = 0.719 nm in the air dried sample to d = 0.725 nm after ethylene glycol treatment is employed as a diagnostic criterion for the presence of kaolinite-smectite interstratification [95,227,228]. This approach was used to identify the presence of mixed-layer K-S clays in the < 0.2 μm fraction of the MC sample. The small relative changes after ethylene glycol treatment for the < 0.2 μm fraction of MC show the presence of kaolinite-smectite with 5–10 % expandability (Figure 5-3c). This conjecture is consistent with published data by Vingiani *et al.*, who found a peak at d = 0.761 nm, which was related to K-S with 90-95 % kaolinite and 5–10 % smectite layers [228]. Conversely, the XRD oriented specimens of the < 0.2 μm fractions for EC, MS, and ES revealed that the kaolinite reflection was not affected by ethylene glycol solvation, indicating the presence of discrete kaolinite without interstratification of expandable layers (Figure 5-3c).

Although chlorite was identified by QXRD using the RockJock program for the < 2 μm and 2–45 μm fractions for the ES and MS samples, it was not observed in the oriented specimens of the < 0.2 μm fractions for those end members (Figure 5-3b). In addition, some non-clay minerals were also identified in the XRD patterns of the oriented preparations of the < 0.2 μm fractions for the petrologic end members. Intense reflections for gypsum (0.759 nm) and calcite (0.303 and 0.383 nm) were observed for MS samples. Weak reflections of these minerals were also identified for the < 0.2 μm fraction of the ES sample. However, gypsum and calcite were not observed for EC and MC samples. The dolomite (0.288 nm) and siderite (0.280 nm) reflections were weak for the XRD oriented preparations for the < 0.2 μm fractions of the MS and ES samples. Many studies have revealed gypsum mineral in the oil sands, most likely produced by oxidation of pyrite [72–74].

5.3.4 ELEMENTAL ANALYSIS

Table 5-4a and b show the total carbon (TC), nitrogen (TN), hydrogen (TH), and sulphur (TS) contents (in wt%) of the bulk samples (before and after bitumen removal using Dean-Stark

extraction) and their various size fractions (i.e. > 45 µm, 2–45 µm, 0.2–2 µm, < 0.2 µm) for ES, EC, MC, and MS. The N/C, H/C, and S/C ratios were also calculated and appear in Table 5-4. After bitumen removal, a reduction in the TN, TC, TH, and TS contents was observed for all end members (with the exception of MC, which is possible due to sample heterogeneity). Elevated N/C, H/C, and S/C ratios were found for all oil sands samples after bitumen removal. The total carbon content of all end member samples increased with decreasing particle size, ranging from 2.2 wt% for the > 45 µm fraction to 7.8 wt% for the < 0.2 µm fraction for MC, from 1.7 to 2.1 wt% for EC, from 0.2 to 6.4 wt% for MS, and from 0.1 to 7.4 wt% for ES. The same trend was observed for the TN and TH contents of the four petrologic end member fractions. However, the amount of TS was quite variable, between 0.002 wt% and 5.9 wt%. The N/C ratio varied between 0.004 and 0.053 for all sample size fractions. The H/C ratio was also different, ranging between 0.096 and 0.749 for all sample size fractions. The S/C ratio was elevated for decreasing size fractions for both MS and MC samples. However, this ratio for ES and EC samples did not follow the same trend as for the marine samples.

5.3.5 SURFACE AREA

The SSA and TSSA results of the bulk samples for the four petrologic end members of NM12 appear in Table 5-5. High surface areas were observed for the clay-rich petrologic end-members EC and MC for both techniques SSA-BET (15.9 ± 1.33 and 15.1 ± 0.41 m^2/g) and TSSA-MB (45.2 ± 1.65 and 57.7 ± 10.68 m^2/g). The bulk sand-rich petrologic end-members (ES and MS) showed low surface areas for either SSA-BET (0.2 ± 0.01 and 1.3 ± 0.38 m^2/g) or TSSA-MB (3.4 ± 0.63 and 11.8 ± 0.53 m^2/g). Comparison between the TSSA-MB and SSA-BET results showed that the TSSA-MB values were significantly higher than the SSA-BET results, due to the basic principles of the different techniques. The TSSA method is based on the adsorption of the MB molecules on both the interlayer spaces of swelling clay minerals and the external surfaces of all particles. The SSA technique, on the other hand, is based on the adsorption of nitrogen on external surfaces of the minerals [114,212].

Table 5-4 a Total carbon (TC), nitrogen (TN), hydrogen (TH), and sulfur (TS) contents (in wt%) in the bulk samples before and after bitumen removal (Dean-Stark) and their size fractions from MC and EC for NM12 determined by elemental analysis. BD and AD – before and after Dean-Stark extraction; TIC – total inorganic carbon; TOC – total organic carbon; n.a. – not analyzed.

CHNS analysis – size fractions										TIC (Q-XRD)	TOC
Sample	Settling time (min)		TN (wt%)	TC (wt%)	TH (wt%)	TS (wt%)	N/C ratio	H/C ratio	S/C ratio		
Marine Clay	Bulk -BD	Ave.	0.081	5.642	0.844	0.003	0.014	0.150	0.001	1.72	3.93
		STDV	0.003	0.079	0.015	0.003					
	Bulk-AD	Ave.	0.081	4.878	0.701	0.041	0.017	0.144	0.008	1.74	3.14
		STDV	0.001	0.030	0.011	0.048					
	>45 µm	Ave.	0.034	2.177	0.209	0.033	0.016	0.096	0.015	0.44	1.73
		STDV	0.000	0.012	0.004	0.001					
	2-45 µm	Ave.	0.10	6.178	0.639	0.120	0.016	0.103	0.019	2.49	3.09
		STDV	0.000	0.452	0.083	0.015					
	<2 µm	Ave.	0.104	3.626	1.247	0.112	0.029	0.346	0.030	0.35	3.28
		STDV	0.001	0.278	0.046	0.061					
	0.2-2 µm	Ave.	0.128	6.010	1.159	0.131	0.021	0.193	0.022	0.34	5.67
		STDV	0.000	0.077	0.015	0.043					
	<0.2µm	Ave.	0.141	7.842	1.089	0.228	0.018	0.139	0.029	0.3	7.54
		STDV	0.003	0.081	0.001	0.039					
Estuarine Clay	Bulk -BD	Ave.	0.057	1.729	0.561	0.072	0.033	0.324	0.041	0.28	1.45
		STDV	0.002	0.048	0.003	0.016					
	Bulk-AD	Ave.	0.051	1.502	0.533	0.051	0.034	0.355	0.034	0.28	1.23
		STDV	0.001	0.022	0.004	0.008					
	>45 µm	Ave.	0.032	0.821	0.158	0.026	0.039	0.192	0.032	0.02	0.83
		STDV	0.001	0.019	0.007	0.011					
	2-45 µm	Ave.	0.047	1.182	0.296	0.039	0.04	0.250	0.033	0.43	0.70
		STDV	0.001	0.027	0.012	0.008					
	<2 µm	Ave.	0.086	1.619	1.206	0.010	0.053	0.749	0.006	0	1.62
		STDV	0.003	0.167	0.066	0.009					
	0.2-2 µm	Ave.	0.067	1.336	0.857	0.002	0.050	0.641	0.001	0	1.34
		STDV	0.001	0.014	0.023	0.003					
	<0.2µm	Ave.	0.102	2.113	1.278	0.013	0.049	0.605	0.006	0	2.11
		STDV	0.002	0.013	0.031	0.011					

Table 5-4 b Total carbon (TC), nitrogen (TN), hydrogen (TH), and sulfur (TS) contents (in wt%) in the bulk samples before and after bitumen removal (Dean-Stark) and their size fractions from MS and ES for NM12 determined by elemental analysis. BD and AD – before and after Dean-Stark extraction; TIC – total inorganic carbon; TOC – total organic carbon; n.a. – not analyzed.

CHNS analysis – size fractions										TIC (Q-XRD)	TOC
Sample	Settling time (min)		TN (wt%)	TC (wt%)	TH (wt%)	TS (wt%)	N/C ratio	H/C ratio	S/C ratio		
Marine Sand	Bulk -BD	Ave.	0.056	8.577	1.189	0.145	0.007	0.139	0.017	0	8.58
		STDV	0.002	0.223	0.033	0.106					
	Bulk-AD	Ave.	0.017	0.627	0.162	0.126	0.028	0.263	0.203	0	0.63
		STDV	0.001	0.097	0.005	0.006					
	>45 µm	Ave.	0.008	0.242	0.072	0.034	0.032	0.299	0.142	0	0.24
		STDV	0.001	0.016	0.004	0.005					
	2-45 µm	Ave.	0.096	3.084	0.939	0.798	0.031	0.304	0.259	0.04	3.04
		STDV	0.001	0.019	0.003	0.020					
	<2 µm	Ave.	0.191	4.932	1.577	1.680	0.039	0.320	0.341	0.1	4.83
		STDV	0.003	0.066	0.011	0.045					
	0.2-2 µm	Ave.	0.202	4.792	1.591	0.265	0.042	0.332	0.055	n.a.	n.a.
		STDV	0.006	0.205	0.034	0.023					
	<0.2µm	Ave.	0.230	6.404	1.525	5.942	0.036	0.238	0.912	n.a.	n.a.
		STDV	0.000	0.153	0.064	0.205					
Estuarine Sand	Bulk -BD	Ave.	0.056	10.029	1.300	0.117	0.006	0.130	0.013	0	10.03
		STDV	0.0003	0.691	0.101	0.058					
	Bulk-AD	Ave.	0.004	0.195	0.060	0.012	0.021	0.315	0.062	0	0.2
		STDV	0.001	0.047	0.011	0.003					
	>45 µm	Ave.	0.003	0.114	0.036	0.005	0.026	0.322	0.044	0	0.11
		STDV	0.000	0.048	0.017	0.000					
	2-45 µm	Ave.	0.054	1.993	0.702	0.111	0.027	0.352	0.056	0.06	1.93
		STDV	0.001	0.026	0.013	0.074					
	<2 µm	Ave.	0.149	3.867	1.591	1.175	0.038	0.411	0.304	0.19	3.97
		STDV	0.001	0.092	0.028	0.059					
	0.2-2 µm	Ave.	0.156	3.675	1.588	0.158	0.042	0.432	0.043	n.a.	n.a.
		STDV	0.002	0.014	0.018	0.032					
	<0.2µm	Ave.	0.235	7.447	1.844	1.820	0.032	0.248	0.245	n.a.	n.a.
		STDV	0.002	0.258	0.049	0.098					

Table 5-5 Surface area of the bulk samples after bitumen removal measured by BET and MB techniques.

Sample	TSSA-MB (m^2/g)	SSA-BET (m^2/g)
EC-Bulk-AD	45.2±1.65	15.9±1.33
MC-Bulk-AD	57.7±10.68	15.1±0.41
ES-Bulk-AD	3.4±0.63	0.2±0.01
MS-Bulk-AD	11.8±0.53	1.3±0.38

5.4 DISCUSSION

5.4.1 DEAN-STARK ANALYSIS

Dean-Stark analysis (Table 5-1) showed that the sand samples (ES and MS) contained high amounts of bitumen, which may be related to the high porosity and permeability of these end members allowing accommodation of bitumen, as reported by Mossop [171]. The clay samples (EC and MC) had high water and low bitumen contents, which may be connected to their high content of clay minerals. According to Carrigy, the amount of bitumen is correlated to the clay-size material (< 2 μm) content in the oil sands samples [196]. The results of the present study were compared with the literature [10,196,224]. The clays (MC and EC) and sands (MS and ES) contained high levels of water and bitumen, respectively, for all three sets of samples (NM09, NM12, and AM10). A high amount of solids was present in EC for all three sets of samples due to its low bitumen content (< 0.4 wt%). The highest bitumen contents were identified in ES for all three sets of samples. Since ES is a black bitumen-rich sand interbedded with a light laminated claystone (EC), the estimation of clay content can be achievable by using large-scale infrared spectroscopy. An accurate approximation improved the aqueous extraction of bitumen by adding adequate caustic soda (or caustic ammonium) [2]. The marine ore, on the other hand, is a mixture of interbedded black sand and a very dark grey claystone, in which the clay content cannot be identified. The estuarine ore is usually mixed with water and hydrotransported to the processing plant, while the marine ore has to be transported on a train and undergoes pre-processing. The estuarine ore is the main production interval (middle McMurray Formation), while the marine ore

interval is usually shallow (upper McMurray Formation) [221,224]. Fustic *et al.* also reported that the marine ore contains higher clay content (30–40 wt%) in the interbedded marine mudstone than that of the estuarine ore (< 20 wt%) [221]. These are some of the important reasons that the estuarine ore is mostly classified as "good-processing" ore, while marine ore can be classified as "middle" or even "poor processing" ore.

Some discrepancies between the NM09 and NM12 samples were observed. The first was that clay samples from NM12 contained higher water and lower bitumen and solids contents than those from NM09, which may be due to the high clay-size material (< 2 μm) content and/or the different collection times (e.g., rainy season for NM12 samples) from the mine. The second discrepancy was that NM12-MS had slightly higher bitumen and lower solids content than NM09-MS, which may be due to more effective sample collection from the mine and/or better separation of end members in the laboratory. Moreover, the very small amounts of clays and sands interbedded (embedded) among NM09-MS and MC, respectively, were hard to distinguish and/or separate before or even after Dean-Stark extraction. Figure 5-4 shows the differences among the physical appearance of four petrologic end members from NM12 and NM09 after Dean-Stark treatment. Thus, the NM12-MS and MC are more representative of marine end members than those of NM09. The bitumen content of NM12-ES was lower by 1 wt% compared with NM09-ES; however, this variation is within the normal range of sampling ore from an oil sands mine.

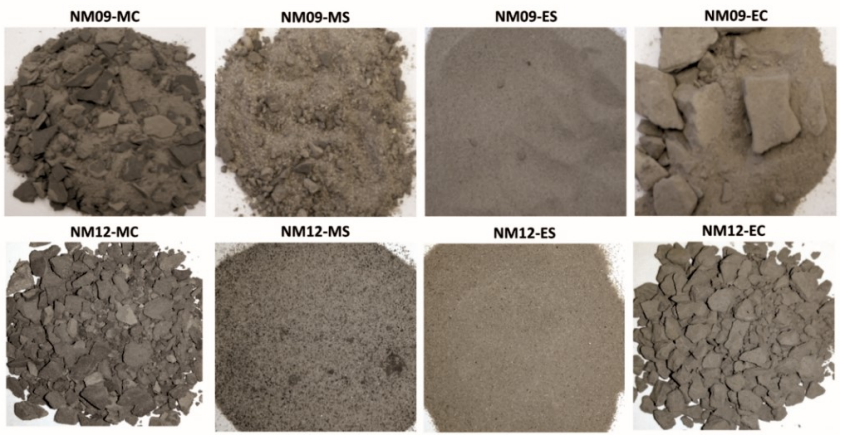

Figure 5-4 Comparison among the physical appearances of four petrologic end members from NM12 and NM09 after Dean-Stark treatment.

5.4.2 PARTICLE SIZE DISTRIBUTION

Comparison of particle size distributions between NM12 and NM09 (Table 5-2) indicates that the marine samples, i.e. MS and MC of NM12, contained higher and lower amounts of coarse (> 45 μm) fractions than the marine samples of NM09, respectively. This is consistent with Dean-Stark extraction results (Table 5-1), where NM12-MS and MC contain higher and lower amounts of bitumen, respectively, relative to NM09. In other words, the NM12-MS and MC samples are more representative of the pure end members with lower impurities than NM09-MS and MC. Conversely, NM12-ES with a lower coarse (> 45 μm) fraction had lower amounts of bitumen than NM09-ES. However, NM12-EC had a very low bitumen content with a high coarse fraction (> 45 μm), which was unexpected.

5.4.3 X-RAY DIFFRACTION

The presence of illite-smectite was only observed in clay end members (EC and MC) and the highest relative amount of mixed layered clay minerals (i.e., illite-smectite and kaolinite-smectite) was identified in the MC sample. The amount of expandability for the EC sample is in agreement with our previously published results [10,203]. However, the expandability for the NM12-MC sample was higher than that of NM09-MC (our previous work), which was 10 % [10,203]. Other researchers have reported expandabilities for illite-smectite between 10 and 40 % in Alberta oil sands ores [20,21,181,182]. Due to the presence of expandable clay minerals in the clay end members, they are more problematic during bitumen extraction (particularly in the aqueous process) than the sand end members. Many studies have revealed clay minerals, particularly expandable clay minerals, as the most problematic minerals affecting an aqueous bitumen extraction process, bitumen recovery and quality, and tailings management [15–17]. Wik *et al.* showed that the small particles and the mineralogical compositions are the two most important parameters affecting bitumen recovery [19]. Therefore, clay minerals in the Alberta oil sands deposits are the most likely species that might negatively affect a non-aqueous extraction process.

The XRD oriented preparations from the ultrafine fractions of the end members can be used to estimate the relative amount of mixed-layer clay minerals (i.e., illite-smectite and kaolinite-smectite). Comparison of the XRD patterns for the < 0.2 μm fractions of the clay end members after ethylene glycol solvation showed a higher intensity peak near 1.21 nm for the MC sample,

which indicates a higher amount of illite-smectite in this sample than that in the EC sample (Figure 5-3c). Meanwhile, the higher intensity kaolinite reflection (0.719 nm) in the < 0.2 μm fraction corresponds to a higher amount of this mineral for EC compared with MC (Figure 5-3c), which is consistent with QXRD (Table 5-3). The presence of kaolinite-smectite and higher smectite content in illite-smectite for marine ore samples are two other factors that further emphasize why marine ore is considered more as a "middle" or even "poor processing" ore relative to estuarine ore.

Moreover, MC contains more carbonate minerals such as calcite and dolomite, which are mostly concentrated in the 2–45 μm fraction (Table 5-3). However, EC has the most siderite in the bulk and the 2–45 μm fraction samples (Table 5-3). The highest amount of calcium sulphate minerals (gypsum) was observed in the < 2 μm fraction for the MS and ES samples (Table 5-3). However, the XRD oriented preparations for the ultrafine fractions revealed that the highest relative amount of gypsum minerals is concentrated in the MS (Figure 5-3b). The highest relative amount of kaolinite was observed in the < 0.2 μm fraction of the sand samples (MS and ES).

5.4.4 ELEMENTAL ANALYSIS

Elemental analysis shows the total carbon (TC), nitrogen (TN), hydrogen (TH), and sulphur (TS) contents (in wt%) in the bulk samples before and after bitumen removal (Dean-Stark), as well as in their size fractions (Table 5-4). The presence of total inorganic carbon (TIC) indicates the elevated inorganic carbon or carbonate minerals (i.e., calcite, dolomite, and siderite) in the MC sample. This result is in agreement with our previously published results [10,203]. On the other hand, the finer fractions of each end member after bitumen removal contain higher amounts of residual toluene insoluble organic carbon (TIOC) (Table 5-4). In other words, TIOC is mainly associated with the clay minerals. Kotlyar *et al.* reported the same observation, showing that the fines fraction (< 44 μm) and particularly the clay fraction (< 3 μm) from the oil sands samples consisted of higher TIOC contents compared with the other fractions [198,229]. In this study, the highest amount of residual TIOC was observed in the < 0.2 μm fraction of MC (7.54 wt%) compared with EC (2.11 wt%) (Table 5-4a). Although the residual TIOC for the 0.2–2 and < 0.2 μm fractions of MS and ES was not determined due to insufficient amounts of these fractions for mineral characterization (QXRD), the results from the < 2 μm fraction of these end members reveal that the TIOC for the MS sample is higher (4.83 wt%) compared with the ES sample (3.67 wt%)

(Table 5-4b). Bensebaa *et al.* and Sparks *et al.* reported that marine oil sands have higher TIOC, similar to asphaltene, compared with estuarine samples [36,230]. TN content increases as the particle size fraction decreases and/or clay content increases (Table 5-4a and b). Since organic matter is the only source of nitrogen in the four end members, the excess TN content indicates the presence of residual organic matter after the Dean-Stark process. This conjecture is consistent with previous thought that the TOC is mainly associated with clay minerals. Moreover, higher amounts (at least double) of residual TOC were observed in all fractions of MC compared with EC (Table 5-4a), which can be responsible for the very dark grey colour of claystone in MC. The amount of TH increases with decreasing size fraction and/or by increasing the clay content (Table 5-4a and b). The TH content in the finer fractions can be correlated to the presence of residual organic matter after Dean-Stark analysis and/or hydroxyl (OH) groups from the clay minerals (surface water and interlayer water). The lowest amounts of TIOC were found in the > 45 μm fractions for all four end members, which may be due to the high amount of quartz minerals (> 90 wt%). This is in agreement with our previous studies as well as other published data [10,203].

The ranges of N/C, H/C, and S/C ratios for organic matter (i.e. bitumen, asphaltene, and kerogen) were calculated from published data and are shown in Table 5-5 [44,224,231]. The S/C ratio varied between 0.001 and 0.912 for all fractions. The fractions with an S/C ratio ≥0.11 (mainly sand samples) signify the possibility of inorganic sulphates (i.e. calcium sulphate) or pyrite. This result is in agreement with QXRD of the fractions (Table 5-3). The derived S/C ratio from previous studies showed that the ratio for organic matter (i.e., bitumen, asphaltene, and kerogen) was ≤ 0.11 (Table 5-6) [44,224,231]. It was also reported in the literature that the H/C ratio for organic matter was in the range of 0.057–0.125, while this ratio for all fractions (with the exceptions of the MC > 45 μm and 2–45 μm fractions) was ≥0.125, which indicates the presence of clay minerals in all fractions (Table 5-3). The ratio generally increased as the size fraction decreased for the sand end members (with the exception of the < 0.2 μm fractions) and was unexpected. However, the H/C ratio varied for the sand end members, which may be related to the effect of carbonate minerals as a source of inorganic carbon and clay minerals as a source of inorganic hydrogen on the H/C ratio. This result is also in good agreement with QXRD for the four end members (Table 5-3).

Table 5-6 N/C, H/C and S/C ratios of bitumen, asphaltene and kerogen calculated from published data [224,231,232].

Sample	N/C ratio	H/C ratio	S/C ratio
Bitumen[1,2]	0.0017-0.0077	0.09-0.125	0.054-0.069
Asphatene[1,2]	0.012-0.016	0.084-0.102	0.06-0.110
Kerogen[3]	>0.019	0.057-0.1	0.03-0.08

The N/C ratio for bulk samples after bitumen removal and for all size fractions of MS, ES, and EC was ≥ 0.021, which may be due to the presence of asphaltene and/or kerogen as residual organic matter. This hypothesis is consistent with published data (Table 5-6) [44,224,231]. However, the N/C ratio for the bulk sample and the > 2 μm fractions of MC was ≤ 0.019, which indicates elevated amounts of inorganic carbon or carbonate minerals (i.e. calcite, dolomite, and siderite). This result is in agreement with QXRD of the various fractions (Table 5-3).

5.4.5 SURFACE AREA

The surface areas results (SSA-BET and TSSA-MB) of the bulk samples for the four petrologic end members revealed a correlation between the surface area and the amount of total clays and/or total 2:1 clays (sum of illite and mixed layer clay minerals). The values of SSA-BET and TSSA-MB increased with increasing the total clays and/or total 2:1 clay content. This conjecture is consistent with previous studies showing that the type and quantity of clay minerals control the surface area [11,199,200]. There is a discrepancy between SSA and TSSA values, which is increased by increasing the total clays and/or total 2:1 clay content (Figure 5-5). This disparity is due to the different techniques principles for the techniques, which were described in the Analytical Methods - Surface Area (section 5.2.3.3). Several studies have reported that the

[1] The chemistry of Alberta oil sand bitumen was reported by Strausz [232].

[2] The elemental analysis of different types of asphaltenes has been thoroughly investigated by Christopher *et al*. [231].

[3] 3The bitumen and kerogen contents for AM10 samples (MC, EC, MS and ES) have been thoroughly investigated by Zheng [224].

presence of organic matter in the rocks may influence the analytical methods for measuring surface properties [114–117]. Although many studies have revealed that organic matter positively affects the SSA-BET results from soil, high amounts of organic carbon lower the SSA-BET results due to larger aggregates forming from smaller particles by attaching to organic matter and/or blocking up holes with sticky organic carbon [24,119,120]. Therefore, in the present study, the Dean-Stark extraction procedure was performed on all petrologic end-members to remove bitumen to prevent the influence of bitumen on surface properties. On the other hand, there are controversial issues about the certainty of TSSA-MB technique due to the selectivity of the exchangeable dye cations and extra adsorption of cations [127,128].

After bitumen removal, a small amount of residual carbon content (TOC) was observed for all bulk samples (with the exception of MC). Therefore, it is assumed that there is an insignificant effect of TOC on BET values. The correlation between the surface area and the quantity of total 2:1 clay minerals (mainly swelling clays)/total clay minerals shows that the surface area (TSSA-MB and SSA-BET) increased with increasing 2:1 clays content (see Table 5-5 and Figure 5-5). Thus, it can be interpreted that mineralogy, mainly the amount of 2:1 clays, has a major effect on the SSA and TSSA values in the petrologic end-members of Alberta oil sands. More precisely, the higher TSSA-MB value for bulk-MC compared with bulk-EC is due to the presence of more smectitic layers in the 2:1 clay minerals (expandability for MC is 30 % versus 10 % for EC), which is discussed in the Results – X-ray Diffraction (section 5.3.3) and shown in Figure 5-3b. Conversely, the SSA-BET value was slightly lower for bulk-MC compared with bulk-EC, which is due to the lower total clays content (29.5 wt% for MC versus 32.4 wt% for EC). In other words, NM12-EC with a large external surface area exhibits a higher SSA-BET value, while NM12-MC with a larger internal surface area has a higher TSSA-MB value.

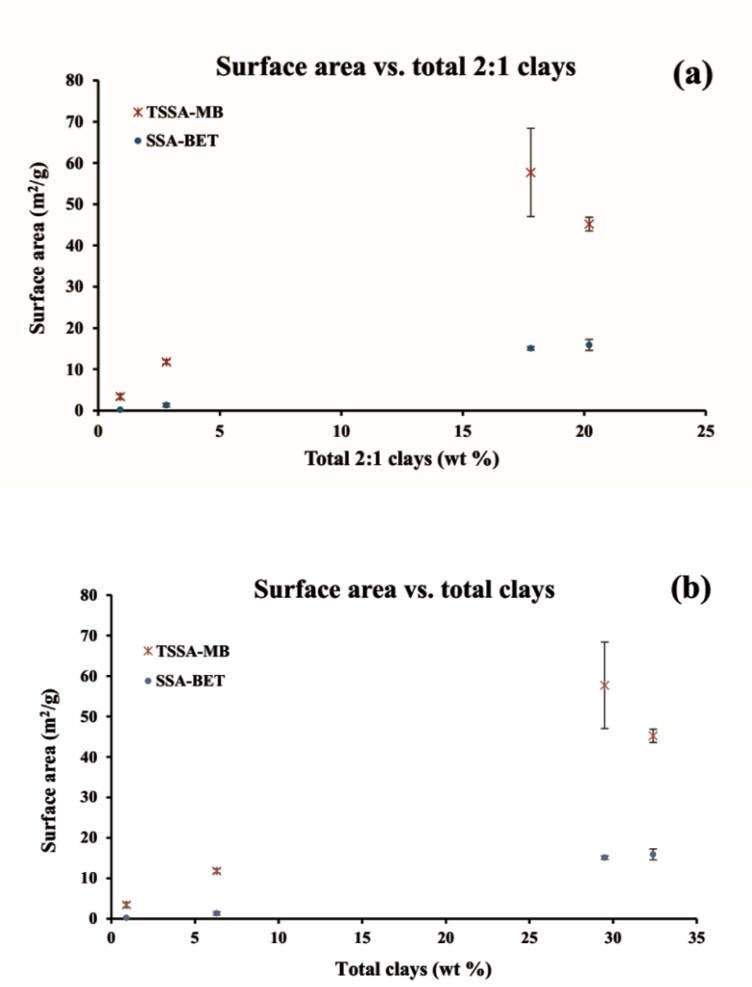

Figure 5-5 TSSA-MB and SSA-BET plotted versus the total 2:1 clays (sum of illite and illite-smectite) and total clays content for the bulk samples of the four petrologic end-members.

5.5 CONCLUSIONS

Samples from an Alberta oil sands ore (North Mine of Syncrude Canada Ltd., taken in 2012 - NM12) were analyzed and the results compared with samples taken previously from the same mine in 2009 (NM09), as well as samples taken from the Aurora Mine in 2010 (AM10). The samples were separated into four petrologic end members, i.e., estuarine clay (EC), estuarine sand (ES), marine clay (MC), and marine sand (MS). The main components were bitumen (0.03 to 15.3 wt%), water (0.6 to 10.2 wt%), and solids (84.1 to 92.9 wt%). ES and EC contained the highest and lowest amounts of bitumen, respectively, for all three samples (NM12, NM09, and AM10). Estuarine ore mostly behaves as "good-processing" ore. The bulk samples after bitumen removal contained two main groups of minerals: non-clay and clay minerals. The non-clay minerals of NM12 mostly included quartz (51.7–99 wt%), carbonates (calcite, dolomite, and siderite, 0–14.1

wt%), and feldspars (K, Na, and Ca feldspars, 0.1–3.8 wt%), with small amounts of pyrite (< 0.2 wt%), TiO_2 minerals (anatase and rutile, < 0.4 wt%), and calcium sulphate mineral (gypsum, 0.5 wt%). The highest relative amount of 2:1 clay minerals (illite and mixed-layer clay minerals) was found in the finest size fractions (< 0.2 μm). The expandability of illite-smectite was 30 ± 4 % and 10 ± 3 % for MC and EC of NM12, respectively. Kaolinite-smectite was only observed in MC from NM12 and the expandability was between 5–10 %. Siderite was concentrated primarily in the coarse fractions of the EC end member. Other carbonates (calcite and dolomite), on the other hand, were found mainly in the bulk sample and the > 2 μm (> 45 and 2–45 μm) fractions of the MC end member. Kerogen and/or asphaltene were identified in all fine (< 45 μm) fractions of end members based on the N/C ratio (> 0.019). The very dark grey colour of MC compared with the beige colour of EC is due to the higher amount of residual TOC in all fractions of MC. The SSA-BET and TSSA-MB values increased as the amount of total clays and/or total 2:1 clay content increased. However, TSSA has higher values than the SSA values due to differences in the two techniques.

CHAPTER 6

6 INFLUENCE OF NON-SWELLING AND SWELLING CLAY MINERALS (ILLITE, KAOLINITE, CHLORITE, SMECTITE AND ILLITE-SMECTITE) DURING ORGANIC SOLVENT-BASED BITUMEN EXTRACTION PROCESS

The contents of this Chapter have been published in the following journals and presented in one peer-reviewed international conference:

M. Geramian, M. Osacky, L. Zheng, D.G. Ivey, Qi Liu and T.H. Etsell, 2013. Influence of Humidity in Swelling and Non-Swelling Clays on Non-Aqueous Bitumen Extraction. The 3rd Oil Sands Clay Conference and Workshop, CONRAD, Feb 20-21, 2013, Edmonton, Alberta.

M. Osacky, **M. Geramian**, D. G. Ivey, Q. Liu and T. H. Etsell, Influence of Nonswelling Clay Minerals (Illite, Kaolinite, and Chlorite) on Nonaqueous Solvent Extraction of Bitumen, Energy Fuels, 29 (2015), 4150-4159.

M. Geramian, M. Osacky, D. G. Ivey, Q. Liu and T. H. Etsell, Effect of Swelling Clay Minerals (Montmorillonite and Illite-smectite) on Non-Aqueous Bitumen Extraction from Alberta Oil Sands, Energy Fuels, 30 (10), (2016), 8083–8090.

6.1 INTRODUCTION

The mined deposits in Alberta oil sands, with 174 billion barrels of recoverable oil, represent the third largest oil reserve in the world [1, 2]. These deposits are highly variable in terms of deposition features, mineral composition and bitumen distribution. The majority of bitumen reserves occurs within the Lower Cretaceous McMurray Formation which consists of several hundred meters of mixed marine and continental sedimentary rocks [171,233]. Hodgson distinguished unconsolidated sands with interbedding of clays within both marine and continental sedimentary rocks [234]. The Alberta oil sands ores are different combinations of these clay-rich and sand-rich rocks deposited in marine and continental sedimentary environments.

Mossop reported that two important parameters, i.e., porosity and permeability of rocks, are controlling factors affecting the degree of bitumen saturation in the McMurray Sedimentary Formation of Alberta oil sands [171]. The sand-rich sediments with high porosity and permeability collected a significant amount of bitumen during the migration of bitumen into the McMurray Formation. Thus, these zones represent high-grade oil sands ores (>10 wt% of bitumen). In contrast, low-grade oil sands ores (<10 wt% of bitumen) occur in clay-rich zones with low porosity and permeability.

The mineral particle surfaces are generally surrounded by a thin film of naturally occurring water in the Alberta oil sands unlike the Utah tar sands [235]. The pores between the water wet particles are filled by bitumen. This condition leads to the liberation of bitumen from hydrophilic particles using water based bitumen extraction processes. Utah oil sands, on the other hand, consist of particles in direct contact with bitumen. For these hydrophobic particles, bitumen extraction is not effective by hot water based extraction processes.

The bitumen from the Alberta oil sands is commercially extracted by water-based processes. The non-aqueous solvent extraction processes have been studied for more than 50 years and have three main comparative advantages such as high bitumen recovery, elimination of waste tailings ponds and reduction/elimination of water consumption [32,174,236].

The Alberta oil sands deposits are a mixture of minerals (i.e., quartz, feldspars and clays), bitumen and salty water. Although quartz has little influence on bitumen extraction from the oil sands ores, clay minerals have a negative influence on bitumen extraction and recovery [35, 36]. Kaolinite,

illite and chlorite are reported as the main non-swelling clay minerals in Alberta oil sands ores [11]. Smectite and illite-smectite with expandability between 10 – 40 % have been determined as the common swelling clay minerals contained in the Alberta oil sands ores [11, 25]. Each clay mineral carries specific properties (e.g., crystal chemistry, structure and surface properties), which are different from other type of clays; thus, each clay may influence differently the bitumen extraction and recovery processes. For instance, interstratified swelling clay minerals (smectite and illite-smectite) may have a significant influence on bitumen extraction and/or bitumen recovery due to the ultrafine particle size fractions and swelling characteristics [10,20,182]

Spark *et al.* and Wallace *et al.* showed that there is a correlation between the mineral composition and the processability of the Alberta oil sands [35, 36]. However, it is difficult to understand the influence of individual clay minerals on bitumen extraction from the oil sands when studying the whole oil sands ore, due to its heterogeneity. Therefore, to minimize these issues, five natural standards of clay minerals from the Clay Minerals Society (the same types of clays present in the Alberta oil sands ores) were used to investigate the individual clay minerals (kaolinite, illite and chlorite) and swelling clays (smectite and illite-smectite). In this part of the work, an experimental set-up was designed and used for the assessment of the major types of clay minerals present in Alberta oil sands ores.

The present chapter is focused on the interaction between bitumen and individual non-swelling clays (kaolinite, illite and chlorite) and swelling clays (smectite and illite-smectite) to determine and better understand the influence of individual clay minerals on non-aqueous bitumen extraction. The comparison between different types of clay minerals allows for evaluation of the influence of both swelling and non-swelling clay minerals on non-aqueous bitumen extraction.

6.2 MATERIALS AND METHODS

6.2.1 MATERIALS

Three non-swelling clays (KGa-2 (kaolinite, Georgia), IMt-1 (illite, Montana) and CCa-2 (chlorite, California)) and two swelling clays: SWy-2 (smectite, Wyoming, USA) and ISCz-1 (illite-smectite, Slovakia) were obtained from the Clay Mineral Repository of the Clay Minerals Society.

In addition, bitumen extracted from a high grade, low fines (<44 μm), good processing oil sands ore was provided by Syncrude Canada Ltd.

6.2.2 SAMPLE PRETREATMENT

Bulk samples of the standard clays were suspended in distilled water and the <2 μm size fractions were separated by centrifugation. The <2 μm clay fractions were washed four times overnight by a 1 M solution of NaCl to prepare the Na^+-exchanged forms of the clays. Centrifugation and dialysis procedures were performed to remove the extra soluble salts from the suspended clays. The dried <2 μm size fractions (overnight at 60˚C) were gently ground using a diamond mortar and pestle. All <2 μm fractions of clays were re-dispersed in distilled water to prepare suspensions for freeze-drying. The clay suspensions were frozen in glass flasks and lyophilized using a SuperModulyo freeze-dryer at −50 °C for around a week. The freeze-dried clays were ground using a Retsch MM 200 mill for 10 min in plastic vials (25 mL) with three plastic balls (9 mm diameter), and sieved through a 250 μm sieve.

A cold wash procedure was performed to collect bitumen from the Syncrude oil sands ore using toluene at room temperature (~20 °C). The oil sands ore sample (~150 g) was placed in a 250 mL FEP centrifuge bottle, to which approximately 100 g (115 mL) of toluene was added. The bottle was sealed and centrifuged at a 2,830 relative centrifugal force (RCF) for 30 min. After centrifugation, the supernatant was gradually poured into the open glass beaker, which was placed on a hot plate at 70 °C for 7 days within a fume-hood. The centrifugation with fresh toluene was repeated three times. The bitumen was then used for the experiments after evaporation of toluene from the collected supernatant.

The <2 μm fractions of pretreated clays (Na^+-exchanged and freeze-dried) were dried overnight (24 h) in an oven at 105 °C and cooled to room temperature for 3 h using a desiccator with relative humidity (RH) of 0.2%. Afterwards, 2.50 g of these clays were placed in 250 mL FEP bottles. The bottles with clays were exposed to 50% and 95% RH in a humidity chamber for 24 h. The untreated samples in the humidity chamber were assumed as 0% RH samples, which were dried in an oven (at 105 °C for 24 h) and cooled to room temperature (0.2% RH for 3 h). The bottles were capped before removal from the humidity chamber to maintain equilibrated samples at 0%, 50%, and 95% RH. Then within a fume hood, 27.5 g of toluene-diluted bitumen (toluene/bitumen ratio = 1/10)

was poured into the above bottles. The blank samples were prepared for comparison, which consisted of mixtures of clays (2.5 g) with pure toluene (25 g) in the same procedure. Afterwards, the blanks and clay−toluene−bitumen (CTB) mixtures were agitated in a sealed bottle with an octagonal magnetic stirring bar (TeflonTM coated-PTFE, 25.4 mm in length and 8 mm in diameter) for 24 h at 40 °C on a hotplate/stirrer. The mixtures (Blanks and CTB) were then stirred and left at 40°C for 7 days in open bottles inside a fume hood to allow the toluene to evaporate. The bitumen was removed from the mixtures using cold-wash technique (three times) with cyclohexane and centrifugation with 3900g for 2 h. The supernatant (containing bitumen and cyclohexane) was slowly siphoned from the bottles to prevent the loss of clays during the cold-wash procedure. Both, supernatant and remaining materials were dried for 7 days at 40 °C within a fume hood and used for analytical experiments.

6.2.3 METHODS

To study the effect of individual clay minerals (swelling and non-swelling clays) on non-aqueous bitumen extraction process, the <2 μm fractions of pretreated standard clay minerals as starting clays, blank samples (0% RH, 50% RH and 95% RH) and clay-bitumen treated samples (0% RH, 50% RH and 95% RH) were examined by X-ray diffraction (XRD) analyses of oriented and random preparations, Fourier transform infrared spectroscopy (FTIR), inductively coupled plasma mass spectroscopy (ICP-MS), elemental analysis, cation exchange capacity (CEC), layer charge density (LCD), specific surface area (SSA), scanning electron microscopy (SEM) and energy dispersive X-ray (EDX).

XRD analyses of oriented and random preparations were carried out using a Rigaku Ultima IV diffractometer (40 kV, 44 mA) with CuKα radiation and a graphite monochromator. The step size was 0.02° 2θ for all samples. The counting time was 1 s and 2 s per step for oriented and random preparations, respectively. The oriented specimens were prepared using ~2 mL of suspension, containing 150 mg of sample on a frosted glass slide (4.6 cm × 2.8 cm). The air-dried oriented samples were exposed overnight at 54% RH before XRD analysis. Ethylene glycol (EG) solvation of oriented specimens was performed overnight at 60°C. Quantitative X-ray diffraction (QXRD) was performed on random preparations using the RockJock program [128]. Sample preparation

was performed according to a modified technique by Omotoso and Eberl, which is also reported by Środoń [141, 142].

XRD analyses on air-dried oriented specimens were performed to identify the crystallite thickness distribution (CTD) and the mean crystallite thickness (T_{MEAN}) for starting, blank and bitumen treated clays by BWA analysis, using the MudMaster computer program [96, 97]. Size distributions for crystallites (coherent X-ray scattering domains) can be determined by XRD through broadening of the XRD reflection widths due to the reduction of crystallite size. The calculations were carried out automatically by the MudMaster computer program [24].

Fourier transform infrared (FTIR) spectroscopy was performed using a Nicolet 6700 spectrometer. The KBr pressed pellet technique was used. To prepare KBr pressed pellets, 0.5 mg of the KGa-2 samples and 1.5 mg of the IMt-1, CCa-2, SWy-2 and ISCz-1 were separately mixed and dispersed in 200 mg of dried KBr (at 120 °C for 3 h). The pressed discs were heated in an oven overnight at 120°C prior to measurement. 128 scans with a resolution of 4 cm^{-1} were recorded for each sample. OMNIC software was used for spectral manipulations, i.e., automatic baseline correction and normalization of FTIR spectra.

Inductively coupled plasma mass spectroscopy (ICP-MS) was performed to identify the chemical composition of samples using multi-acid digestion prior to analysis. The analytical procedure followed standard methods used by Inspectorate Exploration and Mining Services Ltd. (Richmond, British Columbia, Canada).

The total C, H, N and S contents were determined by a Vario MICRO cube elemental analyzer. Approximately 25 mg of each samples were burned at 1150°C in a flowing stream of oxygen. The standard deviation was calculated from three replicates.

Scanning electron microscopy (SEM) was performed using a Zeiss EVO MA 15 instrument operated at 20 kV. The SEM was equipped with a Bruker energy dispersive X-ray (EDX) detector for elemental microanalysis. A secondary electron (SE) detector was used for imaging. The surface of the samples was coated with carbon film using a Leica EM SCD005 carbon coater, prior to SEM examination.

The Cu-triethylenetetramine method was used for cation exchange capacity (CEC) identification. The Pentrák *et al.* procedure was used for sample preparation and calculation of CEC values [126]. The reported values and the standard deviation were calculated from three replicates.

Rhodamine 6G (R6G) cationic dye was used to determine the layer charge density (LCD). The Šucha *et al.* procedure was performed for sample preparation [133]. A UV-Vis spectrophotometer (Varian Cary 50) was used to measure the visible spectra from the dispersed clays in the R6G solution after 24 h of dispersion. The spectra of the clay dispersions without R6G were subtracted from R6G-clay spectra to attain the spectra specific for the adsorbed dye.

Specific surface area (SSA) was determined by N_2 adsorption using the seven points BET technique over the relative pressure (P/P_0) range of 0.05 to 0.3. The samples were outgassed overnight (~24 h) at 130°C under vacuum using a Quantachrome Autosorb-1 MP instrument. The cross-sectional area of a nitrogen molecule was assumed to be 16.2 $Å^2$. The reported values and the standard deviation were calculated from three measurements with different weight loads.

A Hitachi NB 5000 dual beam FIB/SEM was used to prepare cross-section specimens to compare the starting and bitumen-treated clays and to investigate the discernible pattern between clays particles and layers. An air-dried oriented specimen technique was performed to prepare preferred orientation specimens on a glass slide (1×1 cm) followed by drying of the sample into an oven overnight at 105 °C. The samples were coated with a thin Au layer by sputter deposition prior to W deposition as part of the FIB sample preparation process. Tungsten layer was deposited as a protective by ion beam induced deposition. Bulk cutting/milling and polishing processes were carried out using a Ga^+ beam at 40 keV and 10 keV, respectively. The approximate thickness of the final thin section, which was prepared by FIB and placed on Cu grids, was ~100 nm.

6.3 RESULTS AND DISCUSSION

6.3.1 CHARACTERIZATION OF STARTING CLAYS

The mineral composition of the starting clays (<2 μm fractions, Na-saturated and freeze-dried) KGa-2, IMt-1, CCa-2, SWy-2 and ISCz-1, which were determined from the XRD patterns of random preparations by quantitative analysis (QXRD) using the RockJock program, are reported in Table 6-1. Kaolinite, illite, chlorite, smectite and illite-smectite are the main minerals in the

starting KGa-2, IMt-1, CCa-2, SWy-2 and ISCz-1 clays, respectively. Their purities are high and vary between 89 to 97 wt%. The starting KGa-2 clay includes trace quantities of anatase, illite and feldspars. Although, mineral impurities such as quartz, feldspars, palygorskite, talc and illite were not observed for KGa-2, these minerals were identified in the starting CCa-2, IMt-1, SWy-2 and ISCz-1 clays. In other words, CCa-2, IMt-1, SWy-2 and ISCz-1 clays are not pure chlorite, illite, smectite and illite-smectite, respectively. The mineral impurities are mostly quartz and feldspars with amounts between 6 to 11 wt%. However, these minerals (coarse size minerals) have little impact on bitumen extraction compared with clays. This hypothesis is also supported by other researchers in oil sands industry, who concluded the coarse minerals (i.e., quartz and feldspars) do not pose many issues during bitumen extraction process [15–18]. Comparison of XRD patterns from oriented specimens exposed to 54 %RH and ethylene glycol (EG) did not reveal any expandability for non-swelling clay i.e., KGa-2 and CCa-2 (with the exception of IMt-1, which have shown in Figure 6-1 h, i, j).

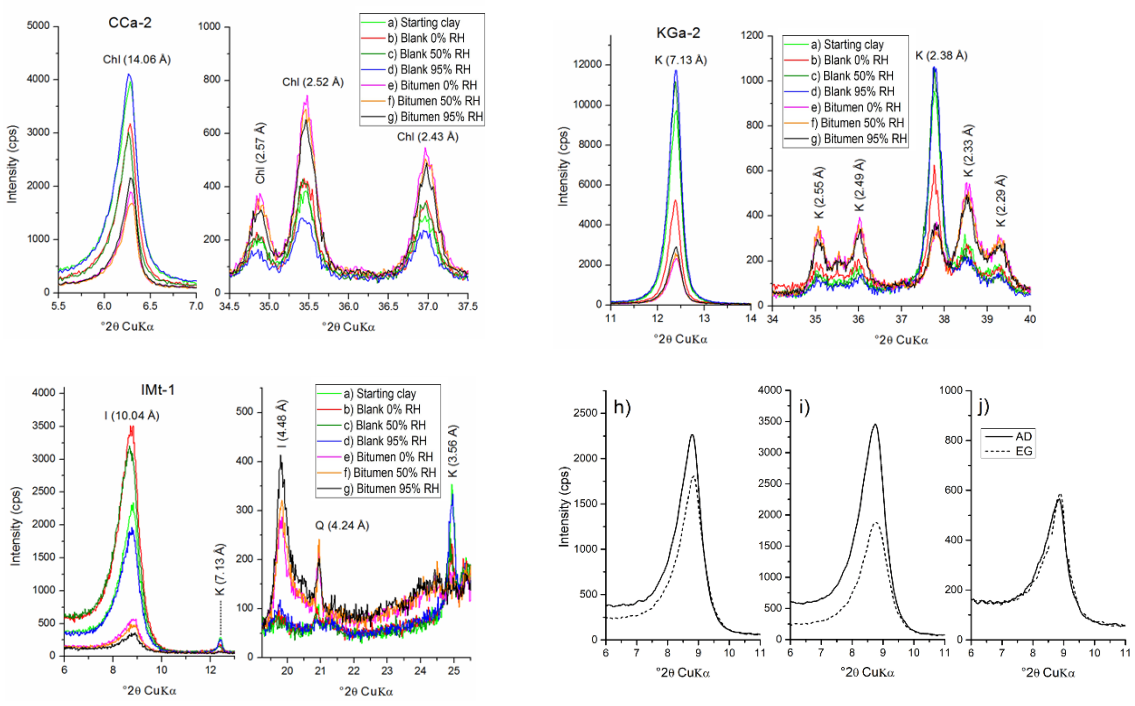

Figure 6-1 XRD patterns of oriented specimens for (a) the starting non-swelling clays; (b) blank 0% RH, (c) 50% RH, and (d) 95% RH; (e) bitumen 0% RH, (f) 50% RH, and (g) 95% RH; and (h) air-dried (AD, solid line) and ethylene glycolated (EG, dash line) illite 001 reflection for starting IMt-1, (i) IMt-1 blank 0% RH, and (j) IMt-1 bitumen 0% RH: I, illite; K, kaolinite; Chl, chlorite; Q – quartz.

A reduction in intensity for the illite 001 reflection (d = 10.04 Å) was observed for IMt-1 after ethylene glycol (EG) solvation compared with the 54% RH treatment. There were not any changes in the position of the IMt-1 illite 001 reflection after EG treatment. The presence of a small amount of smectite (expandable) mineral content was found for the starting IMt-1 clay based on Ir > 1 (Equation 5-1) according to the method described by Środoń [93]. This calculation is consistent with a published paper, which found 5% the expandability for IMt-1 from the Clay Minerals Society [234].

XRD patterns showed that SWy-2 and ISCz-1 were also affected by ethylene glycol treatment (Figure 6-2). The same technique was used for identification of the expandability for ISCz-1. The expandability (S_{XRD}) of the starting ISCz-1 illite-smectite was 17 ± 2%. The specific surface area (SSA) and cation exchange capacity (CEC) for the starting KGa-2, CCa-2, IMt-1, SWy-2 and ISCz-1 are listed in Table 6-2. Starting swelling clays have higher SSA values compared with non-swelling clays. The highest SSA was found for the starting SWy-2 clay and the lowest for the starting CCa-2 clay (Table 6-2). The results of chemical composition of the starting clays can be found in Table 6-2. The starting clays consist of negligible amounts of total C, H, N and S.

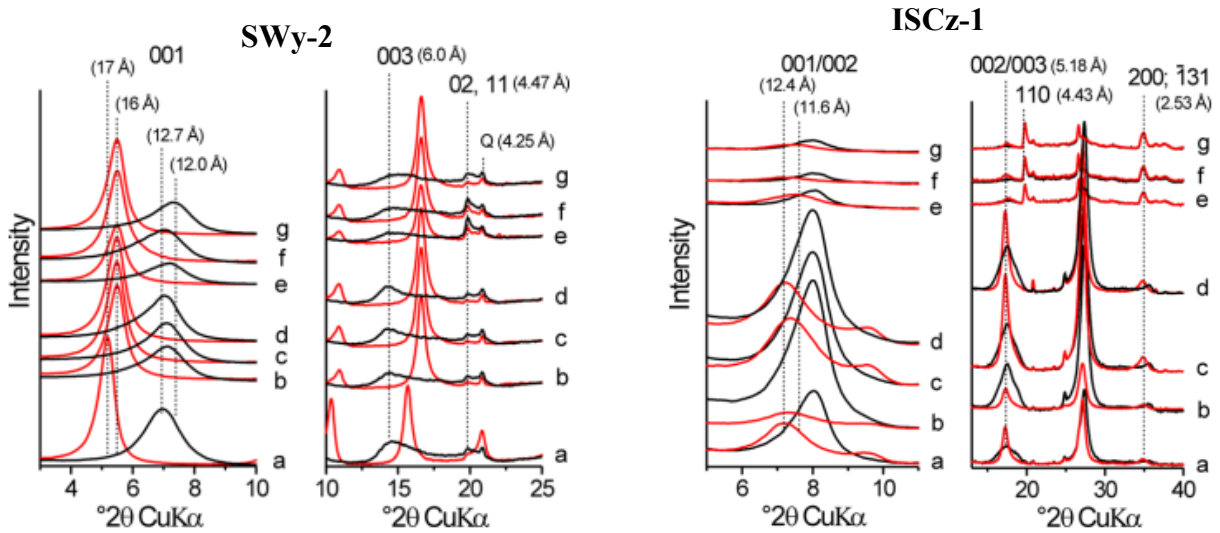

Figure 6-2 Air-dried 54% RH (black) and ethylene glycolated (red) XRD patterns of oriented specimens for (a) the starting swelling clays; the blanks (b) 0% RH, (c) 50% RH, and (d) 95% RH; bitumen treated (d) 0% RH, (e) 50% RH, and (f) 95% RH (g). Q – quartz.

Figure 6-3 shows the crystallite thickness distributions (CTDs) for the starting non-swelling clays using the results of the Bertaut-Warren-Averbach (BWA) analysis. The BWA analysis did not

show any significant changes in the shape of the crystallite thickness distributions (CTDs) for the blanks compared with the starting samples (Figure 6-3 and Table 6-2 a). Accordingly, only small mean crystallite thickness (T_{MEAN}) variations were observed for blank IMt-1 (7.0 ± 0.2 nm), blank KGa-2 (16.1 ± 0.5 nm) and blank CCa-2 (27.6 ± 0.8 nm) samples (Table 6-2 a). The T_{MEAN} values for these clays revealed differences between clays in Table 6-2. The lowest T_{MEAN} (7.5 nm) was found for IMt-1, while the highest T_{MEAN} was calculated for CCa-2. T_{MEAN} for KGa-2 was 16.2 nm. The crystallite thickness distributions (CTDs) for the starting swelling clays were not identified due to instrumental limitation for measuring XRD patterns at very low angles (2θ <1.5°).

Table 6-1 Mineral and chemical composition of the starting standard clays were characterized by quantitative X-ray diffraction (QXRD) analysis and ICP-MS, respectively. tr. – trace (<1 wt%), Loss-on-ignition (LOI) – 1000 °C for 1 h.

Mineral composition (wt%)										
Sample	Kaolinite	Chlorite	Illite	Smectite	Illite-smectite	Feldspars	Palygorskite	Quartz	Talc	Anatase
KGa-2	97	0	tr.	0	0	tr.	0	0	0	tr.
CCa-2	0	92	tr.	0	0	tr.	4	tr.	tr.	0
IMt-1	2	0	89	0	0	4	0	5	0	0
SWy-2	0	0	0	94	0	tr.	0	5	0	0
ISCz-1	tr.	0	0	0	93	4	0	2	0	0

Chemical composition (wt%)											
Sample	SiO2	Al2O3	Fe2O3	CaO	MgO	Na2O	K2O	TiO2	P2O5	LOI	Total
KGa-2	46.42	36.52	1.09	0.02	0.03	0.05	0.04	2.33	0.23	15.91	102.64
CCa-2	31.20	20.55	1.68	0.05	31.74	0.02	0.07	0.16	0.70	14.28	100.45
IMt-1	52.38	21.20	6.65	0.46	2.20	0.13	7.64	0.88	0.29	8.42	100.45
Swy-2	61.54	19.60	4.24	0.06	2.52	2.61	0.09	0.12	0.01	8.77	99.56
ISCz-1	57.06	25.39	1.67	0.03	2.25	0.74	5.93	0.11	0.02	7.92	101.12

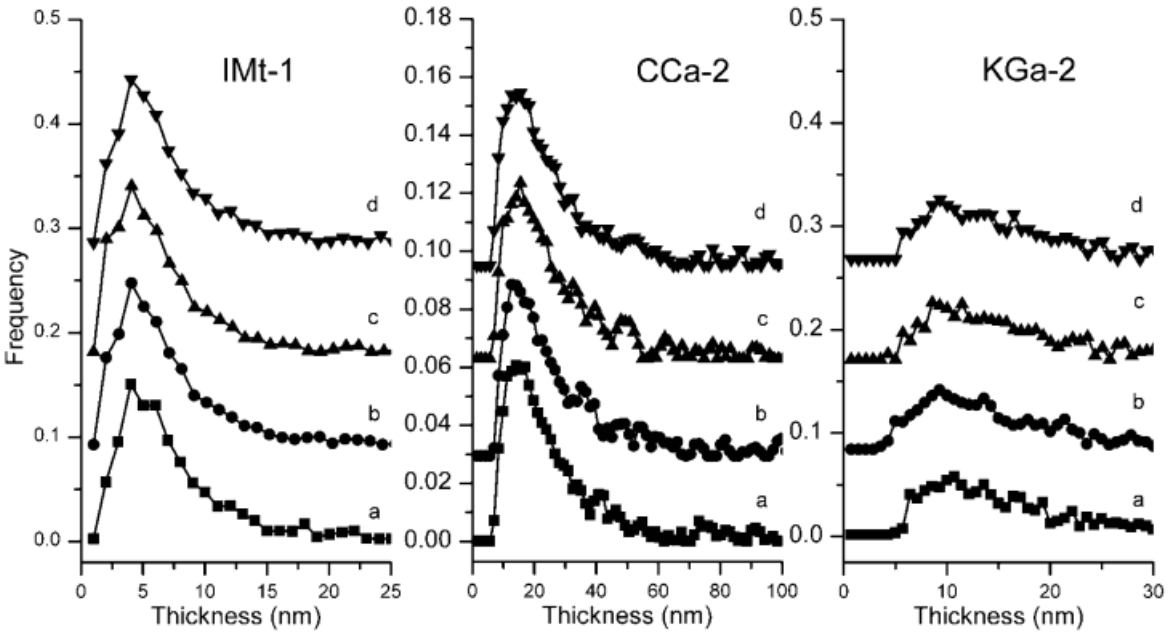

Figure 6-3 Crystallite thickness distributions (CTDs) for (a) starting clays and blanks at (b) 0% RH, (c) 50% RH and (d) 95% RH.

The starting KGa-2 and CCa-2 clays have similar CEC values. The highest CEC value for the starting non-swelling clays was found for the starting IMt-1 clay, which was two times higher than the values for the starting KGa-2 and CCa-2 clays (Table 6-2). Tournassat *et al.* found that the CEC values can be identified from the measurement of cation content, which balances the negative charge sites of the clay. They also determined that the outer surfaces (e.g., edges) of KGa-2 and CCa-2 clays are mainly responsible for the negative charge sites of these clay minerals. However, for IMt-1, the contribution of negative charge sites, which are located at inner surfaces (interlayer space) are the main sources of negative charge for the starting IMt-1 clay. These negative charge sites from the interlayer space lead to CEC values for the starting IMt-1 clay that are more than two times higher than those for the starting KGa-2 and CCa-2 clays. The cation adsorption capacity (CAC) would be more appropriate than cation exchange capacity (CEC) for these samples due to the adsorption of Cu(Trien) molecules mostly at the external surfaces of KGa-2 and CCa-2 clays [237]. The CEC value of the starting ISCz-1 clay was more than two times higher than that for the starting IMt-1 clay. The highest CEC values were identified for the starting SWy-2 clay, which was more than that of the starting ISCz-1 by a factor of 2.3. This phenomenon was expected due

to the higher interlayer space for SWy-2 compared with other clays. The CEC values increased substantially with cation adsorption capacity for the starting clays in the order: CCa-2 ≤ KGa-2 < IMt-1 < ISCz-1 < SWy-2 (Table 6-2).

Figure 6-4 shows the second derivative spectra (SDS) for the starting clays and the SDS for pure R6G solution without any clay admixture. There were no significant changes between the SDS for the starting KGa-2 and CCa-2 clays, and the SDS for the pure R6G solution. Since the starting KGa-2 and CCa-2 clays likely have a relatively low negative layer charge density (LCD), no absorption of R6G molecules was observed on the surface of these clays. In contrast, clear changes were identified for SDS for from the starting IMt-1 clay and the pure R6G solution. More significant changes were observed between the SDS of the starting ISZc-1 and SWy-2 and the SDS for the pure R6G solution (Figure 6-4). The reduction in intensity for the band near 529 nm of the SDS for the starting IMt-1 clay reveals the absorption of R6G molecules on the IMt-1 surface, predominantly due to the monomers on sites with low LCD. The comparison indicated that the spectral changes in the SDS for the starting IMt-1 clay was greater than those for the starting KGa-2 and CCa-2 clays, which are in agreement with the CEC results.

Table 6-2 a Cation exchange capacity (CEC), specific surface area (SSA), mean crystallite thickness, and elemental (H, N, S and C) analysis for non-swelling clays. n.a. – not analyzed.

Sample	CEC (meq/100g)	SSA (m^2/g)	T_{MEAN} (nm)	H (wt%)	N (wt%)	S (wt%)	C (wt%)
Starting materials							
Starting KGa-2	8.4 ± 1.07	21.1	16.2	1.523 ± 0.04	0.022 ± 0.02	0.016 ± 0.01	0.038 ± 0.00
Starting IMt-1	17.9 ± 0.14	42.0	7.5	0.679 ± 0.02	0.040 ± 0.00	0.021 ± 0.01	0.108 ± 0.00
Starting CCa-2	8.2 ± 0.49	14.7	26.6	1.419 ± 0.02	0.008 ± 0.00	0.003 ± 0.00	0.024 ± 0.01
Starting Bitumen	n.a.	n.a.	n.a.	9.899 ± 0.17	1.910 ± 0.56	5.514 ± 0.19	82.086 ± 0.44
Solvent-clay mixtures without bitumen (blanks)							
KGa-2 blank 0% RH	8.2 ± 0.15	19.1	15.7	1.472 ± 0.04	0.030 ±0.01	0.023 ± 0.00	0.490 ± 0.03
KGa-2 blank 50% RH	7.6 ± 0.03	18.6	16.6	1.636 ± 0.03	0.067 ± 0.02	0.025 ± 0.01	0.543 ± 0.02
KGa-2 blank 95% RH	9.1 ± 0.14	20.8	16.1	1.492 ± 0.05	0.047 ± 0.03	0.010 ± 0.01	0.317 ± 0.01
IMt-1 blank 0% RH	17.9 ± 0.21	24.5	7.1	0.751 ± 0.03	0.058 ± 0.02	0.072 ± 0.03	0.885 ± 0.01
IMt-1 blank 50% RH	17.7 ± 0.35	28.9	6.7	0.677 ± 0.01	0.053 ± 0.01	0.000 ± 0.00	0.530 ± 0.00
IMt-1 blank 95% RH	18.4 ± 0.97	31.0	7.1	0.787 ± 0.01	0.110 ± 0.00	0.024 ± 0.00	0.550 ± 0.00
CCa-2 blank 0% RH	8.1 ± 0.20	9.6	28.3	1.476 ± 0.06	0.025 ± 0.01	0.031 ± 0.01	0.758 ± 0.01
CCa-2 blank 50% RH	7.8 ± 0.06	9.7	27.8	1.461 ± 0.04	0.073 ± 0.02	0.023 ± 0.01	0.593 ± 0.01
CCa-2 blank 95% RH	8.5 ± 1.16	10.8	26.8	1.448 ± 0.01	0.030 ± 0.00	0.027 ± 0.01	0.233 ± 0.01
Bitumen-clay mixtures after cyclohexane extraction							
KGa-2 bitumen 0% RH	4.2 ± 0.27	15.4	n.a.	1.901 ± 0.01	0.087 ± 0.01	0.540 ± 0.00	5.460 ± 0.01
KGa-2 bitumen 50% RH	4.4 ± 0.06	17.6	n.a.	1.875 ± 0.13	0.130 ± 0.03	0.378 ± 0.32	5.357 ± 0.02
KGa-2 bitumen 95% RH	5.8 ± 0.24	17.9	n.a.	2.109 ± 0.00	0.113 ± 0.01	0.016 ± 0.00	5.660 ± 0.02
IMt-1 bitumen 0% RH	15.6 ± 0.32	11.6	n.a.	1.254 ± 0.03	0.130 ± 0.01	0.612 ± 0.03	6.588 ± 0.01
IMt-1 bitumen 50% RH	15.5 ± 0.52	11.2	n.a.	1.190 ± 0.01	0.140 ± 0.00	0.626 ± 0.03	6.367 ± 0.04
IMt-1 bitumen 95% RH	16.8 ± 1.07	10.2	n.a.	1.469 ± 0.02	0.163 ± 0.01	0.031 ± 0.01	6.967 ± 0.11
CCa-2 bitumen 0% RH	7.0 ± 2.10	6.5	n.a.	1.711 ± 0.01	0.050 ± 0.00	0.380 ± 0.00	4.075 ± 0.01
CCa-2 bitumen 50% RH	7.8 ± 0.35	5.6	n.a.	1.619 ± 0.01	0.070 ± 0.02	0.370 ± 0.00	3.637 ± 0.01
CCa-2 bitumen 95% RH	7.7 ± 0.07	6.7	n.a.	1.817 ± 0.01	0.080 ± 0.00	0.031 ± 0.00	3.797 ± 0.02

Table 6-2 b Cation exchange capacity (CEC), specific surface area (SSA) and elemental (H, N, S and C) analysis for swelling clays.

Sample	CEC (meq/100g)	SSA (m^2/g)	H (wt%)	N (wt%)	S (wt%)	C (wt%)
Starting materials						
Starting SWy-2	87.1 ± 1.10	31.0	0.736 ± 0.04	0.053 ± 0.01	0.009 ± 0.00	0.133 ± 0.02
Starting ISCz-1	37.5 ± 0.28	49.5	0.687 ± 0.01	0.045 ± 0.01	0.009 ± 0.00	0.100 ± 0.00
Solvent-clay mixtures without bitumen (blanks)						
SWy-2 blank 0% RH	85.6 ± 1.24	13.4	1.010 ± 0.06	0.048 ±0.02	0.049 ± 0.06	0.888 ± 0.01
SWy-2 blank 50% RH	87.5 ± 0.31	12.2	1.114 ± 0.01	0.053 ± 0.01	0.006 ± 0.00	0.750 ± 0.00
SWy-2 blank 95% RH	85.7 ± 1.03	9.3	1.432 ± 0.01	0.120 ± 0.00	0.022 ± 0.00	0.807 ± 0.03
ISCz-1 blank 0% RH	36.9 ± 0.43	38.6	0.774 ± 0.02	0.060 ± 0.01	0.062 ± 0.01	0.898 ± 0.01
ISCz-1 blank 50% RH	37.2 ± 0.63	42.4	0.862 ± 0.02	0.047 ± 0.01	0.021 ± 0.00	0.867 ± 0.02
ISCz-1 blank 95% RH	37.6 ± 0.12	43.9	0.977 ± 0.02	0.120 ± 0.00	0.015 ± 0.00	0.593 ± 0.01
Bitumen-clay mixtures after cyclohexane extraction						
SWy-2 bitumen 0% RH	82.1 ± 0.80	4.7	1.342 ± 0.08	0.123 ± 0.01	0.038 ± 0.01	4.605 ± 0.03
SWy-2 bitumen 50% RH	79.3 ± 0.14	5.6	1.515 ± 0.01	0.123 ± 0.01	0.536 ± 0.02	5.523 ± 0.19
SWy-2 bitumen 95% RH	76.9 ± 0.08	6.0	2.173 ± 0.01	0.193 ± 0.01	0.031 ± 0.01	8.153 ± 0.15
ISCz-1 bitumen 0% RH	32.3 ± 0.03	6.3	1.368 ± 0.08	0.153 ± 0.01	0.048 ± 0.00	7.083 ± 0.04
ISCz-1 bitumen 50% RH	29.2 ± 0.65	6.3	1.570 ± 0.01	0.160 ± 0.01	0.014 ± 0.00	8.180 ± 0.06
ISCz-1 bitumen 95% RH	30.2 ± 2.16	5.5	1.693 ± 0.01	0.203 ± 0.01	0.037 ± 0.00	8.047 ± 0.11

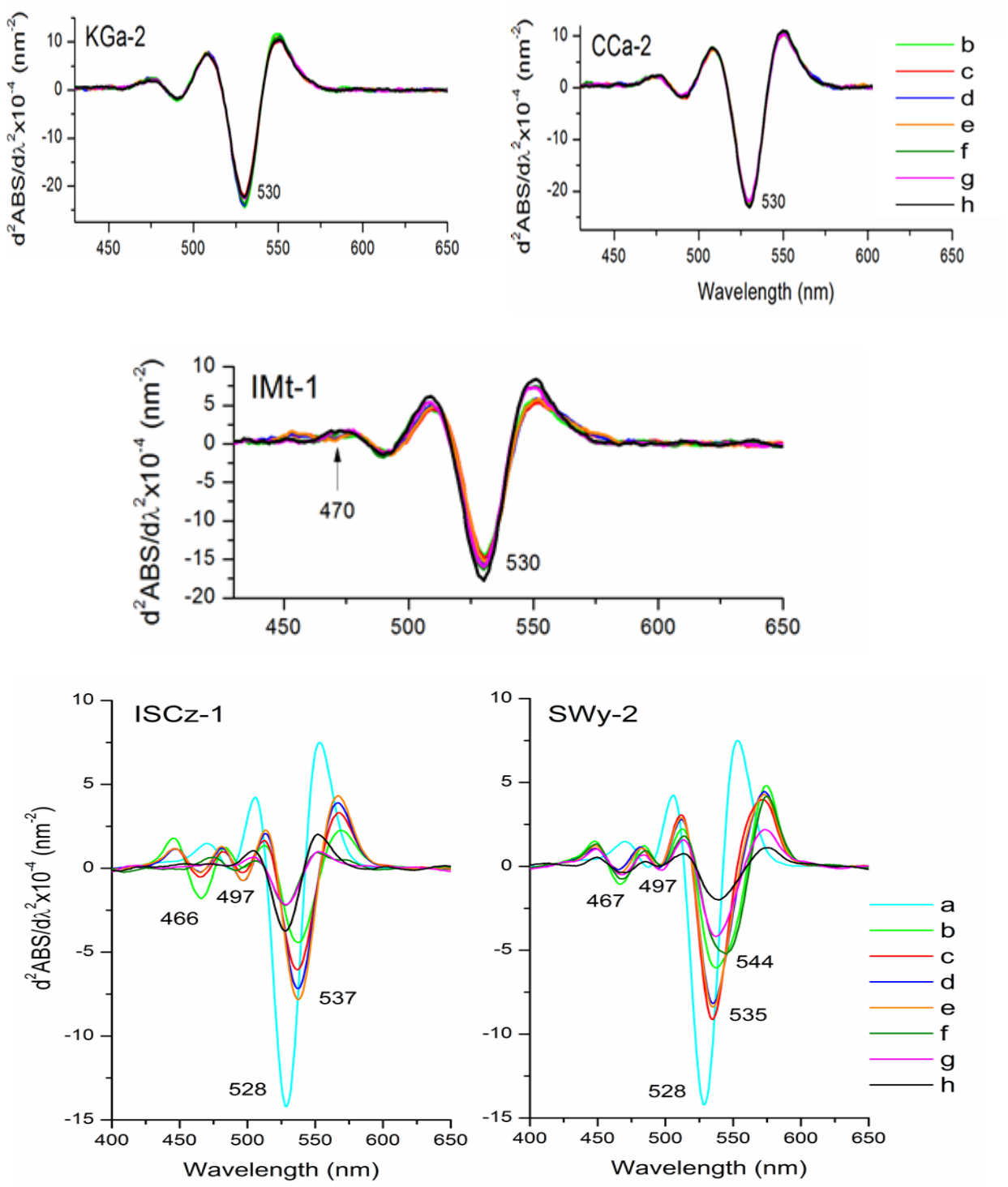

Figure 6-4 SDS for (a) R6G and R6G in dispersions with (b) starting clays, (c) blank 0% RH, (d) blank 50% RH, (e) blank 95% RH, (f) bitumen 0% RH, (g) bitumen 50% RH, and (h) bitumen 95% RH.

6.3.2 CHARACTERIZATION OF BITUMEN MODIFIED CLAY MINERALS

The five distinct types of non-swelling clays (kaolinite, chlorite, and illite) and swelling clays (smectite and illite-smectite), had different carbon contents after bitumen treatment followed by cyclohexane bitumen removal. Swelling clays had higher carbon content (4.6 - 8.2 wt%) than non-swelling clays (3.6 – 7.0 wt%). The illite-smectite ISCz-1 clay at three different humidity conditions (i.e., 0, 50 and 95%) had higher average carbon content (7.1 – 8.2 wt%) than smectite SWy-2 (4.6 – 8.2 wt%). Chlorite CCa-2 had the lowest carbon content for the three different humidity conditions (i.e., 0, 50 and 95%) with values from 3.6 to 4.1 wt%. Illite IMt-1 contained the highest amount of carbon (6.4 – 7.0 wt%) among non-swelling clays (Table 6-2). The variable amount of carbon that remained after bitumen treatment and bitumen removal using toluene and cyclohexane, respectively, revealed that the residual carbon content depends on the nature of clay and sample pre-treatment.

The cyclohexane solvent cannot dissolve and/or extract all components of pure bitumen. The previous experimental results revealed that 95.2 wt% of the initial mass of the pure bitumen sample was dissolved in cyclohexane, while 4.8 wt% of the pure bitumen resisted the cyclohexane extraction process [24]. The analytical techniques, i.e., FTIR and elemental analysis, show that high molecular weight (MW) organic compounds were the majority of the cyclohexane insoluble organic matter remaining from cyclohexane extraction of pure bitumen [24].

6.3.3 IMPACT OF RELATIVE HUMIDITY (RH) ON BITUMEN EXTRACTION

The residual carbon content of the swelling clays after cyclohexane bitumen extraction was remarkably affected by various relative humidity (RH) conditions (0%, 50% and 95% RH). However, the influence of different RH conditions on the amount of residual carbon was insignificant for bitumen-treated non-swelling clays. The extreme variation in the residual carbon content for different RH conditions was observed in smectite SWy-2 clay, where the residual carbon content was gradually elevated in higher RH pre-treatment (Table 6-2 b). This finding is likely due to the opening of the swelling interlayer space of smectite SWy-2 clay, which was exposed at higher RH which was followed by retention of organic matter in the swelling interlayer space after cyclohexane extraction.

Several research results indicate that the basal spacing of smectite clay gradually increased with increasing RH, which is related to the accommodation of one, two or three layers of H_2O molecules in the smectite interlayer [92,238]. Moore and Hower studied the Na-exchange form of smectite SWy-2 and showed that the basal spacing was elevated from 0.96 to ~ 1.2 to 1.8 nm by increasing the RH from 0 to 50 to 100 wt%, respectively [92]. Therefore, the evolution in carbon content with increasing RH for bitumen-treated SWy-2 clays is likely due to the larger basal spacing (i.e., more opened swelling interlayers) leading to trapping of more organic matter after the bitumen treatment. In contrast, the carbon contents for the bitumen-treated ISCz-1 clay with increasing RH varied, which is likely due to the lower expandability of illite-smectite ISCz-1 (one sixth) compared with smectite SWy-2. The highest residual carbon contents for non-swelling clays were determined for bitumen-treated IMt-1 (6.4 – 7 wt%); the lowest residual carbon contents for bitumen-treated CCa-2 (3.6 – 4.1 wt%). The amount of carbon after cyclohexane bitumen extraction was not significantly changed by increasing the RH for the pre-treatment of non-swelling clay minerals (kaolinite, illite and chlorite).

The bitumen-treated ISCz-1 clays had relatively higher carbon contents after cyclohexane bitumen extraction (7.1 – 8.2 wt%) compared with SWy-2 (4.6 – 8.2 wt%) (Table 6-2 b), although the expandability of illite-smectite ISCz-1 is significantly lower than that for smectite SWy-2. The high carbon contents for bitumen-treated ISCz-1 clays are likely due to the high specific surface area (SSA) of ISCz-1 (49.5 m^2/g) compared with SWy-2 (31.0 m^2/g) (Table 6-2). The high carbon contents of bitumen treated ISCz-1 after cyclohexane bitumen removal are likely due to the larger SSA. It seems that the ISCz-1 clay with low expandability (17%) behaved in a manner more characteristic of non-swelling clay minerals than swelling clay minerals during the cyclohexane bitumen extraction process.

6.3.4 CHANGES IN THE ORIENTATION OF CLAY PARTICLES

Clear differences in the intensity of chlorite reflections were found in the XRD oriented patterns for CCa-2 after reaction with bitumen (bitumen-treated clays) and with pure organic solvent (blank clays) (Figure 6-1). The XRD intensity changes were more pronounced for bitumen-treated CCa-2 samples than those for blank CCa-2 clays. However, the position of the 001 reflection for the chlorite samples remained unaffected by the reaction of CCa-2 with bitumen and with pure organic

solvent. After the experiments, two different trends were found in the evolution of the chlorite basal (00l) and non-basal (hkl) reflections for CCa-2. The chlorite non-basal reflections for bitumen-treated CCa-2 increased in intensity in the following order: bitumen 0% RH > bitumen 50% RH > bitumen 95% RH (Figure 6-1).

Kaolinite was the only mineral identified in the XRD patterns of oriented specimen for the starting KGa-2 clay (Figure 6-1). The positions and intensities of the 001 reflection for the starting and reacted (blanks and bitumen-treated) KGa-2 and CCa-2 samples were unaffected by ethylene glycol (EG) treatment, due to lack of mixed-layered clay minerals. The intensity of the kaolinite basal reflections increased for the blanks KGa-2 in the order: blank 0% RH < blank 50% RH < blank 95% RH (Figure 6-1). Among all KGa-2 blanks, only the KGa-2 blank 0% RH sample had a kaolinite basal reflection intensity lower than the starting KGa-2 clay. Kaolinite basal reflection intensities were reduced substantially after reaction with bitumen in the order: KGa-2 bitumen 95% RH < KGa-2 bitumen 50% RH < KGa-2 bitumen 0% RH (Figure 6-1). The non-basal kaolinite reflections showed the opposite trend after reaction with bitumen. Their XRD intensities increased substantially for bitumen-treated KGa-2 samples compared with the starting and the blanks KGa-2 clays (Figure 6-1).

Kaolinite (d = 7.12 Å and 3.56 Å) and quartz (d = 4.24 Å and 1.81 Å) were found in the XRD patterns of oriented specimens for all IMt-1 clays (Figure 6-1). Although, the XRD intensity of the illite 001 reflection (d = 10.04 Å) was reduced for starting IMt-1 after ethylene glycol (EG) solvation, the position for the starting IMt-1 illite 001 reflection remained unaffected by EG treatment (Figure 6-1). The expandability of illite-smectite was calculated based on the comparison of XRD patterns of oriented preparations between air-dried and EG oriented according to the method described by Środoń [94]. The presence of a small quantity of expandable (smectite) interlayers clay was found for the starting IMt-1. This finding is consistent with published data by Hains and van der Pluijm, who found less than 5% of smectite interlayers for IMt-1 [239].

Clear differences are observed between the air-dried (54 % RH) XRD patterns for starting and bitumen-treated swelling clays. The XRD patterns of oriented specimens for both air-dried and EG solvated showed a reduction of the relative intensity of the 00l reflections for bitumen-treated swelling clays (ISCz-1 and SWy-2) compared with the relative intensity of the hkl reflections of the starting and blank clays, which is likely related to the changes in the orientation of clay particles

(Figure 6-2). This conjecture is consistent with the SEM-EDX investigation of XRD oriented preparations, which shows the creation of large clay aggregates in the SEM images as well as the elevation of C and S contents in the EDX spectra of bitumen-treated clays (Figure 6-5). The images show binding between clay particles and large aggregates by residual organic matter. In the wake of this gluing, the preferred orientation specimen of the starting clay particles, which are mostly parallel to the basal plane, became more randomly oriented with the presence of clay-organic aggregates. SEM images also showed that the clay-organic aggregates which formed upon reaction of clays with bitumen were sufficiently stable to resist both cyclohexane bitumen removal and preparation of XRD oriented samples (sonication of bitumen modified clays for 5 min).

6.3.5 OCCUPATION OF INTERLAYER SPACE BY ORGANIC MATTER

No change in the basal spacing of the KGa-2, IMt-1 and CCa-2 samples reveals that the organic solvent did not penetrate the interlayer space of the non-swelling clay minerals; however, it was adsorbed primarily on the external clay mineral surfaces. The reduction of the 001 reflection intensity for all blank IMt-1 samples after ethylene glycol (EG) solvation indicates that the interlayer space was not blocked by the organic solvent coating (Figure 6-1 i).

More pronounced and systematic changes were observed in the XRD oriented patterns for all bitumen-treated non-swelling clays; the XRD intensity decreased substantially for non-swelling clay mineral basal (00l) reflections and the intensity increased for clay mineral non-basal (hkl) reflections. The intensities of the 00l reflections for clay minerals were likely influenced by the particle orientation (preferred vs. random), crystallite size, structural ordering and crystal defects. These observations are also consistent with published data by Uhlik *et al.* and Dohrmann *et al.*, who showed that the 00l reflections are broadened and their intensities decreased with more random orientation, small crystallite size and the presence of stacking defects and structural disorder [240,241]. The changes in the XRD patterns for bitumen-treated clays is likely connected with the changes in the clay particle orientation due to reaction with bitumen.

With a reduction in the degree of preferred orientation, the diffraction intensity of the 00l reflections is decreased in favor of other hkl reflections. These hypotheses were confirmed by SEM images of the XRD oriented preparations of all bitumen-treated samples, which showed the gluing

of small clay particles to large aggregates by organic material. Therefore, the preferred orientation of clay particles changed to more random upon reaction with bitumen (Figure 6-5 and Figure 6-6).

In addition to the XRD intensity variations, the smectite 001 reflection was shifted to smaller d-values in the XRD patterns for the blank and the bitumen-treated clays compared with the air-dried (54% RH) SWy-2 sample (Figure 6-2, patterns in black). Similar changes were observed in the XRD patterns after EG solvation for these samples (Figure 6-2, patterns in red). The relative intensity of the smectite 001 reflection was reduced and changed to smaller d-values after solvation with EG for all blank and bitumen-treated SWy-2 clays. A reduction in the basal spacing (d-values) indicates that the swelling ability was reduced for blank SWy-2 and bitumen-treated SWy-2 clays, which is likely due to the partial penetration of the interlayer space of smectite by organic solvent and bitumen, respectively. The reduction in intensity and shift of the smectite 001 reflection for the air-dried XRD patterns were more distinct for bitumen-treated SWy-2 than for blank SWy-2 clays. These findings are likely due to the chemical nature of bitumen and organic solvent and/or various residual organic contents remaining in the interlayer space of SWy-2 clay.

The XRD patterns for illite-smectite ISCz-1 clays showed different trends compared with the smectite SWy-2 clays. For XRD patterns of the smectite samples, the relative intensity of the smectite 001 reflection decreased in the air-dried XRD patterns for blank SWy-2 clays compared with the starting samples. The relative intensity of the illite-smectite 001/002 reflections increased in the air-dried XRD patterns for blank ISCz-1 clays compared with the starting samples (Figure 6-2). There were negligible shifts in the position of the illite-smectite 001/002 reflection in the air-dried XRD patterns after reaction with bitumen and pure organic solvent. However, the smectite 001 reflection clearly changed to smaller d-values in the air-dried XRD patterns for blank and bitumen-treated SWy-2 samples. After solvation with EG for illite-smectite (patterns in red), the visible changes in the ISCz-1 001/002 reflections to smaller d-values occurred for blank ISCz-1 and bitumen-treated ISCz-1 clays (Figure 6-2).

The basal spacing for illite-smectite after EG solvation shift for blank and bitumen-treated ISCz-1 clays is likely due to the penetration of the interlayer space of illite-smectite by organic solvent and bitumen, respectively. The occupation of the interlayer space by organic matter prevents full EG solvation. The lack of shifting in the Illite-smectite 001/002 reflections for the air-dried blank ISCz-1 and bitumen-treated ISCz-1 XRD patterns contrasts the shift of the SWy-2 smectite 001

reflection, which is likely connected with a significantly lower amount of swelling interlayers for illite-smectite ISCz-1 (17%) compared with smectite SWy-2 (100%).

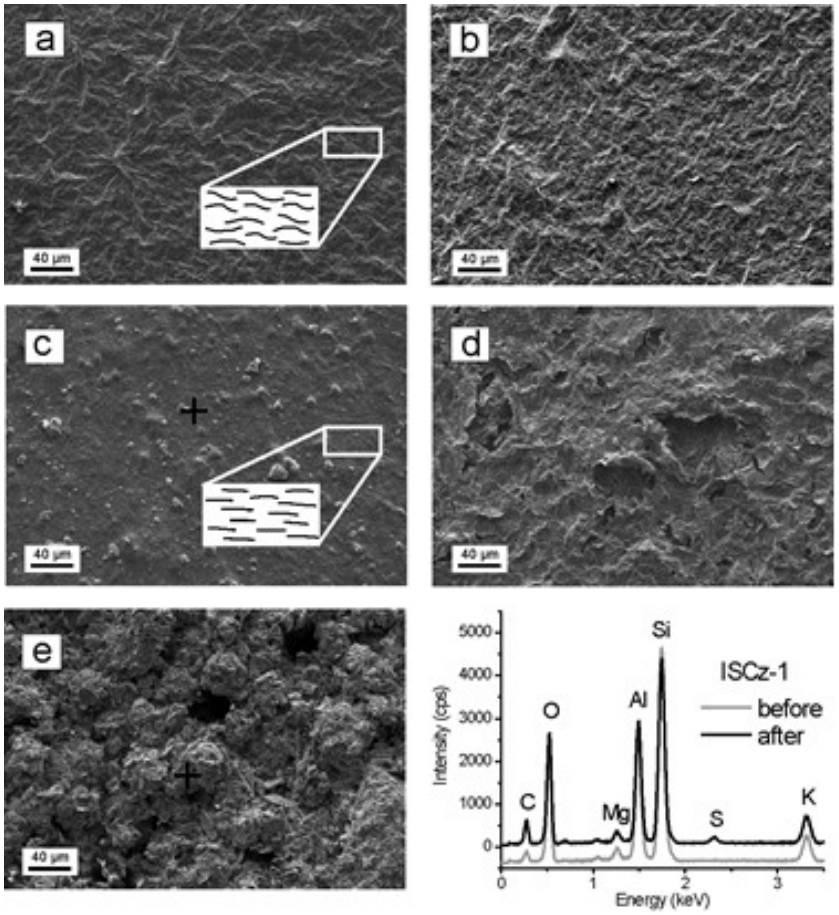

Figure 6-5 SEM SE images for swelling clays. (a) starting SWy-2, (b) SWy-2 blank 50% RH, (c) starting ISCz-1, (d) SWy-2 bitumen 50% RH and (e) ISCz-1 bitumen 50% RH. There were different orientations of clay particles for starting (a) SWy-2 and (c) ISCz-1. EDX spectra for starting ISCz-1 (before treatment) and ISCz-1 bitumen 50% RH (after treatment).

The different relative intensity variations of the 00l reflections between smectite (blank SWy-2) and illite-smectite (blank ISCz-1) show distinct structural ordering of clay crystallites (X-ray scattering domains) upon their reaction with pure organic solvent. The reduction of the relative intensity for the smectite 001 reflections from the initial value for all blank SWy-2 clays may be related to aggregation of smectite particles after reaction with pure organic solvent. This conjecture is in good agreement with the SEM observations, which showed a significantly higher number of small aggregates for the blank SWy-2 clay than for the starting SWy-2 clay (Figure 6-5).

The increased relative intensities of the illite-smectite 001/002 reflections for the blank ISCz-1 clays, indicates higher structural ordering, which is likely due to the interparticle diffraction effect caused by more face-to-face contact between the clay particles after reaction with pure organic

solvent. The additional treatment (agitation, stirring, washing, and drying) performed only for reacted (blanks and bitumen-treated) samples and the specific shape of ISCz-1 clay particles may account for the higher structural ordering of the blank ISCz-1 clays. This conjecture is consistent with previous work showing the interparticle diffraction effect for ISCz-1 clay which resulted from its high ability to build face-to-face contacts between the particles [242]. Sucha *et al.* suggested that this behavior is related to large a and b dimensions and the high flexibility of thin ISCz-1 clay particles. More dense arrangement of clay particles would uniquely reduce pore volume which may have resulted in the reduction of SSA values. This assumption was also confirmed by SSA results, which revealed a reduction in the SSA values for all blank ISCz-1 clays compared with the starting ISCz-1 clay (Table 6-2).

6.3.6 REDUCTION OF CEC UPON BITUMEN EXTRACTION

No significant variations were observed in CEC values for blanks compared with those for the starting non-swelling or swelling clays (Table 6-2). However, the CEC values for all bitumen-treated clays were decreased for both clay groups (non-swelling and swelling), which is likely due to penetration of organic matter into the interlayer space of swelling clay minerals, organic coatings on non-swelling and swelling clay minerals outer surfaces (basal planes and edges), and/or gluing of clay particles to aggregates. The CEC values of swelling clays after bitumen-treatment were reduced only by 6% to 22% compared with the starting clays. However, this reduction varied for non-swelling clays after bitumen-treatment by 5% to 50% compared with the starting clays. The KGa-2 and SWy-2 clays had the highest and lowest reduction ranges of 31% to 50% and 6% to 12%, respectively. These results indicate that a large portion of the negative charge sites on the swelling clay mineral surfaces after bitumen treatment was still accessible to Cu_{TRIEN} molecules used for the CEC determination, whereas a significant number of these negative charge sites on the non-swelling clays, particularly kaolinite (KGa-2), were not reachable to Cu_{TRIEN} molecules due to the different features of clay structures and negative charge sites. Generally, it can be speculated from the CEC results for bitumen-treated clays that the residual organic matter partially occupied the inner (interlayer space) and outer (basal planes and edges) surfaces of clay minerals in the form of patches rather than continuous coatings. Therefore, the patchy surface accumulation of residual organic material mainly occurred on the specific negatively charged sites of the clay mineral surfaces. This assumption has been reported by a few oil sands researchers,

who found a patchy surface distribution of organic matter on marine sediments and Alberta oil sands [36,214,243–245]. Most organic material remained at specific negatively charged sites on the clay mineral surfaces after non-aqueous bitumen removal, likely due to the accumulation of patchy regions of residual organic matter.

The CEC values for bitumen-treated SWy-2 clays were gradually reduced with increasing RH pre-treatment, which is likely related to the increasing amount of residual organic matter for bitumen-treated SWy-2 clays pre-treated under higher RH (Table 6-2 b). More residual organic matter occupied more interlayer space and the larger outer surface area on the clay mineral surfaces, which led to reduced adsorption of Cu_{TRIEN} molecules and subsequently reduced CEC values. This assumption was confirmed by the experimental results showing the carbon content gradually increased with increasing RH pre-treatment for bitumen-treated SWy-2 clays (Table 6-2).

The CEC values dropped for all non-swelling clays after treatment with bitumen compared with the starting clays. The reduction of CEC values for bitumen-treated non-swelling clays was more remarkable for KGa-2 samples (from ~31% to ~50%) than for CCa-2 (from ~5% to ~15%) and IMt-1 (from ~6% to ~13%) samples. However, these reductions were varied for different RH % and residual organic matter. The highest and lowest CEC reduction for bitumen-treated clays belonged to CCa-2 bitumen 50% RH (5%) and to KGa-2 bitumen 0% RH (50%), respectively.

The CEC reduction among the bitumen-treated non-swelling clays (kaolinite KGa-2, illite IMt-1 and chlorite CCa-2) revealed that the negatively charged sites were partially occupied by residual organic matter, which is not constant, but depend on the adsorbing clay material. The distinct clay minerals may consist of various negative layer charges and different densities of negative charged sites on the surface. The differences in CEC reduction between the individual clays after bitumen treatment are likely due to the distinct layer charge and density of negatively charged sites on the surfaces of clay minerals.

6.3.7 INFLUENCE OF SSA ON BITUMEN EXTRACTION

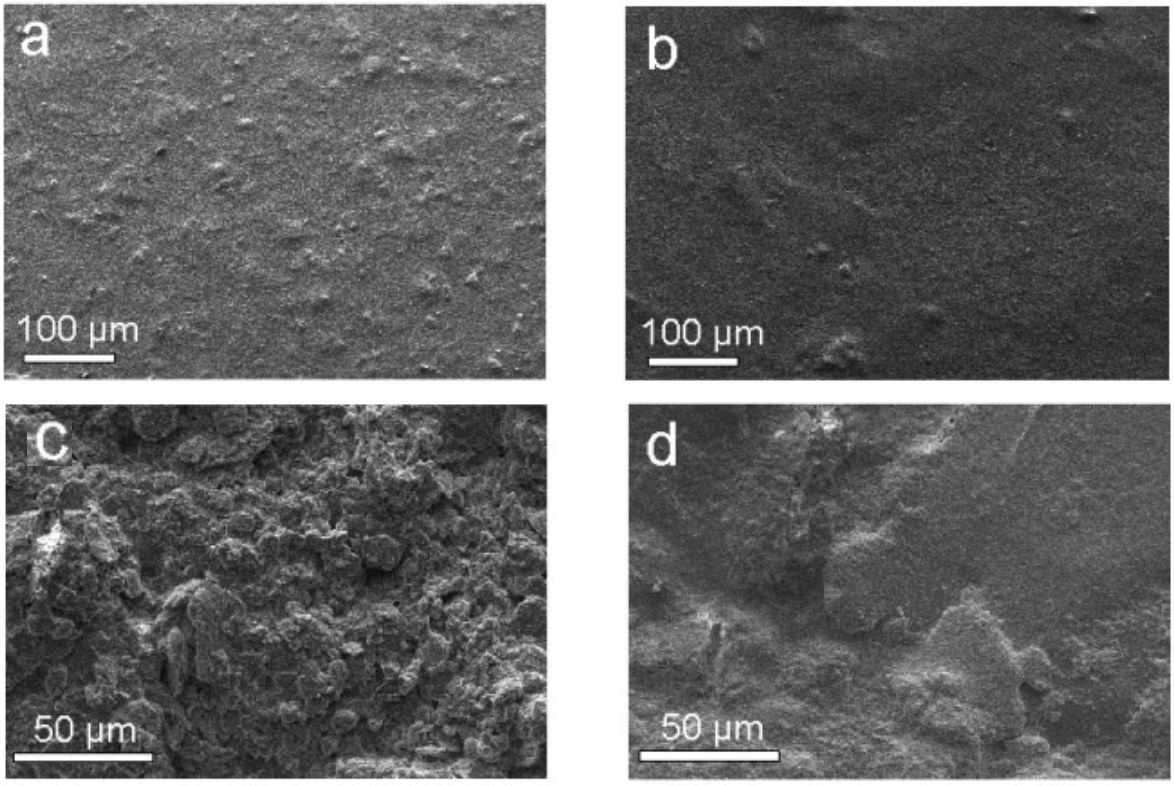

Figure 6-6 SEM SE images of non-swelling clays: (a) starting KGa-2, (b) KGa-2 blank 50% RH, (c) IMt-1bitumen 95%, and (d) KGa-2 bitumen 95% RH.

A reduction in SSA values was found for all blanks and bitumen-treated clays compared with the starting clays, both non-swelling and swelling, which is likely related to the presence of residual organic matter on the clays upon reaction with bitumen and pure organic solvent (Table 6-2). In other words, N_2 adsorption can be affected by inaccessibility due to organic matter filling or blocking pores and/or gluing of clay particles to larger aggregates by organic material [116,214,217].

The reduction in SSA was similar for all bitumen-treated swelling clays (81 – 85% for bitumen SWy-2 and 87 – 89% for bitumen ISCz-1 samples), whereas it differed for all bitumen-treated non-swelling clays (15-27% for bitumen KGa-2, 72 – 76% for bitumen IMt-1 and 5-15% for bitumen CCa-2 samples). However, the reduction in SSA values varied for blank clays, either non-swelling or swelling (1-12% for blank KGa-2, 26-42% for blank IMt-1, 27-35% for blank CCa-2, 11-22% for ISCz-1 and 57-70% for blank SWy-2) (Table 6-2). More significant reduction in SSA

values was found for bitumen-treated clays compared with the blank-clays. This may be related to a higher residual organic content remaining on clays after bitumen treatment than on clays after pure solvent treatment. This indicates that the quantity and/or types of residual organic matter played a crucial role in reduction of the SSA for all non-swelling and swelling clays.

The SSA reduction varied for blank non-swelling clays (KGa-2, IMt-1 and CCa-2) and swelling clays (SWy-2 and ISCz-1), which may be related to the differences in the shape of the starting clay mineral particles (curly shape for SWy-2 vs. flat shape for ISCz-1 and all non-swelling clays (Figure 6-5 and Figure 6-6). Due to the different clay mineral particle shapes, the orientation of the starting clay minerals and subsequent re-arrangement of the clay mineral particles after reaction with pure organic solvent (without bitumen) may be different for all clays, particularly for the SWy-2 and ISCz-1 clays. Distinct rearrangement of the clay mineral particles upon reaction with pure organic solvent (without bitumen) was clearly indicated by XRD analysis, which showed increased relative intensities of the illite-smectite 001/002 reflections for blank ISCz-1. The relative intensities of the smectite 001 reflections were reduced for blank SWy-2 clay (Figure 6-2). Like ISCz-1, the relative intensities of the illite 001 reflections were increased for blank IMt-1 samples. However, the relative intensities of the kaolinite 001 and the chlorite 001 reflections varied for the blank samples (Figure 6-1). Due to different orientations and rearrangement of the clay mineral particles, N_2 adsorption varied among the samples which resulted in variable reduction of the SSA. These observations are also consistent with published data, which showed that the SSA values, determined by N_2 adsorption, can be influenced by the arrangement of particles and aggregates relative to each other (microstructure) [246,247]. Kuila and Prasad stated that clay minerals contained porosity with different dimensions and scales, which was correlated to natural shales and pure clay mineral microstructures [248]. Each clay mineral may have a variety of porosity and pores size distribution, which is likely related to the distinct size and morphology of clay particles [248]. Therefore, it can be speculated that the distribution of organic matter with respect to the clay microstructure is heterogeneous. In natural oil shales, the organic matter may exist in the form of separate particles or laminations where clay porosity may be open to adsorption or organic matter can partially or completely occupy the space between clay aggregates [249].

6.3.8 EFFECT OF LAYER CHARGE DENSITY (LCD) ON BITUMEN RETENTION BY CLAY MINERALS

Minimal changes were observed in the second-derivative spectra (SDS) for reacted (blanks and bitumen-treated) KGa-2 and CCa-2 clays, which may be related to the low negative layer charge density on their surfaces. On the other hand, more pronounced changes were observed in the SDS for blanks and bitumen-treated IMt-1 clays, which likely correlated to the higher density of negatively charged sites on the IMt-1 clay surfaces.

The reduction in the layer charge density, indicated by a band intensity decrease for H-aggregates (~470 nm) and a band intensity increase for monomers (~530 nm), in the SDS for blanks and bitumen-treated IMt-1 samples may be connected with the organic coating on the IMt-1 surface. Coverage of negatively charged sites on the IMt-1 surface by organic matter blocked the adsorption of rhodamine 6G (R6G) on these sites, which led to the reduction in the layer charge density. The disappearance of H-aggregate bands in the IMt-1 SDS after reaction with bitumen indicates that more high charge density sites were inaccessible to R6G adsorption for bitumen-treated samples than those for blanks, likely due to significantly higher amounts (7 to 12 times) of residual organic matter.

Three intensive bands near 467, 497 and 535 nm were found for the SDS of starting SWy-2 and ISCz-1 clays (Figure 6-4). The formation of H-aggregates was detected by the band near 467 nm, which are typically formed on sites with highly negative LCD. The band near 535 nm is characteristic of monomers, which is commonly formed for layers with small negative LCD. The band near 497 nm is preferentially related to H-dimers.

Significant differences were identified for the SDS of starting swelling clays compared with those for blanks and bitumen-treated clays (Figure 6-4). The SDS for blank SWy-2 and ISCz-1 clays showed a clear reduction of the H-aggregates (~497 nm) in favor of monomers (~535 nm), which demonstrated a reduction in the adsorption of R6G molecules on the sites with highly negative LCD in favor of sites with lower negative LCD due to the reaction with only pure organic solvent.

The SDS for blank and bitumen-treated non-swelling clays exhibited slightly changes compared with the starting clay samples. On the other hand, for the SDS for bitumen-treated ISCz-1 clays, the band intensity for monomers (~535 nm) and H-dimers (~497 nm) was reduced and the band attributed to H-aggregates (~466 nm) disappeared (Figure 6-4). The intensity of the bands near 544, 497 and 467 nm was gradually reduced with increasing amount of carbon in the SDS for bitumen-treated SWy-2 clays. This indicates that the amount of areas coated by residual organic

matter increased with increasing carbon content on SWy-2 clay mineral surfaces after bitumen treatment. Therefore, the SDS shows lower adsorption of R6G molecules on clay mineral surfaces due to fewer negatively charged sites accessible for R6G. Due to the presence of residual organic matter, the spectral changes observed in the SDS for bitumen-treated SWy-2 clays reveal a reduction in the LCD, which is consistent with the CEC results (Table 6-2).

6.3.9 FOURIER TRANSFORM INFRARED SPECTROSCOPY

Figure 6-7 shows the FTIR spectra of all starting, blank and bitumen-treated non-swelling and swelling clays. The presence of residual organic matter can be clearly identified from the formation of aliphatic CH stretching bands in the FTIR spectra of all blank and bitumen-treated clays in the 2800 - 3000 cm^{-1} infrared region. The bands near 2927 and 2954 cm^{-1} are related to asymmetric CH_2 and CH_3 stretching vibrations, respectively. The symmetric CH_2 and CH_3 stretching vibrations were identified at bands near 2855 and 2868 cm^{-1}, respectively. The relative intensity of the CH aliphatic bands for bitumen-treated clays (either non-swelling or swelling) was considerably higher than that for blanks, which may be related to the higher residual organic matter content. This conjecture is in a good agreement with the elemental analysis results, which revealed that the carbon content for bitumen-treated clays was substantially higher than that for the blank clays by 5 to 18 times.

The relative intensity of the OH stretching vibrations of water (~3412 cm^{-1}) for bitumen-treated SWy-2 clays was significantly reduced, particularly for pre-treated clays at 50% and 95% RH (Figure 6-7). The spectral changes show a lower amount of interlayer water for bitumen-treated SWy-2 clays compared with the starting SWy-2 clay, which may indicate that some of the interlayer space of smectite was occupied by residual organic matter instead of water. This assumption was confirmed by the XRD results. The results are also in agreement with published data by Mortland, who found that polar organic molecules can be adsorbed in the interlayer space of smectite by replacement of the interlayer water [250].

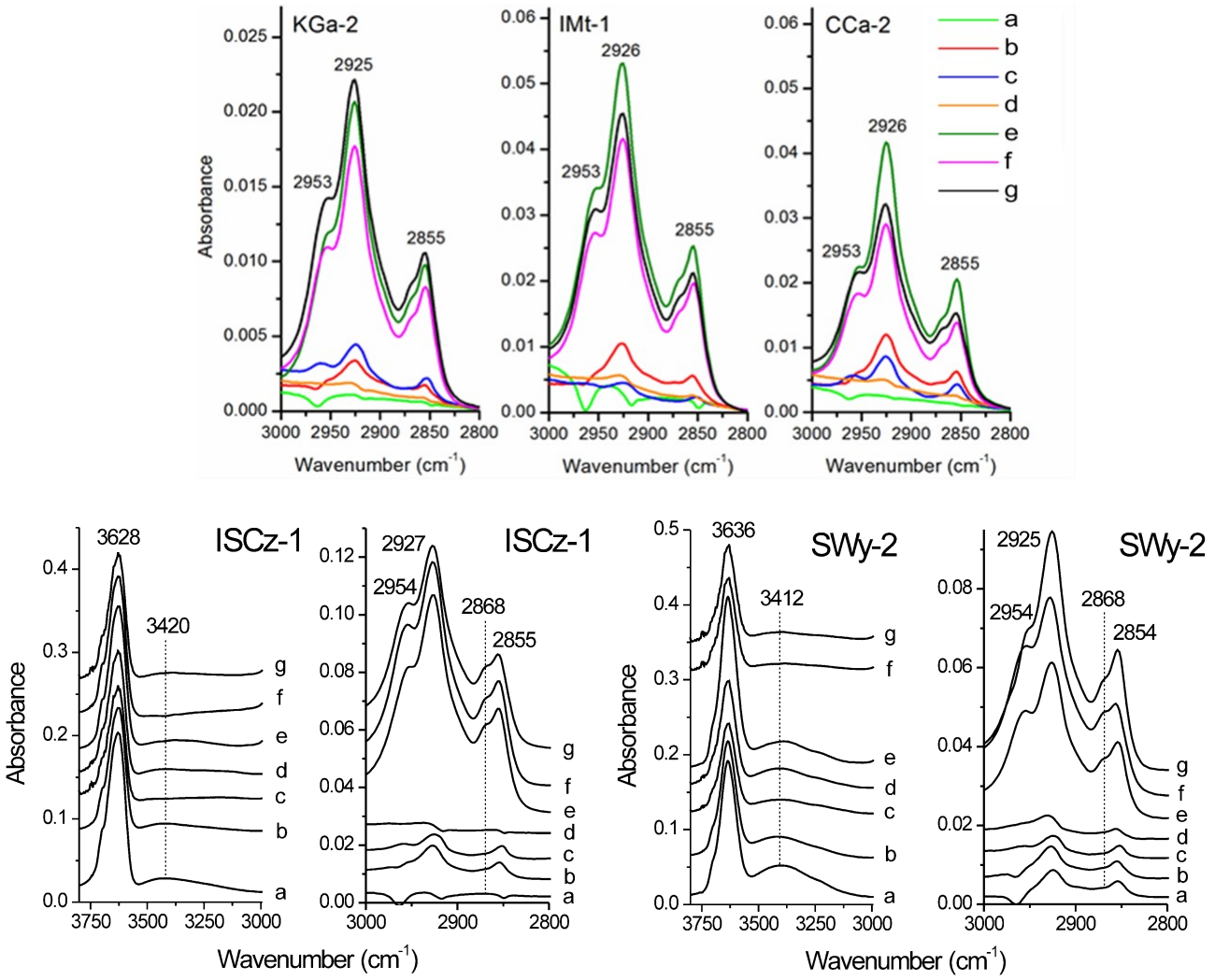

Figure 6-7 FTIR spectra for (a) starting clays; (b) blank 0% RH, (c) 50% RH, and (d) 95% RH; (e) bitumen 0% RH, (f) 50% RH, and (g) 95% RH.

The reduction in the relative intensity of the OH stretching vibrations of water (~3420 cm^{-1}) was ambiguous, which is likely related to significant lower quantity of swelling interlayers for ISCz-1 clays and, therefore, a lower amount of interlayer water compared with smectite SWy-2 clays (Figure 6-7).

6.3.10 FOCUSED ION BEAM-SCANNING ELECTRON MICROSCOPY (FIB-SEM)

Figure 6-8 shows the various stages for cross section preparation, using a FIB-SEM instrument, of clay specimens to investigate the morphology of bitumen-treated ISCz-1 clay compared with the starting ISCz-1 clay.

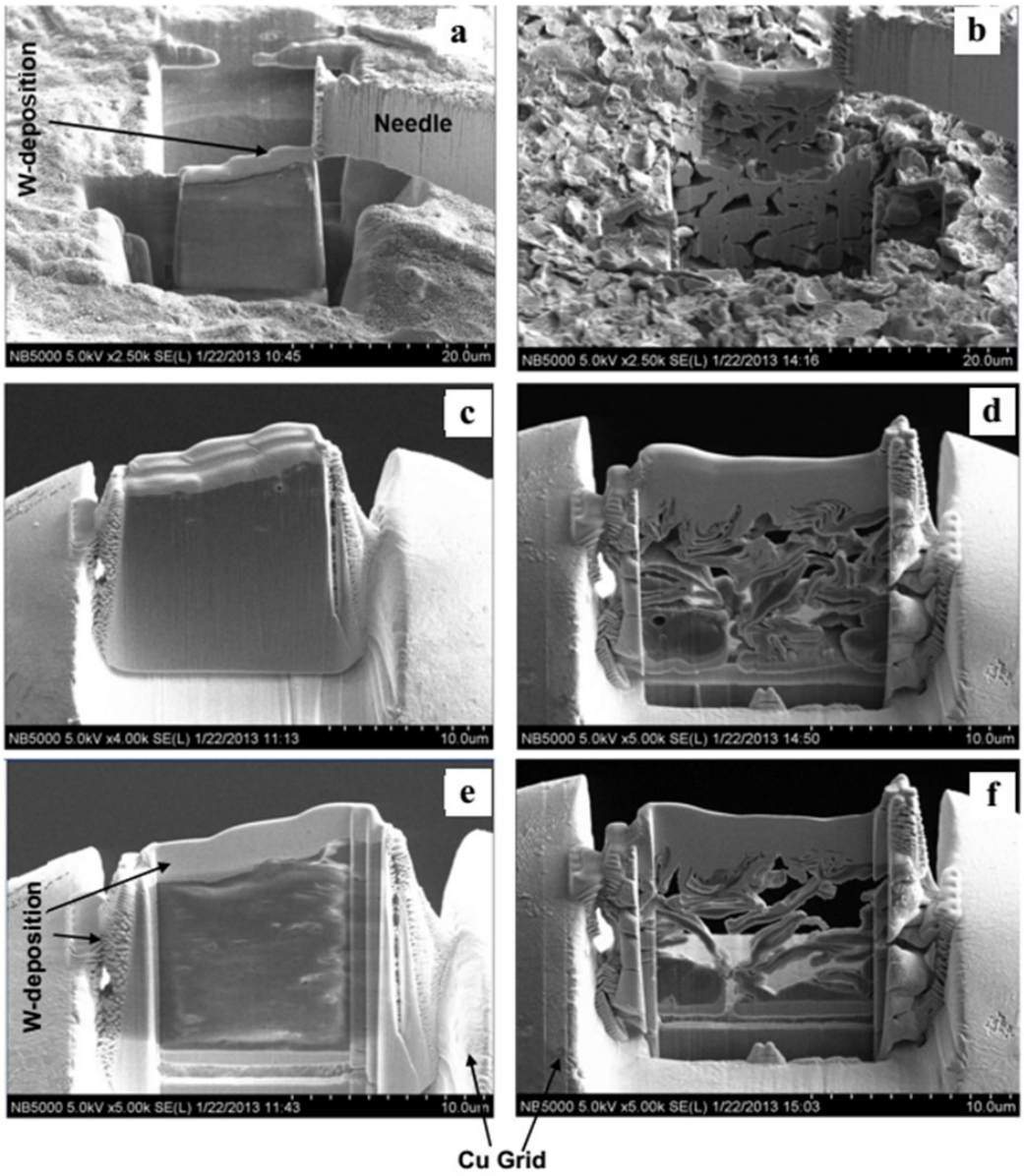

Figure 6-8 Preparation of clay specimens using a FIB-SEM instrument. The region of interest (ROI) was sectioned from the sample (ISCz-1 in this case), welded to the probe, lifted-out and attached to a Cu grid and then milled with Ga ions. a), c), e) Preparation of the starting material and b), d) f) preparation of the bitumen treated material.

The technique was only applied to swelling clays. The region of interest (ROI) was selected, followed by deposition of a protective W layer. A slice was sectioned, welded to a probe and then lifted out (Figure 6-8 a and b). Clear differences were observed for the images from the cross-section and surface of the starting ISCz-1 clay specimen and the bitumen-treated ISCz-1 clay specimen. The differences were more obvious the slice was milled (Figure 6-8 c, e, d, and f).

The images illustrate that the starting ISCz-1clay particles were mostly oriented and laid flat on each other parallel to the basal plane, whereas the bitumen-treated ISCZ-1 samples were more randomly oriented, due to gluing of small clay particles to large aggregates by organic material. These images are consistent with previous XRD results (Figure 6-2) and SEM images (Figure 6-5) from oriented specimens, which showed the formation of the clay-organic aggregates upon reaction of clay with bitumen.

6.4 CONCLUSIONS

The reaction of non-swelling and swelling clays with bitumen showed that bitumen-treated swelling clays contained 4.6 – 8.2 wt% carbon, whereas the non-swelling clays contained only 3.6 – 7.0 wt% carbon after cyclohexane bitumen removal. The residual organic matter remained primarily on the outer surfaces (basal planes and edges) of non-swelling clay mineral particles, while the residual organic matter remained on both outer and inner (interlayer space) surfaces of the swelling clay mineral particles in the form of a patchy rather than continuous coating. The FTIR results revealed that the organic material may be retained in the interlayer space of swelling clay minerals by partial replacement of the interlayer water.

Bitumen treatment of non-swelling clays at various relative humidity conditions (0%, 50% and 95% RH) had no significant influence on the carbon content. On the other hand, bitumen-treatment of swelling clays (mainly smectite SWy-2) under different RH conditions significantly affected the amount of carbon. The amount of carbon increased for bitumen-treated SWy-2 at 95% RH by 56% compared with bitumen-treated SWy-2 at 0% RH. This phenomenon is likely connected with opening of the interlayer space (i.e., swelling) of swelling clay minerals upon exposure to higher RH and subsequent retention of a larger amount of organic material.

Specific surface area (SSA), layer charge density (LCD) and cation exchange capacity (CEC) decreased by reaction with bitumen, due to organic coating on clay mineral surfaces and/or gluing

of clay particles to aggregates. The amount of residual organic matter of swelling clays was influenced by pre-treatment of swelling clays at various RH conditions, the swelling ability, the number of swelling interlayers (i.e., expandability) and the specific surface area (SSA). The SSA was found to be a primary parameter controlling the carbon content of non-swelling clays. The results disclosed that clay minerals with larger SSAs and higher expandability (i.e., numbers of swelling interlayers), exposed under higher RH conditions, generally contained higher amounts of carbon after the bitumen treatment process. Thus, they have the most detrimental influence on cyclohexane bitumen extraction under the studied experimental conditions.

CHAPTER 7

7 INFLUENCE OF OIL SANDS COMPOSITION ON RESIDUAL FINE SOLIDS DURING NON-AQUEOUS BITUMEN EXTRACTION FROM THE ATHABASCA DEPOSIT

The contents of this Chapter have been submitted for publication in a refereed journal and presented at an international conference:

M. Geramian, Qi Liu, D.G. Ivey and T.H. Etsell, Influence of Oil Sands Composition on Bitumen Quality during Non-Aqueous Bitumen Extraction from the Athabasca Deposit, Canadian Journal of Chemical Engineering, (Submitted on November 2017, Manuscript ID: CJCE-17-1124).

M. Geramian, T. H. Etsell, D. G. Ivey, Q. Liu, Characterization of Nano- and Micro-Sized species in the Bitumen product during Non-Aqueous extraction from Oil Sands ores, the MSC 43rd Annual Meeting, June 7-10, 2016, Edmonton, Alberta.

7.1 INTRODUCTION

Oil sands deposits are primarily a mixture of bitumen (4-18 wt%), inorganic materials, i.e., non-clays and clay minerals (55-80 wt%), and salty water (2-15 wt%) [2]. The oil sands deposit in Alberta displays a wide variety of mineral compositions [2,4,10,21]. The mineralogical and textural variability of oil sands are believed to result from mixtures of four petrologically different kinds of rocks, called "end members", representing various sedimentary environments: estuarine sand (ES), estuarine claystone (EC), marine sand (MS), and marine claystone (MC). The different properties of various oil sands ores can be described as an averaged combination of the properties of these four end members [10,22]. Each petrologic type can behave diversely during a bitumen extraction process (either aqueous or non-aqueous), due to the different mineralogical and chemical compositions [11]. Therefore, understanding the influence of the four petrological end members during non-aqueous extraction (NAE) will go a long way towards understanding the behavior of the entire deposit. In this Chapter, each end member was separately mixed with cyclohexane at a constant ratio of 40:60 (cyclohexane:end member), and the collected supernatants (CS) at different settling times (1 min to 30 min) were studied to understand the mineralogical factors affecting NAE.

Applying organic solvents to extract bitumen from the oil sands is a potential alternative to the current commercial aqueous extraction process, which has been in use for more than 50 years. The most significant disadvantages of conventional aqueous extraction include the consumption of large amounts of fresh water and energy, as well as the generation of large quantities of wet tailings requiring long periods of impoundment. Organic solvent based extraction is expected to have fewer environmental issues, as well as the potential advantage of high bitumen recovery from different ore grades (i.e., low, medium and high grade oil sands ores) [10,23,32].

Although the role of various minerals in the oil sands in water-based extraction has been identified, there is insufficient information about the surface properties of various minerals, especially "nano and microsize minerals (NMM)", on non-aqueous bitumen extraction and post-extraction solvent recovery. As learned from previous studies, the most important factor affecting bitumen extraction processes (either aqueous or non-aqueous) is oil sands composition [10,203,251]. Therefore, it is crucial to understand the influence of water, bitumen and solids, particularly nano and microsize species, on the extraction process [11]. Certain NMM, mainly clay minerals, in the oil sands may

affect processability of the ore during non-aqueous extraction [2,20,23]. These minerals may interact with the solvent, bitumen and/or water, due to their high specific surface areas, high cation exchange capacity or redox activity, and specific physicochemical properties [20,34]. The type, quantity and properties of the NMM are related to the sedimentary and diagenetic history of the specific rock.

Previous studies have reported that kaolinite and illite are the main clay constituents in Alberta oil sands, whereas the minor clays are smectite, chlorite and mixed-layer clay minerals [10,21,203]. Different types of clay minerals may have differing effects on the processability of oil sands ore during extraction. The goal of the present study is to characterize the suspended fine solids (SFS) in bitumen products, in order to better understand the most important species affecting non-aqueous bitumen extraction and bitumen quality. The results from the current study are compared with those published in our recent work (Chapter 5), which provides information on the detailed characteristics of the four petrologic end members from Alberta oil sands [251].

7.2 MATERIALS AND METHODS

7.2.1 MATERIALS

Four oil sands ores mined in the Fort McMurray area, collected by Syncrude Canada Ltd. from their North Mine in November 2012 (NM12), were used in the current study. Each mined ore was essentially a representative of one of the four petrologic end members, namely estuarine sand (ES), estuarine claystone (EC), marine sand (MS) and marine claystone (MC) [10,203]. The sands and claystones were manually separated from the as-received (ASRE) samples, disaggregated and passed through a sieve (aperture size of 6.3 mm, according to ASTM E.11). Then, each end member sample was homogenized, stored in sealed containers and kept frozen at -20°C to avoid/stop any weathering degradation [222]. Two solvents used for this study were cyclohexane and toluene, which were purchased from Fisher Scientific, Canada and certified as ACS grade.

7.2.2 EXPERIMENTAL PROCEDURES

The prepared NM12 samples were defrosted for 24 hours at room temperature (20-25°C) in sealed containers prior to use. In order to investigate the role of NMM on the NAE process, an

experimental set-up (Figure 7-1) was designed based on the works of Hooshiar *et al.* and Nikakhtari *et al.* [32,33]. This study was carried out under ambient laboratory conditions, i.e., room temperature (24±0.5°C) and ambient pressure.

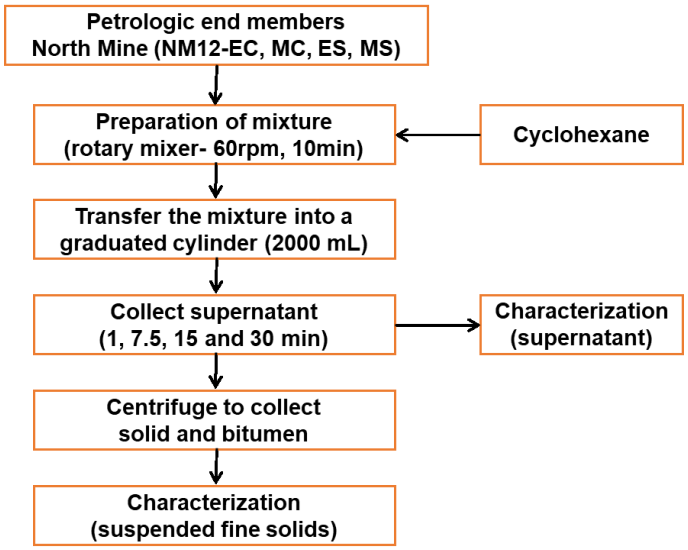

Figure 7-1 Schematic experimental set-up for understanding the migration of different NMM species to bitumen products [223].

The NAE process used was as follows: (I) For each test, 333.3 g of cyclohexane and 500 g of ore (solvent/ore ratio = 40/60) were placed into a 1000 mL glass bottle and sealed. Then the bottles were mounted on a rotary mixer and the bottle content tumbled end-to-end for 10 min at a rotation speed of 60 rpm. (II) Three bottles of prepared mixture for each ore were poured into a 2000 mL graduated cylinder and sealed. (III) The supernatants (100 mL) were slowly siphoned and collected from the top of the mixture after different settling times, i.e., 1 min, 7.5 min, 15 min and 30 min. (IV) The particle size distribution of the suspended fine solids (SFS) and water content of collected supernatants (CS) were measured by focused beam reflectance measurement (FBRM) and Karl Fischer (KF) titration, respectively. (V) The CS were kept in an open glass bottle at 60°C for 7 days within a fume hood, to allow the cyclohexane to evaporate from the supernatant. The weight of the dried CS was then measured for future calculations. (VI) The dried CS in the glass bottle was dissolved by cyclohexane and then transferred into a 50 mL Nalgene™ Teflon FEP (fluorinated ethylene propylene) bottle. The bottle was capped and centrifuged using an Avanti J-30I centrifuge (Beckman Coulter, Mississauga, Ontario, Canada), with a JA-17 rotor, at a 19,500 relative centrifugal force (RCF) for 3 h to separate the SFS from cyclohexane-diluted bitumen

(CDB). The centrifugation was repeated five times, each time with fresh cyclohexane, in order to obtain a clean SFS sample. After each centrifugation, the CDB supernatant was slowly siphoned and then kept in a small glass bottle at 60°C for 7 days within a fume hood, to evaporate the cyclohexane from the CDB. The sediment solids from the bottom of the centrifuge bottle were collected and put in a small glass bottle at 60°C for 3 days within a fume hood, to remove the cyclohexane from the solids. These solids were the same as the SFS in the bitumen product. (VII) The bitumen and solids were then used for future calculations and analysis.

7.2.3 ANALYTICAL METHODS

7.2.3.1 FOCUSED BEAM REFLECTANCE MEASUREMENT

A model G-400 focused beam reflectance measurement (FBRM) particle size analyzer (Mettler-Toledo, Canada) was used to measure the chord length distribution of the collected SFS [165,168]. FBRM is a technique for measuring/studying solid size distribution in-situ in a dark and/or opaque slurry [165,166]. This technique directly tracks changes to the number, shape and dimension of particles in the slurry [167]. The immersed FBRM probe in the slurry counts the reflected laser light from the particle, which impinges upon the probe window. Thousands of individual particles per second hit the window and create pulses of backscattered light, which generates the chord length distribution (CLD) [167].

For each sample analysis, a control test of pure cyclohexane was carried out first. About 150 mL of pure cyclohexane was placed in a 500 mL beaker. A dual-blade impeller and the FBRM probe were immersed into the pure cyclohexane. The same position and depth of the probe were used for all measurements. The sampling interval measurement was 2 s to get the best test resolution. The background medium (pure cyclohexane) was measured with the mixing speed set at 300 rpm (the optimum stirring speed for testing); the counts must be less than 300 in the control test. For SFS particle size determination, 100 mL of collected supernatant was slowly added into the beaker. Then, pure cyclohexane (approximately 150 mL) was added to the supernatant bottle to reach a total mixture of 400 mL. For each measurement, the mixture (collected supernatant and cyclohexane) was recorded after 2 min of premixing time to allow the mixture to completely disperse and temperature to become uniform. Over the next 10 min (2 min to 12 min), the desired

data (i.e., unweighted chord length distribution, mean square weighted percentile c(10), percentile c(50), percentile c(90) and counts of particles) were monitored and recorded.

The D10, D50, and D90 chord length (CL) values were calculated with the software icFBRM 4.2 from a cumulative percent distribution, which was produced from the CLD. The cumulated percent of CL size that accounts for 50% or less of the CL (which is the 50th percentile) is called D50 [169]. The same procedure was used for determination of D10 and D90.

7.2.3.2 KARL FISCHER TITRATION

The water content of the supernatant was determined by the Karl Fischer (KF) titration method (Mettler Toledo DL39 system). The weight of an ~0.1 mL of sample was accurately measured by transferring supernatant using a syringe equipped with a needle. Then, the entire sample was quickly injected into the titration vessel. The titration usually took a few minutes. When the titration was finished, the screen display showed the amount of water detected in every analysis. The percentage of water content was recorded for further calculation. Each supernatant was measured at least four times and the mean value and standard deviation were calculated. The accuracy of titration was repeatedly controlled (every five measurements) by using a standard sample (0.1% water content).

7.2.3.3 X-RAY DIFFRACTION

X-ray diffraction (XRD) patterns were measured for oriented and random specimens using a Rigaku Ultima IV diffractometer, operating at 44 mA and 40 kV, with a graphite monochromator and Cu Kα radiation. The step size was 0.02° 2θ and the exposure time was 2 s per step. Frosted glass slides were used for oriented preparation samples from fully dispersed suspensions of clays or SFS fractions (90 mg) in distilled water (approximately 1.2 mL). In order to disperse the clay particles in distilled water, the suspension was stirred for 5 min using a small magnetic stirring bar (Teflon^{TM} coated-PTFE, 2 mm in length and 2 mm in diameter) and sonicated in an ultrasonic bath for 5 min. The suspension was transferred by a plastic pipette onto a frosted glass slide (2.8×2.8 cm) and left at ambient conditions to dry. According to the procedure described by Moore and Reynolds (1997), the dried glass slides were saturated first at 54% relative humidity and then with ethylene glycol (EG) prior to XRD analysis after each treatment [76]. The specimens were run

from 2θ = 3º to 2θ = 60º. The expandability of kaolinite-smectite and illite–smectite was identified by comparison of XRD patterns of oriented preparations after these treatments according to the procedures described by Moore and Reynolds [76] , Środoń [94] and Dudek *et al* [95].

The mineralogical composition of the SFS at 1 min and 7.5 min settling times from the three petrologic end members, i.e., MC, MS and ES for NM12, was determined by quantitative X-ray diffraction (QXRD) analysis on random preparation specimens using the RockJock-11 program [131]. A sample was sieved using a 250 μm sieve. Then exactly 1.000 g of the sieved sample and 0.250 g of an internal standard (corundum powder) were placed into a grinding cylinder with zirconia grinding balls, to which 4 mL of ethanol was added. Then the sealed grinding cylinder was mounted on a McCrone micronizing mill, mixed and ground for 5 min. The mixture was poured into a ceramic bowl and dried overnight at about 80°C. The dried mixture was put into a 25 mL plastic vial with three plastic balls (10 mm diameter) and shaken to mix and homogenize the contents. Then 0.5 mL of vertel (DuPont™ Vertel XF) was added to the mixture that was shaken again for 10 min using a Retsch MM 200 mill. The amount of vertel added was estimated according to the RockJock user guide (a ratio of 0.5 mL vertel to 1 g of pure clay) [131]. Next, the powder was sieved using a 250 μm sieve and loaded into an XRD side loading holder, which was against a frosted glass slide. The specimens were run from 2θ = 4º to 2θ = 65.5º. JADE 7 software was used to extract the XRD profiles that were entered into the RockJock program to calculate the mineral composition.

7.2.3.4 ELEMENTAL ANALYSIS

The total C, H, N and S contents were determined using a Vario MICRO cube elemental analyzer. A sample was burned in the presence of an oxygen stream at 1150°C and the products of combustion, including CO_2, N_2, H_2O and SO_2, were identified by a thermal conductivity detector. In order to improve the accuracy and reliability, approximately 25 mg of sample was accurately weighed and used for each run and the average of five replicates (at least) were recorded. The total inorganic carbon (TIC) content was obtained by calculation of the carbon content in the carbonate minerals (calcite, dolomite and siderite). The amount of total organic carbon (TOC) for each sample was taken as the difference between the total carbon measured by the elemental analyzer and TIC calculated by QXRD (RockJock program). Since the SFS were washed five times with

fresh cyclohexane, the amount of TOC can be considered as cyclohexane insoluble organic carbon (CIOC).

7.2.3.5 SCANNING ELECTRON MICROSCOPY (SEM)

Scanning electron microscopy (SEM) was used to study samples using a Zeiss EVO MA 15 SEM operated at 20 kV. A secondary electron (SE) detector and a Bruker energy dispersive X-ray (EDX) detector were used for imaging and elemental microanalysis, respectively. Prior to the observation, surfaces of the samples were coated, using a Leica EM SCD005 cool sputter coater, with a thin layer of metal (gold) film to improve the contrast as well as to make the surface of sample electrically conductive for analysis.

7.2.3.6 TRANSMISSION ELECTRON MICROSCOPY (TEM)

Transmission electron microscopy (TEM) was performed to examine samples using a Philips CM20 FEG TEM/STEM instrument with a Schottky field-emission source operated at 200 kV. The TEM utilized with an energy dispersive X-ray (EDX) detector for elemental microanalysis. Several detectors were used for imaging in TEM image mode and diffraction mode. The composition and crystalline structure of the suspended fine solids (SFS) in bitumen products for EC end member were identified by EDX and electron diffraction analysis. To identify the structure of the particles, selected area diffraction (SAD) and nanobeam diffraction were performed on the particles. Like X-ray diffraction, Bragg's law (Equation 2-4) is applicable for the electron diffraction pattern; thus, electrons are scattered elastically by the specimen lattice. The TEM viewing (phosphor) screen and a Gatan Multiscan digital CCD camera at the bottom of the TEM column were used for viewing and recording TEM images and SAD patterns. The camera constant ($\lambda \cdot L$) for the diffraction condition was determined by using a standard gold specimen. According to Equation 2-6, the d value was calculated, by measuring R, L and λ values for gold (where d is the interplanar distance of the lattice planes, R is the measured distance of the diffraction spot on screen, L is the camera length and λ is the wavelength of the X-rays). The camera constant (λL) can be determined for TEM by using a standard specimen (gold). For indexing an unknown single crystal SAD pattern, the distances and angles (R and θ in Figure 2-6) were measured and the Miller

indices (h k l) were then calculated by using the d-spacing formulae for the different crystal systems and interplanar angle formulae [252].

The SFS was diluted in solvent (i.e., cyclohexane) and a droplet of it was transferred onto a carbon-coated copper grid (Formvar/carbon, 400 Mesh, Ted Pella, Inc.). Preparation of TEM samples from dilute SFS helped in separating most of the particles separately and ensured that many were oriented with their larger planes (001 planes) parallel to the grid planes, particularly for clay minerals. This technique was used for minerals and chemical identification of residual solids in bitumen products and particularly for EC end members, due to the very small quantity of SFS in EC, which were difficult to identify by other techniques like XRD.

7.3 RESULTS

7.3.1 KARL FISCHER TITRATION

Figure 7-2 shows the water contents of the supernatants, measured by Karl Fischer (KF) titration, at different settling times for all three end members, i.e., MS, ES and MC. The mean value and the standard deviation of at least four measurements are reported. The water content was found to decrease with increasing settling times from 1 min to 30 min for all three end members, i.e., MS, ES and MC. MC had higher water content than sand samples. The MC and ES samples had the highest and lowest water content at all settling times, respectively. The supernatant of MC at 1 min had the highest standard deviation for the water content by KF titration (±0.016%). The lowest amount of water in the supernatant (diluted bitumen) was 0.03% for the ES samples at 7.5 and 30 min settling times. This amount of water is not easy to measure by other techniques [253].

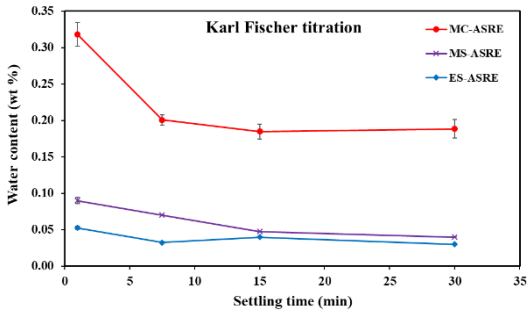

Figure 7-2 Water content measured by the Karl Fischer titration method (KF) for collected supernatants (CS) at different settling times for ES, MS and MC.

7.3.2 FOCUSED BEAM REFLECTANCE MEASUREMENT (FBRM)

Figure 7-3 a, b and c show the counts (% unweighted) vs. chord length distribution (CLD) for MC, MS and ES supernatants at different settling times (i.e., 1 min, 7.5 min, 15 min and 30 min). For all supernatants, the CLD shifted to lower values with increasing settling time from 1 min to 30 min. These changes are shown in Table 7-1, which displays the reduction in the mean square weighted chord length against the settling times. The number of particles (counts) detected by the FBRM probe was reduced with increasing settling time for MC (12400 to 342), MS (14021 to 6833) and ES (8460 to 5230) supernatants. Figure 7-3 d shows the counts of total number of particles vs. settling time (i.e., 1 min, 7.5 min, 15 min, and 30 min) for MC, MS and ES supernatants. Although all samples showed a reduction in the number of particles with increasing settling time for the supernatants, the reduction trend was different for each end member.

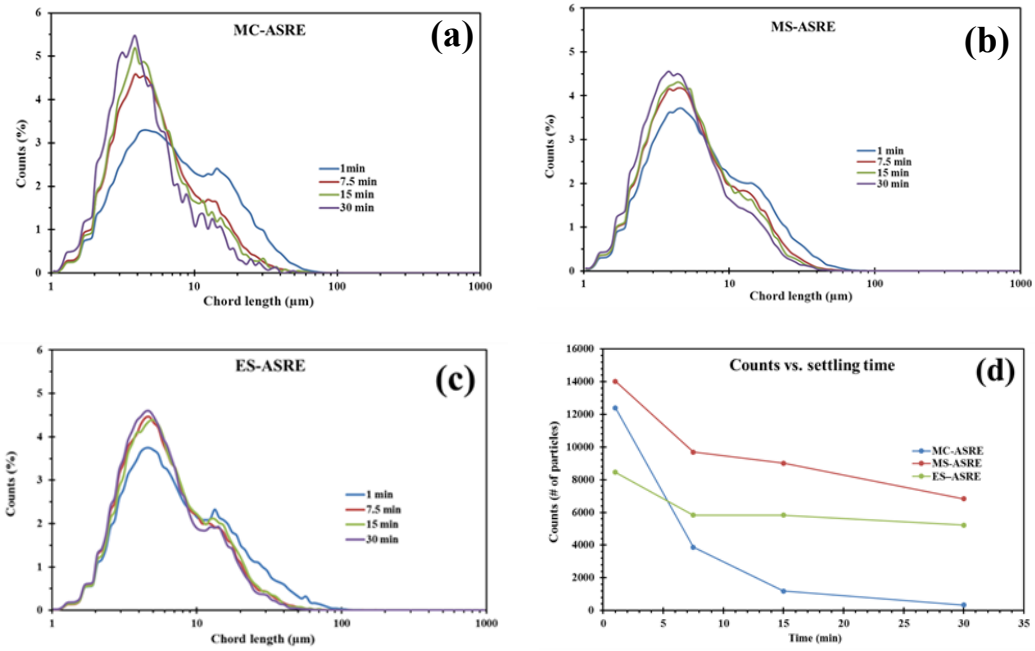

Figure 7-3 Particle size distribution (count % vs. chord length in µm) at different settling times for (a) MC, (b) MS and (c) ES. (d) The number of particles (count) vs. settling time for MC, MS and ES. All measurements were carried out at 200 rpm stirring using the no weight method.

The MC and ES samples displayed the highest and lowest reduction rates, respectively, in the number of particles for settling times from 1 min to 30 min. A similar trend was observed for the D10, D50 and D90 CL for the supernatants of each end member. The EC supernatants were

characterized with the FBRM analyzer, but these data are not reported due to insufficient particle contents in the supernatants for reliable measurement.

Table 7-1 Number of particles and size of particles for C(10), C(50) and (C90) measured by FBRM technique for MC, MS and ES supernatants at different settling times.

Samples	MC-ASRE				MS-ASRE				ES–ASRE			
	1 min	7.5min	15min	30 min	1 min	7.5min	15min	30 min	1 min	7.5min	15min	30 min
Counts (number of particles)	12400	3868	1191	342	14021	9697	9008	6833	8460	5838	5826	5230
D10	2.63	2.42	2.44	2.22	2.49	2.38	2.36	2.24	2.81	2.7	2.75	2.65
D50	6.69	4.85	4.65	4.11	5.76	5.06	4.96	4.55	6.42	5.49	5.66	5.29
D90	21.98	14.18	13.09	11.08	18.82	14.97	14.06	12.66	23.24	16.14	16.57	15.21
Mean Square weighted	28.02	19.43	19.85	16.17	25.93	19.17	9.49	6.07	38.93	24.63	22.65	20.38

7.3.3 SETTLING BEHAVIOR, BITUMEN QUALITY AND SUSPENDED SOLIDS IN THE BITUMEN PRODUCT

After measuring the particle size distribution of the SFS and the water content of the CS, the CS were used to separate and dry the SFS and bitumen from cyclohexane-diluted bitumen (CDB) for each supernatant using the experimental procedure described in section 2.2 and Figure 7-1. The average value and the standard deviation of at least three measurements of the SFS and bitumen are reported for each sample (Table 7-2). As expected, the amount of SFS and bitumen quality decreased and increased, respectively, with increasing settling time for all three end members, i.e., MS, ES and MC. EC supernatants at different settling times were collected, but these data are not reported due to the very small amounts of SFS and bitumen present which were not reliably quantifiable. The SFS and bitumen contents for MC samples were significantly changed from 55.7 to 5.4 wt% and from 44.3 to 94.6 wt%, respectively, with increasing settling time from 1 to 30 min. ES samples displayed the lowest changes for both SFS (5.5 to 2.3 wt%) and bitumen (94.5 to 97.7 wt%) contents when the settling time was increased. MS and ES contained the highest (7.4 wt%) and lowest (2.3 wt%) SFS content, respectively, after 30 min of settling. Figure 7-4 shows

the SFS/bitumen content vs. settling time for ES, MS and MC samples. The amount of SFS/bitumen change for MC was 50.4 wt%, much higher than for MS (7.8 wt%) and ES (3.2 wt%).

Table 7-2 Amounts of bitumen and SFS (in wt%) separated from MC, MS and ES for NM12. The amounts of bitumen and suspended fine solids (SFS) are bitumen product based.

Name	Marine Clay				Marine sand				Estuarine sand			
	SFS (wt%)		Bitumen (wt%)		SFS (wt%)		Bitumen (wt%)		SFS (wt%)		Bitumen (wt%)	
	Ave.	STDEV	Ave.	STDEV	Ave.	STDEV	Ave.	STDEV	Ave.	STDEV	Ave.	STDEV
1min	55.73	3.69	44.27	3.69	15.11	2.59	84.89	2.59	5.46	0.69	94.54	0.69
7.5min	20.32	0.74	79.68	0.74	9.34	2.05	90.66	2.05	2.89	0.13	97.11	0.13
15min	10.68	2.27	89.92	2.27	8.86	1.39	91.14	1.39	2.72	0.43	97.28	0.43
30min	5.38	1.98	94.62	1.98	7.37	2.26	92.63	2.26	2.29	0.27	97.71	0.27

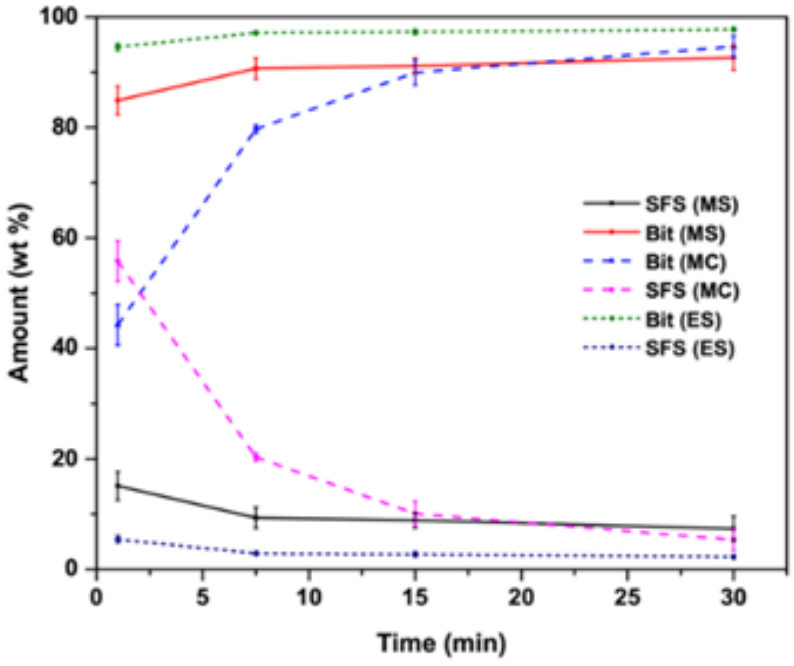

Figure 7-4 Amount of bitumen and SFS collected from supernatants at different settling times for ES, MS and MC.

7.3.4 X-RAY DIFFRACTION

The mineralogical composition of the SFS at 1 min and 7.5 min settling times from the three petrologic end members i.e., MC, MS and ES for NM12 was determined using the RockJock program and is listed in Table 7-3. The amounts of SFS for MC, MS and ES at 15 min and 30 min settling times and for EC at all settling times were insufficient for mineralogical characterization (QXRD).

The SFS of MC, MS and ES included two main groups of minerals: non-clay and clay minerals. The non-clay minerals at 1 min and 7.5 min settling times mostly consisted of quartz (17.4–28.3 wt%), carbonates (calcite, dolomite and siderite, 1.5–16.8 wt%) and feldspars (K, Na and Ca feldspars, 5.3-8.5 wt%), with small amounts of pyrite (<0.9 wt%), TiO_2 minerals (anatase and rutile, 0-1.4 wt%) and calcium sulfate minerals (i.e., gypsum, <1.5 wt%). The clay minerals in these samples included kaolinite (36.3–46.6 wt%), 2:1 clay minerals (illite and mixed-layer clay minerals, 8.5–26.6 wt%), and chlorite (2.6–10.7 wt%). High amounts of quartz were observed in ES after 1 min settling (28.3 wt%). It is interesting to note that a high amount of clay minerals was also identified in sand samples after 7.5 min settling, particularly in ES (70.4 wt%). The highest amount of carbonate minerals was observed in the MC sample, especially after 1 min settling (16.8 wt%). The low and high amounts of quartz and clay minerals were observed, respectively, when the settling times increased from 1 to 7.5 min. The highest amount of quartz accumulated at 1 min settling time (≥ 22.6 wt%) for MC, MS and ES samples.

XRD patterns from oriented preparations of SFS at different settling times for the various petrologic end members were obtained to investigate the clay minerals (Figure 7-5). Kaolinite and illite were determined as the main clay minerals in the XRD patterns of the oriented preparations for all SFS specimens. Kaolinite peaks were observed at 7.13 and 3.57 Å, while illite peaks were observed at 10.0, 4.9 and 3.34 Å. Quartz peaks were observed at 4.25 and 3.34 Å. For all SFS specimens from MC, MS, ES and EC, the relative intensities, shapes and positions of the illite 001 reflections (d = 10 Å) and kaolinite 00l reflections (d = 7.13 Å) were not changed after ethylene glycol solvation, which indicates discrete kaolinite and illite without interstratification of expandable layers (Figure 7-6 and Figure 7-7).

Chlorite was not clearly observed in the oriented preparations for these specimens, although the presence of chlorite was identified by QXRD using the RockJock program for the SFS of ES, MC

and MS samples after 1 min and 7.5 min settling (Table 7-3). In addition, reflections for calcite (3.03 and 3.83 Å) and dolomite (2.88 Å) were observed for MC samples after 1 min and 7.5 min. Weak reflections for siderite (2.80 Å) and Fe-Ti minerals (3.71 Å) were observed for EC (at 1 min) and MC (at 1 min and 7.5 min) samples, respectively.

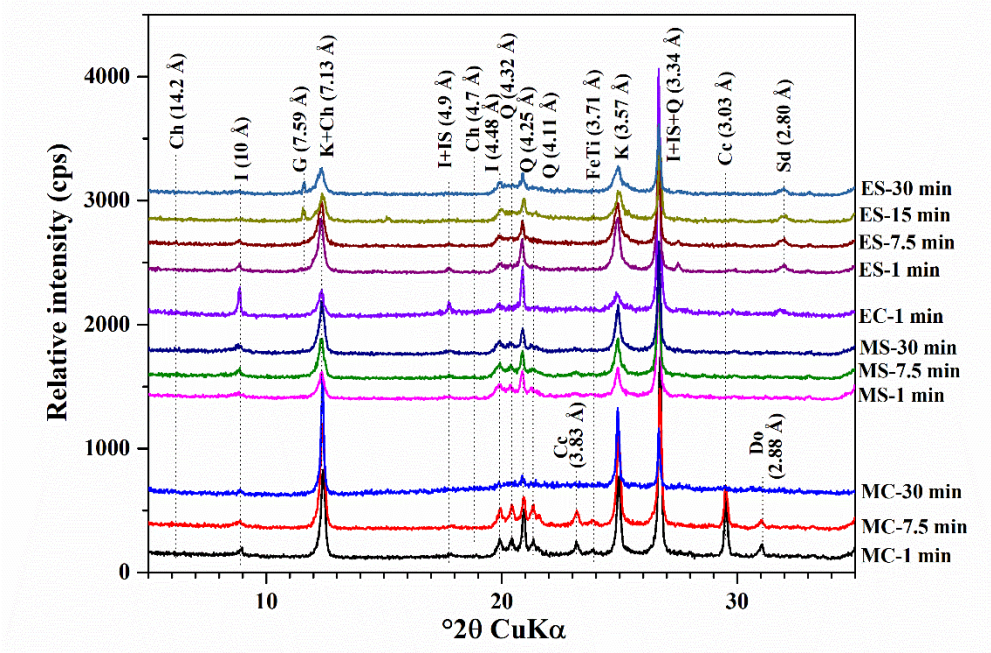

Figure 7-5 XRD patterns for oriented specimens (air-dried) of suspended fine solids (SFS) for MC, MS, EC and ES at different settling times. Ch, chlorite; I, illite; IS, illite–smectite; K, kaolinite; G, gypsum; Q, quartz; Fe-Ti, Fe-Ti and/or Ti oxide mineral; Cc, calcite; Do, dolomite; Sd, siderite.

7.3.5 ELEMENTAL ANALYSIS

The total carbon (TC), nitrogen (TN), hydrogen (TH), and sulfur (TS) contents (in wt%) for ES, MC and MS at different settling times (i.e., 1 min, 7.5 min, 15 min and 30 min) are summarized in Table 7-4. The EC sample was not characterized by the Vario MICRO cube elemental analyzer due to insufficient material. The N/C, H/C and S/C ratios were also calculated and appear in Table 7-4. The total carbon content increased from 7.1 to 11.6 wt% for ES, from 8.3 to 10.9 wt% for MC, and from 8.7 to 10.2 wt% for MS with increasing settling time from 1 min to 30 min. In all samples, an increasing amount of TN was observed with increasing settling time from 1 min to 30 min.

Table 7-3 Mineral composition (in wt%) of different SFS collected from MC, MS and ES for NM12 using the RockJock program. Total 2:1 clays – the sum of illite and illite–smectite, calcium sulfate – i.e., gypsum.

Sample	Settling time (min)	Quartz	Feldspars (K, Na, Ca)	Calcite	Dolomite	Siderite	Calcium sulfate	TiO_2 minerals	Pyrite	Total non-clays	Kaolinite	Total 2:1 clays	Chlorite	Total clays
MC ASRE	1min	24.8	5.8	12.4	3.8	0.6	0.6	0.2	0.4	48.6	36.3	12.5	2.6	51.4
	7.5min	17.1	7.3	9.7	2.6	0.7	0.9	0	0.4	38.7	45.7	12.8	2.8	61.3
ES ASRE	1min	28.3	8.5	0	0.2	3.2	1.5	1.4	0.6	43.7	40.3	8.5	7.5	56.3
	7.5min	17.4	6.1	0	0.2	3	1.2	1.1	0.6	29.7	46.6	13.1	10.7	70.4
MS ASRE	1min	22.6	5.3	0.2	0.9	0.4	0.7	0.3	0.9	31.3	39.1	26.2	3.4	68.7
	7.5min	19.3	7.5	0.5	1.1	0.5	0.7	0.4	0.8	30.8	38.9	26.6	3.7	69.2

It is worth mentioning that the quantity of minerals <1 wt% may not be reliable; however, it was used to calculate the total non-clay minerals.

The marine samples displayed a similar trend for TH content; however, TH varied between 1.43 and 1.89 wt% for ES. In all samples, the amount of TS varied between 0.84 and 1.81 wt%. TS content was higher in sand samples than in the MC sample for the same settling time. The N/C ratio was fairly constant (~0.020) for MC and MS and was 0.018 for ES at all settling times. The S/C ratio decreased with increasing settling time for both MS and MC samples; however, S/C was fairly constant (~0.153) for ES. The H/C ratio varied between 0.155 and 0.202 for all samples.

Table 7-4 Total carbon (TC), nitrogen (TN), hydrogen (TH) and sulfur (TS) contents (in wt%) of SFS from ES, MC and MS for NM12 determined by elemental analysis. TIC – Total inorganic carbon, TOC – Total organic carbon, n.a. – not analyzed.

CHNS analysis – suspended fine solids										TIC	TOC
Sample	Settling time (min)		TN (wt%)	TC (wt%)	TH (wt%)	TS (wt%)	N/C ratio	H/C ratio	S/C ratio	(Q-XRD)	
Marine Clay	1min-ASRE	Ave.	0.16	8.33	1.41	0.93	0.019	0.169	0.112	2.05	6.28
		STDV	0.004	0.17	0.04	0.07					
	7.5min-ASRE	Ave.	0.17	8.43	1.67	0.98	0.020	0.198	0.116	1.58	6.85
		STDV	0.006	0.09	0.06	0.02					
	15min-ASRE	Ave.	0.20	9.47	1.72	0.84	0.021	0.182	0.089	n.a.	n.a.
		STDV	0.005	0.56	0.07	0.12					
	30min-ASRE	Ave.	0.23	10.86	2.01	0.98	0.022	0.185	0.090	n.a.	n.a.
		STDV	0.001	0.24	0.11	0.03					
Marine Sand	1min-ASRE	Ave.	0.19	8.67	1.70	1.75	0.022	0.196	0.201	0.18	8.49
		STDV	0.001	0.08	0.09	0.06					
	7.5min-ASRE	Ave.	0.21	9.72	1.89	1.65	0.022	0.194	0.170	0.26	9.46
		STDV	0.004	0.04	0.60	0.03					
	15min-ASRE	Ave.	0.21	9.87	1.90	1.70	0.021	0.193	0.172	n.a.	n.a.
		STDV	0.003	0.03	0.07	0.02					
	30min-ASRE	Ave.	0.22	10.24	1.91	1.58	0.022	0.187	0.155	n.a.	n.a.
		STDV	0.004	0.04	0.55	0.02					
Estuarine Sand	1min-ASRE	Ave.	0.127	7.085	1.431	1.079	0.018	0.202	0.152	0.36	6.73
		STDV	0.004	0.042	0.010	0.008					
	7.5min-ASRE	Ave.	0.187	10.426	1.886	1.599	0.018	0.181	0.153	0.34	10.09
		STDV	0.002	0.032	0.010	0.061					
	15min-ASRE	Ave.	0.182	10.110	1.856	1.520	0.018	0.184	0.150	n.a.	n.a.
		STDV	0.004	0.060	0.018	0.121					
	30min-ASRE	Ave.	0.213	11.587	1.799	1.809	0.018	0.155	0.156	n.a.	n.a.
		STDV	0.005	0.080	0.416	0.045					

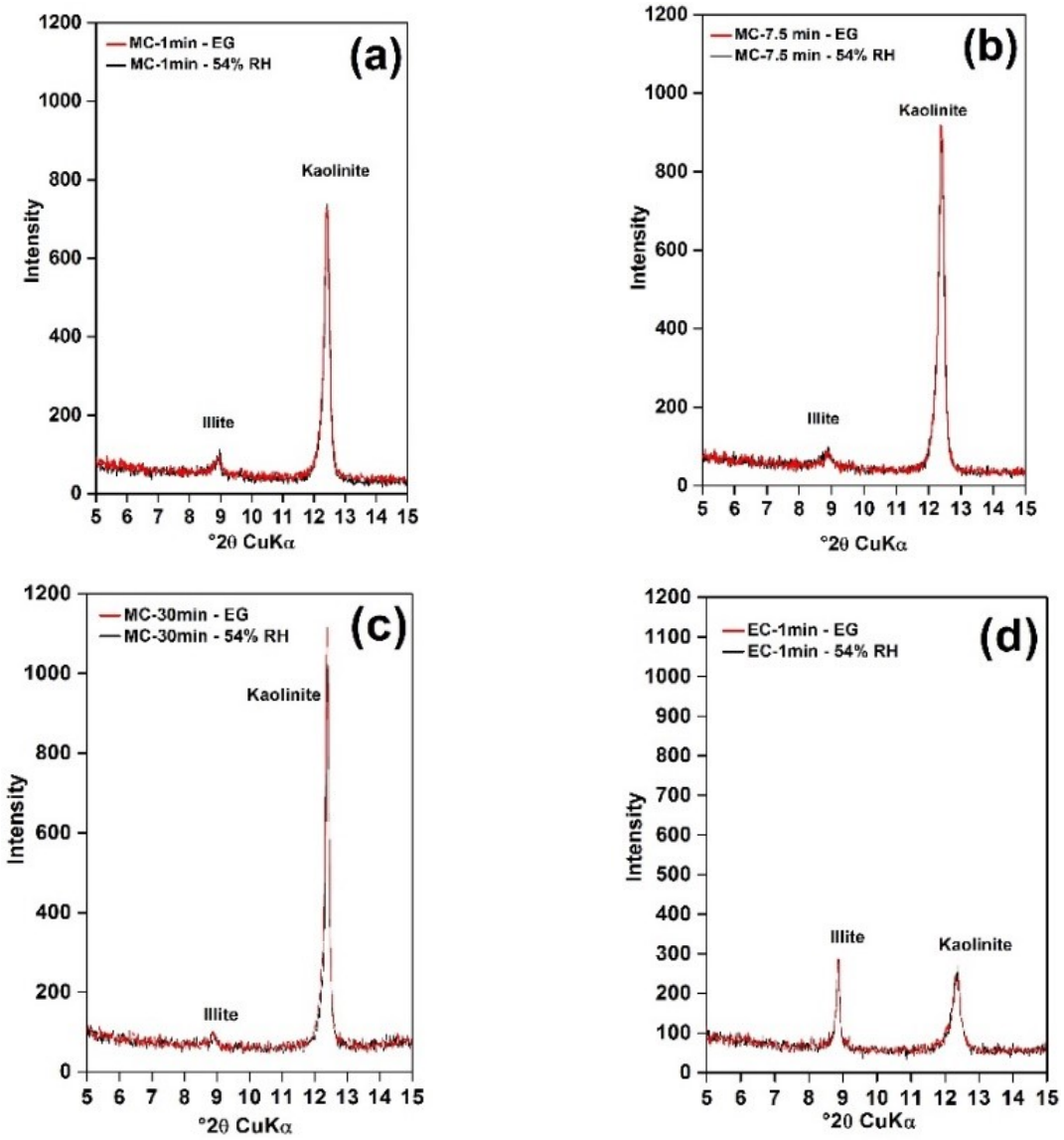

Figure 7-6 XRD patterns for oriented preparations of suspended fine solids (SFS) at different settling times from MC and EC to investigate the clay minerals. (a) MC - 1 min, (b) MC - 7.5 min, (c) MC - 30 min and (d) EC - 1min. Air dried-54% RH (black line) and after ethylene glycol solvation (red line). I, illite and K, kaolinite.

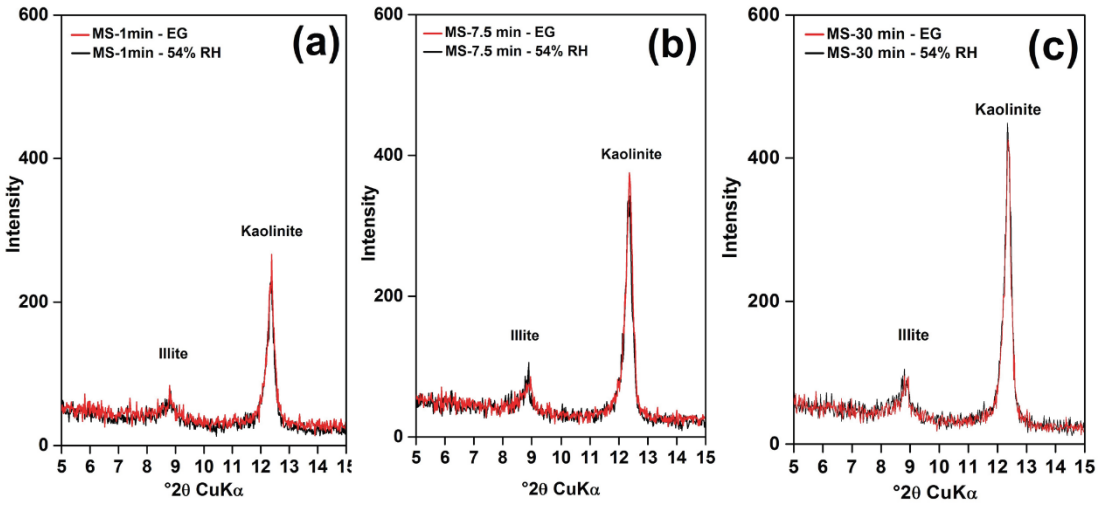

Figure 7-7 XRD patterns for oriented preparations of suspended fine solids (SFS) at different settling times from MS to investigate the clay minerals. (a) MS - 1 min, (b) MS - 7.5 min and (c) MS - 30 min. Air dried-54% RH (black line) and after ethylene glycol solvation (red line). I, illite and K, kaolinite.

7.3.6 SCANNING ELECTRON MICROSCOPY (SEM)

The quantity of suspended solids was not sufficient for some characterization techniques, such as quantitative XRD and cation exchange capacity (CEC), so SEM and EDX spectroscopy were used to characterize some SFS from clay end members after different settling times. SEM SE images of suspended fine solids (SFS) from the bitumen product for the MC sample after 1 min and 7.5 min settling showed a number of large subhedral, anhedral and euhedral particles, ranging in size from 0.2 µm to 40 µm, covered by very fine particles of clays on the surface (Figure 7-8 and Figure 7-9). EDX spectra showed Si, Al, K, Na and O as major components of the large particles. Thus, they were attributed to clay aggregates consisting of several fine clay particles/plates, which were stacked/placed along their larger plane position (Figure 7-8 a and b). A number of cubic pyrite crystals was also observed in MC after 1 min of settling time (Figure 7-8 c). A few anhedral particles rich in Ti and Fe (Figure 7-8 d), which was attributed to Fe–Ti oxide minerals, were found in the bitumen product from the marine petrologic end members (MC and MS). In some cases, the fine clay particles likely influenced the EDX analysis results (enrichment in Si and Al from clays). Therefore, particles coated with clay made mineral identification more difficult. These findings were consistent with the XRD results, which determined the presence of clays (~51 wt%), pyrite

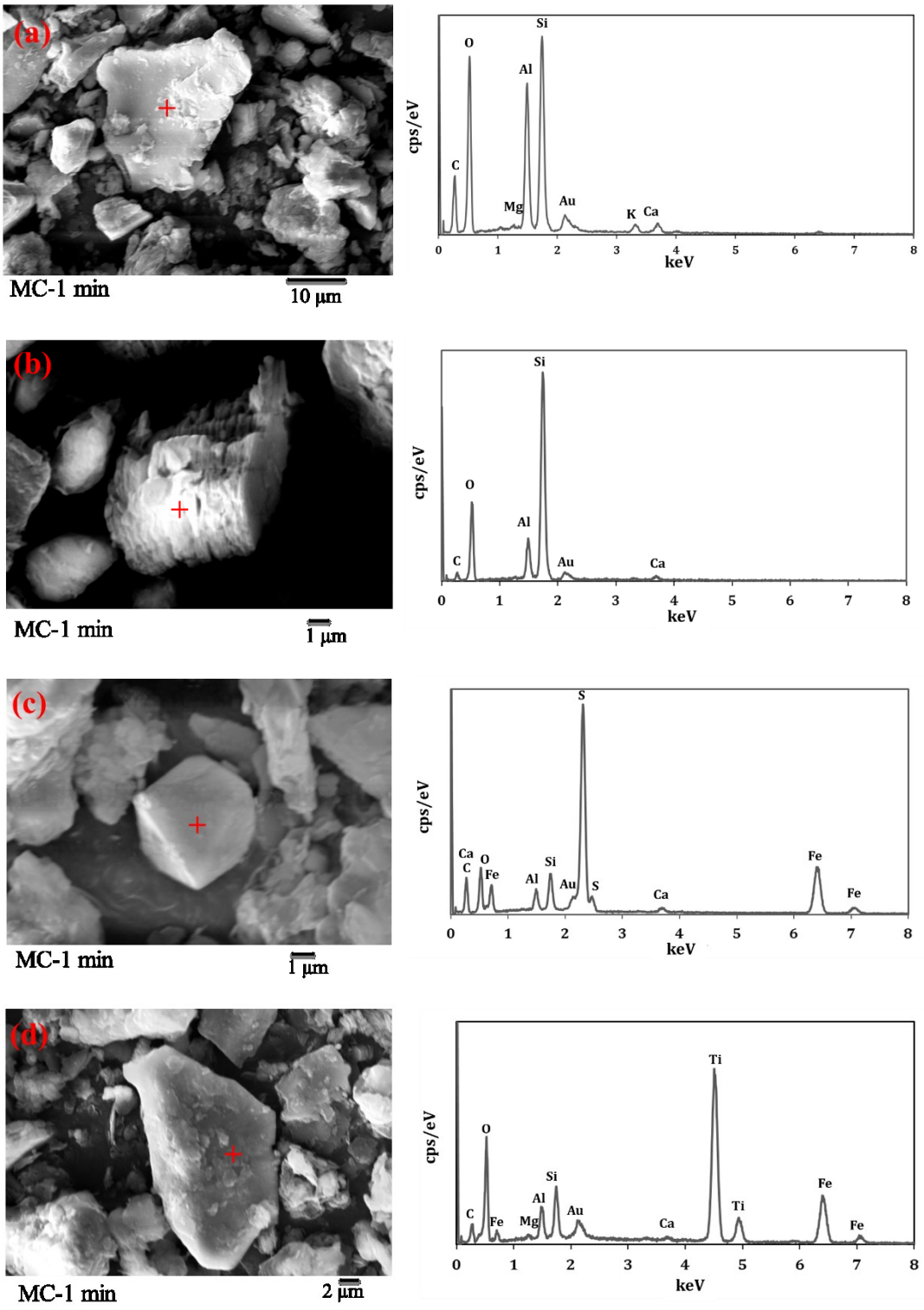

Figure 7-8 SEM SE images (left side) and corresponding EDX spectra (right side) for suspended solids from MC after 1min of settling: (a) clay mineral particle, (b) layers of clay minerals, (c) pyrite and (d) FeTi oxide mineral. The horizontal streaking in some images is an artifact due to charging effects in the SEM.

(0.4 wt%) and TiO_2 minerals (0.2 wt%) in MC after 1 min of settling time. For the SFS from MC after 7.5 min of settling time, the amount of large grains decreased in favour of fine particles mostly consisting of clay particles typically several microns in size (Figure 7-9 a).

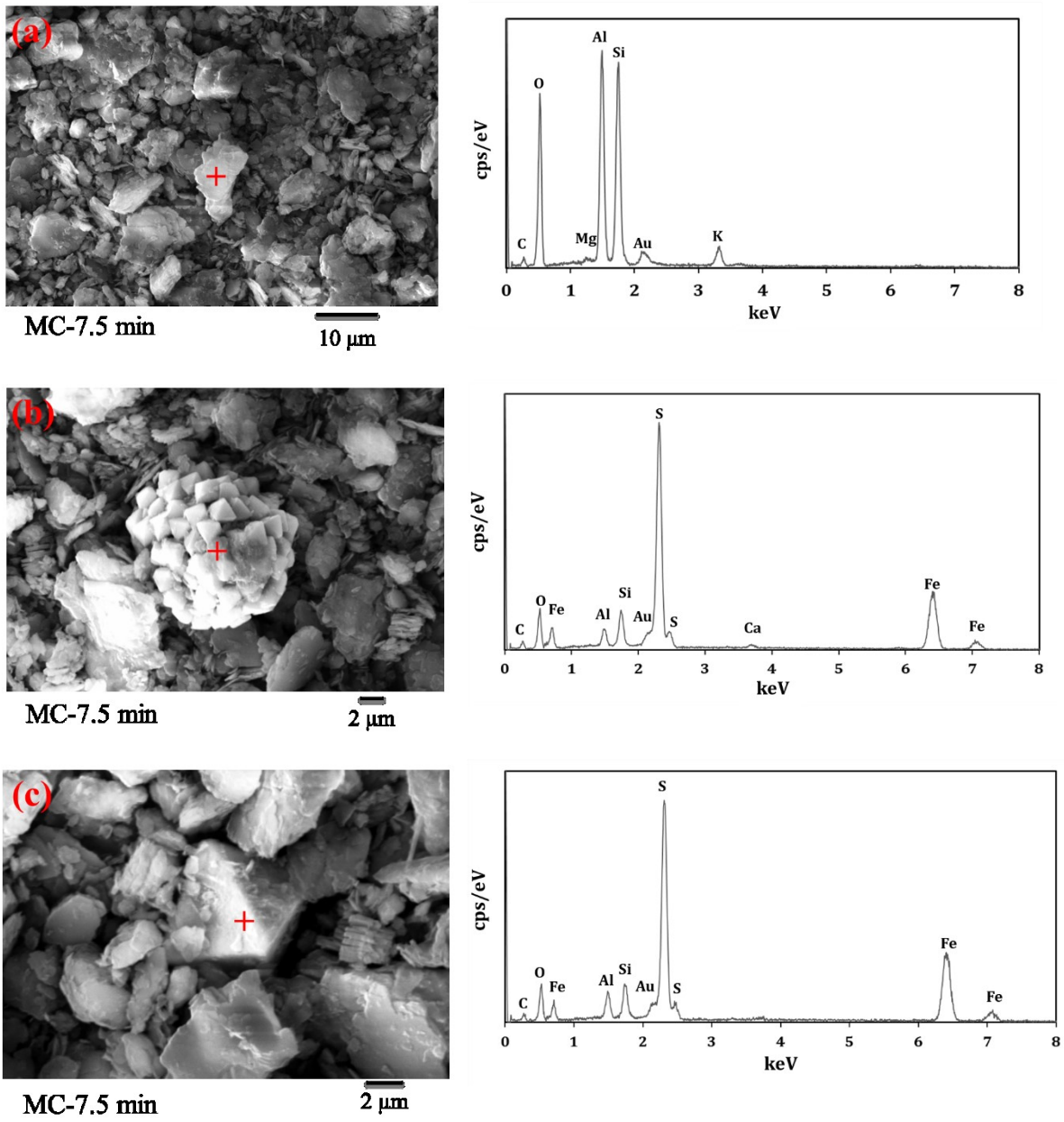

Figure 7-9 SEM SE images (left side) and corresponding EDX spectra (right side) for suspended solids from MC after 7.5 min of settling: (a) clay minerals, (b) pyrite aggregate (framboidal pyrite) and (c) pyrite single particle.

Framboidal pyrite (pyrite aggregate) and cubic pyrite crystal (single particle) were observed in SFS of MC after 7.5 min of settling time (Figure 7-9 b and c). These results are in agreement with the XRD results, and published data showing the presence of framboidal pyrite in the oil sands ore and attachment to the organic matter [224]. Moreover, XRD and SEM analyses showed that the amount of large grains decreased with increasing the settling time. The solids were mostly fine clay particles (kaolinite and illite) and were typically several microns in size.

7.3.7 TRANSMISSION ELECTRON MICROSCOPY (TEM)

Since the amount of SFS collected from the bitumen product for the EC samples was too small for most characterization techniques, TEM, EDX spectroscopy and nanobeam diffraction were used to identify the SFS after 1 min and 7.5 min settling times (Figure 7-10 and Figure 7-11). TEM bright field (BF) image of SFS for EC after 1 min settling time showed the hexagonal plate shape of well crystallized clay particles with a smooth basal surface. The EDX spectra showed Si, Al, and O as major components of this particle. Thus, kaolinite is the most probable mineral, which is likely associated with organic matter as evidenced by the correlation between the intensity of S and C peaks. This conjecture is consistent with previous work showing the hexagonal shape of kaolinite with a smooth basal surface [254].

A few subhedral particles rich in Ti were found in SEM analyses for the SFS of the bitumen product from MC after 1 min and 7.5 min settling (Figure 7-9). TEM BF images from several different TiO_2 particles are shown in Figure 7-11. The particles range is in size from 50 nm to 400 nm. The EDX spectra were taken from the two regions indicated with white circles (1, 2) and the nanobeam diffraction pattern was taken from region 1. The EDX spectra show the presence of both Ti and O in the particles. The SAD pattern is a spot pattern (Figure 7-11b), which indicates a single crystal that is close to the zone axis. The pattern was indexed as the rutile form of TiO_2 (zone axis = [111]). This finding is in agreement with our previous published data (Chapter 4 - section 4.3.2 and Chapter 5 - section5.3.3), which showed the presence of rutile and anatase in the bulk EC sample [10,203,251].

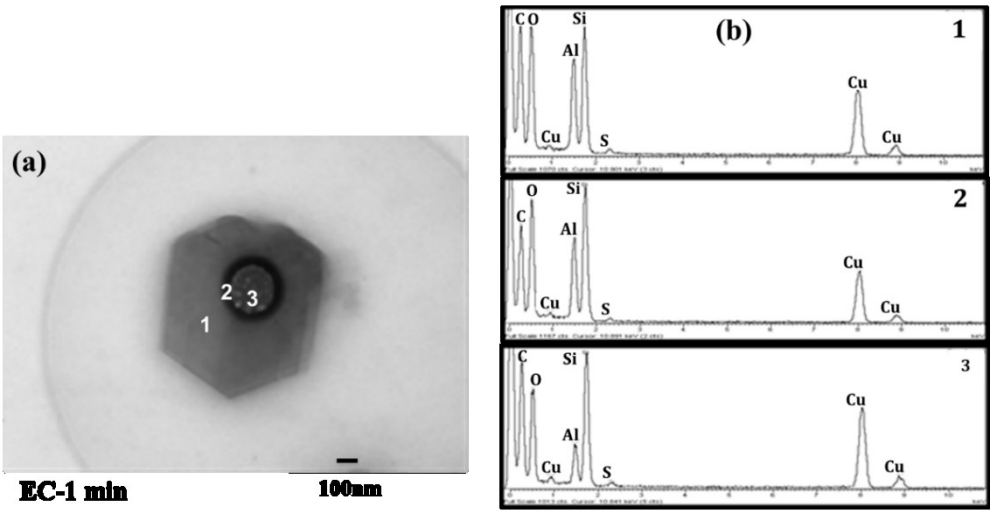

Figure 7-10 a) TEM BF image of clay particle (kaolinite) in supernatant collected from EC-1 min (after 1 min settling); b) EDX spectra from the points indicated in (a). The black ring in (a) is an artifact arising from carbon contamination during EDX analysis.

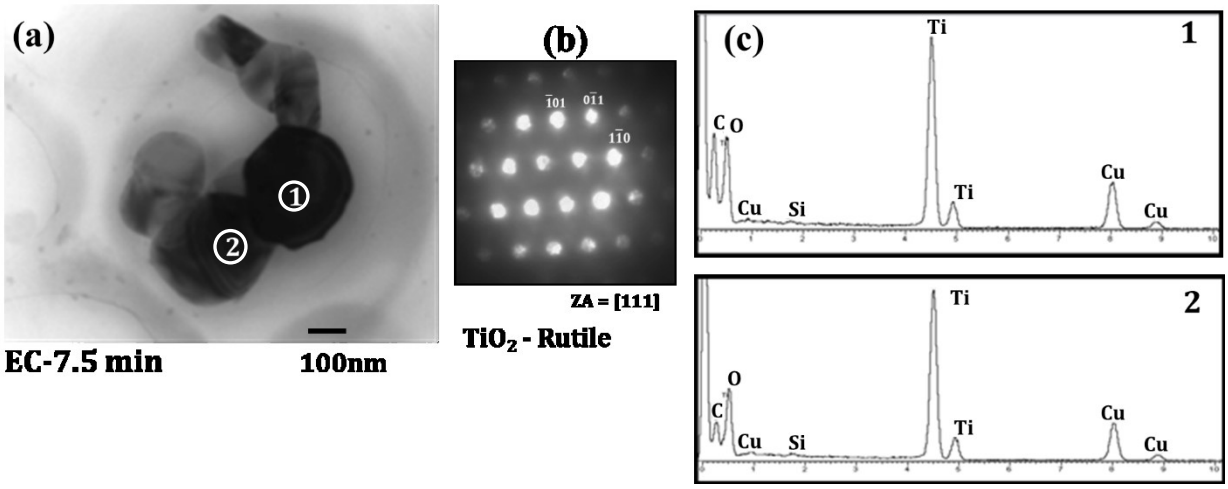

Figure 7-11 a) TEM BF image of rutile nano-size particles from supernatant collected from EC (after 7.5 min settling). b) Nanobeam diffraction pattern from particle labelled as 1 in (a); c) EDX spectra from regions shown in (a).

7.4 DISCUSSION

KF titration (Figure 7-2) showed the presence of water for all three supernatants, i.e., MS, ES and MC. The supernatant of MC showed higher water content compared with the sand samples (ES and MS). The reduction in water content with increasing settling time may be related to the settling of water droplets individually or with hydrophilic solids. The highest standard deviation of the water content was found for the MC supernatant at 1 min (± 0.016%), which could be related to the heterogeneous nature of this end member. This conjecture is consistent with previous published papers [10,203].

The MC supernatant showed the highest rate of decrease in the number of particles with settling time (1 min to 30 min) compared with the other supernatants (Table 7-2). This reduction rate is likely related to the high number of particles coupled with a low bitumen content, which caused high particle settling velocity and a reduction in the number of particles from 12,400 to 342 in the supernatant. The rate of decrease in the number of particles was lowered for all end member supernatants in the order MC>MS>ES, which is in agreement with the settling data (Table 7-2).

The three end members (MC, MS and ES) showed a decrease in SFS and, hence, an increase in bitumen content as the settling time was increased (Figure 7-4). However, the MC supernatant displayed the most significant decrease in SFS and increase in bitumen content compared with the other samples. Although the ES supernatant had the lowest rate change compared with the other samples, the bitumen content of ES was the highest of all four samples. This behavior could be related to the bitumen content of the as-received end members and the SFS during extraction (Table 7-2).

The XRD patterns from oriented preparations of all SFS specimens revealed that the relative amount of all non-clay minerals (with the exception of gypsum and siderite minerals in the ES sample) decreased with increasing settling time (Figure 7-5). Since most of the non-clay minerals, such as quartz, feldspars, pyrite, etc., have high specific gravities (SG >2.5 g/cm^3) and large particle sizes, it was expected that these minerals detached from the bitumen and quickly settled out of the cyclohexane-oil sands mixture in the graduated cylinder. Gypsum and siderite were observed in the ES supernatant samples after 30 min of settling, which may be related to the particle size and/or surface properties of these minerals, leading to attachment with some organic matter and suspension in the solvent-bitumen solution supernatant. This assumption is supported

by several published studies, which identified the presence of significant amounts of pyrite and siderite minerals in the Athabasca oil sands primary froth during aqueous extraction. Besides siderite, other carbonate minerals such as dolomite and calcite were observed in the froth [4,255]. It was also reported that most of the carbonate minerals showed neutral or oil-wet behavior and adsorbed heavy-polar organic matter like asphaltene [256].

The relative amount of kaolinite in the SFS of the marine samples (MS and MC) was elevated with increasing settling time (Figure 7-6 and Figure 7-7), indicating that the residual kaolinite in CS at each settling time was higher than the other minerals (either clay or non-clay minerals), which may be due to kaolinite surface properties and/or particle size distribution. The result is in agreement with the QXRD calculations for MC samples (1 min to 7.5 min); however, the kaolinite content was fairly constant (~39 wt%) for the MS sample (after 1 min and 7.5 min), which was unexpected (Table 7-3). XRD patterns in Figure 7-5 show that the ES samples had higher relative intensities of siderite and gypsum minerals compared with MC and MS. Moreover, MC contains more carbonate minerals such as calcite and dolomite than ES and MS samples. Both results are consistent with QXRD (1 min and 7.5 min settling) (Table 7-3). High amounts of clay minerals were determined in sand samples after 7.5 min settling time, which is probable due to the presence of finer clay minerals in sand samples (particularly in ES) compared with MC. This result is in good agreement with elemental analysis (Table 7-4), which shows that the highest amount of residual CIOC was observed in sand samples, especially in ES (10.1 wt%). This conjecture is consistent with our published papers (Chapter 4 - section 4.3.2 and Chapter 5 - section5.3.3) [10,203,251] and papers by Kotlyar *et al.* [198,229].

The relative amount of gypsum minerals in the ES samples increased with increasing settling time (Figure 7-5). The highest relative amount of kaolinite mineral was observed in the SFS of the marine samples (MS and MC) after 30 min of settling (Figure 7-6 and Figure 7-7). Conversely, the relative amount of illite mineral decreased with increasing settling time for the marine samples (MS and MC). The XRD patterns from oriented preparations for all SFS samples (i.e., EC after 1 min and MC, MS and ES at all settling times) revealed that the kaolinite reflection (7.13 Å) and the illite reflection (10.0 Å) did not change after ethylene glycol treatment, which indicates the presence of discrete kaolinite and illite without interstratification of expandable layers (Figure 7-6 and Figure 7-7). These results highlight the most important reason for higher bitumen quality and/or recovery using NAE methods compared with water extraction techniques. Oil sands

composition has a relatively minor effect on bitumen quality and/or recovery during non-aqueous bitumen extraction; however, oil sands composition significantly influences water based extraction. This idea is consistent with published papers that showed that NAE led to higher bitumen recovery even from low grade ores compared with water based extraction [23,32,33,175,257,258].

Elemental analysis was used to determine total carbon (TC), nitrogen (TN), hydrogen (TH) and sulfur (TS) contents (in wt%) for ES, MC and MS at different settling times (Table 7-4). The total carbon (TC) was elevated with increasing settling time, due to finer fraction enrichment in the SFS at longer settling times, which may contain higher amounts of residual TOC (or CIOC). The correlation of TOC with clay fractions in oil sands samples was reported in recent characterization studies and other publications [198,229,251]. The amount of TC was high for both sand samples (ES and MS), which could be due to the presence of carbonate minerals (dolomite and calcite in MS and siderite in ES). These minerals were observed in the XRD oriented preparations of ES and MS (Figure 7-5).

The N/C ratio for MC and MS was ~0.020, which is possible due to the presence of asphaltene and/or kerogen as residual organic matter. This hypothesis is consistent with published data (Table 7-5) [44,224,231]. The calculated range of N/C, H/C and S/C ratios for organic matter (i.e., bitumen, asphaltene and kerogen) is shown in Table 7-5. The N/C ratio for bitumen, asphaltene and kerogen is in the range of 0.0017-0.007, 0.012-0.016 and ≥0.019, respectively [44,224,231]. The S/C ratio varied between 0.089 and 0.201, which is a sign of possible inorganic sulfates (i.e., calcium sulfate or pyrite) in all SFS samples (with the exception of MC at 15 and 30 min). The calculated S/C ratio from previous studies showed that the ratio for organic matter (i.e., bitumen, asphaltene and kerogen) was ≤0.11 (Table 7-5) [44,224,231]. Table 7-5 shows that the H/C ratio for organic matter was ≤0.1, while this ratio for all SFS samples was ≥0.1 indicating the presence of clay minerals in these SFS samples (Table 7-4). The ratio decreased with increasing settling time for MS sample. However, it varied between 0.155 and 0.202 for ES and MC samples, which is likely related to the effect of carbonate minerals as a source of inorganic carbon (i.e., siderite for ES, and calcite and dolomite for MC) and clay minerals as a source of inorganic hydrogen on the H/C ratio. This result is also in good agreement with the XRD oriented preparations as well as QXRD from the SFS (Figure 7-5 and Table 7-3).

SEM analysis showed that the amount of large particles decreased with increasing settling time. SEM and EDX analysis revealed that the SFS at different settling times were mostly fine clay particles (kaolinite and illite) and were typically several microns in size (Figure 7-8 and Figure 7-9). It was also observed that various subhedral, anhedral and euhedral particles (between 0.2 μm and 40 μm in size), and some heavy minerals, such as Fe–Ti oxide minerals and pyrite (both framboidal and single particles), were found in the SFS from MC after 1 min and 7.5 min settling. These results confirm the XRD results, which identified the presence of clays, pyrite and TiO_2 minerals in the SFS samples.

Table 7-5 N/C, H/C and S/C ratios of bitumen, asphaltene and kerogen calculated from published data [224,231,232].

Sample	N/C ratio	H/C ratio	S/C ratio
Bitumen[1,2]	0.0017-0.0077	0.09-0.125	0.054-0.069
Asphatene[1,2]	0.012-0.016	0.084-0.102	0.06-0.110
Kerogen[3]	>0.019	0.057-0.1	0.03-0.08

TEM-BF images, EDX spectroscopy and electron diffraction revealed that the SFS collected from the bitumen product of the EC samples contained mostly clay (kaolinite) minerals. In addition, trace amounts of subhedral particles of rutile, ranging in size from 50 nm to 400 nm, were also identified from the SFS of the EC sample after 1 and 7.5 min of settling time.

7.5 CONCLUSIONS

The suspended fine solids (SFS) of marine claystone (MC), marine sands (MS) and esturine sands (ES) at all settling times contained two main groups of minerals: non-clay and clay minerals. The non-clay minerals at 1 min and 7.5 min settling times mostly included quartz (17.4–28.3 wt%),

[1] The chemistry of Alberta oil sand bitumen was reported by Strausz [232].

[2] The elemental analysis of different types of asphaltenes has been thoroughly investigated by Christopher *et al*. [231].

[3] 3The bitumen and kerogen contents for AM10 samples (MC, EC, MS and ES) have been thoroughly investigated by Zheng [224].

carbonates (calcite, dolomite and siderite, 1.5–16.8 wt%) and feldspars (K, Na and Ca feldspars, 5.3-8.5 wt%), with small amounts of pyrite (<0.9 wt%), TiO_2 minerals (anatase and rutile, 0-1.4 wt%) and a calcium sulfate mineral (gypsum, <1.5 wt%). The clay minerals in the SFS of MC, MS and ES at 1 min and 7.5 min settling times included kaolinite (36.3–46.6 wt%), 2:1 clay minerals (illite and mixed-layer clay minerals, 8.5–26.6 wt%), and chlorite (2.6–10.7 wt%). The relative concentration of total non-clay minerals in the SFS decreased with increasing settling time in the supernatants of MS, MC and ES. On the other hand, the relative concentration of total clay minerals in SFS increased with increasing the settling time. The supernatant of EC contained traces of bitumen and solids; kaolinite, illite, quartz, siderite and Ti-Fe minerals were observed in this supernatant. Clay (mostly kaolinite) and rutile minerals were also observed in this supernatant using TEM, EDX spectroscopy and electron diffraction techniques. The relative amount of kaolinite in the supernatants of MC, MS and ES increased with increasing settling time. An interesting feature of this study is that mixed-layer clay minerals were not observed in the SFS of MC, MS and ES at all settling times. Kerogen and/or asphaltene were identified in the SFS of end members based on the N/C ratio (>0.018). End member composition affected SFS and bitumen content of the bitumen product; however, the bitumen content was higher than 92% for all three end members (MC, MS and ES) after 30 min of settling.

XRD and SEM analysis showed that the amount of large particles decreased with increasing settling time. The solids were mostly fine clay particles (kaolinite and illite) and were typically several microns in size. Some heavy minerals, such as Fe–Ti oxide minerals and pyrite (both single particle and framboidal pyrite), were found in the suspended solids from MC after 1 min and 7.5 min settling.

CHAPTER 8

8 GENERAL CONCLUSIONS AND FUTURE WORK

8.1 SUMMARY AND CONCLUSIONS

Applying organic solvents in bitumen extraction from oil sands and shales is an alternative approach to aqueous extraction. Certain components of the oil sands may affect processability of the ore during non-aqueous extraction. These minerals are prone to interact with the solvent, bitumen, and/or water due to their high surface area, surface ion exchange capabilities, and specific physicochemical properties. The overall objective of this thesis was to characterize the mineralogical and chemical composition, specifically "nano and microsize minerals (NMM)" and mainly clay minerals of the four petrologic end members that make up the oil sands deposit, where particles are carried into the solvent-bitumen solution. Accordingly, the research work in this thesis was designed to reach the mentioned objectives as described in the following.

1- Characterization of four petrologic end members from Alberta oil sands

In this objective, the four as-received (ASRE) oil sands ores from Syncrude's North Mine taken in 2009 (NM09) and 2012 (NM12) were used for characterization and the results were compared with samples taken from the Aurora Mine in 2010 (AM10) of Syncrude Canada Ltd. (Fort McMurray, Alberta). Each mined ore was essentially a sample of one of the four petrologic end members, namely estuarine sand (ES), estuarine clay (EC), marine sand (MS), and marine clay (MC) [11,203]. In addition, to improve sample collection, clay and sands were manually separated from the ASRE end members.

The four petrologic end members of the Alberta oil sands mainly consisted of bitumen (0.03 to 16.4 wt%), solids (83.3-97.4 wt %) and water (0.6-10.2 wt %). The highest and lowest amounts of bitumen were identified in ES and EC, respectively, for all three samples (NM12, NM09, and AM10). The presence of 0.04 – 6.34 wt% of toluene insoluble organic carbon after bitumen

removal was found in the four end members (NM09) using elemental analysis (CHNS). The quantity of toluene insoluble organic carbon was elevated in the finer fractions, which is most likely due to its association with the clay minerals. The coarse size fractions (with a minimal quantity of clay minerals) have minimal negative effect on bitumen extraction using the soxhlet extractor with hot toluene (Dean-Stark extraction process) compared with fine fractions. Estuarine ore mostly behaves as a “good-processing” ore. The "poor-processing“ ore mostly consisted of marine ore.

The bulk samples after bitumen removal contained two main groups of minerals: non-clay and clay minerals. The non-clay minerals from NM09 and NM12 mostly contained quartz (51.7–99 wt%), carbonates (calcite, dolomite, and siderite, 0–14.1 wt%), and feldspars (K, Na, and Ca feldspars, 0.1–3.8 wt%), with small amounts of pyrite (< 0.2 wt%), TiO_2 minerals (anatase and rutile, < 0.7 wt%), and a calcium sulphate mineral (gypsum, 0.5 wt%). The highest relative amount of 2:1 clay minerals (illite and mixed-layer clay minerals) was mainly found in the finest size fractions (< 0.2 μm). The expandability of illite-smectite was 30 ± 4 % and 10 ± 3 % for MC and EC of NM12, respectively. The expandability of illite-smectite was about 9 % for MC and EC of NM09. Kaolinite-smectite was only observed in MC from NM12 and the expandability was between 5 and 10 %. Siderite was concentrated primarily in the bulk sample and the coarse fractions of the EC end member. Other carbonates (calcite and dolomite), on the other hand, were found mainly in the bulk samples and the > 2 μm (> 45 and 2–45 μm) fractions of the MC end member. However, the highest amount of carbonate was found in the fine fractions (< 2 μm) of MC from NM09. Kerogen and/or asphaltene were identified in all fine (< 45 μm) fractions of end members based on the N/C ratio (> 0.019). The very dark grey colour of MC compared with the beige colour of EC is due to the higher amount of residual TOC in all fractions of MC. There was a direct relation between the mineral and chemical composition of the four petrologic end members.

The surface properties (i.e., CEC, LCD and SA) were determined for four petrologic end members of Alberta oil sands using LCD (R6G and MB), SA (TSSA-MB and SSA-BET) and CEC (Cu_{TRIEN} and MB) techniques. Generally, the surface properties of the samples were influenced by the amount and type of clay minerals present in the petrologic end members. The LCD (R6G and MB), SA (TSSA-MB and SSA-BET) and CEC (Cu_{TRIEN} and MB) values increased due to higher total 2:1 clay minerals content, particularly with mixed layer clay minerals (illite-smectite). The CEC

(Cu_{TRIEN} and MB) values were higher for higher SA (SSA-BET and TSSA-MB) values. TSSA-MB had higher values than those of SSA-BET due to the basic principles of the two techniques.

Different size fractions of petrologic end members diplayed different distributions of layer charge due to different amounts of 2:1 clays, particularly interstratified illite-smectite. A correlation was found between the amount of 2:1 clays and the amount of H-aggregates and monomers. Larger numbers of H-aggregates, lower numbers of monomers and greater layer charges were observed in fractions with higher quantities of 2:1 clay minerals. Molecular aggregation in the SDS spectra of organic dye (MB and R6G) was only identified in petrologic end members consisting of more than 25 wt% of 2:1 clay minerals. The <0.2 μm size fractions of petrologic end members displayed the highest SA (TSSA-MB and SSA-BET), CEC (CuTRIEN and MB) and LCD (R6G and MB) values, due to their higher relative amounts of illite-smectite. The higher SA, CEC and LCD values were characteristic of the fine size fractions of petrologic end members, which is likely due to the higher amounts of illite-smectite compared with other clay minerals in this fraction.

2- Effect of individual clay minerals (swelling and non-swelling clays) on non-aqueous bitumen extraction process

The second underpinning subject of this study was to identify the mechanism of preferential clay segregation. For this purpose, an experimental set up was designed and investigated to examine the effect of individual clay minerals (swelling and non-swelling clays) on non-aqueous bitumen extraction. Since, it is impossible to collect individual types of clay minerals from the oil sands due to the highly heterogeneous nature of these samples, artificial mixtures of bitumen with standard clays (from the Clay Minerals Society) were prepared and the influence of individual clays on the extraction process was investigated.

Bitumen treatment of non-swelling and swelling clay minerals revealed that bitumen-treated swelling clays contained 4.6 – 8.2% of carbon, whereas the non-swelling clays contained only 3.6 – 7.0% of carbon after cyclohexane bitumen removal. Most of the residual organic matter was retained on the outer surfaces (basal planes and edges) of non-swelling clay mineral particles, whereas the residual organic matter remained on both the outer and inner (interlayer space) surfaces of the swelling clay mineral particles in the form of a patchy rather than continuous coating. FTIR results showed that the organic material likely remained in the interlayer space of swelling clay minerals by partial replacement of the interlayer water.

Pre-treatment of non-swelling clay samples at different relative humidity conditions (0%, 50% and 95% RH) had no significant effect on the carbon content. This pre-treatment had a remarkable influence on the amount of carbon after bitumen treatment of swelling clays (mainly smectite SWy-2). The amount of carbon was increased for bitumen treatment of SWy-2 at 95% RH by 56% compared with SWy-2 bitumen-treated at 0% RH. This phenomenon is likely connected with opening of the interlayer space of swelling clay minerals upon exposure to higher RH and subsequent retention of a larger amount of organic material.

The reduction of surface properties (i.e., SSA, LCD and CEC) of clay minerals was observed by reaction with bitumen, which is likely due to organic coating on clay mineral surfaces and/or to gluing of clay particles to aggregates. The pre-treatment of swelling clays at various RH conditions, the swelling ability, the number of swelling interlayers (i.e., expandability) and the specific surface area (SSA) of swelling clays affceted the amount of residual organic matter. SSA was only found to be a primary parameter controlling the carbon content for the non-swelling clays. This can be interpreted as clay minerals with larger SSAs and higher expandability (i.e., numbers of swelling interlayers) that are exposed to higher RH conditions generally contain higher amounts of carbon after bitumen treatment. Thus they have the most detrimental influence on cyclohexane bitumen extraction under the studied experimental conditions.

3- Qualification and quantification of residual fine solids migrated to the bitumen product after cyclohexane extraction of the four petrological end members of Alberta oil sands

The third subject of this study was to design an experimental set up for non-aqueous extraction to collect adequate amounts of suspended fine solids (SFS) from bitumen products after cyclohexane extraction. The type and quantity of these migrated fine solids for different clay species were investigated for the four petrologic end members from the Alberta oil sands to better understand the most important parameters affecting non-aqueous bitumen extraction and bitumen quality.

The SFS of the four petrologic end members at all settling times consisted of two main groups of minerals: non-clay and clay minerals. Quartz and kaolinite were identified as the main non-clay and clay minerals, respectively, after 1 min and 7.5 min settling times. A clear reduction of non-clay minerals (mostly quartz) in favour of clay minerals (mainly kaolinite) in the SFS was identified as the settling time increased in the supernatants of MS, MC and ES. The supernatant of

EC contained traces of bitumen and solids; kaolinite, illite, quartz, siderite and Ti-Fe minerals were observed in this supernatant.

Kaolinite and rutile were also observed in the EC supernatant at 1 min settling time using TEM, EDX spectroscopy and electron diffraction techniques. An interesting feature of this study is that mixed-layer clay minerals were not observed in the SFS of MC, MS and ES at all settling times. Kerogen and/or asphaltene were also determined in the SFS of the end members based on the N/C ratio (>0.018). End member composition affected SFS and bitumen content of the bitumen product; however, the bitumen content was higher than 92% for all three end members (MC, MS and ES) after 30 min of settling.

The XRD results were confirmed by SEM analysis, which showed that the amount of large particles decreased with increasing settling time. The solids were mostly fine clay particles (kaolinite and illite) and were typically several microns in size. Some heavy minerals, such as Fe–Ti oxide minerals and pyrite (both framboidal and single particle), were found in the SFS from MC after 1 min and 7.5 min settling.

8.2 FUTURE WORK

For the future work following this research, the following suggestions and recommendations are proposed:

1- A simplified non-aqueous bitumen extraction process was designed to examine the settling behavior of a mixture of cyclohexane and four petrologic end members with specific solvent/ore ratio (40/60). The results from these experiments revealed that the bitumen quality varied in different end members (93-98 wt%) after 30 min of settling time. The solvent/ore ratio is believed to dramatically influence the bitumen extraction process such as bitumen quality, bitumen recovery, solid precipitation speed and the amount of SFS in the bitumen product. Therefore, the solvent to end member ratio needs to be optimized in the extraction process, since it plays an important role in dissolving bitumen and accelerating solid precipitation. In addition, adding water or surfactants to oil sands solids modifies the wettability, which is likely an effective method to improve solvent recovery and/or bitumen quality.

2- One of the important aims of this study was to identify the migration of SFS in the bitumen product at different settling times for the four as-received (ASRE) petrologic end members from the North Mine samples taken in 2012 (NM12). To gather adequate data, it is beneficial to collect other mine samples (petrologic end members and/or ores), perform the settling behavior experiments, evaluate the migration of fine solids in the bitumen product and characterize them. These studies will help in determining the effect of other factors and/or minerals on non-aqueous extraction.

3- Since nano and microsize clay minerals were found to be the most problematic minerals affecting the bitumen extraction process, bitumen recovery and quality, it is worthwhile to study the influence of the fine (<2 μm) and ultrafine (<0.2 μm) particles of clays on the solvent bitumen extraction process. Therefore, these fractions should be collected from end members and then specific amounts of these particles should be added to each end member to study their migration during non-aqueous bitumen extraction. This will help in understanding how much added fine and ultra-fine particles are found in the bitumen product after certain settling times.

4- The amorphous and poorly crystallized Fe-bearing minerals were characterized using Mössbauer spectroscopy, TEM and electron diffraction in our previous and current studies for oil sands samples NM09 and NM12. The results have shown that very small amounts of siderite ($FeCO_3$) and pyrite (FeS_2), as well as trace amounts of lepidocrocite (γ-FeO(OH)) and wustite (FeO), were present in the original ore (four petrologic end members). Kerogen (sedimentary organic matter) was also identified in the four petrologic end members of NM09, NM12 and AM10. These nano and microsize species are believed to significantly affect the non-aqueous bitumen extraction process and solvent recovery. Therefore, it is of value to investigate the interaction of cyclohexane with kerogen and Fe-bearing minerals (<50 nm) individually and cumulatively, as well as the influence of these nano and microsize species on solvent retention, by adding different amounts of these species to the end members.

REFERENCES

[1] Qabazard HM, Agoawike A, Al-zayer FA. OPEC - Annual Statistical Bulletin. Organ Pet Export Ctries 2012:108. doi:ISSN 0475-0608.

[2] Kasperski KL. Review of research on aqueous extraction of bitumen from mined oil sands. Edmonton: CANMET, Western Research Centre, Natural Resources Canada; 2001.

[3] Zhao S, Kotlyar LS, Sparks BD, Woods JR, Gao J, Chung KH. Solids contents, properties and molecular structures of asphaltenes from different oilsands. Fuel 2001;80:1907–14. doi:10.1016/S0016-2361(01)00044-8.

[4] Kaminsky HAW. Characterization of an Athabasca oil sand ore and process streams. PhD Diss Univ Alberta 2008.

[5] Masliyah J, Czarnecki J, Xu Z. Handbook on theory and practice of bitumen recovery from athabasca oil sands. vol. 1–Theoreti. Kingsley publishing services; 2011. doi:10.1017/CBO9781107415324.004.

[6] Teare M, Cruickshank R, Miller S, Overland S, Marsh R, Willwerth A, et al. ST98-2014 Alberta's energy reserves 2013 and supply/demand outlook 2014-2023. Calgary: 2014.

[7] Mikula RJ, Munoz VA, Wang N, Bjornson B, Cox D, Moisan B, et al. Characterization of bitumen properties using microscopy and near infrared spectroscopy: Processability of oxidized or degraded ores. J Can Pet Technol 2003;42:50–4. doi:10.2118/03-08-04.

[8] Liu J, Xu Z, Masliyah J. Role of fine clays in bitumen extraction from oil sands. AIChE J 2004;50:1917–27. doi:10.1002/aic.10174.

[9] Alberta Energy. Oil sands tailings, Alberta Government 2013:2. www.energy.alberta.ca/OilSands/pdfs/FSTailings.pdf (accessed March 23, 2015).

[10] Osacky M, Geramian M, Ivey DG, Liu Q, Etsell TH. Mineralogical and chemical composition of petrologic end members of Alberta oil sands. Fuel 2013;113:148–57.

doi:10.1016/j.fuel.2013.05.099.

[11] Osacky M, Geramian M, Liu Q, Ivey DG, Etsell TH. Surface properties of petrologic end-members from alberta oil sands and their relationship with mineralogical and chemical composition. Energy Fuels 2014;28:934–44. doi:10.1021/ef402150z.

[12] Alberta Energy. Alberta Culture and Tourism. Alberta Geol Serv Alberta-Oil-Sands-Map n.d. doi:http://history.alberta.ca/energyheritage/sands/origins/default.aspx#page-1.

[13] Langenberg CW, Hein FJ, Berhane H. Three-Dimensional Geometry of Fluvial-Estuarine Oil Sand Deposits of the Clarke Creek Area (NTS 74D), Northeastern Alberta. Edmonton, Alberta: 2003.

[14] Etsell TH, Liu Q, Ivey DG. Nano and Microsize Minerals in Non-aqueous Bitumen Extraction from Oil Sands 2010:21.

[15] Sandford EC, Seyer FA. Processibility of Athabasca tar sand using a batch extraction unit: the role of NaOH. CIM Bull 1979;72:164–9.

[16] Takamura K, Wallace D. The physical chemistry of the hot water process. J Can Pet Technol 1988;27:98–106. doi:10.2118/88-06-08.

[17] Smith RG, Schramm LL. The influence of mineral components on the generation of natural surfactants from Athabasca oil sands in the alkaline hot water process. Fuel Process Technol 1992;30:1–14. doi:10.1016/0378-3820(92)90072-X.

[18] Zhou ZA, Xu Z, Masliyah JH, Czarnecki J. Coagulation of bitumen with fine silica in model systems. Colloids Surfaces A Physicochem Eng Asp 1999;148:199–211. doi:10.1016/S0927-7757(98)00677-3.

[19] Wik S, Sparks BD, Ng S, Tu Y, Li Z, Chung KH, et al. Effect of process water chemistry and particulate mineralogy on model oilsands separation using a warm slurry extraction process simulation. Fuel 2008;87:1394–412. doi:10.1016/j.fuel.2006.05.034.

[20] Omotoso OE, Mikula RJ. High surface areas caused by smectitic interstratification of kaolinite and illite in Athabasca oil sands. Appl Clay Sci 2004;25:37–47. doi:10.1016/j.clay.2003.08.002.

[21] Hooshiar A, Uhllik P, Kaminsky HW, Shinbine A, Omotoso O, Liu Q, et al. High resolution

transmission electron microscopy study of clay mineral particles from streams of simulated water based bitumen extraction of Athabasca oil sands. Appl Clay Sci 2010;48:466–74. doi:10.1016/j.clay.2010.02.008.

[22] Mercier PHJ, Patarachao B, Kung J, Kingston DM, Woods JR, Sparks BD, et al. X-ray diffraction (XRD)-derived processability markers for oil sands based on clay mineralogy and crystallite thickness distributions. Energy Fuels 2008;22:3174–93. doi:10.1021/ef8002203.

[23] Hooshiar A, Uhlik P, Ivey DG, Liu Q, Etsell TH. Clay minerals in nonaqueous extraction of bitumen from Alberta oil sands: Part 2. Characterization of clay minerals. Fuel Process Technol 2012;96:183–94. doi:10.1016/j.fuproc.2011.10.010.

[24] Osacky M, Geramian M, Ivey DG, Liu Q, Etsell TH. Influence of nonswelling clay minerals (illite, kaolinite, and chlorite) on nonaqueous solvent extraction of bitumen. Energy and Fuels 2015;29:4150–9. doi:10.1021/acs.energyfuels.5b00269.

[25] Camp FW. The tar sands of Alberta, Canada. 3rd ed. Denver, Colorado: Cameron Engineers Inc.; 1976.

[26] Alberta Energy. Alberta Energy, Oil sands, Alberta Government 2010. http://www.energy.gov.ab.ca/OurBusiness/oilsands.asp.

[27] Utah Heavy Oil Program, Institute for Clean and Secure Energy. A Technical, Economic, and Legal Assessment of North American Heavy Oil, Oil Sands, and Oil Shale Resources. Salt Lake City, Utah: 2007. doi:DE-FC-06NT15569.

[28] MacKinnon MD. Development of the tailings pond at Syncrude's oil sands plant 1978-1987. AOSTRA J Res 1989;5:109–33.

[29] Veliotti TR, Johnson KF, editors. Energy Research Developments : Tidal Energy, Energy Efficiency and Solar Energy. New York: Nova Science Publishers, Inc.; 2009.

[30] Moorhouse J, Huot M, Dyer S. Drilling Deeper: The In Situ Oil Sands Report Card. Drayton Valley, Alberta: 2010.

[31] Thermal In-situ oil sands. Can Nat 2016. http://www.cnrl.com/operations/north-america/north-american-crude-oil-and-ngls/thermal-insitu-oilsands.

[32] Hooshiar A, Uhlik P, Liu Q, Etsell TH, Ivey DG. Clay minerals in nonaqueous extraction of bitumen from Alberta oil sands: Part 1. Nonaqueous extraction procedure. Fuel Process Technol 2012;94:80–5. doi:10.1016/j.fuproc.2011.10.008.

[33] Nikakhtari H, Vagi L, Choi P, Liu Q, Gray MR. Solvent screening for non-aqueous extraction of Alberta oil sands. Can J Chem Eng 2013;91:1153–60. doi:10.1002/cjce.21751.

[34] Bayliss P, Levinson AA. Mineralogical review of the Alberta oil sand deposits (Lower Cretaceous, Mannville Group). Bull Can Pet Geol 1976;24:211–4.

[35] Ignasiak TM, Kotlyar L, Longstaffe FJ, Strausz OP, Montgomery DS. Separation and characterization of clay from Athabasca asphaltene. Fuel 1983;62:353–62. doi:10.1016/0016-2361(83)90096-0.

[36] Sparks BD, Kotlyar LS, O'Carroll JB, Chung KH. Athabasca oil sands: Effect of organic coated solids on bitumen recovery and quality. J Pet Sci Eng 2003;39:417–30. doi:10.1016/S0920-4105(03)00080-9.

[37] Wallace D, Tipman R, Komishke B, Wallwork V, Perkins E. Fines/water interactions and consequences of the presence of degraded illite on oil sands extractability. Can J Chem Eng 2004;82:667–77. doi:10.1002/cjce.5450820405.

[38] Eslahpazir R, Liu Q, Ivey DG. Characterization of iron-bearing particles in Athabasca oil sands. Energy and Fuels 2012;26:5036–47. doi:10.1021/ef300597p.

[39] Kaminsky HAW, Etsell TH, Ivey DG, Omotoso O. Characterization of heavy minerals in the Athabasca oil sands. Miner Eng 2008;21:264–71. doi:10.1016/j.mineng.2007.09.011.

[40] Ciu Z, Liu Q, Etsell TH, Oxenford J, Coward J. Heavy Minerals in the Athabasca Oil Sands Tailings – Potential and Recovery Processes. Can Metall Q 2003;42:383–92. doi:10.1179/cmq.2003.42.4.383.

[41] Wang C, Geramian M, Liu Q, Ivey DG, Etsell TH. Comparison of different methods to determine the surface wettability of fine solids isolated from Alberta oil sands. Energy and Fuels 2015;29. doi:10.1021/ef502709r.

[42] BUTT AS. Shale Characterization using X-Ray Diffraction. MSc Eng Diss Dalhousie Univ 2012.

[43] Bichard J. Oil sands composition and behaviour research. Alberta Oil Sands Technol Res Auth 1987;3:626.

[44] Strausz OP, Lown EM. The chemistry of alberta oil sands, bitumen and heavy oils. Calgary: Alberta Energy Research Institute; 2003.

[45] Alberta Research Council., Alberta. Alberta Environment. Clay tailings from Alberta oil sands and other sources : a review. Reports ; 1978/2 1978:87.

[46] Spiers GA, Dudas MJ, Turchenek LW. The Chemical and Mineralogical Composition of Soil Parent Materials in Northeast Alberta. Can J SOIL Sci 1989;69. doi:10.4141/cjss89-074.

[47] Sands versus Carbonates. Laricina Energy Ltd n.d. http://www.laricinaenergy.com/about-oil-sands/oil-sands-versus-carbonates.html.

[48] Couillard M, Mercier PHJ. Analytical Electron Microscopy of Carbon-Rich Mineral Aggregates in Solvent-Diluted Bitumen Products from Mined Alberta Oil Sands. Energy Fuels 2016;30:5513–24. doi:10.1021/acs.energyfuels.6b00708.

[49] Ellwood BB, Burkart B, Rajeshwar K, Darwin RL, Neeley RA, McCall AB, et al. Are the iron carbonate minerals, ankerite and ferroan dolomite, like siderite, important in paleomagnetism? J Geophys Res 1989;94:7321–31. doi:89 JB00044.

[50] Baker P, Burns S. Occurrence and formation of dolomite in organic-rich continental margin sediments. Am Assoc Pet Geol Bull 1985;69:1917–30. doi:10.1306/94885570-1704-11D7-8645000102C1865D.

[51] Hepler LG, Hsi C, Alberta Oil Sands Technology and Research Authority. AOSTRA technical handbook on oil sands, bitumens and heavy oils. 1989.

[52] Kasperski KL. A review of properties and treatment of oil sands tailings. AOSTRA J Res 1992;8:11–53.

[53] Wills BA. Mineral processing technology. Oxford: Butterworth-Heinemann; 2006.

[54] Chopra S, Lines L, Schmitt DR, Batzle M. Heavy-oil Reservoirs : Their Characterization and Production Heavy Oil as an Important Resource for the Future, 2000, p. 1–70.

[55] Procter RM, Taylor GC, Wade JA. Oil and natural gas resources of Canada 1983. Inst

Sediment Pet Geol 1984:59. doi:10.4095/119739.

[56] Rossenfoss S, Rassenfoss S. Finding Pathways to Produce Heavy Oil From Canadian Carbonates. J Pet Technol 2013. doi:10.2118/0813-0058-JPT.

[57] Hein FJ, Marsh RA, Boddy MJ. Overview of the Oil Sands and Carbonate Bitumen of Alberta: Regional Geologic Framework and Influence of Salt-Dissolution Effects 2008;10144:1–5. doi:Search and Discovery Article #10144.

[58] Wo E, Song L, Hurst T, Sitek N. Geological Review and Bitumen Resource Appraisal of the Grosmont Formation within the Athabasca Oil Sands Area. 2010 AAPG Int Conv Exhib 2010;80130. doi:AAPG Search and Discovery Article #90108.

[59] Machel HG, Luz Borrero M, Dembicki E, Huebscher H, Ping L, Zhao Y. The Grosmont : a complex dolomitized, fractured and karstified heavy oil reservoir in a Devonian carbonate-evaporite platform. GeoConvention 2012 Vis 2012;10576:1–24.

[60] Snyder J. Sleeping giant: Can Canada's other mammoth bitumen deposit be commercialized? Ventur Publ Inc 2014. https://www.albertaoilmagazine.com/2014/09/sleeping-giant/.

[61] Geology Division-Research Council of Alberta. Notes on the Occurence of Iron-Bearing Minerals Associated with the Athabasca Oil Sands. Edmonton: 1973.

[62] Kramers JW, Brown RAA. Survey of heavy minerals in the athabasca oil sand deposit., Edmonton, Alberta: Annual Meeting of CIM, October 26–29; 1975.

[63] Omotoso O, Munoz VA, Mikula RJ. Valuable Minerals in The UTS Fort Hill Oil Sands Lease Core Samples. Edmonton: 2005. doi:CETC—DEVON 05-48 (CE).

[64] Young J, Healy RE. Mineralogical Characterization of Ti- and Zr-Bearing Heavy Minerals in Syncrude and Suncor oil sands. Winnipeg: 1996.

[65] Chachula F, Liu Q. Upgrading a rutile concentrate produced from athabasca oil sands tailings. Fuel 2003;82:929–42. doi:10.1016/S0016-2361(02)00401-5.

[66] Klein C, Hurlbut CS, Dana JD. Manual of mineralogy (after James D. Dana). 20th ed. New York: Wiley; 1985.

[67] Adams GL. Gypsum deposits in the United States. Econ Geol 1904;Series A:1–125.

doi:10.1016/S0016-0032(21)91174-8.

[68] Indiana Gelogical Survey. Anhydrite and Gypsum n.d. https://igs.indiana.edu/ReferenceDocs/GypsumAndAnhydrite_Card.pdf.

[69] Motta Cabrera SC. Characterization of Oil Sands Tailings Using Low Field Nuclear Magnetic Resonance (NMR) Technique. 2008.

[70] Beier N. The Oil Sands Tailings Research Facility 2007:1423–30.

[71] Chalaturnyk RJ, Don Scott J, Özüm B. Management of Oil Sands Tailings. Pet Sci Technol 2002;20:1025–46. doi:10.1081/LFT-120003695.

[72] Todd EC, Sherman DM, Purton JA. Surface oxidation of pyrite under ambient atmospheric and aqueous (pH = 2 to 10) conditions: Electronic structure and mineralogy from X-ray absorption spectroscopy. Geochim Cosmochim Acta 2003;67:881–93. doi:10.1016/S0016-7037(02)00957-2.

[73] Craen MD, Geet M Van, Honty M, Weetjens E, Sillen X. Extent of oxidation in Boom Clay as a result of excavation and ventilation of the HADES URF: Experimental and modelling assessments. Phys Chem Earth 2008;33:6–8. doi:10.1016/j.pce.2008.10.032.

[74] Honty M, De Craen M, Wang L, Madejová J, Czímerová A, Pentrák M, et al. The effect of high pH alkaline solutions on the mineral stability of the Boom Clay - Batch experiments at 60°C. Appl Geochem 2010;25:825–40. doi:10.1016/j.apgeochem.2010.03.002.

[75] Borrrero ML. Hondo evaporites within the grosmont heavy oil carbonate platform, Alberta, Canada. MSc Diss Univ Alberta 2010.

[76] Moore DM, Reynolds RC. X-ray diffraction and the identification and analysis of clay minerals. 2nd ed. US. Oxford University Press; 1997.

[77] Bergaya F, Theng BKG, Lagaly G. Handbook of Clay Science. Developments in Clay Science, Volume 1. 1st ed. Amsterdam: Elsevier Science; 2006.

[78] Holtz RD, William KD. An Introduction to Geotechnical Engineering. Eng Geol 1986;22:377. doi:10.1016/0013-7952(86)90005-0.

[79] Grim RE. Applied clay mineralogy. McGraw-Hill Book Company, Inc., USA; 1962.

[80] Clementz DM. Interaction of petroleum heavy ends with montmorillonite. Clays Clay Miner

1976;24:312–9. doi:10.1346/CCMN.1976.0240607.

[81] Dongbao F, Woods JR, Kung J, Kingston DM, Kotlyar LS, Sparks BD, et al. Residual organic matter associated with toluene-extracted oil sands solids and its potential role in bitumen recovery via adsorption onto clay minerals. Energy Fuels 2010;24:2249–56. doi:10.1021/ef900885p.

[82] Kasongo T, Zhou Z, Xu Z, Masliyah J. Effect of clays and calcium ions on bitumen extraction from Athabasca oil sands using flotation. Can J Chem Eng 2000;78:674–81. doi:10.1002/cjce.5450780409.

[83] Tu Y, O'Carroll JB, Kotlyar LS, Sparks BD, Ng S, Chung KH, et al. Recovery of bitumen from oilsands: Gelation of ultra-fine clay in the primary separation vessel. Fuel 2005;84:653–60. doi:10.1016/j.fuel.2004.03.020.

[84] Odebunmi EO, Olaremu AG. Extraction of Chemical Constituents of Bitumen Using a Mixed Solvent System 2015:485–94. doi:10.4236/ojapps.2015.58047.

[85] Adams JJ, Rostron BJ, Mendoza CA. Coupled fluid flow, heat and mass transport, and erosion in the Alberta basin: Implications for the origin of the Athabasca oil sands. Can J Earth Sci 2004;41:1077–95. doi:10.1139/e04-052.

[86] Peters KE, Cassa MR. Applied Source Rock Geochemistry. In: Magoon LB, Dow WG, editors. Pet. Syst. source to trap AAPG Mem. 60., 1994, p. 93–120.

[87] McCarthy K, Rojas K, Niemann M, Palmowski D, Peters K, Stankiewicz A. Basic Petroleum Geochemistry for Source Rock Evaluation. Oilf Rev 2011;23:32–43. doi:10.1016/j.epsl.2006.01.027.

[88] Schoonheydt RA, Johnston CT. The surface properties of clay minerals. Layer Miner Struct Their Appl Adv Technol 2011:335–70. doi:10.1180/EMU-notes.11.10.

[89] Mitchell JK, Soga K. Fundamentals of soil behaviour. 3rd ed. New York, NY, United States: John Wiley and Sons; 2005.

[90] Klobe WD, Cast RG. Reactions Affecting Cation Exchange Kinetics in Vermiculite 1. Soil Sci. Soc. Am. Proc. 31, 1967, p. 744–9.

[91] Sawhney BL. Selective sorption and fixation of cations by clay minerals. A review. Clays

Clay Miner 1972;20:93–100. doi:10.1346/CCMN.1972.0200208.

[92] Moore DM, Hower J. Ordered Interstratification of Dehydrated and Hydrated Na-smectite. Clays Clay Miner 1986;34:379–84. doi:10.1346/CCMN.1986.0340404.

[93] Srodo J. Nature of Mixed-Layer Clays and Mechanisms of Their Formation and Alteration. Annu Rev Earth Planet Sci 1999;27:19–53. doi:10.1146/annurev.earth.27.1.19.

[94] Środoń J. X-ray powder diffraction identification of illitic materials. Clays Clay Miner 1984;32:337–49. doi:10.1346/CCMN.1984.0320501.

[95] Dudek T, Cuadros J, Huertas J. Structure of mixed-layer kaolinite-smectite and smectite-to-kaolinite transformation mechanism from synthesis experiments. Am Mineral 2007;92:179–92. doi:10.2138/am.2007.2218.

[96] Dudek T, Środoón J, Eberl DD, Elsass F, Uhlik P. Thickness distribution of illite crystals in shales. I: X-ray diffraction vs. high-resolution transmission electron microscopy measurements. Clays Clay Miner 2002;50:562–77. doi:10.1346/000986002320679305.

[97] Eberl DD, Drits VA, Srodon J, Nüesch R. Mudmaster: A program for calculating crystallite size distributions and strain for the shapes of X-ray Diffraction peaks. US Geol Surv Open-File Rep 96-171 2000:53.

[98] Drits VA, Eberl DD, Srodoi JI. XRD Measurement of Mean Thickness, Thickness Distribution and Strain for Illite and Illite-Smectite Crystallites by the Bertaut-Warren-Averbach Technique 1998;46:38–50.

[99] Eberl DD, Nüesch R, Sucha V, Tsipursky S. Measurement of fundamental illite particle thicknesses by X-ray diffraction using PVP-10 intercalation. Clays Clay Miner 1998;46:89–97. doi:10.1346/CCMN.1998.0460110.

[100] Srodon J, Elsass F, Mchardy WJ, Morgan DJ. Chemistry of Illite-Smectite Inferred from Tem Measurements of Fundamental Particles. Clay Miner 1992;27:137–58. doi:10.1180/claymin.1992.027.2.01.

[101] Brindley GW, Brown G, editors. Crystal structures of clay minerals and their x-ray identification. London: Mineralogical Society; 1980.

[102] Takeda H, Ross M. Mica polytypism: identification and origin. Am Mineral 1995;80:715–

24. doi:10.1144/GSL.QJEGH.1993.026.004.04.

[103] Baronnet A. Some aspects of polytypism in crystals. Prog Cryst Growth Charact 1978;1:151–211. doi:10.1016/0146-3535(78)90009-6.

[104] Brigatti MF, Guggenheim S. Mica Crystal Chemistry and the Influence of Pressure, Temperature, and Solid Solution on Atomistic Models. Rev Mineral Geochemistry 2002;46:1–97. doi:10.2138/rmg.2002.46.01.

[105] Giuseppetti G, Tadini C. The crystal structure of 2 O brittle mica: Anandite. TMPM Tschermaks Mineral Und Petrogr Mitteilungen 1972;18:169–84. doi:10.1007/BF01134206.

[106] Brindley GW, F.Inst.P, Robinson Keiti. X-ray studies of halloysite and metahalloysite, Part I. The structure of metahalloysite, an example of random layer lattice. Mineral Mag 1948;28:393–406.

[107] Churchman GJ, Theng BKG. Interactions of Halloysites with Amides : Mineralogical Factors Affecting Complex Formation. Clay Miner 1984;19:161–75. doi:10.1180/claymin.1984.019.2.04.

[108] García FJG, Rodríguez SG, Kalytta A, Reller A. Study of natural halloysite from the Dragon Mine, Utah (USA). Zeitschrift Fur Anorg Und Allg Chemie 2009;635:790–5. doi:10.1002/zaac.200900076.

[109] Lvov YM, DeVilliers MM, Fakhrullin RF. The application of halloysite tubule nanoclay in drug delivery. Expert Opin Drug Deliv 2016;13:977–86. doi:10.1517/17425247.2016.1169271.

[110] Massaro M, Lazzara G, Milioto S, Noto R, Riela S. Covalently modified halloysite clay nanotubes: synthesis, properties, biological and medical applications. J Mater Chem B 2017;5:2867–82. doi:10.1039/C7TB00316A.

[111] Brigatti MF, Malferrari D, Laurora A, Elmi C. Structure and mineralogy of layer silicates: recent perspectives and new trends. Eur Mineral Union Notes Mineral 2011;11:1–71. doi:10.1180/EMU-notes.11.1.

[112] Brunauer S, Emmett PH, Teller E. Adsorption of Gases in Multimolecular Layers. J Am Chem Soc 1938;60:309–19. doi:citeulike-article-id:4074706.

[113] Gregg SJ, Sing KSW. Adsorption, Surface Area and Porosity. Academic Press INC. (London) LTD; 1982.

[114] Chiou CT, Rutherford DW, Manes M. Sorption of N2 and Egme Vapors on Some Soils, Clays, and Mineral Oxides and Determination of Sample Surface-Areas by Use of Sorption Data. Environ Sci Technol 1993;27:1587–94. doi:0013-936X/93/0927-1587$04.00/0.

[115] Chiou C, Kile D, Malcolm R. Sorption of vapors of some organic liquids on soil humic acid and its relation to partitioning of organic compounds in soil organic matter. Environ Sci … 1988;22:298–303. doi:10.1021/es00168a010.

[116] Chiou CT, Lee JF, Boyd SA. The Surface Area of Soil Organic Matter. Environ Sci Technol 1990;24:1164–6. doi:0013-936X/90/0924-1164$02.50/0 0.

[117] De Jonge H, Mittelmeijer-Hazeleger MC. Adsorption of CO 2 and N 2 on Soil Organic Matter: Nature of Porosity, Surface Area, and Diffusion Mechanisms. Environ Sci Technol 1996;30:408–13. doi:10.1021/es950043t.

[118] Środoń J. Correlation between coal and clay diagenesis in the Carboniferous of the Upper Silesian Coal Basin. In: Mortland MM, Farmer VC, editors. Proc. Int. Clay Conf., Amsterdam: Elsevier; 1979, p. 251–60. doi:10.1016/S0070-4571(08)70721-0.

[119] Kaiser K, Zech W. Soil dissolved organic matter sorption as influenced by organic and sesquioxide coatings and sorbed sulfate. Soil Sci Soc Am J 1998;62:129–36. doi:10.2136/sssaj1998.03615995006200010017x.

[120] Celis R, Hermosin MC, Cox L, Cornejo J. Sorption of 2,4-dichlorophenoxyacetic acid by model particles simulating naturally occurring soil colloids. Environ Sci Technol 1999;33:1200–6. doi:10.1021/es980659t.

[121] Bérend I, Cases JM, François M, Uriot JP, Michot L, Masion A, et al. Mechanism of Adsorption and Desorption of Water Vapor by Homoionic Montmorillonites: 2. The Li+, Na+, K+, Rb+, and Cs+-exchanged Forms. Clays Clay Miner 1995;43:324–36. doi:10.1346/CCMN.1995.0430307.

[122] Cases J, Berend I, Francois M, Uriot J, Michot LI, Thomas E. Mechanism of adsorption and desorption of water vapor by homoionic montmorillonite: 3. The Mg2+, Ca2+, Sr2+ and Ba2+ exchanged forms. Clays Clay Miner 1997;45:8–22.

doi:10.1346/CCMN.1997.0450102.

[123] Hedley CB, Saggar S, Theng BKG, Whitton JS. Surface area of soils of contrasting mineralogies using para-nitrophenol adsorption and its relation to air-dry moisture content of soils 2000;38:155–67. doi:10.1071/SR99114.

[124] Quirk JP, Murray RS. Appraisal of the ethylene glycol monoethyl ether method for measuring hydratable surface area of clays and soils. Soil Sci Soc Am J 1999;63, 4:839–49. doi:10.2136/sssaj1999.634839x.

[125] Helmy AK, Ferreiro EA, de Bussetti SG. Surface Area Evaluation of Montmorillonite. J Colloid Interface Sci 1999;210:167–71. doi:10.1006/jcis.1998.5930.

[126] Bujdák J, Komadel P. Interaction of methylene blue with reduced charge montmorillonite. J Phys Chem B 1997;101:9065–8. doi:10.1021/jp9718515.

[127] Kahr G, Madsen FT. Determination of the cation exchange capacity and the surface area of bentonite, illite and kaolinite by methylene blue adsorption. Appl Clay Sci 1995;9:327–36. doi:10.1016/0169-1317(94)00028-O.

[128] Kaufhold S, Dohrmann R. Beyond the Methylene Blue method : determination of the smectite content using the Cu-triene method. Angew Geol 2003;49:13–7.

[129] Pentrák M, Czímerová A, Madejová J, Komadel P. Changes in layer charge of clay minerals upon acid treatment as obtained from their interactions with methylene blue. Appl Clay Sci 2012;55:100–7. doi:10.1016/j.clay.2011.10.012.

[130] Syncrude-Research. Determination of bitumen, water and solids content of oil sands,reject and slurry samples (classical). In: Bulmer JT, Starr J, editors. Syncrude Anal. methods oil sand Bitum. Process., Edmonton: The Alberta Oil Sands Technology and Research Authority; 1979, p. 46–52.

[131] Eberl DD. User's guide to RockJock - A program for determining quantitative mineralogy from powder X-ray diffraction data. Boulder: 2003.

[132] Farmer VC. The layer silicates. Infrared Spectra Miner., London: Mineralogical Society; 1974, p. 331–363.

[133] Hang PT, Brindley GW. Methylene blue absorption by clay minerals. Determination of

surface areas and cation exchange capacities (clay-organic studies XVIII). Clays Clay Miner 1970;18:203–12. doi:10.1346/CCMN.1970.0180404.

[134] Meier LP, Kahr G. Determination of the cation exchange capacity (CEC) of clay minerals using the complexes of copper(II) ion with triethylenetetramine and tetraethylenepentamine. Clays Clay Miner 1999;47:386–8. doi:10.1346/CCMN.1999.0470315.

[135] Kaminsky H. Demystifying the methylene blue index. 4th Int. Oil Sands Tailings Conf. December 7-10, Lake Louis, Alberta, Lake Louis: The University of Alberta Geotechnical Centre and the Oil Sands Tailings Research Facility (OSTRF); 2014.

[136] Ŝucha V, Czímerová A, Bujdák J. Surface properties of illite-smectite minerals as detected by interactions with Rhodamine 6G dye. Clays Clay Miner 2009;57:361–70. doi:10.1346/CCMN.2009.0570308.

[137] Bujdák J, Iyi N, Sasai R. Spectral Properties, Formation of Dye Molecular Aggregates, and Reactions in Rhodamine 6G/Layered Silicate Dispersions. J Phys Chem B 2004;108:4470–7. doi:10.1021/jp037607x.

[138] Breen C, Rock B. The Competitive Adsorption of Methylene Blue on to Montmorillonite from Binary Solution wih Thioflavin T, Proflavine and Acridine Yellow. Steady-State and Dynamic Studies. Clay Miner 1994;29:179–89. doi:10.1180/claymin.1994.029.2.04.

[139] Michot LJ, Villiéras F. Surface Area and Porosity. In: Bergaya F, Theng BKG, Lagaly G, editors. Handb. Clay Sci. 1st ed., Elsevier Ltd; 2006, p. 965–78.

[140] William Lawrence Bragg. From Wikipedia, Free Encycl n.d. https://en.wikipedia.org/wiki/William_Lawrence_Bragg (accessed January 1, 2017).

[141] Prendergast R. Structure determination of small and large molecules using single crystal X-ray crystallography. MSc Diss Univ Manchester 2010:127.

[142] Lin W, Barron AR. An Introduction to X-ray Diffraction 1 History of X-ray crystallography. OpenStax-CNX 2014:1–11. http://creativecommons.org/licenses/by/4.0/.

[143] Cullity BD. Elements of X-Ray Diffraction. 2nd ed. Reading, Mass: Addison-Wesley Pub. Co; 1978.

[144] Omotoso O, Eberl D. Sample preparation and data collection strategies for X-ray diffraction quantitative phase analysis of clay-bearing rocks. 46th Annu. Meet. Clay Miner. Soc., Billings, Montana USA: 2009, p. 209.

[145] Środoń J, Drits VA, McCarty DK, Hsieh JCC, Eberl DD. Quantitative X-ray diffraction analysis of clay-bearing rocks from random preparations. Clays Clay Miner 2001;49:514–28. doi:10.1346/CCMN.2001.0490604.

[146] Vario MICRO Cube Elemental Analyzer 2016:4.

[147] Thermo Scientific. FLASH 2000 Series CHN/CHNS/Oxygen Automatic Elemental Analyzer FLASH 2000 Series 2008:4.

[148] Williams DB, Carter CB. Transmission Electron Microscopy-A Textbook for Materials Science. Part 1 Basics. Second, New York, NY, United States: Springer; 2009, p. 760.

[149] Reimer L, Kohl H. Transmission Electron Microscopy - Physics of Image Formation. Fifth. Springer; 2008.

[150] Myers B. TEM Sample Preparation with the FIB/SEM 2009:1–41.

[151] Stuart BH. Infrared Spectroscopy: Fundamentals and Applications. vol. 8. 2004. doi:10.1002/0470011149.

[152] McKelvy M, Britt TR, Davis BL, Gillie JK, Lentz LA, Leugers A, et al. Infrared spectroscopy. Anal Chem 1996;68:93–160. doi:10.1021/a1980006k.

[153] Farmer VC. Infrared spectroscopy. In: Olphen H van, Fripiat JJ, editors. Data Handb. Clay Mater. other Non-metallic Miner., Pergamon Press, Oxford, UK; 1979, p. 285–337.

[154] Farmer V., Russell JD. Effects of particle size and structure on the vibrational frequencies of layer silicates. Spectrochim Acta 1966;22:389–98. doi:10.1016/0371-1951(66)80069-3.

[155] Lazarev YUA, Lazareva A V. Infrared spectra and structure of synthetic polytripeptides 1978;17:1197–214. doi:10.1002/bip.1978.360170508.

[156] Madejov J, Komadel P, Madejova J, Madejová J. Base line studies of the clay minerals society source clays: infrared methods. Clay Clay Miner 2001;49:410–32. doi:10.1346/CCMN.2001.0490508.

[157] Farmer VC, Russell JD. The infra-red spectra of layer silicates. Spectrochim Acta

1964;20:1149–73. doi:10.1016/0371-1951(64)80165-X.

[158] Russell JD, Fraser AR. Infrared methods. In: Wilson MJ, editor. Clay Mineral. Spectrosc. Chem. Determ. Methods, Chapman & Hall, London; 1994, p. 11–67. doi:10.1007/978-94-011-0727-3_2.

[159] Chen F, Finch J a., Xu Z, Czarnecki J. Wettability of fine solids extracted from bitumen froth. J Adhes Sci Technol 1999;13:1209–24. doi:10.1163/156856199X00884.

[160] Muhr H-J, Rohner R. Good Titration Practice ™ in Karl Fischer Titration. Mettler Toledo 2011:98.

[161] Eberl DD, Drits VA, Środoń J. Deducing growth mechanisms for minerals from the shapes of crystal size distributions. Am J Sci 1998;298:499–533. doi:10.2475/ajs.298.6.499.

[162] Kile DE, Eberl DD, Hoch AR, Reddy MM. An assessment of calcite crystal growth mechanisms based on crystal size distributions. Geochim Cosmochim Acta 2000;64:2937–50. doi:10.1016/S0016-7037(00)00394-X.

[163] Środoń J, Eberl DD, Drits VA. Evolution of fundamental-particle size during illitization of smectite and implications for reaction mechanism. Clays Clay Miner 2000;48:446–58. doi:10.1346/CCMN.2000.0480405.

[164] Mercier PHJ, Le Page Y, Tu Y, Kotlyar L. Powder X-ray Diffraction Determination of Phyllosilicate Mass and Area versus Particle Thickness Distributions for Clays from the Athabasca Oil Sands. Pet Sci Technol 2008;26:307–21. doi:10.1080/10916460600806069.

[165] Kirwan LJ. Investigating bauxite residue flocculation by hydroxamate and polyacrylate flocculants utilising the focussed beam reflectance measurement probe. Int J Miner Process 2009;90:74–80. doi:10.1016/j.minpro.2008.10.010.

[166] De Clercq B, Lant PA, Vanrolleghem PA. Focused beam reflectance technique for in situ particle sizing in wastewater treatment settling tanks. J Chem Technol Biotechnol 2004;79:610–8. doi:10.1002/jctb.1028.

[167] Pandey A, Smith B, Redman T. Best practice for separations in mining and oil sands operations a review of modern technologies: optimizing thickeners, flotation and mature fine tailings (MFT) dewatering 2013:7.

[168] Heath AR, Fawell PD, Bahri PA, Swift JD. Estimating average particle size by focused beam reflectance measurement (FBRM). Part Part Syst Charact 2002;19:84–95. doi:10.1002/1521-4117(200205)19:2<84::AID-PPSC84>3.0.CO;2-.

[169] Kumar V, Taylor MK, Mehrotra A, Stagner WC. Real-time particle size analysis using focused beam reflectance measurement as a process analytical technology tool for a continuous granulation-drying-milling process. AAPS PharmSciTech 2013;14:523–30. doi:10.1208/s12249-013-9934-4.

[170] Higley DK, Lewan MD, Roberts LNR, Henry M. Timing and petroleum sources for the Lower Cretaceous Mannville Group oil sands of northern Alberta based on 4-D modeling. Am Assoc Pet Geol Bull 2009;93:203–30. doi:10.1306/09150808060.

[171] Grant D. Mossop. Geology of the Athabasca oil sands. Am Assoc Adv Sci 1980;207:145–52. doi:10.1126/science.207.4427.145.

[172] ASTM E11-17 Standard Specification for Woven Wire Test Sieve Cloth and Test Sieves 2017:1–18. doi:https://doi.org/10.1520/E0011-17.

[173] Bulmer JT, Starr J, editors. Determination of Bitumen, Water and Soiids Content of Oil Sand, Reject and Slurry Samples (Classical). Method 2.7. Syncrude Anal. methods oil sand Bitum. Process., Edmonton: Syncrude Canada Limited; 1979, p. 46–51.

[174] Cormack DE, Kenchington JM, Phillips CR, Leblanc PJ. Parameters and mechanisms in the solvent extraction of mined athabasca oil sand. Can J Chem Eng 1977;55:572–80. doi:10.1002/cjce.5450550515.

[175] Nikakhtari H, Wolf S, Choi P, Liu Q, Gray MR. Migration of fine solids into product bitumen from solvent extraction of Alberta oilsands. Energy Fuels 2014;28:2925–32. doi:10.1021/ef500021y.

[176] Meadus FW, Bassaw BP, Sparks BD. Solvent extraction of athabasca oil-sand in a rotating mill Part 2. Solids-liquid separation and bitumen quality. Fuel Process Technol 1982;6:289–300. doi:10.1016/0378-3820(82)90008-X.

[177] Yong RN, Elmonayeri D. On the stability and settling of suspended solids in settling ponds. Part II. Diffusion analysis of initial settling of suspended solids. Can Geotech J 1984;21:644–56. doi:10.1139/t84-071.

[178] Angle CW, Zrobok R, Hamza HA. Surface properties and elasticity of oil-sands-derived clays found in a sludge pond. Appl Clay Sci 1993;7:455–70. doi:10.1016/0169-1317(93)90015-S.

[179] Kotlyar LS, Deslandes Y, Sparks BD, Kodama H, Schutte R. Characterization of colloidal solids from Athabasca fine tails. Clays Clay Miner 1993;41:341–5. doi:10.1346/CCMN.1993.0410309.

[180] Mercier PHJ, Ng S, Moran K, Sparks BD, Kingston D, Kotlyar LS, et al. Colloidal Clay Gelation : Relevance to Current Oil Sands Operations. Pet Sci Technol 2012;30:915–23. doi:10.1080/10916466.2010.45959.

[181] Kaminsky HAW, Etsell TH, Ivey DG, Omotoso O. Distribution of clay minerals in the process streams produced by the extraction of bitumen from athabasca oil sands. Can J Chem Eng 2009;87:85–93. doi:10.1002/cjce.20133.

[182] Adeyinka OB, Samiei S, Xu Z, Masliyah JH. Effect of particle size on the rheology of athabasca clay suspensions. Can J Chem Eng 2009;87:422–34. doi:10.1002/cjce.20168.

[183] Tournassat C, Ferrage E, Poinsignon C, Charlet L. The titration of clay minerals: II. Structure-based model and implications for clay reactivity. J Colloid Interface Sci 2004;273:234–46. doi:10.1016/j.jcis.2003.11.022.

[184] Czímerová A, Jankovič L, Bujdák J. Spectral properties of rhodamine 6G in smectite dispersions: Effect of the monovalent cations. J Colloid Interface Sci 2011;357:322–30. doi:10.1016/j.jcis.2011.01.069.

[185] Bujdák J, Janek M, Madejová J, Komadel P. Influence of the layer charge density of smectites on the interaction with methylene blue. J Chem Soc - Faraday Trans 1998;94:3487–92. doi:10.1039/a805341c.

[186] Yoon S, Bhatt SD, Lee W, Lee HY, Jeong SY, Baeg J, et al. Separation and characterization of bitumen from Athabasca oil sand. Korean J Chem Eng 2009;26:64–71. doi:10.1007/s11814-009-0011-3.

[187] Cuadros J, Dudek T. FTIR investigation of the evolution of the octahedral sheet of kaolinite-smectite with progressive kaolinization. Clays Clay Miner 2006;54:1–11. doi:10.1346/CCMN.2006.0540101.

[188] Petit S, Decarreau A. Hydrothermal (200 °C) synthesis and crystal chemistry of iron-rich kaolinites starting materials. Clay Miner 1990;25:181–96. doi:10.1180/claymin.1990.025.2.04.

[189] Miller FA, Wilkins CH. Infrared Spectra and Characteristic Frequencies of Inorganic Ions. Anal Chem 1952;24:1253–94. doi:10.1021/ac60068a007.

[190] Saikia BJ, Parthasarathy G. Fourier Transform Infrared Spectroscopic Characterization of Kaolinite from Assam and Meghalaya, Northeastern India. J Mod Phys 2010;1:206–10. doi:10.4236/jmp.2010.14031.

[191] Estévez MJT, Arbeloa FL, Arbeloa TL, Arbeloa IL. Absorption and Fluorescence Properties of Rhodamine 6G Adsorbed on Aqueous Suspensions of Wyoming Montmorillonite. Langmuir 1993;9:3629–34. doi:10.1021/la00036a045.

[192] Lopez Arbeloa F, Tapia Estevez MJ, Lopez Arbeloa T, LOPEZ Arbeloa I. Spectroscopic Study of the Adsorption of Rhodamine 6G on Clay Minerals in Aqueous Suspensions. Clay Miner 1997;32:97–106. doi:10.1180/claymin.1997.032.1.11.

[193] Kikteva T, Star D, Zhao Z, Baisley TL, Leach GW. Molecular Orientation, Aggregation, and Order in Rhodamine Films at the Fused Silica/Air Interface. J Phys Chem B 1999;103:1124–33. doi:10.1021/jp9835824.

[194] Bujdák J. Effect of the layer charge of clay minerals on optical properties of organic dyes. A review. Appl Clay Sci 2006;34:58–73. doi:10.1016/j.clay.2006.02.011.

[195] Bergmann K, O'Konski CT. A Spectroscopic Study of Methylene Blue Monomer, Dimer, and Complexes With Montmorillonite. J Phys Chem 1963;67:2169–77. doi:10.1021/j100804a048.

[196] Carrigy MA. Effect of texture on the distribution of oil in the Athabasca oil sands, Alberta, Canada. J Sediment Pet 1962;32:312–25. doi:10.1306/74D70CB3-2B21-11D7-8648000102C1865D.

[197] Omotoso O, McCarty DK, Hillier S, Kleeberg R. Some successful approaches to quantitative mineral analysis as revealed by the 3rd reynolds cup contest. Clays Clay Miner 2006;54:748–60. doi:10.1346/CCMN.2006.0540609.

[198] Kotlyar LS, Kodama H, Sparks BD, Grattan-Bellew PE. Non-crystalline inorganic matter-

humic complexes in Athabasca oil sand and their relationship to bitumen recovery. Appl Clay Sci 1987;2:253–71. doi:10.1016/0169-1317(87)90035-4.

[199] Środoń J. Quantification of illite and smectite and their layer charges in sandstones and shales from shallow burial depth. Clay Miner 2009;44:421–34. doi:DOI 10.1180/claymin.2009.044.4.421.

[200] Woodruff WF, Revil A. CEC-normalized clay-water sorption isotherm. Water Resour Res 2011;47:1–15. doi:10.1029/2011WR010919.

[201] Środoń J, Zeelmaekers E, Derkowski A. The charge of component layers of illite-smectite in bentonites and the nature of end-member illite. Clays Clay Miner 2009;57:649–71. doi:10.1346/CCMN.2009.0570511.

[202] Grygar T, Hradil D, Bezdička P, Doušová B, Čapek L, Schneeweiss O. Fe(III)-modified montmorillonite and bentonite: Synthesis, chemical and UV-Vis spectral characterization, arsenic sorption, and catalysis of oxidative dehydrogenation of propane. Clays Clay Miner 2007;55:165–76. doi:10.1346/CCMN.2007.0550206.

[203] Osacky M, Geramian M, Dyar MD, Sklute EC, Valter M, Ivey DG, et al. Characterisation of petrologic end members of oil sands from the Athabasca region, Alberta, Canada. Can J Chem Eng 2013;91:1402–15. doi:10.1002/cjce.21860.

[204] Dohrmann R, Kaufhold S. Determination of exchangeable calcium of calcareous and gypsiferous bentonites. Clays Clay Miner 2010;58:79–88. doi:10.1346/CCMN.2010.0580108.

[205] Derkowski A, Bristow TF. On the problems of total specific surface area and cation exchange capacity measurements in organic-rich sedimentary rocks. Clays Clay Miner 2012;60:348–62. doi:10.1346/CCMN.2012.0600402.

[206] Dohrmann R. Problems in CEC determination of calcareous clayey sediments using the ammonium acetate method. J Plant Nutr Soil Sci 2006;169:330–4. doi:10.1002/jpln.200621975.

[207] Dohrmann R. Cation exchange capacity methodology III: Correct exchangeable calcium determination of calcareous clays using a new silver-thiourea method. Appl Clay Sci 2006;34:47–57. doi:10.1016/j.clay.2006.02.010.

[208] Dohrmann R, Kaufhold S. Three new, quick CEC methods for determining the amounts of exchangeable calcium cations in calcareous clays. Clays Clay Miner 2009;57:338–52. doi:10.1346/CCMN.2009.0570306.

[209] Helling CS, Chesters G, Corey RB. Contribution of organic matter and clay to soil cation-exchange capacity as affected by the pH of the saturating solution. Soil Sci Soc Am Proc 1964;28:517–20. doi:10.2136/sssaj1964.03615995002800040020x.

[210] Rashid MA. Contribution of Humic Substances to the Cation Exchange Capacity of Different Marine Sediments. Marit Sediments 1969;5:40–3.

[211] Czímerová A, Bujdák J, Dohrmann R. Traditional and novel methods for estimating the layer charge of smectites. Appl Clay Sci 2006;34:2–13. doi:10.1016/j.clay.2006.02.008.

[212] Derkowski A, Drits VA, McCarty DK. Rehydration of dehydrated-dehydroxylated smectite in a low water vapor environment. Am Mineral 2012;97:110–27. doi:10.2138/am.2012.3872.

[213] Dyal RS, Hendricks SB. Total surface of clays in polar liquids as a characteristic index. Soil Sci 1950;69:503. doi:10.1097/00010694-195006000-00014.

[214] Kaiser K, Guggenberger G. Mineral surfaces and soil organic matter. Eur J Soil Sci 2003;54:219–36. doi:10.1046/j.1365-2389.2003.00544.x.

[215] Burford JR, Deshpande TL, Greenland DJ, Quirk JP. Influence of Organic Materials on Determination of Specific Surface Areas of Soils. Eur J Soil Sci 1964;15:192–201.

[216] Echeverria JC, Morera MT, Mazkiaran C, Garrido JJ. Characterization of the porous structure of soils: adsorption of nitrogen (77K) and carbon dioxide (273K), and mercury porosimetry. Eur J Soil Sci 1999;50:497–503. doi:10.1046/j.1365-2389.1999.00261.x.

[217] Feller C, Schouller E, Thomas F, Rouiller J, Herbillon AJ. N2-Bet Specific surface areas of some low activity clay soils and their relationships with secondary constituents and organic matter contents. Soil Sci 1992;153:293–9. doi:10.1097/00010694-199204000-00005.

[218] Bujdák J, Iyi N, Fujita T. The aggregation of methylene blue in montmorillonite dispersions. Clay Miner 2002;37:121–33. doi:10.1180/0009855023710022.

[219] Bujdák J, Janek MN, Madejova J, Komadel P. Methylene Blue Interactions with Reduced-

Charge Smectites. Clay Clay Miner 2001;49:244–51. doi:10.1346/CCMN.2001.0490307.

[220] Oil Sands - Alberta's Energy Heritage 2016. http://history.alberta.ca/energyheritage/sands/default.aspx (accessed July 29, 2016).

[221] Fustic M, Ahmed K, Brough S, Bennett B, Bloom L, Asgar-Deen M, et al. Reservoir and bitumen heterogeneity in Athabasca oil sands. 2006 CSPG-CSEG-CWLS Jt Conf 2006:640–52.

[222] Ren S, Zhao H, Dang-Vu T, Xu Z, Masliyah JH. Effect of weathering on oil sands processability. Can J Chem Eng 2009;87:879–86. doi:10.1002/cjce.20234.

[223] Geramian M, Ardakani OH, Sanei H, Etsell TH, Ivey DG, Liu Q. Nano and micro-sized species in non- aqueous bitumen extraction from alberta oil sands. COSIA/PTAC Oil Sands Clay Work. Conf. April 28-29, Edmonton, Alberta: 2015.

[224] Zheng L. Characterization of Clay Minerals and Kerogen in Alberta Oil Sands Geological End Members. University of Alberta, 2013.

[225] Entezari I, Rivard B, Geramian M, Lipsett MG. Predicting the abundance of clays and quartz in oil sands using hyperspectral measurements. Int J Appl Earth Obs Geoinf 2017;59:1–8. doi:10.1016/j.jag.2017.02.018.

[226] Srivastava P, Parkash B, Pal DK. Clay minerals in soils as evidence of Holocene climatic change, central indo-gangetic plains, north-central India. Quat Res 1998;239:230–9. doi:10.1006/qres.1998.1994.

[227] Schultz LG, Shepard AO, Blackmon PD, Starkey HC. Mixed-layer kaolinite-montmorillonite from the yucatan peninsula, Mexico. Clays Clay Miner 1971;19:137–50. doi:10.1346/CCMN.1971.0190302.

[228] Vingiani S, Righi D, Petit S, Terribile F. Mixed-layer kaolinite-smectite minerals in a red-black soil sequence from basalt in Sardinia (Italy). Clays Clay Miner 2004;52:473–83. doi:10.1346/CCMN.2004.0520408.

[229] Kotlyar LS, Ripmeester JA, Montgomery DS, Sparks D. Characterization of oil sands solids closely associated with Athabasca bitumen. Fuel 1988;67:808–14. doi:10.1016/0016-2361(88)90155-X.

[230] Bensebaa F, Kotlyar LS, Sparks BD, Chung KH. Organic coated solids in Athabasca bitumen: charactrization and process implications. Can J Chem Eng 2000;78:610–6. doi:10.1002/cjce.5450780402.

[231] Christopher J, Sarpal a S, Kapur GS, Krishna A, Tyagi BR, Jain MC, et al. Chemical structure of bitumen-derived asphaltenes by nuclear magnetic resonance spectroscopy and x-ray diffractometry. Fuel 1996;75:999–1008. doi:10.1016/0016-2361(96)00023-3.

[232] Strausz OP. The chemistry of Alberta Oil Sand Bitumen. Fuels 1977;22:171–6.

[233] Crerar EE, Arnott RWC. Facies distribution and stratigraphic architecture of the Lower Cretaceous McMurray Formation, Lewis Property, northeastern Alberta. Bull Can Pet Geol 2007;55:99–124. doi:10.2113/gscpgbull.55.2.99.

[234] Hodgson GW. The McMurray oil field. Alberta Soc Pet Geol News Bull 1954;2:2–3.

[235] Misra M, Aguilar R, Miller JD. Surface Chemistry Features in the Hot Water Processing of Utah Tar Sand. Sep Sci Technol 1981;16:1523–44. doi:10.1080/01496398108058314.

[236] Sparks BD, Meadus FW, Kumar A, Woods JR. The effect of asphaltene content on solvent selection for bitumen extraction by the SESA process. Fuel 1992;71:1349–53. doi:10.1016/0016-2361(92)90205-3.

[237] Mehlich A. Effect of type of soil colloid on cation-adsorption capacity and on exchangeable hydrogen and calcium as measured by different methods. Soil Sci 1945;60:289–304. doi:10.1097/00010694-194510000-00003.

[238] Norrish K. The swelling of montmorillonite. Discuss Faraday Soc 1954;18:120. doi:10.1039/df9541800120.

[239] Haines SH, van der Pluijm BA. Clay quantification and Ar-Ar dating of synthetic and natural gouge: Application to the Miocene Sierra Mazatan detachment fault, Sonora, Mexico. J Struct Geol 2008;30:525–38. doi:10.1016/j.jsg.2007.11.012.

[240] Dohrmann R, Rüping KB, Kleber M, Ufer K, Jahn R. Variation of preferred orientation in oriented clay mounts as a result of sample preparation and composition. Clays Clay Miner 2009;57:686–94. doi:10.1346/CCMN.2009.0570602.

[241] Uhlik P, Sucha V, Eberl DD, Puskelova L, Caplovicova M. Evolution of pyrophyllite

particle sizes during dry grinding. Clay Miner 2000;35:423–32. doi:10.1180/000985500546774.

[242] Sucha V, Srodolq JAN, Elsass F, Mchardy WJ. Particle shape versus coherent scattering domain of illite/smectite: Evidence from HRTEM of Dolna Ves clays 1996;44:665–71.

[243] Mayer LM. Extent of coverage of mineral surfaces by organic matter in marine sediments. Geochim Cosmochim Acta 1999;63:207–15. doi:10.1016/S0016-7037(99)00028-9.

[244] Ransom B, Kim D-B, Kastner M, Wainwright S. Organic matter preservation on continental slopes:Importance of mineralogy and surface area. GeochimCosmochimActa 1998;62_ _:1329–45. doi:10.1016/S0016-7037(98)00050-7.

[245] Ransom B, Bennett RH, Baerwald R, Shea K. TEM study of in situ organic matter on continental margins: Occurrence and the "monolayer" hypothesis. Mar Geol 1997;138:1–9. doi:10.1016/S0025-3227(97)00012-1.

[246] Kaufhold S, Dohrmann R, Klinkenberg M, Siegesmund S, Ufer K. N2-BET specific surface area of bentonites. J Colloid Interface Sci 2010;349:275–82. doi:10.1016/j.jcis.2010.05.018.

[247] Schoonheydt AR. Clay mineral surfaces. In: Vaughan DJ, Pattrick RAD, editors. Miner. surfaces. 1st ed., London: Chapman and Hall; 1995, p. 303–32.

[248] Kuila U, Prasad M. Specific surface area and pore-size distribution in clays and shales. Geophys Prospect 2013;61:341–62. doi:10.1111/1365-2478.12028.

[249] Kuila U, McCarty DK, Derkowski A, Fischer TB, Topór T, Prasad M. Nano-scale texture and porosity of organic matter and clay minerals in organic-rich mudrocks. Fuel 2014;135:359–73. doi:10.1016/j.fuel.2014.06.036.

[250] Mortland MM. Clay-Organic Complexes and Interactions. Adv Agron 1970;22:75–117. doi:10.1016/S0065-2113(08)60266-7.

[251] Geramian M, Ivey DG, Liu Q, Etsell TH. Characterization of four petrologic end members from Alberta oil sands and comparison between different mines and sampling times. Can J Chem Eng 2017. doi:10.1002/cjce.23034.

[252] Andrews KW, Dyson DJ, Keown SR. Interpretation of electron diffraction patterns. Hilger

and Watts Ltd.; 1967. doi:10.1007/978-1-4899-6475-5.

[253] Jiang T. Diluted bitumen emulsion characterization and separation. PhD Diss RICE Univ 2009.

[254] Wilson MJ, Wilson L, Patey I. The influence of individual clay minerals on formation damage of reservoir sandstones: a critical review with some new insights. Clay Miner 2014;49:147–64. doi:10.1180/claymin.2014.049.2.02.

[255] Hepler LG, Smith RG. The Alberta oil sands: Industrial procedures for extraction and some recent fundamental research. Alberta oil sands technology and research authority; 1994.

[256] Bennion DB, Thomas F., Sheppard DA. Formation damage due to mineral alteration and wettability changes during hot water and steam injection in clay-bearing sandstone reservoirs. SPE Form. Damage Control Symp. Febr. 26-27, Lafayette, Louisiana: Society of Petroleum engineers, Inc.; 1992, p. 165–77. doi:10.2118/23783-MS.

[257] Pal K, Nogueira Branco LDP, Heintz A, Choi P, Liu Q, Seidl PR, et al. Performance of solvent mixtures for non-aqueous extraction of Alberta oil sands. Energy Fuels 2015;29:2261–7. doi:10.1021/ef502882c.

[258] Dang-Vu T, Jha R, Wu SY, Tannant DD, Masliyah J, Xu Z. Effect of solid wettability on processability of oil sands ores. Energy Fuels 2009;23:2628–36. doi:10.1021/ef9000117.

APPENDIX

I- LIST OF REFEREED JOURNAL PUBLICATIONS

- **M. Geramian**, Q. Liu, D.G. Ivey and T.H. Etsell, "Influence of Oil Sands Composition on Bitumen Quality during Non-Aqueous Bitumen Extraction from the Athabasca Deposit", Canadian Journal of Chemical Engineering, (Submitted on November 2017, Manuscript ID: CJCE-17-1124).
- **M. Geramian**, D. G. Ivey, Q. Liu and T. H. Etsell "Characterization of Four Petrologic End Members from Alberta Oil Sands and Comparison between Different Mines and Sampling Times" Canadian Journal of Chemical Engineering, 1–13, (2017), DOI: 10.1002/cjce.23034).
- M. Osacky, **M. Geramian**, P. Uhlík, M. Caplovicova, Z. Dankova, H. Palkova, M. Vítkova, M. Kovaćova, D.G. Ivey, Q. Liu, and T. H. Etsell "Mineralogy and Surface Chemistry of Alberta Oil Sands: Relevance to Nonaqueous Solvent Bitumen Extraction", Energy Fuels, 31, (2017), 8910–8924.
- I. Entezari, B. Rivarda, **M. Geramian**, M. G. Lipsett, "Predicting the abundance of clays and quartz in oil sands using hyperspectral measurements", International Journal of Applied Earth Observation and Geoinformation, 59 (2017), 1–8.
- **M. Geramian**, M. Osacky, D. G. Ivey, Q. Liu and T. H. Etsell, "Effect of Swelling Clay Minerals (Smectite and Illite-smectite) on Non-Aqueous Bitumen Extraction from Alberta Oil Sands", Energy Fuels, 30 (10), (2016), 8083–8090.
- C. Wang, **M. Geramian**, Q. Liu, D. G. Ivey, T. H. Etsell, "Comparison of Different Methods to Determine the Surface Wettability of Fine Solids Isolated from Alberta Oil Sands, Energy Fuels, 29 (2015), 3556–3565.
- M. Osacky, **M. Geramian**, D. G. Ivey, Q. Liu and T. H. Etsell, "Influence of Nonswelling Clay Minerals (Illite, Kaolinite, and Chlorite) on Nonaqueous Solvent Extraction of Bitumen", Energy Fuels, 29 (2015), 4150-4159.
- M. Osacky, **M. Geramian**, Q. Liu, D.G. Ivey and T.H. Etsell, "Surface properties of petrologic end members from Alberta oil sands and their relationship with mineralogical and chemical composition", Energy Fuels, 28 (2014), 934–944.

- M. Osacky, **M. Geramian**, M.D. Dyar, E.C. Sklute, M. Valter, D.G. Ivey, Qi Liu and T.H. Etsell, 2013. "Characterization of petrologic end members of oil sands from the Athabasca region, Alberta, Canada", Canadian Journal of Chemical Engineering, 91 (2013), 1402–1415.
- M. Osacky, **M. Geramian**, D.G. Ivey, Q. Liu and T.H. Etsell, "Mineralogical and chemical composition of petrologic end members of Alberta oil sands", Fuel. 113 (2013), 148–157.

II- LIST OF CONFERENCE PROCEEDINGS AND PRESENTATIONS

- M. Osacky, **M. Geramian**, P. Uhlík, M. Caplovicova, Z. Dankova, H. Palkova, M. Vítkova, M. Kovaćova, D.G. Ivey, Q. Liu, and T. H. Etsell, "Mineralogy, chemistry and surface properties of Alberta oil sands: implications for non-aqueous bitumen extraction", 54th Annual Clay Minerals Society Conference, June 5-8, 2017, Edmonton, Alberta, Canada.
- **M. Geramian**, T. H. Etsell, D. G. Ivey, Q. Liu, "Characterization of Nano- and Micro-Sized species in the Bitumen product during Non-Aqueous extraction from Oil Sands ores", the MSC 43rd Annual Meeting, June 7-10, 2016, Edmonton, Alberta, Canada.
- **M. Geramian**, O. H. Ardakani, H. Sanei, T. H. Etsell, D. G. Ivey and Q. Liu, "Nano and Micro-Sized Species in NonAqueous Bitumen Extraction from Alberta Oil Sands", COSIA/PTAC Oil Sands Clay Workshop and Conference, April 28-29, 2015, Edmonton, Alberta, Canada.
- I. Entezari, M. Speta, B. Rivard, and **M. Geramian**, "Hyperspectral Characteristics of Oil Sands Clay Mineral Assemblages", COSIA/PTAC Oil Sands Clay Workshop and Conference, April 28-29, 2015, Edmonton, Alberta, Canada.
- **M. Geramian**, T. H. Etsell, D. G. Ivey and Q. Liu, "Migration of Fine Solids to Bitumen Solution after Cyclohexane Extraction of the Four Petrological End Members of Alberta Oil Sands", was presented at the Oil Sands 2014 Conference, University of Alberta, April 28 - 29, 2014, Edmonton, Alberta, Canada.
- **M. Geramian**, M. Osacky, D. Dyar, E. Sklute, M. Valter, T.H. Etsell, D.G. Ivey, Qi Liu, "Characterization of petrologic end members of Athabasca oil sands. The 3rd Oil Sands Clay Conference and Workshop, CONRAD, Feb 20-21, 2013, Edmonton, Alberta, Canada.
- **M. Geramian**, M. Osacky, L. Zheng, D.G. Ivey, Qi Liu and T.H. Etsell, "Effect of Various Clay Minerals on non-Aqueous Bitumen Extraction", Oilsands 2012, August 28-30, 2012. Edmonton, Alberta, Canada.

- M. Osacky, **M. Geramian**, D.G. Ivey, Qi Liu and T.H. Etsell, "Surface properties, mineralogical properties and chemical composition of petrologic end members of Alberta oil sands", Oilsands 2012, August 28-30, 2012. Edmonton, Alberta, Canada.
- M. Osacky, **M. Geramian**, D.G. Ivey, Qi Liu and T.H. Etsell, "Mineralogical and Chemical Characterization of Petrologic End Members of Alberta Oil Sands", 48th Annual Meeting of the Clay Minerals Society, Stateline, Nevada, USA.